
Development of advanced mathematical models for
analysis of hydraulic channel fracturing technique

By

Hao Thanh Luong

A thesis submitted for the degree of Master of Philosophy at the

School of Mechanical Engineering

The University of Adelaide

Australia

November 2018

Abstract

The channel fracturing technique is a Schlumberger's recent development in the area of hydraulic fracture stimulations, which allows for discontinuous proppant placement within the fracture opening. The discontinuous placement of proppant creates a highly conductive network of interconnected open channels, which can significantly increase the overall fluid conductivity of the fracture. Modelling, analysis and prediction of the fluid conductivity of openings created using the channel fracturing technique is of a great interest in both industrial and research contexts. Subsequently, the main objective of this research is to study the channel fracturing technique. Specific aims include the investigation of the effects of different confining stress, proppant placement patterns, and mechanical properties of the rock formation and proppant on the enhancement of the fluid conductivity.

The general methodology adopted in this thesis is based on the Distributed Dislocation Technique, which is a powerful analytical tool for the analysis of fracture problems. To meet the main objective, a number of nonlinear mathematical models were developed to predict the fluid conductivity. These models are presented in separate chapters of this thesis. A number of case studies were considered for typical combinations of mechanical properties of rock and proppant, proppant placement patterns as well as confining stress conditions. It was demonstrated that an appropriate selection of proppant and its placement pattern within the openings can significantly increase the well production rates, which is essentially the ultimate goal of hydraulic fracture stimulations.

From practical point of view, the outcomes of this thesis can provide a valuable guidance for designing efficient proppant injection schedules and selecting a suitable proppant type in order to maximise the well productivity, decrease environmental impact as well as to reduce the overall cost of oil and gas recovery, which are currently the main concerns for the relevant industries and

government organisations.

The main body of the thesis represents a compendium of papers submitted to or published in international journals or conference proceedings. These papers are united by the same topic as well as the research methodology mentioned above.

The percentage and contribution of the candidate are specified in the Statement of Authorship for each article with more than one author.

Declaration

I certify that this work contains no material which has been accepted for the award of any other degree or diploma in my name, in any university or other tertiary institution and, to the best of my knowledge and belief, contains no material previously published or written by another person, except where due reference has been made in the text. In addition, I certify that no part of this work will, in the future, be used in a submission for any other degree or diploma in any university or tertiary institution without the prior approval of the University of Adelaide.

I give consent to this copy of my thesis when deposited in the University Library, being made available for loan and photocopying, subject to the provisions of the Copyright Act 1968.

The author acknowledges that copyright of published works contained within this thesis resides with the copyright holder(s) of those works.

I also give permission for the digital version of my thesis to be made available on the web, via the University's digital research repository, the Library Search also through web search engines.

Hao Thanh Luong

Date

Acknowledgements

First, I would like to express my deepest gratitude to my principal supervisor, Prof. Andrei Kotousov, for his guidance and support during my Master program. He sketched an appropriate plan to improve my ability and continuously encouraged me moving forwards. My special appreciation goes to my co-supervisor, Dr. Aditya Khanna, for his great support during these past two years. Working under his guidance is a golden chance for me to accumulate professional knowledge and develop research skills which are essential to pursuing a research career.

I greatly appreciate A/Prof. Giang Nguyen and Mr. Linh Le for their support of modeling rock formation. Special thanks go to Dr. Francis Rose for his comments on my computational models and manuscripts. In addition, I would like to thank Ms. Alison Hunter for her proof-reading the thesis.

The thesis would not be possible without the financial support in the form of scholarship offered by the Ministry of Education and Training of the Vietnam government and the University of Adelaide.

I dedicate the thesis to my loving wife, Huyen Pham, and my son, Anh Luong, for their continuous encouragement and support that help me overcome the hard times.

Table of contents

Abstract	i
Declaration	iii
Acknowledgements	iv
Table of contents	v
1. Introduction	1
1.1. Hydraulic fracturing techniques	2
1.2. Research motivation and objectives	3
1.3. Organization of the thesis.....	5
References	7
2. Mechanics of hydraulic fracturing	9
2.1. Background to hydraulic fracturing	10
2.2. Open-channel hydraulic fracturing	14
2.3. Hydraulic fracture processes	17
2.3.1. Fracture initiation criteria	18
2.3.2. Hydraulic fracture propagation	21

2.3.3.	Fluid flow and fluid loss	24
2.3.4.	Transportation and placement of the proppant	28
2.4.	Hydraulic fracture modeling	31
2.4.1.	Sneddon’s model for penny-shaped fracture	31
2.4.2.	PKN and KGD models for planar fracture	33
2.4.3.	Pseudo three-dimensional (P3D) models for planar fracture	35
2.4.4.	Three-dimensional models for hydraulic fractures.....	37
2.5.	Residual opening of hydraulic fractures	40
2.6.	Conductivity of proppant packs	42
2.7.	Well performance	45
2.8.	Research gaps	47
2.9.	Conclusion	48
	References.....	49
3.	Fracture mechanics and distributed dislocation technique	59
3.1.	Linear elastic fracture mechanics.....	60
3.2.	Distributed dislocation technique	64
3.3.	Gauss-Chebyshev quadrature for integral equations	68
3.4.	Conclusion	70

References	71
4. Residual opening of hydraulic fractures created using the channel fracturing technique.....	72
Statement of authorship.....	73
Abstract	75
1. Introduction	75
2. Problem formulation	76
3. Solution procedure	79
4. Numerical results.....	80
5. Conclusion.....	87
References	87
5. Optimisation of proppant use in the application of the channel fracturing technique	89
Abstract	90
1. Introduction	90
2. Problem formulation	91
3. Mathematical model.....	91
4. Results and discussion.....	93

5. Conclusion	95
6. Acknowledgements	95
7. References	95
6. On the application of the channel-fracturing technique to soft rock formations	98
Statement of authorship	99
Summary	100
Introduction.....	100
Problem formulation and modeling assumptions	101
Mechanical behaviour of rock and proppant columns.....	102
Governing equations for the residual opening of the unit cell.....	104
Effective conductivity of the unit cell.....	105
Parametric study	107
Conclusions.....	111
Nomenclature	111
References.....	112
Appendix A: Singular integral equation for dislocation density	114
Appendix B: Numerical solution procedure of the singular integral equation	116

7. On the coarse-scale residual opening of hydraulic fractures created using the channel fracturing technique.....	118
Statement of authorship.....	119
Abstract	121
Introduction	122
Formulation of the unit-cell problem	123
Method of solution: Distributed Dislocation Technique.....	125
Homogenisation procedure	127
Numerical results	129
Conclusion.....	131
References	132
8. Summary and recommendations.....	133
8.1. Summary of the outcomes.....	134
8.2. Recommendations for future work.....	136

Chapter 1

Introduction

Chapter 1

Introduction

Hydraulic fracturing is a well stimulation technique that is commonly used to enhance the production of underground resources, such as oil, natural gas, geothermal energy and water. The application of this technology has opened up vast unconventional energy resources, including low permeability shale formations, coal seam gas, and tight-sand reservoirs. The technique has contributed significantly to the success of petroleum industries across the world. Over the last ten years, the natural gas production of the United States increased by more than 30%, and in 2012, the total production from unconventional reservoirs was 34% of the total hydrocarbon production (d'Huteau et al. 2011). In Australia, the recent transition from conventional reservoirs to unconventional reservoirs recently has increased attention to the hydraulic fracturing technologies (Medvedev et al. 2013). This chapter introduces the basic concepts of hydraulic fracturing techniques, the significance of this research, and the main objectives of the current thesis.

1.1. Hydraulic fracturing techniques

Hydraulic fracturing involves fluid injection into the wellbore to initiate new fractures in the rock and widen the existing natural fractures. Granular particles called “proppants”, are mixed with the fracturing fluid and injected into the fracture to hold open, or “prop” the fracture once the fracturing fluid pressure is relieved. The proppant-filled fracture provides a narrow but very conductive pathway for fluid flow from the rock formation towards the wellbore (Bortolan et al. 2015), and significantly increases the well productivity (Khanna et al. 2014).

Since the early application of hydraulic fracturing, producers have tried to create a continuous proppant pack along the entire fracture length. However,

maintaining the high fluid conductivity of the proppant pack over the lifetime of a fluid producing well represents a major challenge for the industry. To overcome this challenge, early pioneers, Darin and Huitt (1960) proposed using a single layer of proppant, and Tinsley and Williams (1975) suggested discontinuous placement of multiple proppant layers. Both concepts envisaged the creation of a network of open channels, which can provide alternative pathways for gas or fluid to flow freely within the fracture (Bedrikovetsky et al. 2012; Khanna et al. 2013). The concept of discontinuous proppant placement was implemented in practice recently, with the development of the open-channel fracturing technique by Schlumberger scientists (d'Huteau et al. 2011; Medvedev et al. 2013).

The conductivity of the open channels is several orders higher than the conductivity of the porous proppant pack and it is estimated that fractures created using open-channel fracturing have a higher initial and long-term conductivity than conventional fractures filled with a continuous proppant pack (d'Huteau et al. 2011). Between the years 2010-2013, more than 10,000 open-channel fracturing treatments had been successfully performed in shale-carbonate and sandstone-rich reservoirs in various countries (Medvedev et al. 2013). The collective data shows two common trends, namely a reduction in proppant use and an improvement in the average initial and long term well productivity when compared to continuous proppant placement (Medvedev et al. 2013).

1.2. Research motivation and objectives

For the petroleum industries, the demand for economic efficiency has drawn great interest towards improving the hydraulic fracture conductivity for both conventional fracturing techniques and the novel channel fracturing technique (Bortolan Neto et al. 2015). Among many parameters, the conductivity of a hydraulic fracture strongly depends on the response of the proppant pack under compressive in-situ stresses as well as the placement of proppant within the fracture (Khanna et al. 2014). Modelling the influence of these parameters on the

fracture opening and conductivity can facilitate the optimal real-world implementation and significantly improve the economic efficiency of the hydraulic fracturing procedures.

Although a wealth of literature exists on this topic, some of the most widely utilised models suffer from drawbacks highlighted in Chapter 2. The overall aim of this research is to develop and validate an advanced and more realistic modelling approach for analysing the effectiveness of the channel fracturing technique under various reservoir conditions. The overall aim can be separated into the following objectives:

- 1) Develop an empirical model to describe the combined effect of proppant consolidation and embedment upon the net residual opening of the proppant-filled fractures under compressive loading. The model must describe the nonlinear consolidation response of a wide range of proppants under uniaxial compression. It must also describe the dependence of the embedment depth upon the confining stress. The model is to be calibrated using experimental data.
- 2) Develop an analytical model, based on the Distributed Dislocation Technique, for obtaining the residual opening profile of hydraulic fractures with a discontinuous distribution of proppant columns. Perform an extensive parametric study to investigate the effects of the mechanical properties of the rock and proppant column, and the in-situ stresses.
- 3) Develop an analytical model for evaluating the effective fluid conductivity of a heterogeneous medium composed of porous proppant columns and open channels. The model will provide upper and lower bounds for the effective fluid conductivity of the fracture as a function of the residual opening of the channels and the permeability of the proppant pack.
- 4) Integrate the analytical models developed in objectives (2) and (3) to identify the optimal proppant column spacing which maximises the effective fracture conductivity of given reservoir conditions and rock and proppant mechanical

properties.

- 5) Validate the outcomes of the modelling approach by comparing the theoretically obtained tendencies with field observations and previous engineering estimations. Due to a scale-effect and certain modelling assumptions, it is not possible to directly compare the theoretical outcomes with experimental data obtained for laboratory-scale specimens.

1.3. Organization of the thesis

The thesis is organised in seven chapters and the contents of each chapter are summarised below:

Chapter 1 starts with a brief description of hydraulic fracturing and its contribution to the growth of petroleum industries across the world. In addition, the channel fracturing technique, which is the focus of the current thesis, is briefly introduced in this chapter. The economic incentives of cost-efficient oil and gas production is introduced as the motivation for the present work and previous modelling studies. Finally, the research objectives of this thesis are identified, with the overall aim to develop advanced analytical models for the residual opening and conductivity of open-channel fractures under different reservoir conditions. The modelling outcomes can guide the design of optimal hydraulic stimulations.

Chapter 2 provides a detailed overview of the various stages of conventional and open-channel hydraulic fracturing treatments. The processes of fracture initiation and propagation, as well as fluid and proppant transport in the fracture, are described. Following that, hydraulic fracture propagation models of varying complexity are reviewed, ranging from simplified 2D analytical models to more sophisticated 3D numerical models. Some of the shortcomings of existing modelling approaches are discussed and the research gaps to be addressed in the thesis are identified.

Chapter 3 provides an overview of Linear Elastic Fracture Mechanics (LEFM)

and describes the research methodology, which is based on the Distributed Dislocation Technique (DDT). The method for deriving singular integral equations for crack problems using DDT and the numerical procedures for solving singular equations are also discussed.

Chapter 4 considers the problem of a partially-filled hydraulic fracture created in a hard rock formation, i.e. the effect of proppant embedment into the rock is excluded from the analysis. The problem geometry is idealised as two-dimensional and periodic and the governing equations are derived for a unit-cell of the periodic geometry. The integral equation is reduced to a system of nonlinear algebraic equations by using Gauss-Chebyshev quadrature, which are solved numerically using the Newton-Raphson iteration. An extensive parametric study is conducted to investigate the influence of the proppant column size and the space between columns on the fracture residual opening as well as fracture conductivity.

Chapter 5 further extends the parametric study conducted in Chapter 3 to investigate the effect of the rock Young's modulus on the optimal values of proppant column spacing and effective fracture conductivity. It is demonstrated that the benefits of the channel fracturing technique, i.e. increased fracture conductivity and reduced proppant use, are most pronounced for rock formations with high Young's modulus. The obtained results are used to identify the range of rock Young's modulus for which the implementation of the channel fracturing technique is suitable.

Chapter 6 considers the same problem geometry as Chapters 3 and 4, but the further develops the problem formulation and modelling approach to incorporate the effect of proppant embedment into the rock. This development is essential for modelling channel fracturing in soft rock formations, where the influence of proppant embedment on the fracture residual opening is significant. A parametric study is conducted to demonstrate the interplay between proppant consolidation and proppant embedment and their combined influence on the residual opening

and conductivity of the fracture. The outcomes can guide the selection of the optimal proppant column spacing in soft rock formations.

Chapter 7 considers the more realistic non-periodic problem geometry, where the proppant column spacing as well as the confining stress can vary along the length of the fracture. It is proposed that the numerous discrete proppant columns along the fracture length can be replaced by a continuous distribution of nonlinear springs. A homogenisation procedure, based on the energy conservation principle, is developed to determine the "traction law" i.e. the load-displacement relationship for the continuous distribution of nonlinear springs in terms of the "unit-cell" solution presented in the earlier chapters.

Chapter 8 presents the concluding remarks and recommendations for future work. Based on the work completed in this thesis, it only remains to solve the boundary value problem for a hydraulic fracture supported by uniformly distributed springs between the crack-faces, which satisfy the traction law obtained in Chapter 6. The lengthwise variation of the initial fracture opening, fluid pressure within the fracture, remote in-situ stress normal to the fracture plane and irregular proppant column spacing can be incorporated at this stage. The method of solution of the latter boundary problem would be the same as developed in Chapters 3-5.

References

Bedrikovetsky, P.G., Keshavarz, A., Khanna, A., McKenzie, K.M. & Kotousov, A. 2012, 'Stimulation of natural cleats for gas production from coal beds by graded proppant injection', paper presented at SPE Asia Pacific Oil and Gas Conference and Exhibition, Perth, Australia.

Bortolan Neto, L., Khanna, A. & Kotousov, A. 2015, 'Conductivity and performance of hydraulic fractures partially filled with compressible proppant packs', *International Journal of Rock Mechanics and Mining Sciences*, vol. 74, pp. 1-9, DOI <https://doi.org/10.1016/j.ijrmms.2014.11.005>.

Bortolan, N.L., Khanna, A. & Kotousov, A. 2015, 'Conductivity and performance of hydraulic fractures partially filled with compressible proppant packs', *International*

Journal of Rock Mechanics and Mining Sciences, vol. 74, pp. 1-9, DOI <https://doi.org/10.1016/j.ijrmms.2014.11.005>.

d'Huteau, E., Gillard, M., Miller, M., Pena, A., Johnson, J., Turner, M., Medvedev, O., Rhein, T. & Willberg, D. 2011, 'Open-channel fracturing-a fast track to production', *Schlumberger*, vol. Oilfield Review Autumn 2011, 23, no. 3.

Darin, S.R. & Huitt, J.L. 1960, 'Effect of a partial monolayer of propping agent on fracture flow capacity', paper presented at 34th Annual Fall Meeting of SPE, Dallas.

Khanna, A., Bortolan Neto, L. & Kotousov, A. 2014, 'Effect of residual opening on the inflow performance of a hydraulic fracture', *International Journal of Engineering Science*, vol. 74, pp. 80-90, DOI <https://doi.org/10.1016/j.ijengsci.2013.08.012>.

Khanna, A., Keshavarz, A., Mobbs, K., Davis, M. & Bedrikovetsky, P. 2013, 'Stimulation of the natural fracture system by graded proppant injection', *Journal of Petroleum Science and Engineering*, vol. 111, pp. 71-77, DOI <https://doi.org/10.1016/j.petrol.2013.07.004>.

Medvedev, A.V., Kraemer, C.C., Pena, A.A. & Panga, M.K.R. 2013, 'On the mechanisms of channel fracturing', paper presented at SPE Hydraulic Fracturing Technology Conference, The Woodlands, Texas, USA.

Tinsley, J.M. & Williams, J.R., Jr. 1975, 'A new method for providing increased fracture conductivity and improving stimulation results', vol. 27, no. 11, DOI 10.2118/4676-PA.

Chapter 2

Mechanics of Hydraulic Fracturing

Chapter 2

Mechanics of Hydraulic Fracturing

Hydraulic fracturing is a stimulation technique widely adopted in the oil, gas and some other industries for enhancement of the permeability of low-permeable reservoirs. Successful application of this technique has significantly increased the production rate and efficiency of oil and gas wells. Presently, the main issue faced by the petroleum industry is minimising the cost of this technique and reducing the risk of environmental damage due to its implementation. Consequently, much research effort has been directed to predicting the stimulation outcomes and selecting the optimal parameters for particular conditions and applications. In this literature review, it is impossible to cover every aspect of this stimulation technique. It will focus only on specific issues that are important for the current work, namely: background on hydraulic Fracturing, open-channel hydraulic fracturing and modelling of hydraulic fracturing processes.

2.1. Background to Hydraulic Fracturing

The history of the technology began in the 1930s, with the Dow Chemical Company exploring how rock formations can be cracked and deformed by using downhole fluid pressure, so that the efficiency of acid stimulation is significantly increased (Grebe & Stoesser 1935). The first hydraulic treatment performed in 1947 by the Stanolind Oil and Gas Corporation in Kansas showed that this technique was more effective than the current technology of the time, well acidizing (Adachi et al. 2007). Since then, hydraulic fracturing techniques have been used in a variety of field conditions. Annually, thousands of hydraulic fracture treatments are successfully performed in diverse geological regions.

The American Petroleum Institute reports that the hydraulic fracturing technique has been applied to more than 1.1 million wells in U.S since 1940

(Adams & Rowe 2013). According to Montgomery and Smith (2010), the number of hydraulic fracturing treatments performed globally is approximately 2.5 million, and approximately 60% of the total number of wells drilled undergo the hydraulic fracturing treatment. In 2008, there were more than 50,000 hydraulic fracture treatments completed worldwide, and the cost for a single treatment lied between 10,000 and 6 million US dollars. The worldwide commercial market for hydraulic fracturing per year is estimated at nearly \$30 billion. As per the report in (Adams & Rowe 2013), hydraulic fracturing has significantly increased US recoverable reserves by at least 30% for oil and 90% for gas.

Additional applications of hydraulic fracturing lie in the areas of water production, in-situ stress measurement, geothermal energy extraction, tunnel and dam construction, and block cave mining. For water well production enhancement, existing fractures within aquifers are washed out, propagated and connected to each other using high pressure injection water (Rummel & Kappelmeyer 1983). For in-situ stress measurement in rock masses, the fracturing fluid is pumped into a borehole at a controlled rate and variation in fluid pressure according to the different stages of crack evolution, such as fracture initiation, fracture propagation, and fracture closure, is tracked. The obtained fluid pressure history is used to determine the state of rock stress. Hydraulic fractures are also utilised to create flow pathways in low permeability hot rocks, thereby allowing the extraction of geothermal energy using a system of injection and the extraction wells (Economides & Nolte 2000).

Conventional hydraulic stimulation for oil/gas reservoirs can be illustrated as per the schematic in Figure 1. The fracturing process begins with the perforation operation, whereby specially designed shaped-charges blast through the steel casing, the cement, and rock formation with predefined orientations to create perforation tunnels, which form an initial path for fractures (Montgomery & Smith 2010). A viscous liquid, known as the fracturing fluid, is injected into the borehole under high, controlled pressure to initiate fractures at the perforated interval

(Economides & Nolte 2000). By controlling the pumping parameters, such as the pumping rate, fluid pressure, and the duration of fluid injection, the fractures are propagated from the wellbore towards the desired distance, which can be extended up to several hundred meters (Economides & Nolte 2000).

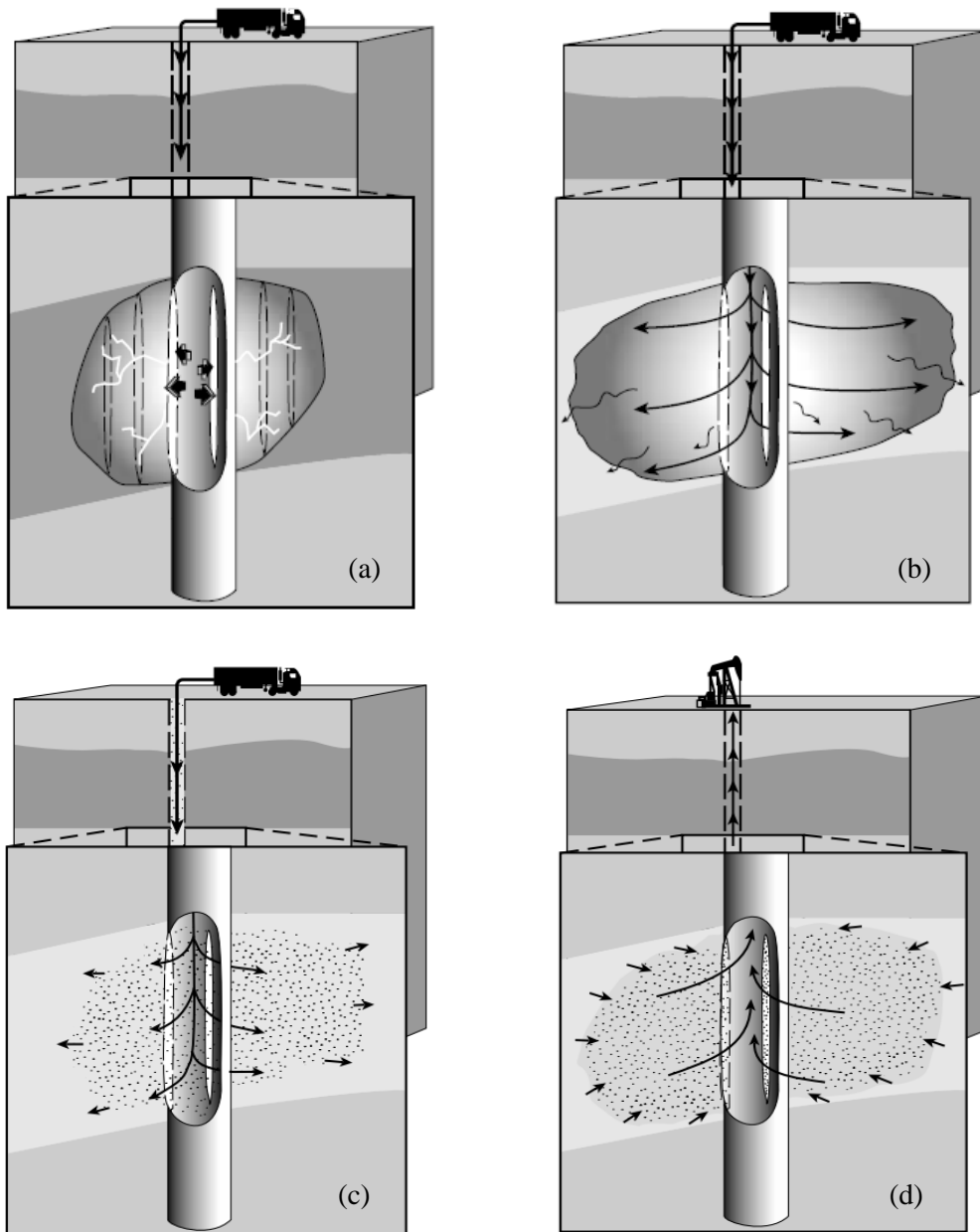


Figure 1: Schematic illustration of hydraulic fracture: (a) internal pressure breaking a vertical wellbore, (b) propagating a fracture, (c) introducing proppant into the fracture and (d) fluid production from the fractured well (Economides & Nolte 2000)

Clean fluid is commonly injected first to increase the fracture width for the proppant particles, which is injected in later stages as a semi-liquid mixture or slurry, and can migrate through the fracture (Economides & Nolte 2000). For the last stage of the hydraulic treatment, once pumping has ceased, the decrease in liquid pressure and the flow of the residual hydraulic fluid through the fracture faces into the porous formation result in the closure of the fracture surfaces under the action of far-field compressive stresses. The remaining proppant-pack provides not only mechanical support to keep the fracture open but also a conductive pathway that allows the fluid to flow within the fracture (Cipolla et al. 2008). The conductivity of a propped fracture is several orders of magnitude higher than that of an un-propped fracture, especially under high in-situ stress conditions (Gillard et al. 2010; Zhang et al. 2013b).

The conductivity of the hydraulic fracture is limited by the permeability of the porous proppant pack. It is well known that several damage mechanisms can impair the permeability of proppant packs by blocking the pore space between the proppant particles. The mechanisms include: improper fracture clean-up resulting in residual fracturing gel in the proppant pack, mineral precipitation in the pore space and accumulation of fine debris resulting from proppant crushing and embedment into the rock (Vincent 2009). The impairment of fluid flow through the proppant pack reduces the overall efficiency of the fracturing treatment (Sammuel et al. 2009). Extensive research has been conducted over the past several decades to counteract these effects and develop new fracturing fluids (Bang et al. 2008; Cramer et al. 2004; Friehauf & Sharma 2009; Stephens et al. 2007) and proppants (Nor-Azlan et al. 2003). These solutions are generally cost intensive and can offset any economic benefits of increased fracture conductivity. An alternative and cost-effective approach to addressing this challenging, known as the open-channel fracture technique, has been developed recently by Schlumberger scientists and widely applied throughout the petroleum industry. The method of implementation of this technique is described in the next section.

2.2. Open-channel Hydraulic Fracturing

The Open-Channel Fracturing Technique is based on the concept that proppant should be deposited discontinuously throughout the fractures, so a homogeneous proppant pack is substituted by a heterogeneous structure consisting of proppant columns and a network of open channels (Gillard et al. 2010), see Figure 2. The open channels occupy only a small fraction of the fracture volume but provide the dominant fluid pathway towards the wellbore due to their high conductivity. Hence, the low permeability of the proppant packs has an insignificant influence on the overall conductivity of the fractures. Discontinuous placement of the proppant also results in a decrease in proppant use for the treatment, especially for large scale fractures that can consume hundred tons of proppant, so eventually this leads to cost savings (Khanna & Kotousov 2016). Moreover, the novel technique results in a smaller operational footprint and significantly reduces the environment impact (d'Huteau et al. 2011).

The efficiency of open-channel hydraulic fracturing treatment was evaluated in a wide range of oil fields. A study was conducted in Argentina to compare use of the new technique with conventional treatment in moderately permeable oil reservoirs. The results showed that for the first 30 days, the production in wells stimulated by the open-channel hydraulic fracturing technique was 53% higher than that of wells where conventional treatments were applied, and accumulative hydrocarbon production over two years was 29% higher than the corresponding production using the conventional treatments (d'Huteau et al. 2011). A study on the implementation of the channel fracturing technique for tight-gas reservoirs in Jonah Field, USA, showed that the technique increased accumulated production by 26% and saved 44% of proppant use, compared with conventional treatments (d'Huteau et al. 2011). Another study was conducted in the Eagle Ford Shale region in the USA, which stores a large volume of both gas and oil. The channel fracturing technique increased the long term production of recovered hydrocarbons: by 76% for gas production and by 54% for condensate production

(d'Huteau et al. 2011). The proven efficiency of this technique has encouraged the application of the novel technique for reservoir stimulation. d'Huteau et al. (2011) shows that more than 2600 open-channel hydraulic fracturing treatments have been performed in eight countries, including the USA, Canada, Argentina, India, etc. On a global scale, this novel technique has saved more than 86,180 tons of proppant usage in comparison with the amount of proppant that would have been used for conventional treatments.

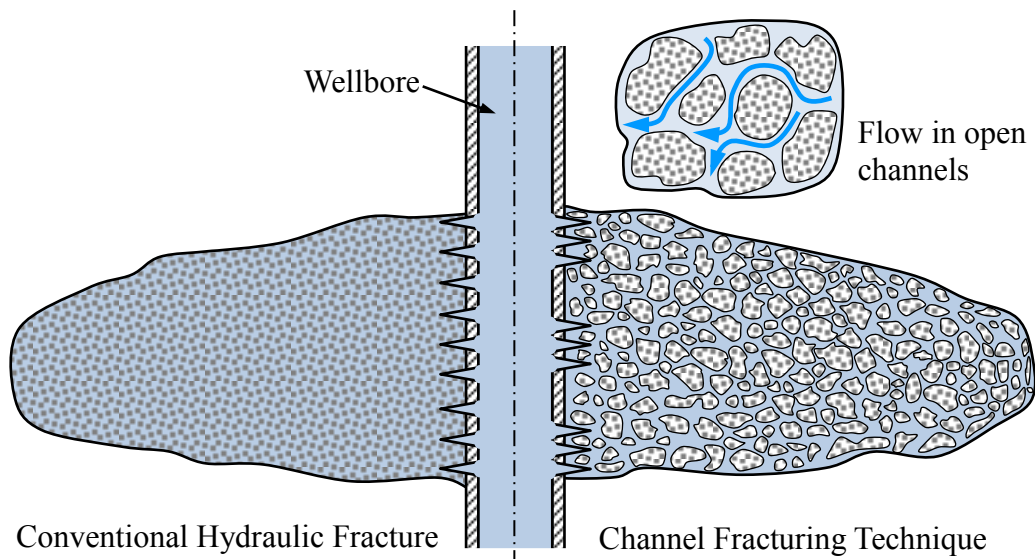


Figure 2: Conventional (left) and Channel Fracturing Technique (right) (Gillard et al. 2010).

The discontinuous deposit of proppant along the fracture length is created by injecting proppant-laden fluid into the fracture in short pulses which are separated by pulses of clean fluid. The periodicity of proppant injection schedule leads to the formation of proppant columns (pillars) inside the fracture (Gillard et al. 2010). A comparison between proppant pumping schedule for conventional and open-channel technique is presented in Figure 3. In both techniques, the proppant concentration is increased in a step-wise manner with pumping time. In conventional treatments, shown as the red line, proppant is continuously mixed with the fracturing fluid. For the channel fracturing treatment, shown as the green

line, the proppant pulse is alternated with clean fluid (d'Huteau et al. 2011). The size and distance between the proppant columns is controlled by varying the duration of the proppant laden and clean fluid pulses. In addition, at the last stage of open-channel treatment, the proppant is added continuously to ensure the connection between the fractures and the wellbore is stable, uniform, and reliable. This stage is also referred to the tail-in stage (Barasia & Pankaj 2014).

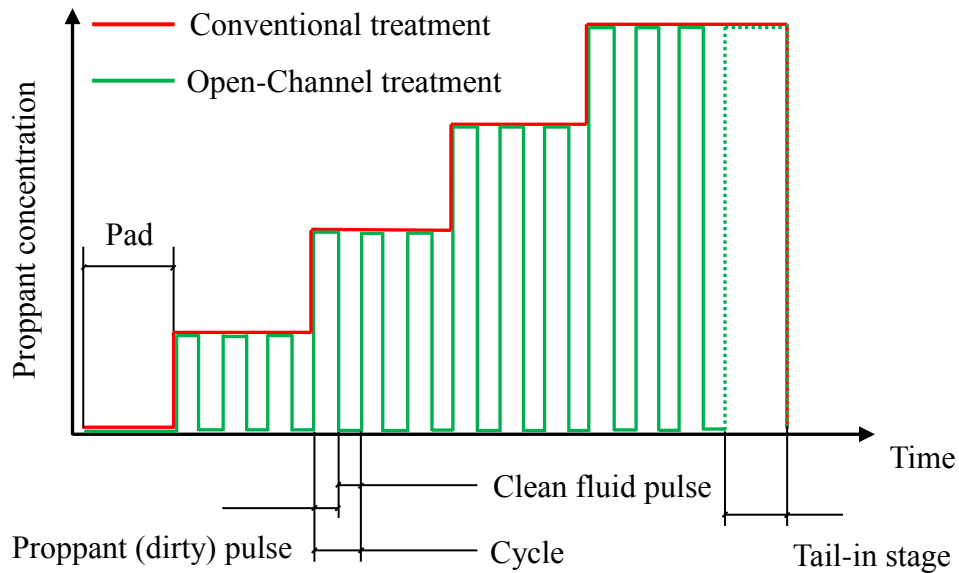


Figure 3: Proppant schedule for Channel Hydraulic Fracturing and Conventional Fracturing (Gillard et al. 2010).

The discontinuous deposit of proppant along the fracture height is achieved by using a special perforation interval. In conventional hydraulic fracturing, the perforations are made evenly along the height of the pay zone. For open-channel treatment, a heterogeneous arrangement of perforations is created by letting clusters of perforations be separated by non-perforated intervals, as per Figure 4 (Gillard et al. 2010).

A key factor affecting the successful application of the channel fracturing technique is maintaining the heterogeneous distribution of proppant within the fracture during the pumping procedure, as well as during fracture closure. The

dispersion or spreading of proppant slugs during movement within the fracture reduces the column height prior to fracture closure as well as the spacing between the proppant columns. Hence, proppant dispersion has a negative impact on the efficiency of the open-channel technique and must be minimised. For this purpose, the proppant slurry is mixed with fibers which entangle the proppant particles and minimise the dispersion of proppant-laden pulses whilst they are carried through equipment pipes, the wellbore, and throughout the fracture. The effectiveness of fibrous materials for mitigating the dispersion of proppant inside the fracture was documented experimentally in several previous studies (Bulova et al. 2006).

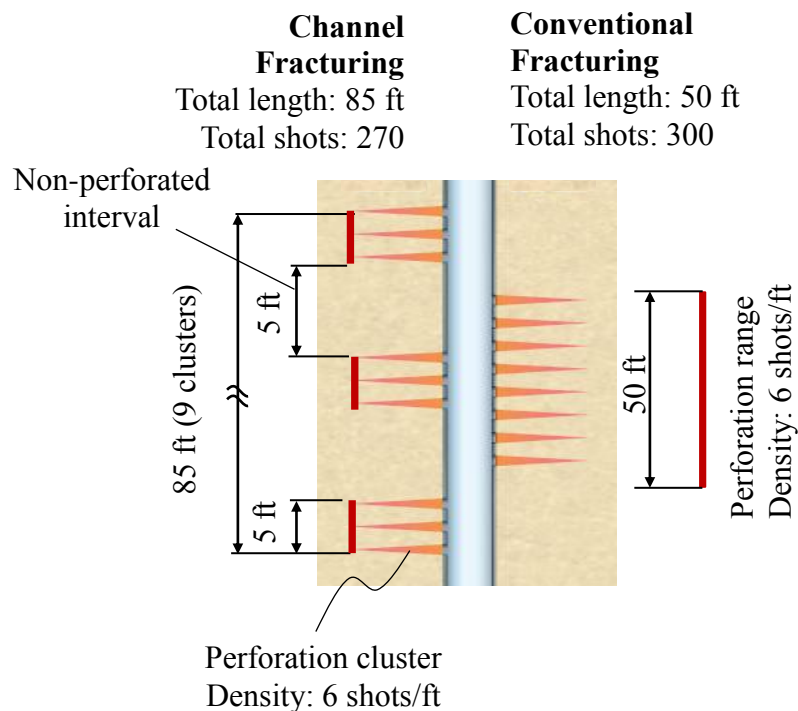


Figure 4: A perforation scheme used to facilitate the formation of open channels

2.3. Hydraulic fracture processes

Modelling of hydraulic fracture initiation and propagation is of great importance from the point of view of the design of fracturing operations. For given

in-situ stress state, mechanical properties of the reservoir rock and fracturing fluid injection schedule, hydraulic fracture propagation models aim to predict the dimensions of the fracture, i.e. its aperture, span and height as a function of the injection time. The processes of hydraulic fracture initiation, propagation and fluid flow in the fracture and porous rock are discussed in the following sections.

2.3.1. Fracture initiation criterion

Hydraulic fracture initiation is generally predicted using the tensile strength criterion, i.e. fracture initiation occurs if the principal tensile stress at the wellbore surpasses the tensile strength of the rock formation (Economides & Nolte 2000). This criteria is widely utilised for brittle materials, however, it must be adapted for practical use since the quantity of interest is the wellbore fluid pressure at fracture initiation, commonly known as the breakdown pressure. The breakdown pressure depends upon the in-situ stress field near the wellbore, as well as the orientation of the wellbore with respect to the principal stresses (Hossain et al. 2000).

The in-situ stress state in underground rock formations can be described by three orthogonal principal stresses, such that maximum principal stresses is generally aligned with the vertical direction and caused by the overburden or self-weight of the rock. The remaining principal stress components are aligned with the horizontal plane and are generally unequal due to tectonic activity and heterogeneity of the rock formation. The vertical (maximum) principal stress component is denoted by σ_v . The minimum and intermediate principal stresses are denoted by σ_h and σ_H , respectively (Hossain et al. 2000). When a borehole is drilled into the rock formation, it distorts the in-situ stress field in the rock (Hossain et al. 2000). An approximate calculation of the distorted stress field can be made using the technique proposed by Hubbert and Willis (1957), in which the rock formation is assumed to be a homogeneous, linearly elastic, and isotropic medium (Aadnoy 1987; Hsiao 1988; Valko & Economides 1995). The stress state on the wall of an oriented wellbore, shown in Figure 5, has been derived by

several researchers (Aadnoy 1987; Aadnoy & Chenevert 1987; Bradley 1979; Deily & Owens 1969; Richardson 1981) and described in Eqs (1)-(5).

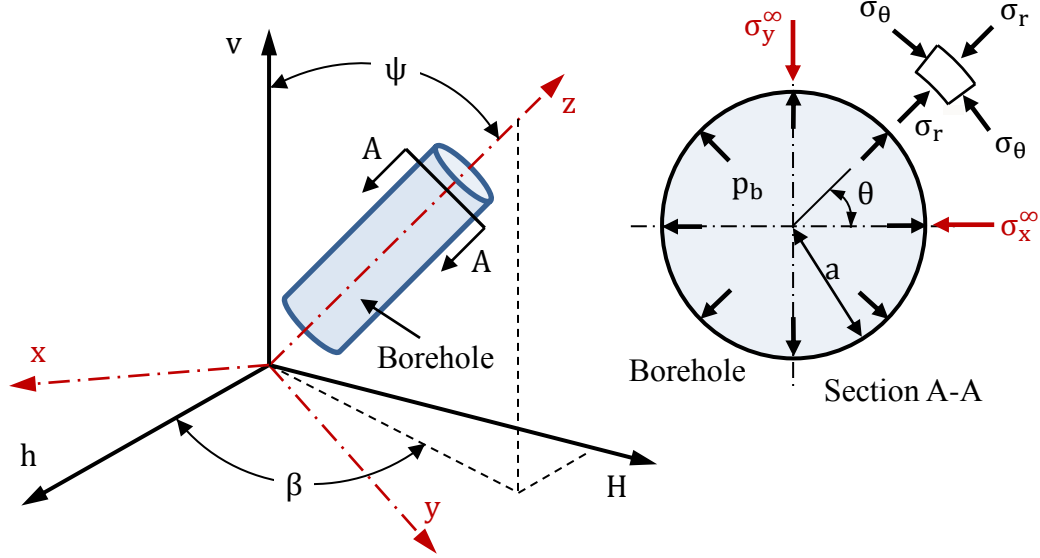


Figure 5: Schematic of an arbitrarily oriented borehole showing the principle stress directions and the stress components near the borehole (Hossain et al. 2000).

$$\sigma_r(r = a) = p_b, \quad (1)$$

$$\sigma_\theta(r = a) = \sigma_x^\infty + \sigma_y^\infty - 2(\sigma_x^\infty - \sigma_y^\infty) \cos 2\theta - p_b - 4\tau_{xy}^\infty \sin 2\theta, \quad (2)$$

$$\sigma_{z\theta} = \sigma_z^\infty - 2\nu(\sigma_x^\infty - \sigma_y^\infty) \cos 2\theta - 4\nu\tau_{xy}^\infty \sin 2\theta, \quad (3)$$

$$\tau_{r\theta}(r = a) = \tau_{rz}(r = a) = 0, \quad (4)$$

$$\tau_{\theta z}(r = a) = 2(-\tau_{xz}^\infty \sin \theta + \tau_{yz}^\infty \cos \theta). \quad (5)$$

where p_b is wellbore pressure; σ_r , σ_θ , $\sigma_{z\theta}$ are radial, tangential and axial stresses, respectively; $\tau_{r\theta}$, τ_{rz} , and $\tau_{\theta z}$ are shear stresses with the first subscript denotes shear stress direction and the second subscript denotes the plane that perpendicular to the shear stress; σ_x^∞ , σ_y^∞ , σ_z^∞ , τ_{xy}^∞ , τ_{xz}^∞ and τ_{yz}^∞ are the in-situ stress components in the absence of the borehole and can be obtained in terms of the principal in-situ stresses, σ_v , σ_h and σ_H using the three-dimensional stress transformation equations

(Hossain et al. 2000).

Based on the tensile strength criterion, the breakdown pressure p_b for fracture initiation can be determined by the following equation (Hossain et al. 2000).

$$p_b \geq \sigma_x^\infty + \sigma_y^\infty - 2(\sigma_x^\infty - \sigma_y^\infty) \cos 2\theta - 4\tau_{xy} \sin 2\theta - \frac{\tau_{\theta z}^2}{\sigma_{z\theta}}, \quad (6)$$

Fractures on the wellbore wall are initiated at an angular position θ_{cr} with the minimum wellbore pressure p_{bf}

$$p_{bf} = \sigma_x^\infty + \sigma_y^\infty - 2(\sigma_x^\infty - \sigma_y^\infty) \cos 2\theta_{cr} - 4\tau_{xy} \sin 2\theta_{cr} - \frac{\tau_{\theta z_{cr}}^2}{\sigma_{z\theta_{cr}}}, \quad (7)$$

where $\tau_{\theta z_{cr}}$ and $\sigma_{z\theta_{cr}}$ are $\tau_{\theta z}$ and $\sigma_{z\theta}$, respectively, at the crack initiation angle θ_{cr} , which is found by minimising the breakdown pressure in Eq. (6).

For a vertical wellbore ($\psi = 0^\circ$, $\beta = 90^\circ$ and $\theta_{cr} = 90^\circ$), the critical pressure for crack initiation is simply given by Eq. (8) (Economides & Nolte 2000).

$$p_{bf} = 3\sigma_h - \sigma_H - p_p + \sigma_t, \quad (8)$$

where p_p is the pore pressure in the rock near the wellbore and σ_t is the tensile strength of the rock. Generally, both of these terms are much smaller in magnitude than the in-situ stress components and the breakdown pressure can also be estimated as $p_{bf} = 3\sigma_h - \sigma_H$. Eq. (8) provides an upper bound for the fracture initiation pressure due to the assumption of no fluid infiltration in the rock formation. However, in practice, the infiltration of fluid into the formation results in an increase in the pore pressure, which in turn decreases the effective stresses and fracture initiation pressures. A lower bound for the fracture initiation pressure was obtained by (Economides & Nolte 2000) based on poroelasticity considerations:

$$p_{bf} = \frac{3\sigma_h - \sigma_H - 2\eta p_w + \sigma_t}{2(1 - \nu)}, \quad \eta = \frac{\alpha(1 - 2\nu)}{2(1 - \nu)}, \quad (9)$$

where ν is Poisson's ratio, and α is Biot's coefficient. Similar expressions can be obtained for horizontal wells.

For certain orientations of the wellbore, the direction of the minimum principal stress can vary significantly in the near-wellbore and far-field regions. Abass et al. (2009) demonstrated that during the early stages of fracture propagation, the orientation of the fracture plane is controlled by a near-wellbore stress field. When the fracture propagates sufficiently far from the wellbore, further propagation is governed by the in-situ stress field. Hence, in order to propagate a hydraulic fracture in desired orientation, such as longitudinal, angularly, or perpendicular to the wellbore, the perforations must extend beyond the near wellbore stress field (Li et al. 2015b).

2.3.2. Hydraulic fracture propagation

After initiation, if the wellbore fluid pressure is sufficient, a fracture will propagate from the wellbore towards the formation. The propagation criterion is generally obtained using linear elastic fracture mechanics, i.e. the stress intensity factor K_I at the tip of the fracture must be equal to the fracture toughness of the rock K_{IC} , i.e. (Irwin 1957)

$$K_I = K_{IC}. \quad (10)$$

The stress intensity factor K_I is a function of the fracture size and geometry as well as the loading conditions. For a short fracture with length comparable to the wellbore radius, as shown in Figure 6, K_I can be estimated as (Economides & Nolte 2000).

$$K_I = 1.12(p_f - \bar{\sigma}_{\theta\theta})\sqrt{\pi L} \quad (11)$$

where L is the fracture length; p_f is the fluid pressure inside the fracture; and $\bar{\sigma}_{\theta\theta}$ is the average normal stress acting on the fracture surfaces, which is a function of the pressure in the wellbore and the stresses at far-field region. In geological structures, $\bar{\sigma}_{\theta\theta}$ is compressive and known as closure stress. To propagate the fracture, p_f must be higher than the closure stress. Thus, for a given fracture with predefined wellbore pressure, the pressure of the fluid inside the fracture is the dominant factor controlling fracture growth.

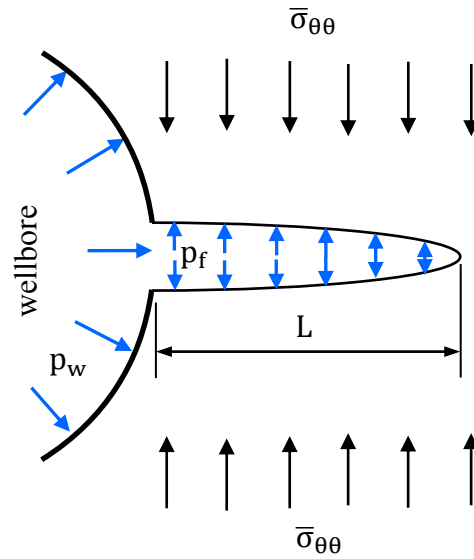


Figure 6: A small fracture at the wellbore

The propagation of a planar hydraulic fracture in a homogenous rock formation can be modelled analytically by adopting a number of simplifications. For example, in a classical model presented in a review paper by Feng et al. (2016), the rock formation is assumed to be isotropic, linearly elastic and impermeable; the fluid is considered as incompressible, and liquid pressure within the fracture is equal to wellbore pressure. By using a coupled solid and liquid mechanic method, the fracture half-length and fluid pressure within the fracture during fracture propagation can be written as:

$$L(t) = \left[\frac{E'Q(t - t_0)}{2\pi^{1/2}K_{IC}} \right]^{2/3} \quad (12)$$

$$p_f(t) = \frac{E'Q(t - t_0)}{2\pi L^2}, \quad (13)$$

respectively, where Q is the injection rate, t is the injection time, $L(t)$ is the half length of the fracture at time t , $p_f(t)$ is the net pressure within the fracture at time t , E' is Young's modulus in plane strain condition, and t_0 is the start time for fracture propagation.

Detournay (2004) reviewed various analytical models for hydraulic fracture propagation in plane strain and radial geometries and described two main energy dissipation processes, which govern the different modes of fracture propagation. The first process is the fracture of the rock, and the dissipation is governed by the fracture toughness, K_{IC} . The second process is the viscous flow of the fracturing fluid, which is governed by the viscosity, μ . The limiting solutions, corresponding to zero toughness and zero viscosity are reviewed in Detournay (2004), and the parameter governing the transition between these two asymptotic solutions is obtained for the special case of fracture in impermeable rocks. as follows:

$$\mathcal{K} = \frac{K'}{(E'^3 \mu' Q_0)^{1/4}}, \quad K' = 4 \left(\frac{2}{\pi} \right)^{1/2} K_{IC}, \quad E' = \frac{E}{1 - \nu^2}, \quad \mu' = 12\mu. \quad (14)$$

when $\mathcal{K} \leq 1$, the propagation regime is viscosity dominated, since most of the energy dissipation occurs in the fluid. In this regime, the limit solution based on the assumption of zero fracture toughness of the rock can be utilised. When $\mathcal{K} \geq 4$, the propagation regime is toughness dominated, since most of the energy dissipation is associated with the creation of new fracture surfaces in the rock. In this regime, the limit solution based on the assumption of zero fluid viscosity can be utilised. For intermediate values of this dimensionless parameter, the solution

for fracturing length and opening as well as fluid pressure within the fracture can be obtained numerically (Detournay 2004).

The above considerations are based on the assumption of a homogenous rock formation. Hydraulic fractures are also created in multilayered rock formations, where the variation of elastic properties and in-situ stress state across interfaces can influence the fracture propagation (Teufel & Clark 1984). If the fracture propagates across the interfaces, the width of the hydraulic fracture, which relates directly to the proppant movement and final proppant placement, can be significantly influenced by the difference in Young's modulus and the permeability in the rock layers (Daneshy 2009; Smith et al. 2001).

In naturally-fractured rock formations, fluid injection at the wellbore can lead to the slip or opening of the pre-existing natural fractures in addition to the creation of the fluid-driven fracture. If the propagation path of the hydraulic fracture intersects the natural fractures, the hydraulic fracture can transverse the natural fractures or divert and become aligned with the orientation of the natural fracture (Blanton 1982; Lamont & Jessen 1963; Warpinski et al. 1998). The outcome is influenced, among many other parameters, by the frictional properties of the natural fracture or interface and the local stress state (Anderson 1981; Casas et al. 2006; He et al. 2017; Kaufman et al. 2008). The stimulation of natural fractures due to the interaction with the hydraulic fracture can significantly increase the permeability of the rock formation, however, modelling of this phenomenon is a complex task, since the position, orientation and geometry of underground natural fractures is generally estimated to a high degree of uncertainty based on indirect measurements, such as core logs, excavations, wellbore pressure history and acoustic emissions from the fracturing rock.

2.3.3. Fluid flow and fluid loss

Modelling of the single-phase flow of a Newtonian fluid in a single rock

fracture is one of the most basic steps for the analysis of hydraulic fracture propagation. It is a starting point for the modelling of more realistic situations, such as two-phase flow (for e.g. oil and water), flow of non-Newtonian fracturing fluids containing proppants, and flow in a network of fractures. This problem has been investigated thoroughly over the past several decades, and briefly recapped in this section.

The Navier-Stokes equations, supplemented with the equation for the conservation of mass, provide a complete mathematical description of the flow of incompressible Newtonian fluids (Currie 2003). For the general case of three-dimensional flow, these equations can be written in component form as (Currie 2003):

$$\begin{aligned} \rho \left(\frac{\partial u_x}{\partial t} + u_x \frac{\partial u_x}{\partial x} + u_y \frac{\partial u_x}{\partial y} + u_z \frac{\partial u_x}{\partial z} \right) \\ = -\frac{\partial p_f}{\partial x} + \rho g_x + \mu \left(\frac{\partial^2 u_x}{\partial x^2} + \frac{\partial^2 u_x}{\partial y^2} + \frac{\partial^2 u_x}{\partial z^2} \right), \end{aligned} \quad (15)$$

$$\begin{aligned} \rho \left(\frac{\partial u_y}{\partial t} + u_x \frac{\partial u_y}{\partial x} + u_y \frac{\partial u_y}{\partial y} + u_z \frac{\partial u_y}{\partial z} \right) \\ = -\frac{\partial p_f}{\partial y} + \rho g_y + \mu \left(\frac{\partial^2 u_y}{\partial x^2} + \frac{\partial^2 u_y}{\partial y^2} + \frac{\partial^2 u_y}{\partial z^2} \right), \end{aligned} \quad (16)$$

$$\begin{aligned} \rho \left(\frac{\partial u_z}{\partial t} + u_x \frac{\partial u_z}{\partial x} + u_y \frac{\partial u_z}{\partial y} + u_z \frac{\partial u_z}{\partial z} \right) \\ = -\frac{\partial p_f}{\partial z} + \rho g_z + \mu \left(\frac{\partial^2 u_z}{\partial x^2} + \frac{\partial^2 u_z}{\partial y^2} + \frac{\partial^2 u_z}{\partial z^2} \right), \end{aligned} \quad (17)$$

$$\frac{\partial u_x}{\partial x} + \frac{\partial u_y}{\partial y} + \frac{\partial u_z}{\partial z} = 0, \quad (18)$$

where ρ is the density, \mathbf{u} is the velocity vector with components u_x , u_y and u_z , μ is

the viscosity, p_f is the fluid pressure, and g is the acceleration due to gravity.

The coupled system of equations (15)-(18) is too difficult to solve, either analytically or numerically, for realistic fracture geometries. Therefore, various simplifications are adopted to reduce the Navier-Stokes equations to a more tractable form. The first level of simplification is to linearize the Navier-Stokes equations by discarding the acceleration terms, $\rho(\dot{\mathbf{u}} + (\mathbf{u} \cdot \nabla)\mathbf{u})$, i.e. the left hand side of Eqs. (15)-(17). This simplification is acceptable for ‘creeping’ flows, i.e. when the Reynolds number is less than about 10, a condition which is generally satisfied for fluid flow in hydraulic fractures (Currie 2003). If the hydraulic fracture geometry is planar, with the fracture plane perpendicular to the z -axis, and the fluid flow occurs in the x -direction, the linearised Stokes equations can be written in component form as:

$$\frac{\partial p_f}{\partial x} = \rho g_x + \mu \left(\frac{\partial^2 u_x}{\partial x^2} + \frac{\partial^2 u_x}{\partial z^2} \right), \quad (19)$$

$$\frac{\partial p_f}{\partial z} = \rho g_z + \mu \left(\frac{\partial^2 u_z}{\partial x^2} + \frac{\partial^2 u_z}{\partial z^2} \right). \quad (20)$$

All terms in Eq. (20), which represents the momentum balance in the direction perpendicular to the fracture plane, are very small, i.e. this equation can be ignored. The remaining one dimensional Stokes Eq. (19) can be further simplified, provided that the aperture of the fracture varies gradually along the x -direction, i.e. $\partial^2 u_x / \partial x^2 \ll \partial^2 u_x / \partial z^2$. If these conditions are met, the governing equation for fluid flow in the fracture is reduced to

$$\frac{\partial p_f}{\partial x} = \rho g_x + \mu \frac{\partial^2 u_x}{\partial z^2}. \quad (21)$$

Eq. (21) can be integrated twice with respect to z to obtain the well-known expression for the parabolic velocity profile for flow between parallel plates. For $g_x = 0$,

$$u_x = \frac{1}{2\mu} \frac{\partial p_f}{\partial x} \left(z^2 - \left(\frac{w}{2} \right)^2 \right), \quad (22)$$

where w is the aperture of the fracture at location x . Substituting Eq. (22) into the mass conservation equation (18) and integrating once more with respect to z with limits $-w/2$ to $w/2$ yields the steady-state Reynolds lubrication equation (Currie 2003)

$$\frac{\partial}{\partial x} \left(w^3 \frac{\partial p_f}{\partial x} \right) = 0. \quad (23)$$

During a hydraulic fracture treatment, a part of the fracturing fluid penetrates through the fracture surfaces into the porous rock formation due to the difference between the liquid pressure within the fracture and the pressure in the formation. This fluid flow is named fluid loss or leak-off (Yi & Peden 1994). Leak-off is known as the key parameter controlling the geometry and the size of a hydraulic fracture. A widely used model for fluid leak-off is based on the pioneering work of Carter (1957). In the Carter's leak-off model, leak-off flow is approximated as one-dimensional flow that is perpendicular to the fracture surfaces. The model proposes that the volume of fluid leak-off per unit length of the fracture is inversely proportional to the square root of time and is defined as

$$g(x, t) = \frac{C_L}{\sqrt{t - t_L(x)}}, \quad t - t_L(x) > 0, \quad (24)$$

where C_L is the fluid loss coefficient factor which is dependent on the rock permeability (Howard & Fast 1957), t is the time, and $t_L(x)$ is the time it takes for the fracturing fluid to reach location x along the fracture.

The global balance of injected volume of the incompressible fluid injected at the wellbore can be stated as

$$V_{\text{inject}}(t) = V_{\text{fracture}}(t) + V_{\text{leak}}(t), \quad (25)$$

For the particular case of constant injection rate, $V_{\text{inject}}(t) = Q_0 t$ and the volume of the fluid in the fracture and the leak-off into the porous rock can be written as

$$V_{\text{fracture}}(t) = 2 \int_0^{L(t)} w(x, t) dx, \quad t > 0, \quad (26)$$

$$V_{\text{leak}}(t) = 2 \int_0^t \frac{C_L L(t_L)}{\sqrt{t - t_L(x)}} dt_L, \quad t > 0. \quad (27)$$

The Reynolds lubrication equation for the non-steady case and including leak-off can be derived in a similar manner to Eq. (23) as

$$\frac{\partial w}{\partial t} + g(x, t) = \frac{1}{12\mu} \frac{\partial}{\partial x} \left(w^3 \frac{\partial p_f}{\partial x} \right), \quad t > 0, \quad x < L(t). \quad (28)$$

A similar equation can be derived for the case of radial flow in a penny-shaped fracture (Currie 2003)

2.3.4. Transportation and placement of the proppant

The previous section provided the governing equations for the flow of ‘clean’ fracturing fluid in the fracture. However, during the proppant injection stage, a mixture of proppant particles and the fracturing fluid, known as slurry, is injected into the fracture. Proppant particles alter the properties of fracturing fluid and incorporating the effects on fluid flow caused by their presence is a necessary but challenging task. A number of simplifying assumptions are generally introduced when modelling slurry transport within the fracture. According to Adachi et al. (2007), the slurry is commonly modelled as a Newtonian fluid, whose viscosity depends on the concentration fraction of proppant and is determined empirically.

Gravitational settling is considered as the dominant mechanism for slip between the fracturing fluid and proppant particles.

Dontsov and Peirce (2014) analysed the steady flow of slurry within a channel using an empirical constitutive model introduced by Boyer et al. (2011). This model captures the non-uniform distribution of proppant particles across the channel, slip velocity due to the slurry flow, and the transition from Poiseuille's flow corresponding to low proppant concentration to Darcy's law corresponding to high proppant concentration. In this model, the distribution of proppant inside the fracture is defined via volumetric concentration, ψ , and normalized as

$$\bar{\psi} = \frac{\psi}{\psi_{\max}} \quad (29)$$

where ψ_{\max} is the maximum allowable volumetric concentration determined from geometrical considerations. The proppant particles are assumed to be spherical with radius r , and both proppant and fluid are considered as incompressible.

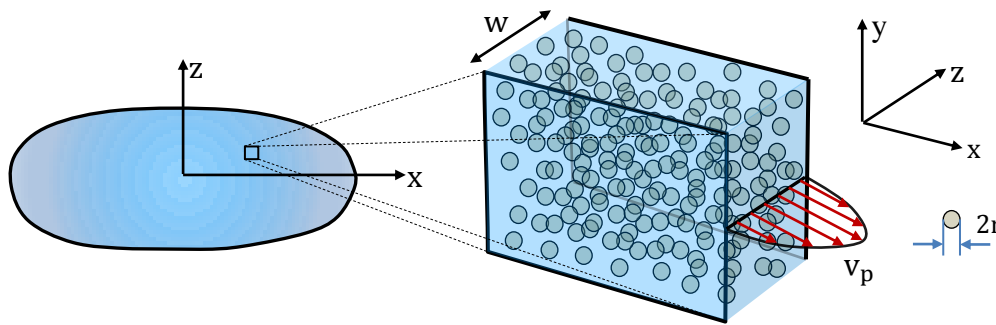


Figure 7: A schematic of the hydraulic fracture and the slurry flow inside it (Dontsov & Peirce 2014).

A schematic of the fracture and the associated coordinate system is shown in Figure 7, where x is the axis along the fracture length in horizontal direction, y is the axis along the fracture height, and z is the axis perpendicular to the fracture plane. To describe the flow of proppant-laden fluid in the fracture, Dontsov and Peirce (2014) proposed a modified form of the lubrication equation (28) derived in

the previous section, i.e.

$$\frac{\partial w}{\partial t} + g(x, t) = \frac{1}{12\mu} \frac{\partial}{\partial x} \left(w^3 \widehat{Q}_s \frac{\partial p_f}{\partial x} \right), \quad (30)$$

where the dimensionless function \widehat{Q}_s depends upon the proppant volumetric concentration, $\bar{\psi}$, and the normalised fracture opening, w/r . Dontsov and Peirce (2014) proposed the function \widehat{Q}_s based on the empirical model of Boyer et al. (2011) as follows

$$\widehat{Q}_s \left(\bar{\psi}, \frac{w}{r} \right) = Q_s(\bar{\psi}) + \frac{r^2}{w^2} \bar{\psi} D \quad (31)$$

where Q_s represents the reciprocal of the effective velocity of the slurry and $D = 8(1 - \psi_{\max})^{\bar{\alpha}}/3 \psi_{\max}$ is a constant related to the permeability of the proppant pack. The function \widehat{Q}_s defined in Eq. (31) allows for the governing equation (30) to capture the transition from Poiseuille's flow at low proppant concentration to Darcy's flow as the proppant concentration reaches its maximum value.

The conservation of mass equation for the proppant particles in the slurry can be written as

$$\frac{\partial w(x, t) \bar{\psi}(x, t)}{\partial t} + \frac{\partial q_{px}(x, t)}{\partial x} + \frac{\partial q_{py}(x, t)}{\partial y} = 0 \quad (32)$$

where q_{px} and q_{py} present the proppant flux in x and y direction, respectively. The second term in Eq. (32) corresponds to the pressure-driven flux of the proppant particles and the last term corresponds to the gravitational settling of the proppant particles. These fluxes are expressed as

$$q_{px} = -B \left(\frac{w}{r} \right) \frac{w^3}{12\mu} \widehat{Q}_s \frac{\partial p_f}{\partial x} \widehat{Q}_p \left(\bar{\psi}, \frac{w}{r} \right) \quad (33)$$

$$q_{py} = -B\left(\frac{w}{r}\right) \frac{r^2 w}{12\mu} (\rho_p - \rho_f) g \widehat{G}_p\left(\bar{\psi}, \frac{w}{r}\right) \quad (34)$$

where ρ_p and ρ_f are the densities of proppant and the clear fracturing fluid, respectively, g is the gravitational acceleration, B is blocking function, \widehat{Q}_p and \widehat{G}_p are two dimensionless functions of the normalized proppant concentration $\bar{\psi}$ and the ratio of w/r . Eq. (33) captures the clustering of proppant particles towards the central region of the flow channel and away from the fracture walls. Eq. (34) is a modified form of the Stokes law for steady state settlement of a sphere in a viscous fluid. Both \widehat{Q}_p and \widehat{G}_p tend to zero as the normalised proppant concentration $\bar{\psi}$ approaches unity, indicating that an immobile proppant pack has formed.

2.4. Hydraulic fracture modelling

The previous section described the basic equations governing the initiation and propagation of a rock fracture, as well as fluid flow and transport within the fracture. In practical applications, hydraulic fracture simulators based on the previously presented equations, are utilised to predict the propagation of fractures under a given set of reservoir conditions and pumping schedules. For computational efficiency, the simulators adopt a number of simplifying assumptions regarding the geometry of the propagating fracture. In this section, some of the most notable models are reviewed.

2.4.1. Sneddon's model for penny-shaped fracture

One of the simplest models for hydraulic fracture propagation was developed for a penny-shaped fracture, with the assumption of constant injection rate, constant fluid pressure within the fracture, and no fluid leak off (see Figure 8).

Sneddon (1946) and Sneddon and Elliott (1946) obtained the analytical solution for the opening profile of a penny-shaped crack subjected to uniform pressure, as

follows

$$w(r) = \frac{8p_f R(1 - \nu^2)}{\pi E} \sqrt{\left(1 - \left(\frac{r}{R}\right)^2\right)} \quad (35)$$

where E is Young's modulus, ν is Poisson's ratio, R is the crack radius and p_f is the uniform pressure acting on the crack faces. For hydraulic fracturing applications, p_f can be interpreted as the net-fluid pressure in the fracture, i.e. the fluid pressure minus the minimum in-situ principal stress. The volume of the ellipsoidal crack can be obtained from Eq. (35) as

$$V = \frac{2}{3} R^2 w(0) = \frac{16}{3\pi} R^3 \frac{(1 - \nu^2)}{E} p_f. \quad (36)$$

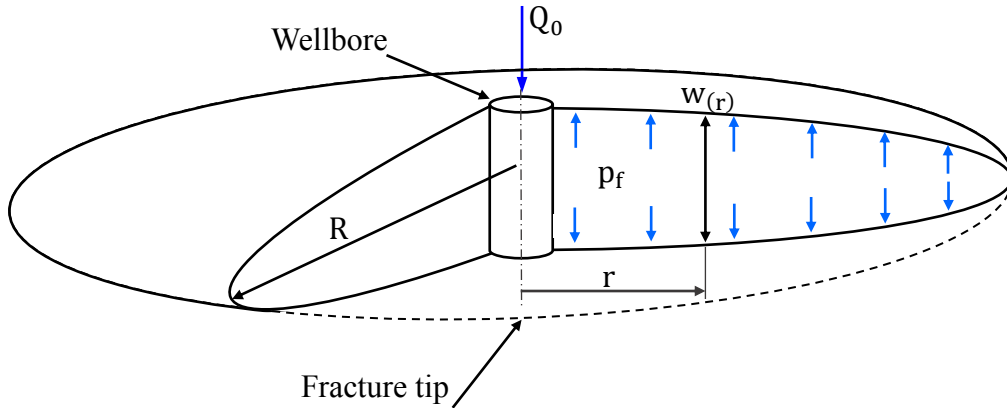


Figure 8: A penny shaped fracture subjected to uniform fluid pressure.

Based on Griffith's energy criterion, Sack (1946) showed that fracture propagation occurs when the net fluid pressure reaches a critical value

$$p_f = \sqrt{\frac{\pi \gamma_s E}{2(1 - \nu^2)R}} \quad (37)$$

where γ_s is the specific fracture surface energy. Combining Eqs. (36) and (37), Perkins and Kern (1961) showed that the propagation criterion for a radial fracture

can be written as

$$p_f = \left(\frac{2\pi^3 \gamma_s^3 E^2}{3(1 - \nu^2)^2 V} \right)^{1/5} . \quad (38)$$

For constant injection rate and no fluid leak-off, the fracture volume can be related to the injection rate and pumping time according to

$$V = Q_o t, \quad t > 0. \quad (39)$$

Rearranging and solving for R yields the fracture propagation model

$$R = \left(\frac{9EQ_o^2 t^2}{128\pi\gamma_s(1 - \nu^2)} \right)^{1/5} . \quad (40)$$

2.4.2. PKN and KGD models for planar fracture

Several key papers on the propagation of planar fractures from vertical wellbores were published from the late 1950s to early 1970s. Of the several proposed models, two of the most widely utilised are the PKN (Nordgren 1972; Perkins & Kern 1961) and KGD models (Geertsma & De Klerk 1969; Khristianovich & Zheltov 1955), named after their respective developers. Both models share a number of common simplifying assumptions, they assume that (1) the fracture is planar and propagates perpendicular to the direction of the minimum principal in-situ stress, (2) the fracture height remains constant along the entire length of the fracture, (3) the fluid flow in the fracture is one-dimensional and along the direction of fracture propagation, (4) the flow of the Newtonian fluid is described by Poiseuille's law, and (4) the rock is homogenous, isotropic and linearly elastic.

Both models adopt the plane-strain assumption, except along different directions. The PKN model assumes plane strain conditions along the horizontal direction and considers an elliptical cross-section of the fracture. Although the maximum width of the elliptical section, w varies with distance along the fracture

length, x , the width at any given cross-section, $w(x)$ solely depends upon the net fluid pressure, $p_f(x)$ and is independent of width along other cross-sections. This model was developed for long fractures, i.e. fractures whose length is much greater in comparison to the height (Economides & Nolte 2000). The KGD model assumes plane strain conditions along the vertical direction and considers a rectangular fracture cross-section. This model was developed for short fractures, i.e. fractures whose length is much smaller in comparison to the height (Economides & Nolte 2000).

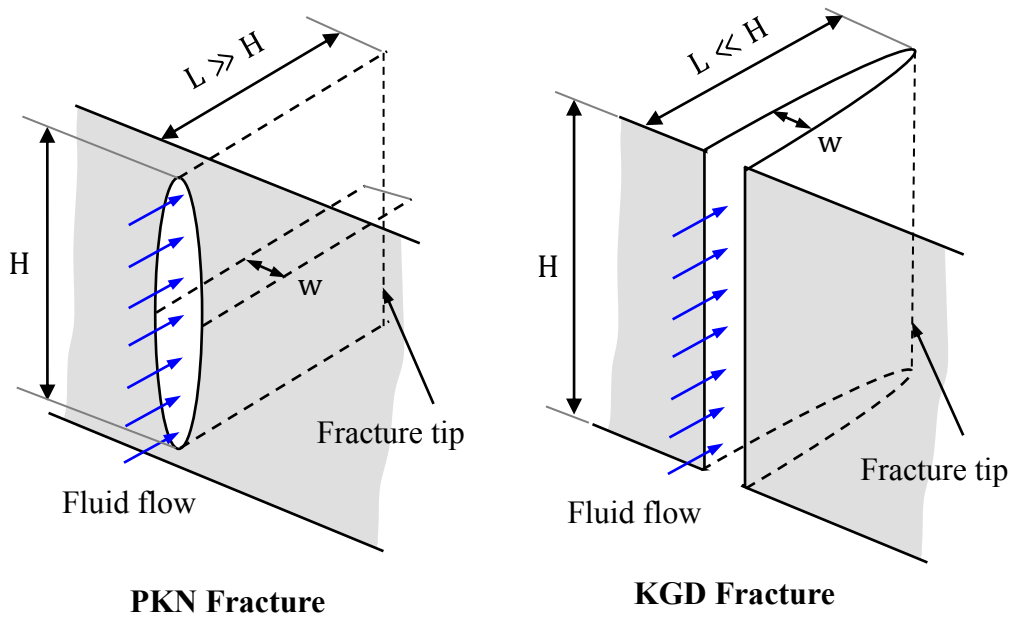


Figure 9: Basic two-dimensional models for planar fracture geometry.

For negligible leak-off into the rock formation and constant fluid injection rate, analytical solutions for the fracture opening at the wellbore, denoted by w_w and the fracture half-length, L can be obtained for both PKN and KGD fracture geometries. For PKN geometry, the solution is given by (Nordgren 1972)

$$w_w(t) = 2.18 \left(\frac{\mu Q_o^2 (1 - \nu^2)}{EH} \right)^{\frac{1}{5}} t^{\frac{1}{5}}, \quad (41)$$

$$L(t) = 0.39 \left(\frac{EQ_0^3}{\mu(1-\nu^2)H^4} \right)^{\frac{1}{5}} t^{\frac{4}{5}}. \quad (42)$$

For the KGD geometry, the solution is given by Geertsma and De Klerk (1969)

$$w_w(t) = 1.48 \left(\frac{\mu Q_0^3 (1-\nu^2)}{EH^3} \right)^{\frac{1}{6}} t^{\frac{1}{3}}, \quad (43)$$

$$L(t) = 0.38 \left(\frac{EQ_0^3}{\mu(1-\nu^2)H^3} \right)^{\frac{1}{6}} t^{\frac{2}{3}}. \quad (44)$$

The effect of fluid leak-off, described by Eq. (24) was incorporated into the above solutions in later studies, however the resulting expressions are complex and require numerical solution. The KGD model was further refined by Detournay and colleagues (Detournay 2004; Detournay & Cheng 1993), who modelled in crack-tip region in greater detail and investigated the effects of the fluid lag region behind the crack tip as well as poro-elasticity effects.

2.4.3. Pseudo three-dimensional (P3D) models for planar fracture

The PKN and KGD models described previously assume constant fracture height along the entire length. In multilayered rock formations, or for significant spatial variation in the minimum in-situ stress, the height of the fracture can vary with distance from the wellbore. Like the simpler PKN and KGD models, the P3D models also assume a planar fracture geometry, however, they do not impose any restrictions on the fracture height. The models generally assume plane strain conditions and do not fully couple the equations of fluid flow and rock deformation (Adachi et al. 2007). Although P3D models are crude, their principal advantage lies in their simplicity and low computational cost (Adachi et al. 2007).

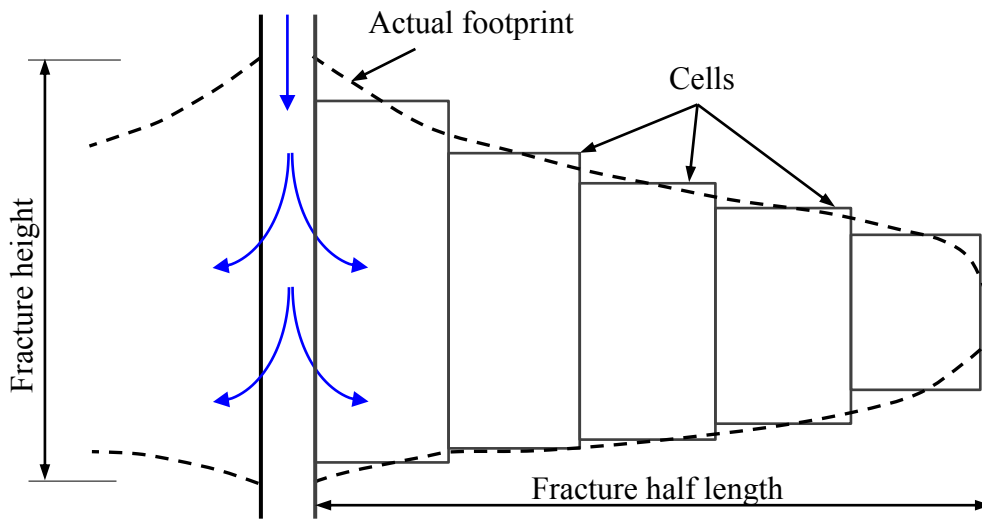


Figure 10: Cell-based pseudo-3D model (Adachi et al. 2007)

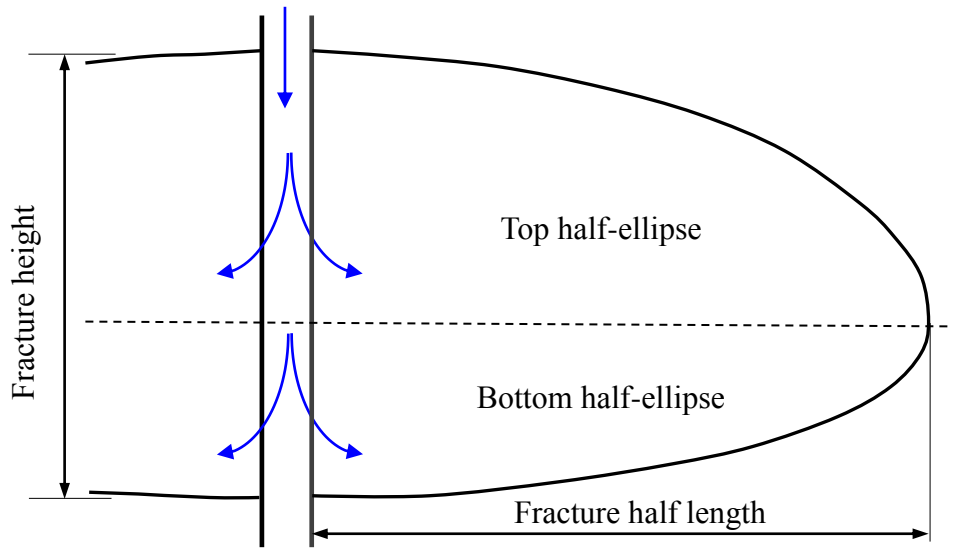


Figure 11: Lumped pseudo-3D model (Adachi et al. 2007)

The P3D models are categorised as cell-based and lumped models (Economides & Nolte 2000). In the cell-based approach, see Fig. 10, the fracture length is considered as a series of PKN cells. The fluid flow is considered as one-dimensional (along the fracture length) and the variation in fluid velocity with vertical position is ignored. Hence, each cell is subjected to uniform pressure. The

height and cross-section opening of each cell are determined using two-dimensional linear elasticity solutions (Palmer & Carroll 1983; Settari & Cleary 1986). For the lumped approach as shown in Figure 11, the geometry of a fracture is composed of two half elliptical profiles with equal lateral extent, but different vertical extent (McLennan & Picardy 1985; Xiujuan et al. 2010). For each time increment, the fracture length and height at the wellbore are determined and the assumed shape is fitted to these position (Adachi et al. 2007).

2.4.4. Three-dimensional models for hydraulic fractures

Three-dimensional (3D) models relax several simplifying assumptions adopted by simpler models discussed earlier, such as fracture containment in a single rock layer, planar fracture geometry, and one-dimensional fluid flow within the fracture. 3D models utilise various numerical schemes to solve the coupled equations of linear elasticity and fluid transport. As a result, these models are computationally expensive and their use is generally restricted to research environments. In this section, four main methodologies for numerical modelling are briefly discussed, namely, the Finite Element Method (FEM), the eXtended Finite Element Method (XFEM), the Boundary Element Method (BEM), and the Discrete Element Method (DEM). Some examples of complex phenomena modelled using numerical techniques are presented.

In the FEM, the entire problem domain (fracture and rock) is discretised into a mesh of interconnected elements. The solution for each element is expressed by a linear combination of simple shape functions that can approximate the global solution for local regions (Shahid et al. 2016). For crack problems, the conventional finite elements are not able to capture the high-stress gradient near the crack and properly reproduce the singularity of the stress field surrounding the crack tips. The accuracy of stress singularity around the crack tips is significantly improved when Barsoum (1976) and Henshell and Shaw (1975) adopted the idea using singular elements, which are formed by placing the mid-side node near the

crack tip at the quarter-point position. Based on a nonlinear mapping, these singular elements can properly reproduce square root stress singularity at the crack tips. Through the years, different types of singular elements have been developed and used for modelling 2D and 3D crack problems (Nejati et al. 2015). Modelling evolving crack problems using the FEM requires very fine mesh generation at the crack tip, and mesh adjustment is required to capture the moving geometry. Hence, during the fracture propagation, a new mesh needs to be generated and aligned along the fracture.

For hydraulic fracture modelling, the FEM was used by Carter et al. (2000), Martha et al. (1993), and Bouchard et al. (2000) to model fracture propagation using different re-meshing strategies. Settari and Raisbeck (1981) developed a two-dimensional finite element model, which is similar to the PKN model, to describe the flow of compressible fluid in a linearly elastic porous medium containing a fracture caused by tensile stress. The fracture was represented by special cohesive elements obeying a user-defined traction law or stress-displacement relationship (Chen et al. 2009). Although the method can simulate fracture propagation in real time, it is unable to predict fracture propagation directions under complex loading conditions because the propagation path is pre-selected based on the location of the cohesive elements (Zhang et al. 2010). FEM was also implemented with continuum damage mechanics, in which a fracture is considered as a series of continuous elements having minimal strength. The permeability of these elements is governed by the corresponding state of strain and stress (Wangen 2013). This method can simulate non-planar fractures, but it requires very small elements to predict the growth path as well as the geometry of the hydraulic fracture properly (Li et al. 2012). FEM was also utilised to investigate hydraulic fracture growth in multilayered reservoirs, in which the layers have been assumed to be elastic and perfectly bonded together. Advani et al. (1990) developed a FEM solution for modelling 3D hydraulic fractures to analyse the hydraulic fracture propagation in layered reservoirs under tensile loading.

The XFEM was first utilised for modelling fracture problems in the works of Belytschko and Black (1999) by using a local partition of unity where a subset of nodes is enriched to allow fractures can be modelled within an element. Due to the XFEM is originated from the conventional FEM, most theoretical background of the FEM can be easily extended and applied in the XFEM. Lecampion (2009) utilised the XFEM to develop a solution of hydraulic fractures by proposing special tip functions that encapsulate asymptotic functions commonly encountered in hydraulic fracture problems. Khoei et al. (2012) developed an XFEM technique for the thermo-hydro-mechanical modelling of impermeable discontinuities in saturated porous media. Gordeliy and Peirce (2013) utilised an XFEM strategy that can solve elastic hydrodynamic equations to investigate the propagation of hydraulic fractures in an elastic formation. Dahi et al. (2011) used the XFEM to investigate the intersection between a hydraulic fracture with a single natural fracture. The research also estimated the effects of the intersection angles on the evolution of the hydraulic fracture as well as the natural fracture.

In the Boundary Element Method (BEM), the problem domain is classified into two regions: the boundary, which is the fracture, and the interior regions which is the intact rock (Shahid et al. 2016). Only the fracture surfaces, or boundaries, are discretised into elements and each element has its own contributions to the stress and strain of the medium. Since the discretisation is imposed only on the boundary, the problem dimensionality and computational cost are reduced. Wilson and Witherspoon (1974) used BEM to study a steady flow in a net of planar fractures. Penny-shaped hydraulic fractures were modelled by Shapiro et al. (2007) and Cleary and Wong (1985). However, BEM loses its computational efficiency for multilayered rocks because the solution for the continuity conditions on the boundary between layers is very complicated (Peirce & Siebrits 2001).

DEM uses a mutual interaction between discrete elements to simulate a discontinuous system. The failure of materials can be modelled as the destruction of the bond between the elements. The motion of each element during fracture is

computed by using Newton's equations (Cundall & Strack 1979). Zhang et al. (2013a) utilised DEM to analyse the evolution of a hydraulic fracture in a granular media at different pumping rates of hydraulic fluid. The growth and mutual interaction between two hydraulic fractures in dense and unconsolidated formations, such as sand or highly fractured medium, are investigated by Thallak et al. (1991). These authors successfully defined the influence of the stress field induced by one fracture on the propagation of the other and found that these two hydraulic fractures tend to avoid a tip to tip connection with each other. The disadvantage of DEM is its very highly computational cost, especially for field-scale applications (Li et al. 2015b).

2.5. Residual opening of hydraulic fractures

Once the fluid injection is stopped, however, the compressive stress, σ_{yy}^∞ , results in the reduction of the fracture opening, $\Delta\delta_r(x)$, as illustrated in Figure 12. The reduction of the fracture opening is due to the consolidation and the embedment of the proppant pack (Bortolan Neto & Kotousov 2013), and the main mechanisms (rearrangement, embedment and damage) are schematically shown in Figure 13.

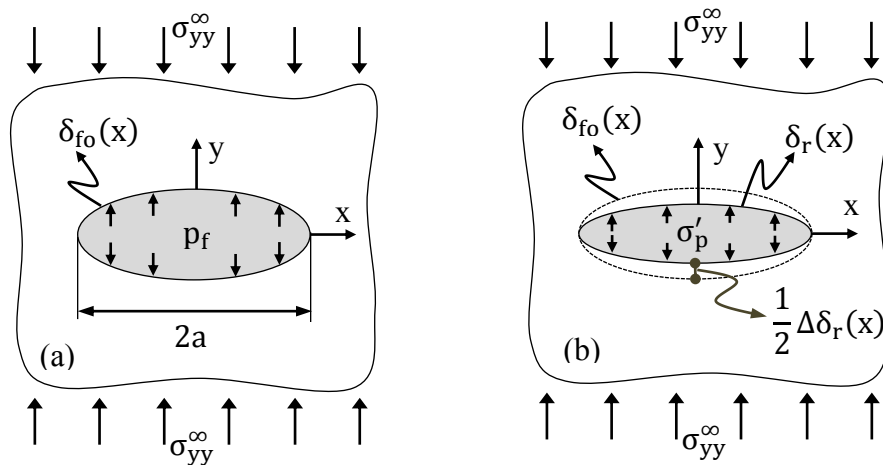


Figure 12: Opening of a fracture during injection stage (a) and during recovery stage (b) (Bortolan Neto & Kotousov 2012)

As mentioned above, the consolidation of the proppant pack is mainly driven by the rearrangement of proppant particles into a tighter pack due to the slip or rotation between particles and the particle damage (Mesri & Vardhanabhuti 2009). The rotation and slip between particles normally occurs at the beginning of the relieved stage under small compressive stress. The particle damage usually occurs at high compressive stress due to numerous mechanisms, including the abrasion or grinding between particle surfaces, the breaking or crushing of particles, and the split or shattering of particles. The degree of the rotation or slip between particles and the particle damage are considered to be the key factors to determine the mechanical response of the proppant pack (Coop 1990; Mesri & Vardhanabhuti 2009).

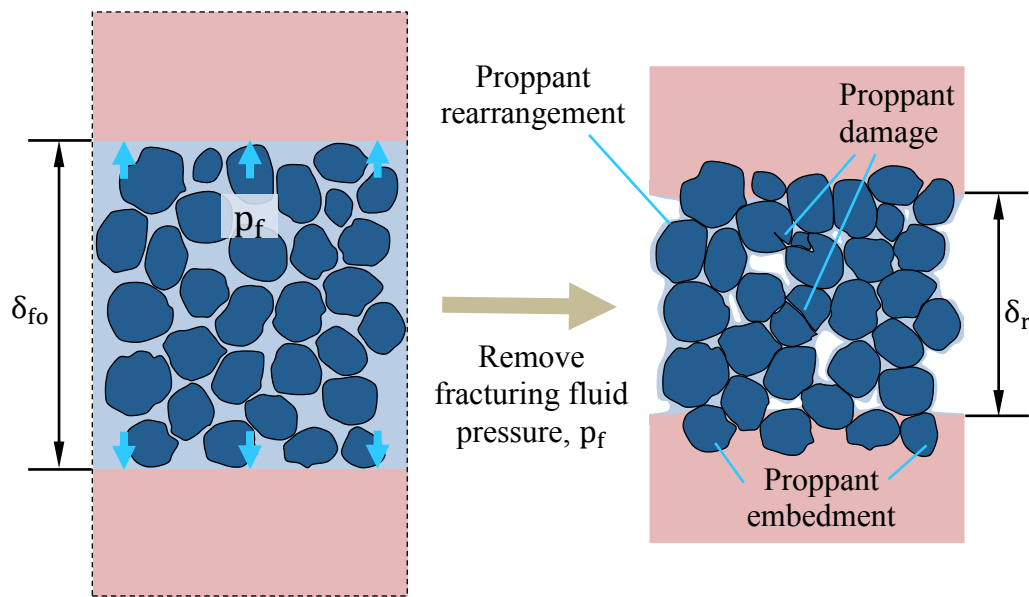


Figure 13: Schematic of main mechanisms leading to fracture close under compression

Terzaghi et al. (1996) proposed a consolidation model for sand and cohesionless soils, in which the consolidation is described as

$$\sigma'_p(x) = \exp\left(\frac{\varepsilon(x)}{C_p}\right) \sigma'_{p0} \quad (45)$$

where $\sigma'_p(x)$ is normal compressive stress, σ'_{p0} is the initial normal compressive stress acting on the particles, C_p is compressibility of the soil defined in Coduto (2001), and $\varepsilon(x)$ is dimensionless parameter representing the proppant settlement ratio and it is defined as

$$\varepsilon(x) = \frac{\delta_{f0}(x) - \delta_r(x)}{\delta_{f0}(x)} \quad (46)$$

where $\delta_{f0}(x)$ is the fracture opening under the initial compressive stress σ'_{p0} , and $\delta_r(x)$ is the effective fracture opening under the compressive stress $\sigma'_p(x)$ (Bortolan Neto & Kotousov 2013). This popular model was widely applied to model behaviour of granular materials and it will be also utilised in the current thesis.

The embedment of proppant into rock formation leads to the reduction of the fracture opening and is demonstrated in Figure 13. Experiments in hard rocks indicate that the depths of embedment is approximate a half of the particle diameter (Much & Penny 1987). For soft rock like sandstone, the embedment depths can up to three times of the particle diameter (Lacy et al. 1998). Modelling proppant embedment is a challenging task due to the complexity of the forces transmitted by friction between adjacent particles (Deng et al. 2014; Reinicke et al. 2010) and the non-linear response of indentation in the rock formation (Momber 2004). Several empirical models have been developed to calculate embedment depths for monolayer proppant (Huitt & McGlothlin 1958; Volk et al. 1981) and for multilayers of proppant (Li et al. 2015a).

2.6. Conductivity of proppant packs

The conductivity of a fracture, which is commonly defined as the product of the permeability of the fracture and its opening, is considered as a key parameter to evaluate the capacity of the fracture for fluid flow during the hydrocarbon

resources recovery stage (Diyashev & Economides 2006). Hence, the permeability of the proppant pack together with the fracture residual opening play an important role to assess the fluid flow within the propped fracture as well as the performance of a well.

The consolidation and damage during the recovery stage lead to numerous mechanisms impairing the permeability of a hydraulic fracture. The decrease in porous space between the particles due to compression leads to the reduction of the permeability of the proppant pack (Bortolan Neto et al. 2015). The pore space is also filled with various substances, such as fracturing gel residual, mineral precipitates (Barree et al. 2003; Weaver et al. 2006), and fine particles formed due to the damage of rock and proppant particles at high confining stresses (Reinicke et al. 2010; Wen et al. 2007). The behaviour of porosity and permeability can be incorporated using empirical models.

One simple theoretical model was suggested by Bortolan Neto et al. (2015). In this model, the porosity ζ of a proppant pack is defined as

$$\zeta = \frac{V_s}{V} = 1 - \frac{V_p}{V} \quad (47)$$

where V is the volume of the proppant pack, V_s is the total volume of porous space within the proppant pack, V_p is the total volume of proppant particles, and $V = V_s + V_p$.

The relationship between the porosity of the proppant pack during the recovery stage and the porosity during the injection stage is presented in Eq. (48) (Bortolan Neto et al. 2015)

$$\zeta = 1 - \frac{V_0}{V} (1 - \zeta_0). \quad (48)$$

where V_0 , ζ_0 are the volume and the porosity of the proppant pack during the

injection stage, respectively, V is the proppant pack volume during the recovery stage. The volumes of the proppant pack at these stages are calculated as (Bortolan Neto et al. 2015)

$$V_0 = 2h \int_{-a}^{+a} \delta_{f0}(x) dx, \quad V = 2h \int_{-a}^{+a} \delta_r(x) dx. \quad (49)$$

where h is the fracture height, $\delta_{f0}(x)$ and $\delta_r(x)$ are the fracture opening corresponding to the injection and recovery stages, respectively, and can be seen in Figure 12.

The relationship between the porosity and permeability of the proppant pack is modelled using Kozeny-Carman equation (Mavko & Nur 1997)

$$\kappa_p = \frac{G_f}{A^2} \frac{\zeta^3}{(1 - \zeta)^2}. \quad (50)$$

where κ_p is the proppant permeability, G_f is a geometric factor, and A is the surface area

From Eq.(50), the relation between permeability of the proppant pack before and after compaction is obtained as (Bortolan Neto et al. 2015)

$$\frac{\kappa_p}{\kappa_{p0}} = \left(\frac{\zeta}{\zeta_0}\right)^3 \left(\frac{1 - \zeta_0}{1 - \zeta}\right)^2 \quad (51)$$

where κ_{p0} is the permeability of the proppant pack during the injection stage.

Equations from (47) to (51) show a significant dependence of proppant permeability on the residual opening of the fracture. This particular conclusion justifies some of the research aims of this thesis presented in Chapter 1. In addition, the discussed above models will be extended for the analysis of channel fracturing techniques.

2.7. Well performance

The well performance is conventionally estimated based on the well productivity index, J_w , which is typically defined as the ratio of the production rate of the well, Q_w , and the difference between the reservoir pressure and the borehole pressure (Diyashev & Economides 2006) as the following equation

$$J_w = \frac{Q_w}{p_o - p_i} \quad (52)$$

where p_o is the pressure within the reservoir, p_i is pressure in the wellbore. For simplification purpose, the well productivity index can be substituted by the normalised productivity index \bar{J}_w (Bortolan Neto et al. 2015).

The conductivity of a hydraulic fracture during the recovery stage is normally calculated based on several assumptions: the rock formation is the linear, homogeneous and isotropic; the fluid flow within the fracture is laminar flow and can be governed using Darcy's law for steady-state (Economides & Nolte 2000). Hence, key parameters controlling the fluid flow include the viscosity of fluid, pressure gradient, permeability of the reservoir and the fracture, and dimensions. Several approaches have been developed from these simplifications for evaluating the performance of a well (Entov & Murzenko 1994; Kanevskaya & Kats 1996; Li et al. 1996; Murzenko 1994). These researches based on the assumption that the fracture is fully filled with proppant. However, the transportation of proppant is prohibited by the sedimentation and the screen out of the proppant particles during the proppant injection stage. Hence, the effective length of the fracture is much smaller than the initial crack length created during the fluid injection stage (Barree et al. 2005; Cutler et al. 1985; Montgomery & Steanson 1985).

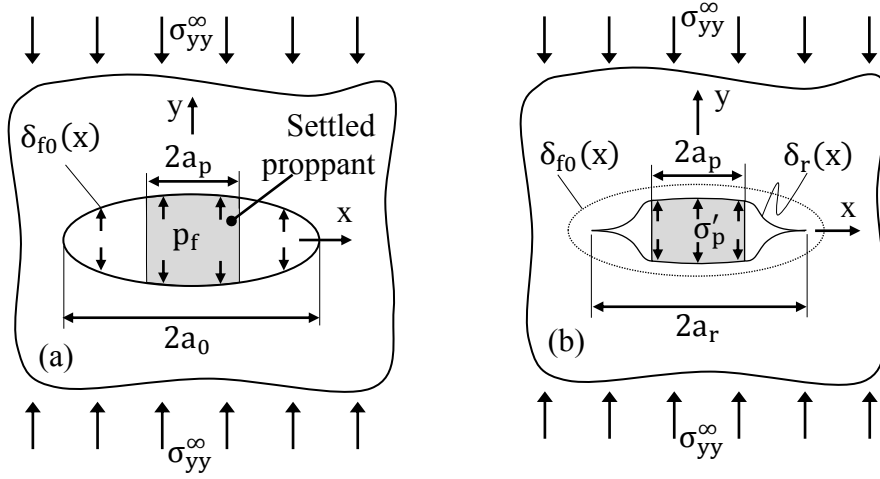


Figure 14: Partially propped hydraulic fracture. (a) fracture opening during injection stage and (b) residual fracture opening during recovery stage (Bortolan Neto et al. 2015).

Bortolan Neto et al. (2015) investigated a fracture partially filled by a proppant pack with compressibility C_p and permeability κ_p . Under the refining stress during the recovery stage, the residual opening $\delta_r(x)$ and residual length a_r of the fracture are described as Figure 14. The reduction of fracture opening and the fracture length significantly affects the permeability and the conductivity of the fracture.

The steady-state flow of fluid within the fracture is governed as a function of the fracture opening and permeability along the fracture (Zazovskii & Todua 1990)

$$\begin{aligned}
 S_f(x)\kappa_f(x) \int_{-a_r}^{+a_r} \frac{\phi(t)}{x-t} dt + 4\pi h\kappa_r \int_{-a_r}^x \phi(t) dt \\
 = Q_w \mu \frac{\pi}{2} (1 + \text{sgn}(x - a_r))
 \end{aligned} \tag{53}$$

where the unknown function $\phi(t)$ is relevant to the fluid flux into the fracture, h is the fracture height, κ_r is the permeability of the rock formation, $S_f(x) = 2h\delta_r(x)$ is the cross sectional area of the fracture, and $\kappa_f(x)$ is the fracture permeability and

it is distinguished in the propped region ($|x| < a_p$) and the un-propped region ($a_p < |x| \leq a_r$) as (Barree et al. 2003)

$$\kappa_f(x) = \begin{cases} \kappa_p & |x| < a_p \\ \frac{\delta_f^2(x)}{12} & a_p < |x| \leq a_r \end{cases} \quad (54)$$

The normalised productivity index of the fracture is normally defined as

$$\bar{J}_w = \left[\ln 2 - \ln \left(\frac{1}{K_{x,0}} \right) \right] \left[\ln \left(\frac{1}{K_{x,0}} \frac{1}{A_r} \right) - \int_{-1}^1 \Phi(X) \ln(X) dX \right]^{-1}, \quad (55)$$

where $X = x/a_r$ is normalised distance from the borehole along the fracture length, $K_{x,0} = a_0/r_r$ is the design value of the penetration ratio with r_r is the radius of the circular reservoir surrounding the wellbore, $A_r = a_r/a_0$ is normalised of the fracture residual length, and the terms $\int_{-1}^1 \Phi(X) \ln(X) dX = -\ln 2$ (Bortolan Neto et al. 2015). A similar approach will be adopted in the current thesis.

2.8. Research gaps

Among numerous parameters, residual opening of the fracture during recovery stage is defined as a key factor controlling the permeability and conductivity of the fracture and consequently influencing the well performance. Extensive research has focused on modelling the behaviour of the proppant pack under compressive loading to define the residual opening and its effect on the fracture conductivity (Bortolan Neto & Kotousov 2012, 2013; Bortolan et al. 2015; Khanna et al. 2014; Morris et al. 2014; Yan et al. 2016). Although the influence of proppant compressibility is incorporated, these models are limited in specific cases because the influence of proppant embedment was not accounted or modelled correctly (Gao et al. 2012; Li et al. 2015a).

The influence of the proppant placement was investigated in various case from

fully filled fractures to partially filled fractures (Bortolan Neto et al. 2015; Bortolan Neto & Kotousov 2012, 2013; Khanna et al. 2014). These studies mostly focus on the continuous placement of proppant within the fracture. The development of the channel fracturing technique is raising demand for developing models that can capture the influence of discontinuous placement of proppant on the fracture conductivity. Several modelling studies to optimise the implementation of the channel fracturing technique have been produced recently (Hou et al. 2016a; Hou et al. 2016b; Morris et al. 2014; Yan et al. 2016; Zhang & Hou 2016; Zheng et al. 2017). Although these models can be applied in several specific cases, they do not capture the nonlinear behaviour as well as the compressibility of the proppant columns. In addition, the models for fracture deformation utilised in these studies do not describe the real context of channel fracturing sufficiently.

The current thesis is aimed to overcome the above mentioned shortcomings and extend the theoretical framework developed in papers by Bortolan Neto, Khanna and Kotousov to the analysis of channelling fracturing stimulations.

2.9. Conclusion

Hydraulic fracture modelling is extensively used by the petroleum industry to perform economic optimisation (i.e. determine the appropriate fracture size which yields the best return on investment), to design fluid and proppant injection schedules, to predict the fracture propagation, and to evaluate the effectiveness of a fracturing treatment by comparing the modelling predictions to the observed behaviour. In this chapter, basic equations governing the initiation and propagation of fluid-driven fractures in rock as well the equations for fluid and proppant transport are presented. Some of the most notable analytical models for hydraulic fracture propagation are reviewed and the applications of numerical methods for the exact solution of governing equations are briefly discussed.

It is highlighted that the widely-utilised hydraulic fracture models neglect the important phenomenon of partial fracture closure and loss of fracture opening due to the consolidation of the compressible proppant particles once fluid injection is ceases and the fracture fluid pressure tends to the pore pressure of the surrounding rock. The residual opening and conductivity of fractures can be significantly lower than anticipated due to proppant consolidation, embedment and crushing. For fractures created using the channel-fracturing technique, the deformation of the open channels must also be taken into consideration. The present thesis is dedicated to the modelling and investigation of the latter phenomena. It is expected that the models developed herein can further extent the understanding of hydraulic fracturing and enhance the underlying economic benefits.

References

Aadnoy, B.S. 1987, 'Modelling of the stability of highly inclined boreholes in anisotropic rock formations', paper presented at Offshore Europe, Aberdeen, United Kingdom.

Aadnoy, B.S. & Chenevert, M.E. 1987, 'Stability of highly inclined boreholes (includes associated papers 18596 and 18736)', DOI 10.2118/16052-PA.

Abass, H.H., Soliman, M.Y., Al-Tahini, A.M., Surjaatmadja, J.B., Meadows, D.L. & Sierra, L. 2009, 'Oriented fracturing: A new technique to hydraulically fracture an openhole horizontal well', paper presented at SPE Annual Technical Conference and Exhibition, New Orleans, Louisiana.

Adachi, J., Siebrits, E., Peirce, A. & Desroches, J. 2007, 'Computer simulation of hydraulic fractures', *International Journal of Rock Mechanics and Mining Sciences*, vol. 44, no. 5, pp. 739-757, DOI <https://doi.org/10.1016/j.ijrmms.2006.11.006>.

Adams, J. & Rowe, C. 2013, 'Differentiating applications of hydraulic fracturing', paper presented at ISRM International Conference for Effective and Sustainable Hydraulic Fracturing, Brisbane, Australia.

Advani, S.H., Lee, T.S. & Lee, J.K. 1990, 'Three-dimensional modeling of hydraulic fractures in layered media: Part i—finite element formulations', *Journal of Energy Resources Technology*, vol. 112, no. 1, pp. 1-9, DOI 10.1115/1.2905706.

Anderson, G.D. 1981, 'Effects of friction on hydraulic fracture growth near unbonded interfaces in rocks', vol. 21, no. 01, DOI 10.2118/8347-PA.

Bang, V.S.S., Yuan, C., Pope, G.A., Sharma, M.M., Baran, J.R., Jr., Skildum, J. &

Linnemeyer, H.C. 2008, 'Improving productivity of hydraulically fractured gas condensate wells by chemical treatment', paper presented at Offshore Technology Conference, Houston, Texas, USA.

Barasia, A. & Pankaj, P. 2014, 'Tail-in proppant and its importance in channel fracturing technique', paper presented at SPE Bergen One Day Seminar, Bergen, Norway.

Barree, R.D., Cox, S.A., Barree, V.L. & Conway, M.W. 2003, 'Realistic assessment of proppant pack conductivity for material selection', paper presented at SPE Annual Technical Conference and Exhibition, Denver, Colorado.

Barree, R.D., Cox, S.A., Gilbert, J.V. & Dobson, M.L. 2005, 'Closing the gap: Fracture half length from design, buildup, and production analysis', vol. 20, no. 04, DOI 10.2118/84491-PA.

Barsoum, R.S. 1976, 'On the use of isoparametric finite elements in linear fracture mechanics', *International Journal for Numerical Methods in Engineering*, vol. 10, no. 1, pp. 25-37, DOI doi:10.1002/nme.1620100103.

Belytschko, T. & Black, T. 1999, 'Elastic crack growth in finite elements with minimal remeshing', *International Journal for Numerical Methods in Engineering*, vol. 45, no. 5, pp. 601-620, DOI doi:10.1002/(SICI)1097-0207(19990620)45:5<601::AID-NME598>3.0.CO;2-S.

Blanton, T.L. 1982, 'An experimental study of interaction between hydraulically induced and pre-existing fractures', paper presented at SPE Unconventional Gas Recovery Symposium, Pittsburgh, Pennsylvania.

Bortolan Neto, L., Khanna, A. & Kotousov, A. 2015, 'Conductivity and performance of hydraulic fractures partially filled with compressible proppant packs', *International Journal of Rock Mechanics and Mining Sciences*, vol. 74, pp. 1-9, DOI <https://doi.org/10.1016/j.ijrmms.2014.11.005>.

Bortolan Neto, L. & Kotousov, A. 2012, 'Residual opening of hydraulically stimulated fractures filled with granular particles', *Journal of Petroleum Science and Engineering*, vol. 100, pp. 24-29, DOI <https://doi.org/10.1016/j.petrol.2012.11.014>.

Bortolan Neto, L. & Kotousov, A. 2013, 'Residual opening of hydraulic fractures filled with compressible proppant', *International Journal of Rock Mechanics and Mining Sciences*, vol. 61, pp. 223-230, DOI <https://doi.org/10.1016/j.ijrmms.2013.02.012>.

Bortolan, N.L., Khanna, A. & Kotousov, A. 2015, 'Conductivity and performance of hydraulic fractures partially filled with compressible proppant packs', *International Journal of Rock Mechanics and Mining Sciences*, vol. 74, pp. 1-9, DOI <https://doi.org/10.1016/j.ijrmms.2014.11.005>.

Bouchard, P.O., Bay, F., Chastel, Y. & Toveña, I. 2000, 'Crack propagation modelling using an advanced remeshing technique', *Computer Methods in Applied Mechanics and Engineering*, vol. 189, no. 3, pp. 723-742, DOI <https://doi.org/10.1016/S0045->

[7825\(99\)00324-2.](#)

Boyer, F., Guazzelli, É. & Pouliquen, O. 2011, 'Unifying suspension and granular rheology', *Physical Review Letters*, vol. 107, no. 18, p. 188301.

Bradley, W.B. 1979, 'Failure of inclined boreholes', *Journal of Energy Resources Technology*, vol. 101, no. 4, pp. 232-239, DOI 10.1115/1.3446925.

Bulova, M.N., Nosova, K.E., Willberg, D.M. & Lassek, J.T. 2006, 'Benefits of the novel fiber-laden low-viscosity fluid system in fracturing low-permeability tight gas formations', paper presented at SPE Annual Technical Conference and Exhibition, San Antonio, Texas, USA.

Carter, B., Wawrzynek, P.A. & Ingraea, J. 2000, 'Automated 3-d crack growth simulation', *International Journal for Numerical Methods in Engineering*, vol. 47, pp. 1-3.

Carter, R.D. 1957, 'Derivation of the general equation for estimating the extent of the fractured area', in GC Howard & CR Fast (eds), *Drilling and production practice*, American Petroleum Institute, New York, USA, pp. 261-269.

Casas, L.A., Miskimins, J.L., Black, A.D. & Green, S.J. 2006, 'Laboratory hydraulic fracturing test on a rock with artificial discontinuities', paper presented at SPE Annual Technical Conference and Exhibition, San Antonio, Texas, USA.

Chen, Z., Bungler, A.P., Zhang, X. & Jeffrey, R.G. 2009, 'Cohesive zone finite element-based modeling of hydraulic fractures', *Acta Mechanica Sinica*, vol. 22, no. 5, pp. 443-452, DOI [https://doi.org/10.1016/S0894-9166\(09\)60295-0](https://doi.org/10.1016/S0894-9166(09)60295-0).

Cipolla, C.L., Lolon, E. & Mayerhofer, M.J. 2008, 'Resolving created, propped and effective hydraulic fracture length', paper presented at International Petroleum Technology Conference, Kuala Lumpur, Malaysia.

Cleary, M.P. & Wong, S.K. 1985, 'Numerical simulation of unsteady fluid flow and propagation of a circular hydraulic fracture', *International Journal for Numerical and Analytical Methods in Geomechanics*, vol. 9, no. 1, pp. 1-14, DOI doi:10.1002/nag.1610090102.

Coduto, D.P. 2001, *Foundation design: Principles and practices*, Prentice Hall, Upper Saddle River, New Jersey.

Coop, M.R. 1990, 'The mechanics of uncemented carbonate sands', *Geotechnique*, vol. 40, no. 4, pp. 607-626, DOI 10.1680/geot.1990.40.4.607.

Cramer, D.D., Woo, G.T. & Dawson, J.C. 2004, 'Development and implementation of a low-polymer-concentration crosslinked fracturing fluid for low-temperature applications', paper presented at SPE Eastern Regional Meeting, Charleston, West Virginia.

Cundall, P.A. & Strack, O.D.L. 1979, 'A discrete numerical model for granular assemblies', *Geotechnique*, vol. 29, no. 1, pp. 47-65, DOI 10.1680/geot.1979.29.1.47.

Currie, I.G. 2003, *Fundamental of fluids*, 3rd edn, vol. 154, Marcel Dekker, Inc, New York.

Cutler, R.A., Enniss, D.O., Jones, A.H. & Swanson, S.R. 1985, 'Fracture conductivity comparison of ceramic proppants', vol. 25, no. 02, DOI 10.2118/11634-PA.

d'Huteau, E., Gillard, M., Miller, M., Pena, A., Johnson, J., Turner, M., Medvedev, O., Rhein, T. & Willberg, D. 2011, 'Open-channel fracturing-a fast track to production', *Schlumberger*, vol. Oilfield Review Autumn 2011, 23, no. 3.

Dahi, T., Arash, O. & Jon, E. 2011, 'Numerical modeling of multistranded-hydraulic-fracture propagation: Accounting for the interaction between induced and natural fractures', *SPE Journal*, vol. 16, no. 03, pp. 575-581, DOI 10.2118/124884-PA.

Daneshy, A.A. 2009, 'Factors controlling the vertical growth of hydraulic fractures', paper presented at SPE Hydraulic Fracturing Technology Conference, The Woodlands, Texas.

Deily, F.H. & Owens, T.C. 1969, 'Stress around a wellbore', paper presented at Fall Meeting of the Society of Petroleum Engineers of AIME, Denver, Colorado.

Deng, S., Li, H., Ma, G., Huang, H. & Li, X. 2014, 'Simulation of shale-proppant interaction in hydraulic fracturing by the discrete element method', *International Journal of Rock Mechanics and Mining Sciences*, vol. 70, pp. 219-228, DOI <https://doi.org/10.1016/j.ijrmms.2014.04.011>.

Detournay, E. 2004, 'Propagation regimes of fluid-driven fractures in impermeable rocks', *International Journal of Geomechanics*, vol. 4, no. 1, pp. 35-45, DOI doi:10.1061/(ASCE)1532-3641(2004)4:1(35).

Detournay, E. & Cheng, A.H.D. 1993, 'Fundamentals of poroelasticity', *Comprehensive Rock Engineering: Principles, Practice and Projects*, vol. 2, chapter 5, pp. 113-171.

Diyashev, I.R. & Economides, M.J. 2006, 'The dimensionless productivity index as a general approach to well evaluation', vol. 21, no. 03, DOI 10.2118/94644-PA.

Dontsov, E.V. & Peirce, A.P. 2014, 'Slurry flow, gravitational settling and a proppant transport model for hydraulic fractures', *Journal of Fluid Mechanics*, vol. 760, pp. 567-590, DOI 10.1017/jfm.2014.606.

Economides, M.J. & Nolte, K.G. 2000, *Reservoir stimulation*, 3rd edn, Wiley, Chichester, England.

Entov, V.M. & Murzenko, V.V. 1994, 'Steady flow of homogeneous fluid in an oil reservoir recovery element with a hydrofracture', *Fluid Dynamics*, vol. 29, no. 1, pp. 81-87, DOI 10.1007/bf02330626.

Feng, Y., Jones, J.F. & Gray, K.E. 2016, 'A review on fracture-initiation and -propagation pressures for lost circulation and wellbore strengthening', vol. 31, no. 02, DOI 10.2118/181747-PA.

- Friehauf, K.E. & Sharma, M.M. 2009, 'Fluid selection for energized hydraulic fractures', paper presented at SPE Annual Technical Conference and Exhibition, New Orleans, Louisiana.
- Gao, Y., Lv, Y., Wang, M. & Li, K. 2012, 'New mathematical models for calculating the proppant embedment and fracture conductivity', paper presented at SPE Annual Technical Conference and Exhibition, San Antonio, Texas, USA.
- Geertsma, J. & De Klerk, F. 1969, 'A rapid method of predicting width and extent of hydraulically induced fractures', vol. 21, no. 12, DOI 10.2118/2458-PA.
- Gillard, M.R., Medvedev, O.O., Hosein, P.R., Medvedev, A., Peñacorada, F., apos & Huteau, E. 2010, 'A new approach to generating fracture conductivity', paper presented at SPE Annual Technical Conference and Exhibition, Florence, Italy.
- Gordeliy, E. & Peirce, A. 2013, 'Coupling schemes for modeling hydraulic fracture propagation using the xfem', *Computer Methods in Applied Mechanics and Engineering*, vol. 253, pp. 305-322, DOI <https://doi.org/10.1016/j.cma.2012.08.017>.
- Grebe, J.J. & Stoesser, M. 1935, 'Increasing crude production 20,000,000 bbl. From established fields', *World Petroleum J*, vol. August, pp. 473-485.
- He, J., Pasternak, E., Dyskin, A., Lebedev, M. & Gurevich, B. 2017, 'The effect of constriction in hydraulic fracturing', in Springer International Publishing, Cham, pp. 613-619.
- Henshell, R.D. & Shaw, K.G. 1975, 'Crack tip finite elements are unnecessary', *International Journal for Numerical Methods in Engineering*, vol. 9, no. 3, pp. 495-507, DOI doi:10.1002/nme.1620090302.
- Hossain, M.M., Rahman, M.K. & Rahman, S.S. 2000, 'Hydraulic fracture initiation and propagation: Roles of wellbore trajectory, perforation and stress regimes', *Journal of Petroleum Science and Engineering*, vol. 27, no. 3, pp. 129-149, DOI [https://doi.org/10.1016/S0920-4105\(00\)00056-5](https://doi.org/10.1016/S0920-4105(00)00056-5).
- Hou, B., Zheng, X., Chen, M., Ye, Z. & Chen, D. 2016a, 'Parameter simulation and optimization in channel fracturing', *Journal of Natural Gas Science and Engineering*, vol. 35, pp. 122-130, DOI <https://doi.org/10.1016/j.jngse.2016.08.046>.
- Hou, T., Zhang, S., Yu, B., Lv, X., Zhang, J., Han, J. & Li, D. 2016b, 'Theoretical analysis and experimental research of channel fracturing in unconventional reservoir', paper presented at SPE Europec featured at 78th EAGE Conference and Exhibition, Vienna, Austria.
- Howard, G.C. & Fast, C.R. 1957, 'Optimum fluid characteristics for fracture extension', paper presented at Drilling and Production Practice, New York, New York.
- Hsiao, C. 1988, 'A study of horizontal-wellbore failure', *Society of Petroleum Engineers*, vol. 3, no. 04, DOI 10.2118/16927-PA.

- Hubbert, M.K. & Willis, D.G. 1957, 'Mechanics of hydraulic fracturing', *Trans. AIME*, vol. 210, pp. 153–166.
- Huitt, J.L. & McGlothlin, B.B., Jr. 1958, 'The propping of fractures in formations susceptible to propping-sand embedment', paper presented at Drilling and Production Practice, New York, New York.
- Kanevskaya, R.D. & Kats, R.M. 1996, 'Exact solutions of problems of fluid inflow into a well with a vertical hydrofracture and their use in numerical models of flow through porous media', *Fluid Dynamics*, vol. 31, no. 6, pp. 854-864, DOI 10.1007/bf02030104.
- Kaufman, P.B., Penny, G.S. & Paktinat, J. 2008, 'Critical evaluation of additives used in shale slickwater fracs', paper presented at SPE Shale Gas Production Conference, Fort Worth, Texas, USA.
- Khanna, A., Bortolan Neto, L. & Kotousov, A. 2014, 'Effect of residual opening on the inflow performance of a hydraulic fracture', *International Journal of Engineering Science*, vol. 74, pp. 80-90, DOI <https://doi.org/10.1016/j.ijengsci.2013.08.012>.
- Khanna, A. & Kotousov, A. 2016, 'Controlling the height of multiple hydraulic fractures in layered media', *Society of Petroleum Engineers*, DOI 10.2118/176017-PA.
- Khoei, A.R., Moallemi, S. & Haghghat, E. 2012, 'Thermo-hydro-mechanical modeling of impermeable discontinuity in saturated porous media with x-fem technique', *Engineering Fracture Mechanics*, vol. 96, pp. 701-723, DOI <https://doi.org/10.1016/j.engfracmech.2012.10.003>.
- Khristianovich, S.A. & Zheltov, Y.P. 1955, 'Formation of vertical fractures by means of highly viscous liquid', paper presented at 4th World Petroleum Congress, Rome, Italy.
- Lacy, L.L., Rickards, A.R. & Bilden, D.M. 1998, 'Fracture width and embedment testing in soft reservoir sandstone', vol. 13, no. 01, DOI 10.2118/36421-PA.
- Lamont, N. & Jessen, F.W. 1963, 'The effects of existing fractures in rocks on the extension of hydraulic fractures', vol. 15, no. 02, DOI 10.2118/419-PA.
- Lecampion, B. 2009, 'An extended finite element method for hydraulic fracture problems', *Communications in Numerical Methods in Engineering*, vol. 25, no. 2, pp. 121-133, DOI doi:10.1002/cnm.1111.
- Li, H., Jia, Z. & Wei, Z. 1996, 'A new method to predict performance of fractured horizontal wells', paper presented at International Conference on Horizontal Well Technology, Calgary, Alberta, Canada.
- Li, K., Gao, Y., Lyu, Y. & Wang, M. 2015a, 'New mathematical models for calculating proppant embedment and fracture conductivity', vol. 20, no. 03, DOI 10.2118/155954-PA.
- Li, L.C., Tang, C.A., Li, G., Wang, S.Y., Liang, Z.Z. & Zhang, Y.B. 2012, 'Numerical simulation of 3d hydraulic fracturing based on an improved flow-stress-damage model

and a parallel fem technique', *Rock Mechanics and Rock Engineering*, vol. 45, no. 5, pp. 801-818, DOI 10.1007/s00603-012-0252-z.

Li, Q., Xing, H., Liu, J. & Liu, X. 2015b, 'A review on hydraulic fracturing of unconventional reservoir', *Petroleum*, vol. 1, no. 1, pp. 8-15, DOI <https://doi.org/10.1016/j.petlm.2015.03.008>.

Martha, L.F., Wawrzynek, P.A. & Ingraffea, A.R. 1993, 'Arbitrary crack representation using solid modeling', *Engineering with Computers*, vol. 9, no. 2, pp. 63-82, DOI 10.1007/BF01199046.

Mavko, G. & Nur, A. 1997, 'The effect of a percolation threshold in the kozeny-carman relation', *GEOPHYSICS*, vol. 62, no. 5, pp. 1480-1482, DOI 10.1190/1.1444251.

McLennan, J.D. & Picardy, J.C. 1985, 'Pseudo-three-dimensional fracture growth modeling', paper presented at The 26th U.S. Symposium on Rock Mechanics (USRMS), Rapid City, South Dakota.

Mesri, G. & Vardhanabhuti, B. 2009, 'Compression of granular materials', *Canadian Geotechnical Journal*, vol. 46, no. 4, pp. 369-392, DOI 10.1139/T08-123.

Momber, A.W. 2004, 'Deformation and fracture of rocks loaded with spherical indenters', *International Journal of Fracture*, vol. 125, no. 3, pp. 263-279, DOI 10.1023/B:FRAC.0000022240.64448.2f.

Montgomery, C.T. & Smith, M.B. 2010, 'Hydraulic fracturing: History of an enduring technology', DOI 10.2118/1210-0026-JPT.

Montgomery, C.T. & Steanson, R.E. 1985, 'Proppant selection: The key to successful fracture stimulation', vol. 37, no. 12, DOI 10.2118/12616-PA.

Morris, J.P., Chugunov, N. & Meouchy, G. 2014, 'Understanding heterogeneously propped hydraulic fractures through combined fluid mechanics, geomechanics, and statistical analysis', paper presented at 48th U.S. Rock Mechanics/Geomechanics Symposium, Minneapolis, Minnesota.

Much, M.G. & Penny, G.S. 1987, 'Long-term performance of proppants under simulated reservoir conditions', paper presented at Low Permeability Reservoirs Symposium, Denver, Colorado.

Murzenko, V.V. 1994, 'Exact solutions of problems of steady fluid flow in reservoirs with hydrofractures', *Fluid Dynamics*, vol. 29, no. 2, pp. 214-220, DOI 10.1007/bf02324310.

Nejati, M., Paluszny, A. & Zimmerman, R.W. 2015, 'On the use of quarter-point tetrahedral finite elements in linear elastic fracture mechanics', *Engineering Fracture Mechanics*, vol. 144, pp. 194-221, DOI <https://doi.org/10.1016/j.engfracmech.2015.06.055>.

Nor-Azlan, N., Sanchez, A.I. & Diyashev, I.R. 2003, 'Massive hydraulic fracturing - a

case history in western siberia, russia', paper presented at SPE International Improved Oil Recovery Conference in Asia Pacific, Kuala Lumpur, Malaysia.

Nordgren, R.P. 1972, 'Propagation of a vertical hydraulic fracture', vol. 12, no. 04, DOI 10.2118/3009-PA.

Palmer, I.D. & Carroll, H.B., Jr. 1983, 'Numerical solution for height and elongated hydraulic fractures', paper presented at SPE/DOE Low Permeability Gas Reservoirs Symposium, Denver, Colorado.

Peirce, A.P. & Siebrits, E. 2001, 'Uniform asymptotic approximations for accurate modeling of cracks in layered elastic media*', *International Journal of Fracture*, vol. 110, no. 3, pp. 205-239, DOI 10.1023/A:1010861821959.

Perkins, T.K. & Kern, L.R. 1961, 'Widths of hydraulic fractures', vol. 13, no. 09, DOI 10.2118/89-PA.

Reinicke, A., Rybacki, E., Stanchits, S., Huenges, E. & Dresen, G. 2010, 'Hydraulic fracturing stimulation techniques and formation damage mechanisms—implications from laboratory testing of tight sandstone–proppant systems', *Chemie der Erde - Geochemistry*, vol. 70, pp. 107-117, DOI <https://doi.org/10.1016/j.chemer.2010.05.016>.

Richardson, R.M. 1981, 'Hydraulic fracture in arbitrarily oriented boreholes: An analytical solution', *Proc. Workshop on Hydraulic Fracturing Stress Measurements, Monterey, CA, Dec.*

Rummel, F. & Kappelmeyer, O. 1983, 'The falkenberg geothermal frac-project: Concepts and experimental results', in S Nemat-Nasser, H Abé & S Hirakawa (eds), *Hydraulic fracturing and geothermal energy*, Springer Netherlands, Dordrecht, pp. 59-74.

Sack, R.A. 1946, 'Extension of griffith's theory of rupture to three dimensions', *Proceedings of the Physical Society*, vol. 58, no. 6, p. 729.

Sammuel, M., Mohden, A.H., Ejan, A.B., Ooi, Y.S., Ashraf, S. & Nasr-El_din, H.A. 2009, 'Anovel alpha-amylase enzyme for applications at high temperature', *Paper SPE 125024 presented at the SPE Annual Technical Conference and Exhibition, New Orleans, USA, 4-7 October.*

Settari, A. & Cleary, M.P. 1986, 'Development and testing of a pseudo-three-dimensional model of hydraulic fracture geometry', vol. 1, no. 06, DOI 10.2118/10505-PA.

Settari, A. & Raisbeck, J.M. 1981, 'Analysis and numerical modeling of hydraulic fracturing during cyclic steam stimulation in oil sands', vol. 33, no. 11, DOI 10.2118/9078-PA.

Shahid, A.S.A., Fokker, P.A. & Rocca, V. 2016, 'A review of numerical simulation strategies for hydraulic fracturing, natural fracture reactivation and induced microseismicity prediction', *Open Petroleum Engineering Journal*, vol. 9, pp. 72-91.

- Shapiro, A.A., Bedrikovetsky, P.G., Santos, A. & Medvedev, O.O. 2007, 'A stochastic model for filtration of particulate suspensions with incomplete pore plugging', *Transport in Porous Media*, vol. 67, no. 1, pp. 135-164, DOI 10.1007/s11242-006-0029-5.
- Smith, M.B., Bale, A.B., Britt, L.K., Klein, H.H., Siebrits, E. & Dang, X. 2001, 'Layered modulus effects on fracture propagation, proppant placement, and fracture modeling', paper presented at SPE Annual Technical Conference and Exhibition, New Orleans, Louisiana.
- Sneddon, I.N. 1946, 'The distribution of stress in the neighbourhood of a crack in an elastic solid', *Proceedings of the Royal Society of London. Series A, Mathematical and Physical Sciences*, vol. 187, no. 1009, pp. 229-260.
- Sneddon, I.N. & Elliott, H.A. 1946, 'The opening of a griffith crack under internal pressure', *Quarterly of Applied Mathematics*, vol. 4, no. 3, pp. 262-267.
- Stephens, W.T., Schubarth, S.K., Dickson, K.R., Snyder, E.M., Doles, K. & Herndon, D.C. 2007, 'Behavior of proppants under cyclic stress', paper presented at SPE Hydraulic Fracturing Technology Conference, College Station, Texas, U.S.A.
- Terzaghi, K., Peck, R.B. & Mesri, G. 1996, *Soilmechanicsinengineeringpractice*, 3rd edn, ohnWiley&Sons, NewYork.
- Teufel, L.W. & Clark, J.A. 1984, 'Hydraulic fracture propagation in layered rock: Experimental studies of fracture containment', DOI 10.2118/9878-PA.
- Thallak, S., Rothenburg, L. & Dusseault, M. 1991, 'Simulation of multiple hydraulic fractures in a discrete element system', paper presented at The 32nd U.S. Symposium on Rock Mechanics (USRMS), Norman, Oklahoma.
- Valko, P. & Economides, M.J. 1995, *Hydraulic fracture mechanics*, Wiley, Chichester, England.
- Vincent, M.C. 2009, 'Examining our assumptions -- have oversimplifications jeopardized our ability to design optimal fracture treatments?', paper presented at SPE Hydraulic Fracturing Technology Conference, The Woodlands, Texas.
- Volk, L.J., Raible, C.J., Carroll, H.B. & Spears, J.S. 1981, 'Embedment of high strength proppant into low-permeability reservoir rock', paper presented at SPE/DOE Low Permeability Gas Reservoirs Symposium, Denver, Colorado.
- Wangen, M. 2013, 'Finite element modeling of hydraulic fracturing in 3d', *Computational Geosciences*, vol. 17, no. 4, pp. 647-659, DOI 10.1007/s10596-013-9346-2.
- Warpinski, N.R., Branagan, P.T., Peterson, R.E. & Wolhart, S.L. 1998, 'An interpretation of m-site hydraulic fracture diagnostic results', paper presented at SPE Rocky Mountain Regional/Low-Permeability Reservoirs Symposium, Denver, Colorado.
- Weaver, J.D., van Batenburg, D.W. & Nguyen, P.D. 2006, 'Sustaining conductivity', paper presented at SPE International Symposium and Exhibition on Formation Damage Control,

Lafayette, Louisiana, USA.

Wen, Q., Zhang, S., Wang, L., Liu, Y. & Li, X. 2007, 'The effect of proppant embedment upon the long-term conductivity of fractures', *Journal of Petroleum Science and Engineering*, vol. 55, no. 3, pp. 221-227, DOI <https://doi.org/10.1016/j.petrol.2006.08.010>.

Wilson, C.R. & Witherspoon, P.A. 1974, 'Steady state flow in rigid networks of fractures', *Water Resources Research*, vol. 10, no. 2, pp. 328-335, DOI doi:10.1029/WR010i002p00328.

Xiujian, Y., Tongtao, W., Xiangzhen, Y. & Xin, W. 2010, 'A pseudo-3d model with 2d flow of hydraulic fracture propagation in thin interbedded sandstone reservoir', paper presented at International Symposium on In-Situ Rock Stress, Beijing, China.

Yan, X., Huang, Z., Yao, J., Song, W., Li, Y. & Gong, L. 2016, 'Theoretical analysis of fracture conductivity created by the channel fracturing technique', *Journal of Natural Gas Science and Engineering*, vol. 31, pp. 320-330, DOI <https://doi.org/10.1016/j.jngse.2016.03.038>.

Yi, T. & Peden, J.M. 1994, 'A comprehensive model of fluid loss in hydraulic fracturing', vol. 9, no. 04, DOI 10.2118/25493-PA.

Zazovskii, A.F. & Todua, G.T. 1990, 'Steady inflow into a well with a long vertical fracture', *Fluid Dynamics*, vol. 25, no. 4, pp. 584-593, DOI 10.1007/bf01049867.

Zhang, F., Damjanac, B. & Huang, H. 2013a, 'Coupled discrete element modeling of fluid injection into dense granular media', *Journal of Geophysical Research: Solid Earth*, vol. 118, no. 6, pp. 2703-2722, DOI doi:10.1002/jgrb.50204.

Zhang, G.M., Liu, H., Zhang, J., Wu, H.A. & Wang, X.X. 2010, 'Three-dimensional finite element simulation and parametric study for horizontal well hydraulic fracture', *Journal of Petroleum Science and Engineering*, vol. 72, no. 3, pp. 310-317, DOI <https://doi.org/10.1016/j.petrol.2010.03.032>.

Zhang, J. & Hou, J. 2016, 'Theoretical conductivity analysis of surface modification agent treated proppant ii – channel fracturing application', *Fuel*, vol. 165, pp. 28-32, DOI <https://doi.org/10.1016/j.fuel.2015.10.026>.

Zhang, J., Kamenov, A., Zhu, D. & Hill, A.D. 2013b, 'Propped fracture conductivity in shales', paper presented at 32nd International Conference on Ocean, Offshore and Arctic Engineering, Nantes, France, June 9–14.

Zheng, X., Chen, M., Hou, B., Ye, Z., Wang, W., Yin, C. & Chen, X. 2017, 'Effect of proppant distribution pattern on fracture conductivity and permeability in channel fracturing', *Journal of Petroleum Science and Engineering*, vol. 149, pp. 98-106, DOI <https://doi.org/10.1016/j.petrol.2016.10.023>.

Chapter 3

Fracture Mechanics and Distributed Dislocation Technique

Chapter 3

Fracture Mechanics and Distributed Dislocation Technique

The application of Linear Elastic Fracture Mechanics (LEFM) to predict the propagation of a crack under hydraulic pressure was started in the 1960s with the work of some pioneers (Perkins & Kern 1961). Through the years, several models based on the LEFM theory have been proposed to simulate the initiation and propagation of hydraulic fractures. The analytical models for hydraulic fracture were built based on solutions for crack problems in 2D configurations. The 2D theory leads to simpler solutions for real hydraulic fractures when it just accounts two dimensions into the model: Crack length and crack width. Even though the appearance of more comprehensive numerical solution for 3D problems, the 2D models based on LEFM are still be utilised widely in modelling hydraulic stimulation. Among numerous techniques, Distributed Dislocation Technique (DDT) is an effective tool to derive equations governing 2D model of hydraulic fractures. The DDT can give entire solutions for the fracture problem and these solutions can be solved at a relatively low computational cost. This Chapter will briefly review the basic of the LEFM, the DDT, and numerical procedure to solve singular integral equations derived from the DDT method.

3.1. Linear elastic fracture mechanics

In the LEFM, a cracked subject is assumed to be a linearly elastic medium, while nonlinear effects are insignificant and ignored. The criteria for the initiation and growth of a crack have been developed based on two basic approaches. The first approach is based on the balance of global energy during crack growth, and the other one considers the stress distribution around the crack tips.

An energy balance approach was first proposed by Griffith (1921) when he considered the propagation of cracks in brittle materials. Griffith introduced a

well-known concept that an existing crack will start propagating if the energy supplied to the subject exceeds that required to form new cracked surfaces. The Griffith theory provides a clear, physical mechanism that governs the failure process and explains the huge discrepancy between the theoretical and experimental results in defining material strength (Sun & Jin 2012). Irwin (1948) proposed a fracture criterion based on the concept of energy release rate, G , which is the change of potential energy per one unit of crack growth. According to this criterion, a crack will propagate if G exceeds a critical value G_c , which is defined as the fracture toughness.

Further, based on Westergaard's solution (Westergaard 1939) for stress and displacement in a cracked plate, Irwin (1957) introduced stress intensity factor, K , and classified it according to three basic crack modes: Mode I, Mode II, and Mode III as presented in Figure 1. Crack propagation occurs if the value of K at the crack tip reaches the critical value, K_c . The condition to apply this criterion is that the plastic deformation zone is well defined within the K dominance, see Figure 2. As the ease of calculating K and the ease of measuring the fracture toughness, this approach has been generally used in the analyses of fracture mechanics.

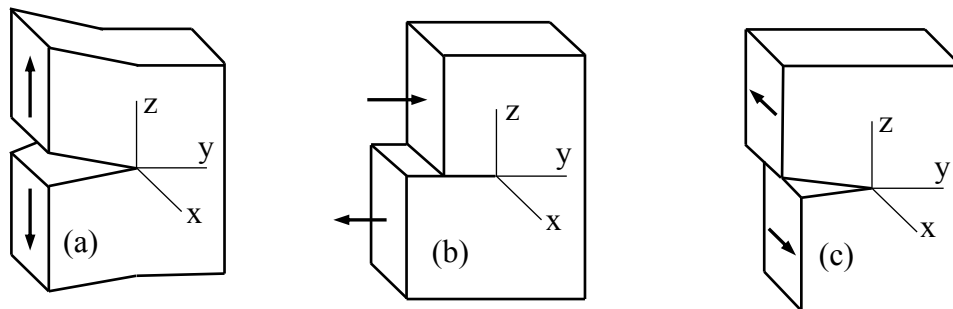


Figure 1: Basic fracture modes: (a) Mode I, (b) Mode II, (c) Mode III (Sun & Jin 2012)

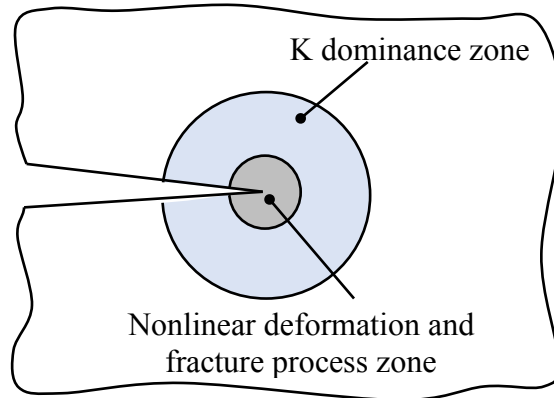


Figure 2: The process zone and the K dominance zone (Sun & Jin 2012)

By defining a coordinate system with the origin is placed at the crack tip as shown in Figure 3, Williams (1956) developed an asymptotic solution to provide a general expression for the stress field around a crack tip, which is independent of the external load as well as the crack geometry. The influence of crack geometry and external load on the singular stresses is described by the stress intensity factors. The stress and displacement fields in the near crack tip region corresponding to different crack modes are summarised in Table 1.

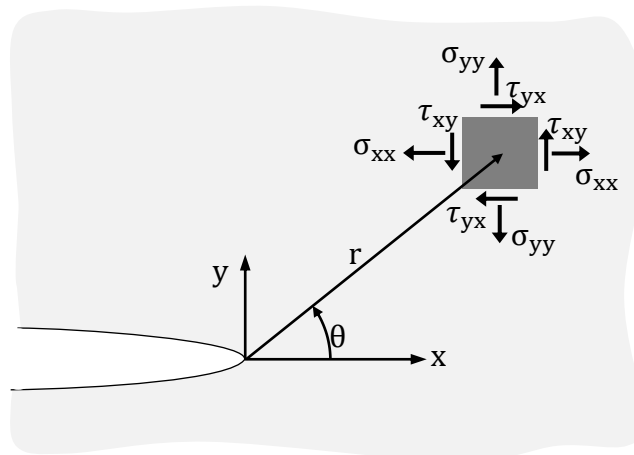


Figure 3: Schematic of stresses surrounding a crack tip adapted from Bortolan Neto (2013)

Table 1: Summary of crack tip elastic stress and displacement fields (Hills et al. 1996)

	Mode I	Mode II	Mode III
σ_{xx}	$\frac{K_I}{\sqrt{2\pi r}} \cos \frac{\theta}{2} \left[1 - \sin \frac{\theta}{2} \sin \frac{3\theta}{2} \right]$	$\frac{K_{II}}{\sqrt{2\pi r}} \sin \frac{\theta}{2} \left[2 + \cos \frac{\theta}{2} \cos \frac{3\theta}{2} \right]$	0
σ_{yy}	$\frac{K_I}{\sqrt{2\pi r}} \cos \frac{\theta}{2} \left[1 + \sin \frac{\theta}{2} \sin \frac{3\theta}{2} \right]$	$\frac{K_{II}}{\sqrt{2\pi r}} \sin \frac{\theta}{2} \cos \frac{\theta}{2} \cos \frac{3\theta}{2}$	0
σ_{xy}	$\frac{K_I}{\sqrt{2\pi r}} \sin \frac{\theta}{2} \cos \frac{\theta}{2} \cos \frac{3\theta}{2}$	$\frac{K_{II}}{\sqrt{2\pi r}} \cos \frac{\theta}{2} \left[1 - \sin \frac{\theta}{2} \sin \frac{3\theta}{2} \right]$	0
σ_{zz}	0	0	0
σ_{zx}	0	0	$-\frac{K_{III}}{\sqrt{2\pi r}} \sin \frac{\theta}{2}$
σ_{zy}	0	0	$\frac{K_{III}}{\sqrt{2\pi r}} \cos \frac{\theta}{2}$
u_x	$\frac{K_I}{2\mu} \sqrt{\frac{r}{2\pi}} \cos \frac{\theta}{2} (\kappa - \cos \theta)$	$\frac{K_{II}}{2\mu} \sqrt{\frac{r}{2\pi}} \sin \frac{\theta}{2} (2 + \kappa + \cos \theta)$	0
u_y	$\frac{K_I}{2\mu} \sqrt{\frac{r}{2\pi}} \sin \frac{\theta}{2} (\kappa - \cos \theta)$	$\frac{K_{II}}{2\mu} \sqrt{\frac{r}{2\pi}} \cos \frac{\theta}{2} (2 - \kappa - \cos \theta)$	0
u_z	0	0	$\frac{K_{III}}{2\mu} \sqrt{\frac{r}{2\pi}} \sin \frac{\theta}{2}$

$\kappa = (3 - \nu)/(1 + \nu)$ for plane stress and $\kappa = 3 - 4\nu$ for plane strain, ν is Poisson's ratio

After the work of Williams (1956), there were many papers devoted to the development of mathematical methods and obtaining exact and approximate solutions for various geometries and boundary conditions (Dyskin 1997; Dyskin et al. 2015). One of such methods is the Distributed Dislocation Techniques, which will be briefly discussed next.

3.2. The Distributed Dislocation Technique

In this section, the Distributed Dislocation Technique (DDT) is introduced by developing a solution for the simplest crack problem: an embedded straight crack in an infinite sheet of material loaded by a remote tensile stress, as Figure 4(a). By using the principle of superposition, the problem can be deconstructed into two separate problems. The first problem is defining the stress induced by the remote tensile stress in an uncracked infinite plate, see Figure 4(b). The second problem considers to a free plate in which a crack is created by inserting rigid material between the crack faces. The material is inserted in such a manner that the induced tractions along the crack faces balance with the stresses induced in the first problem, as illustrated in Figure 4(c).

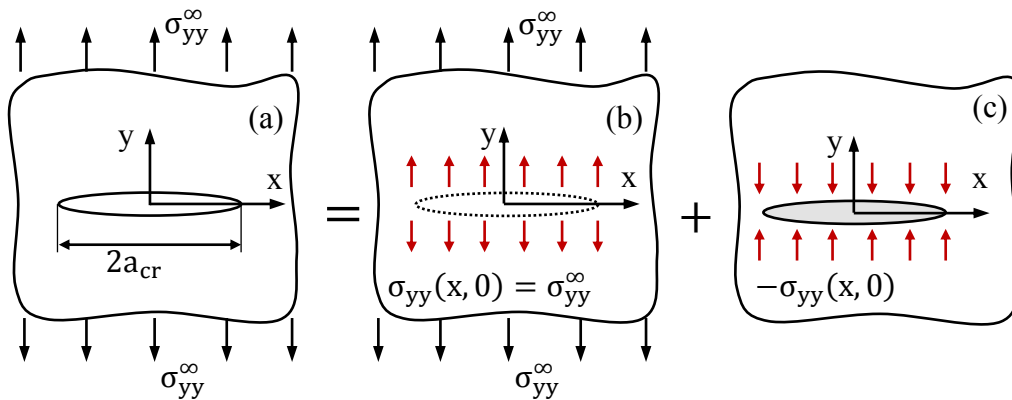


Figure 4: Superposition principle: (a) the straight crack problem; (b) the stress in an uncracked sheet; and (c) the corrective traction on the crack surfaces (Hills et al. 1996)

The inserted material can be imagined as the addition of many infinitesimal bands, which are first added at the crack tip, then extended along the crack line, as shown in Figure 5. Each single band is considered as an edge dislocation, so the crack can be examined as a number of edge dislocations distributed continuously along its length.

In the DDT, the stress field and relative displacements induced by a single edge dislocation in an infinite body are the foundations from which to compute the

stress field induced by the continuous edge dislocations. When considering an edge dislocation placed at $x = 0, y = 0$ with Burger's vector $b = 0\vec{i} + b_y\vec{j}$ as shown in Figure 6, a displacement jump is produced (Hills et al. 1996)

$$u_y(x, y = 0^+) - u_y(x, y = 0^-) = b_y \quad (1)$$

where $u_y(x, y)$ is the y component of the displacement field.

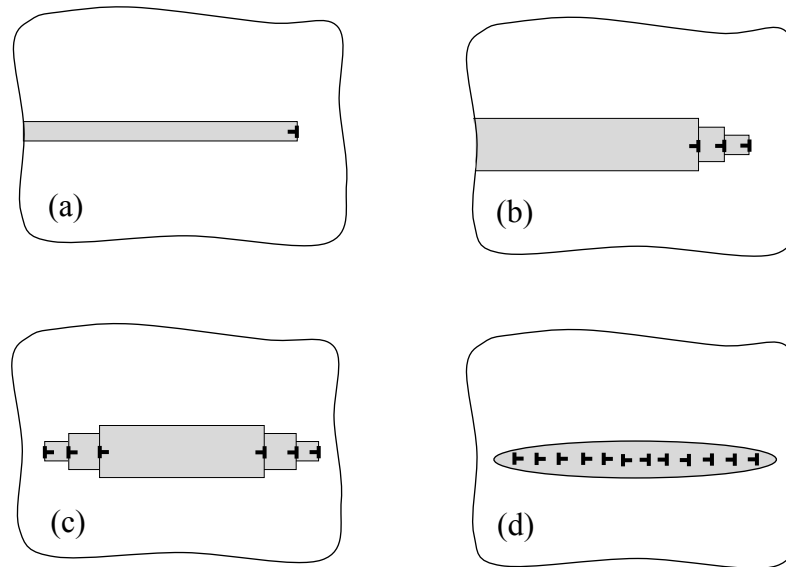


Figure 5: Inserted material between two faces of a crack; (a) a single edge dislocation; (b) additional dislocations; (c) taken away dislocation; (d) final geometry of the crack

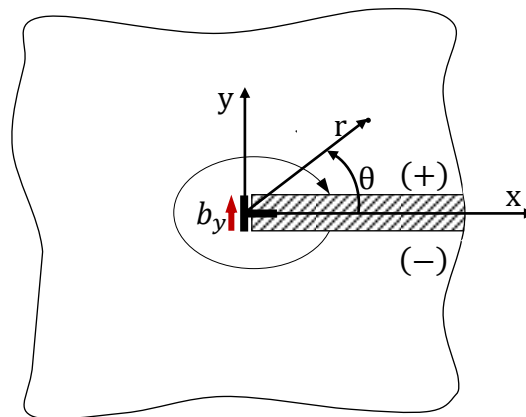


Figure 6: Schematic of an edge dislocation and Burger's vector

The stress fields arising from this displacement jump are presented in the following equations (Hills et al. 1996).

$$\bar{\sigma}_{xx}(x, y) = \frac{\bar{E}}{4\pi} b_y \frac{x}{r^4} (x^2 - y^2) \quad (2)$$

$$\bar{\sigma}_{yy}(x, y) = \frac{\bar{E}}{4\pi} b_y \frac{x}{r^4} (x^2 + 3y^2) \quad (3)$$

$$\bar{\sigma}_{xy}(x, y) = \frac{\bar{E}}{4\pi} b_y \frac{y}{r^4} (x^2 - y^2) \quad (4)$$

where $r^2 = x^2 + y^2$; b_y is Burger's vector; \bar{E} is the generalised Young's modulus, which is defined as $\bar{E} = E$ in plane stress or $\bar{E} = E/(1 - \nu^2)$ in plane strain with ν is Poisson's ratio.

To obtain a stress field induced by edge dislocations continuously distributed along $-a_{cr} < x < +a_{cr}$, $y = 0$, the set of dislocations distributed along an infinitesimal crack element between the points φ and $\varphi + \delta\varphi$ need to be considered to calculate infinitesimal Burger's vector

$$db_y = \Gamma_y(\varphi)d\varphi \quad (5)$$

where $\Gamma_y(\varphi)$ is the dislocation density at point φ (Hills et al. 1996).

The stress field is obtained by integrating the fundamental solution for an edge dislocation (Hills et al. 1996).

$$\bar{\sigma}_{xx}(x, y) = \frac{\bar{E}}{4\pi} \int_{-a_{cr}}^{+a_{cr}} \Gamma_y(\varphi) \frac{(x - \varphi)((x - \varphi)^2 - y^2)}{((x - \varphi)^2 + y^2)^2} d\varphi \quad (6)$$

$$\bar{\sigma}_{yy}(x, y) = \frac{\bar{E}}{4\pi} \int_{-a_{cr}}^{+a_{cr}} \Gamma_y(\varphi) \frac{(x - \varphi)((x - \varphi)^2 + 3y^2)}{((x - \varphi)^2 + y^2)^2} d\varphi \quad (7)$$

$$\bar{\sigma}_{xy}(x, y) = \frac{\bar{E}}{4\pi} \int_{-a_{cr}}^{+a_{cr}} \Gamma_y(\varphi) \frac{y((x - \varphi)^2 - y^2)}{((x - \varphi)^2 + y^2)^2} d\varphi \quad (8)$$

Using the superposition principle, the total stresses in the material, $\sigma_{ij}(x, y)$, are the result of a simple addition of stresses induced in the plate without the crack, $\hat{\sigma}_{ij}(x, y)$, and stresses induced by the continuous dislocation along the crack, $\bar{\sigma}_{ij}(x, y)$, and described by Eq. (9)

$$\sigma_{ij}(x, y) = \hat{\sigma}_{ij}(x, y) + \bar{\sigma}_{ij}(x, y) \quad (9)$$

The set of boundary conditions for the crack is described as

$$\bar{\sigma}_{xx} = \bar{\sigma}_{yy} = \bar{\sigma}_{xy} = 0, \quad x, y \rightarrow \infty, \quad (10)$$

$$\sigma_{yy}(x, y = 0) = \bar{\sigma}_{yy}(x, y = 0) + \sigma_{yy}^{\infty}(x, y = 0) = 0, \quad -a_{cr} < x < +a_{cr}, \quad (11)$$

$$\sigma_{xy}(x, y = 0) = \bar{\sigma}_{xy}(x, y = 0) = 0, \quad (12)$$

Combining the boundary conditions with Eq. (7), the following equation can be obtained

$$\frac{\bar{E}}{4\pi} \int_{-a_{cr}}^{+a_{cr}} \frac{\Gamma_y(\varphi)}{(x - \varphi)} d\varphi + \sigma_{yy}^{\infty} = 0 \quad |x| < a_{cr}. \quad (13)$$

The dislocation density $\Gamma_y(\varphi)$ is firstly solved from Eq.(13), then utilised to calculate the opening profile of the fracture based on the following equation (Hills et al. 1996).

$$\delta_{cr}(x) = - \int_{-a_{cr}}^x \Gamma_y(\varphi) d\varphi. \quad (14)$$

The Eq. (14) is very important to calculate the residual opening profile of the fractures considered in the current thesis as discussed in Chapters 4 to 7.

Due to the physical requirement that the crack surfaces are bonded with each other at both ends or $\delta_{cr}(x = -a_{cr}) = \delta_{cr}(+a_{cr}) = 0$, the condition of no net dislocation needs to be satisfied and described as (Hills et al. 1996)

$$\int_{-a_{cr}}^{+a_{cr}} \Gamma_y(\varphi) d\varphi = 0. \quad (15)$$

The exact solution for singular integral equation, as Eq. (13), and Eq. (15) cannot be obtained directly due to the inversion of the non-linear terms in the integral. Among several numerical solutions have been developed to deal with this issue, Gauss-Chebyshev quadrature is known as an effective solution to solve singular integral equations containing Cauchy kernels (Hills et al. 1996). Hence, the Gauss-Chebyshev quadrature is used throughout the current thesis and will be reviewed in the next section.

3.3. Gauss-Chebyshev quadrature for integral equations

In order to apply the Gauss-Chebyshev quadrature solution, some manipulations for Eq. (13) need to be performed first. The interval $[-a_{cr}, +a_{cr}]$ is normalised to be $[-1, +1]$ using the following scale transformation

$$s = \frac{\varphi}{a_{cr}}, \quad (16)$$

$$t = \frac{x}{a_{cr}}, \quad (17)$$

Eq. (13) and (15) can be written as

$$\frac{\bar{E}}{4\pi} \int_{-1}^{+1} \frac{\Gamma_y(s)}{(t-s)} ds = \sigma_{yy}^{\infty}(t) \quad |t| < 1. \quad (18)$$

$$\int_{-1}^{+1} \Gamma_y(s) ds = 0. \quad (19)$$

where $\Gamma_y(s)$ is described as the product of a fundamental solution, $\chi(s)$, and a bounded function, $\psi(s)$, as below (Hills et al. 1996)

$$\Gamma_y(s) = \chi(s)\psi(s) \quad (20)$$

Using the Gauss-Chebyshev quadrature, Eq. (18) is transformed to a set of $M - n$ algebraic equations as below (Hills et al. 1996)

$$\frac{\bar{E}}{4\pi} \sum_{i=1}^M V_i \frac{\psi(s_i)}{t_k - s_i} = \sigma_{yy}^{\infty}(t_k) \quad k = 1 \dots M - n \quad (21)$$

where M is the number of the integration points s_i , t_k are the collocation points, and V_i are weight function. The expression of these quantities is obtained from Hills et al. (1996) as following

$$s_i = \cos\left(\pi \frac{2i-1}{2M}\right), \quad i = 1 \dots M, \quad (22)$$

$$t_k = \cos\left(\pi \frac{k}{M}\right), \quad k = 1 \dots M - 1, \quad (23)$$

$$V_i = \frac{1}{M} \quad (24)$$

$$n = 1, \quad (25)$$

Hence, Eq. (21) can be written as

$$\frac{\bar{E}}{4M} \sum_{i=1}^M \frac{\psi(s_i)}{t_k - s_i} = \sigma_{yy}^{\infty}(t_k) \quad k = 1 \dots M - 1 \quad (26)$$

Eq. (19) is discretised as

$$\frac{\pi}{M} \sum_{i=1}^M \psi(s_i) = 0 \quad (27)$$

Eq. (26) and Eq. (27) form a system of M non-linear algebraic equations with M unknown, $\psi(s_i)$. These equations are solved numerically using standard iterative procedure.

From the obtained $\psi(s_i)$, the fracture opening profile is calculated from Eq. (14) employing the Gauss-Chebyshev quadrature and expressed as

$$\delta_{cr}(t_j) = -\frac{\pi a}{M} \sum_{i=1}^j \psi(s_i) \quad (28)$$

The numerical procedure has been introduced above is utilised to solve problems in Chapters 4 to 7 with some modifications corresponding to the changes of boundary conditions. For the problems considered in the thesis, proppant pack induces a pressure on the fracture faces and keeps the fracture open during the recovery of hydrocarbon resources, so the non-linear behaviour of the pressure needs to be modelled and added to the boundary conditions.

3.4. Conclusion

In this chapter, the criterion for the initiation and propagation of a hydraulic fracture are reviewed by introducing the LEM. The DDT is reviewed as the general approach for the current thesis. The Gauss-Chebyshev quadrature, an effective numerical solution for singular integral equations, is also discussed

briefly. The following chapters are the candidate's papers developed by employing the general approach discussed above.

References

Bortolan Neto, L. 2013, 'Non-linear models for evaluating the residual opening of hydraulically stimulated fractures and its impact on well performance', School of Mechanical Engineering, Publications thesis, Doctor of Philosophy thesis, The University of Adelaide.

Dyskin, A. 1997, 'Mechanism of dilatancy and fracture of brittle materials in uniaxial compression', *International Journal of Fracture*, vol. 86, pp. 45-50.

Dyskin, A., Pasternak, E. & Esin, M. 2015, 'Multiscale rotational mechanism of fracture propagation in geomaterials', *Philosophical Magazine*, vol. 95, no. 28-30, pp. 3167-3191, DOI 10.1080/14786435.2015.1013073.

Griffith, A.A. 1921, 'Vi. The phenomena of rupture and flow in solids', *Philosophical Transactions of the Royal Society of London. Series A, Containing Papers of a Mathematical or physical Character*, vol. 221, no. 582-593, pp. 163-198, DOI 10.1098/rsta.1921.0006.

Hills, D.A., Kelly, P.A., Dai, D.N. & Korsunsky, A.M. 1996, *Solution of crack problems: The distributed dislocation technique*, Kluwer Academic Publishers, Dordrecht/Boston/London.

Irwin, G.R. 1948, 'Fracture dynamics', in: *Fracture of Metals*, ASM, Cleveland, OH, pp. 147-166.

Irwin, G.R. 1957, 'Relation of stresses near a crack to the crack extension force', in: *Proceedings of the International Congresses of Applied Mechanics*, vol. 3, pp. 245-251.

Perkins, T.K. & Kern, L.R. 1961, 'Widths of hydraulic fractures', vol. 13, no. 09, DOI 10.2118/89-PA.

Sun, C.T. & Jin, Z.H. 2012, *Fracture mechanics*, Academic Press, Elsevier. DOI <https://doi.org/10.1016/C2009-0-63512-1>.

Westergaard, H.M. 1939, 'Bearing pressure and cracks', *Journal of Applied Mechanics*, vol. 6, pp. 49-53.

Williams, M.L. 1956, 'On the stress distribution at the base of a stationary crack', *Journal of Applied Mechanics*, vol. 24, no. 1, pp. 109-114.

Chapter 4

Residual opening of hydraulic fractures created
using the channel fracturing technique

Statement of Authorship

Title of Paper	Residual opening of hydraulic fractures created using the channel fracturing technique
Publication Status	<input checked="" type="checkbox"/> Published <input type="checkbox"/> Accepted for Publication <input type="checkbox"/> Submitted for Publication <input type="checkbox"/> Unpublished and Unsubmitted work written in manuscript style
Publication Details	Khanna, A., Luong, H., Kotousov, A., Nguyen, G. D., & Rose, L. R. F. (2017). Residual opening of hydraulic fractures created using the channel fracturing technique. International Journal of Rock Mechanics and Mining Sciences, 100(Supplement C), 124-137. doi: https://doi.org/10.1016/j.ijrmms.2017.10.023

Principal Author

Name of Principal Author	Aditya Khanna		
Contribution to the Paper	Supervised the development of the theoretical models, wrote manuscript and acted as corresponding author.		
Overall percentage (%)	40		
Signature		Date	06/06/2018


Co-Author Contributions



By signing the Statement of Authorship, each author certifies that:

- i. the candidate's stated contribution to the publication is accurate (as detailed above);
- ii. permission is granted for the candidate to include the publication in the thesis; and
- iii. the sum of all co-author contributions is equal to 100% less the candidate's stated contribution.

Name of Co-Author (Candidate)	Hao Thanh Luong		
Contribution to the Paper	Developed the models and performed analyses		
Overall percentage (%)	30		
Certification:	This paper reports on original research I conducted during the period of my Higher Degree by Research candidature and is not subject to any obligations or contractual agreements with a third party that would constrain its inclusion in this thesis. I am the 2 nd author of this paper		
Signature		Date	06/06/2018

Name of Co-Author	Andrei Kotousov		
Contribution to the Paper	Supervised development of work, helped in data interpretation and manuscript evaluation.		
Overall percentage (%)	10		
Signature		Date	06/06/2018

Name of Co-Author	Giang Nguyen		
Contribution to the Paper	Helped to evaluate and edit the manuscript.		
Overall percentage (%)	10		
Signature		Date	06/06/2018

Name of Co-Author	Francis Rose		
Contribution to the Paper	Helped to evaluate and edit the manuscript.		
Overall percentage (%)	10 		
Signature		Date	06/06/2018



Contents lists available at ScienceDirect

International Journal of Rock Mechanics and Mining Sciences

journal homepage: www.elsevier.com/locate/ijrmms

Residual opening of hydraulic fractures created using the channel fracturing technique

Aditya Khanna^{a,*}, Hao Luong^a, Andrei Kotousov^a, Giang D. Nguyen^b, L.R. Francis Rose^c^a School of Mechanical Engineering, The University of Adelaide, Adelaide, SA 5005, Australia^b School of Civil, Environmental and Mining Engineering, The University of Adelaide, Adelaide, SA 5005, Australia^c Aerospace Division, DST Group, Melbourne, VIC 3207, Australia

ARTICLE INFO

Keywords:

Channel fracturing
Fracture opening
Proppant deformation
Optimal arrangement

ABSTRACT

The channel fracturing technique aims for discontinuous placement of proppant particles along the length of a hydraulic fracture in a way that a network of open channels or voids can be created between the proppant-filled regions of the fracture. In this paper, a simple theoretical model is developed to identify the optimal proppant volume fraction that maximises the effective conductivity of the partially-filled fracture while reducing the amount of proppant used.

The fracture geometry is idealised as two-dimensional and a regular arrangement of proppant columns is considered. The residual opening profile of the fracture is determined as a function of the proppant column width and spacing, the mechanical properties of the rock and the proppant pack as well the magnitude of the compressive in-situ stress acting normal to the fracture plane. The effective fracture conductivity is then determined as a function of its residual opening profile. Some optimal estimates are provided for the conductivity enhancement and reduction in proppant use which can be useful for the application of the channel fracturing technique.

1. Introduction

Hydraulic fracturing is a well-stimulation technology used in the oil and gas industry for enhancing hydrocarbon recovery and alleviating near-wellbore damage. This technique consists of initiating, propagating and opening a fracture from the wellbore towards a hydrocarbon-bearing layer by a pressurised fluid. Granular particles called “proppants”, which range from natural sands to synthetic materials, are pumped into the created fracture along with the fracturing fluid. Once the injection pressure is relieved, the assembly of proppant particles, referred to as the proppant pack, plays the dual role of providing mechanical support and a porous pathway for fluid flow within the fracture.¹

In practice, several damage mechanisms tend to impair the permeability of the proppant pack and hence, the efficacy of the fracturing treatment. For e.g., fracturing gel residue and mineral precipitates tend to deposit in the pore space of the proppant pack leading to reduced porosity and permeability.^{2,3} Fine particles produced due to the localised crushing of the rock and proppant pack at high confining stresses can also plug the pore space of the proppant pack.^{4,5} Attempts to alleviate the adverse impact of these damage mechanisms on fracture

conductivity generally results in increased cost of the fracturing treatment.⁶

An alternative and cost-effective solution is to decouple the load bearing task of the proppant pack from that of providing a fluid pathway. This decoupling can be achieved through the discontinuous placement of proppant in the fracture, thereby creating open channels or voids between the proppant columns, as illustrated in Fig. 1. The technique of non-uniform proppant placement is known as ‘channel fracturing’ and although the idea of discontinuous proppant placement was proposed in the early days of hydraulic fracturing,⁷ the technique was adopted in practice only recently.^{8–11} Such a proppant placement is analogous to the partial proppant monolayer placement often employed in the stimulation of natural fractures.^{12–14}

In such partially-filled fractures, fluid seeping into the fracture from the porous reservoir would flow locally through the proppant columns into the surrounding channels and globally along the network of open channels into the wellbore. Under such flow conditions, the poor permeability of the proppant pack would not severely limit the overall conductivity of the fracture. Discontinuous proppant placement could also result in significant cost savings, especially in the case of large fracturing jobs, such as multiple vertical fractures emanating from a

* Corresponding author.

E-mail addresses: aditya.khanna@adelaide.edu.au (A. Khanna), hao.luong@adelaide.edu.au (H. Luong), andrei.kotousov@adelaide.edu.au (A. Kotousov), g.nguyen@adelaide.edu.au (G.D. Nguyen), francis.rose@dsto.defence.gov.au (L.R.F. Rose).

<http://dx.doi.org/10.1016/j.ijrmms.2017.10.023>

Received 8 February 2017; Received in revised form 27 September 2017; Accepted 19 October 2017

Available online 05 November 2017

1365-1609/ © 2017 Elsevier Ltd. All rights reserved.

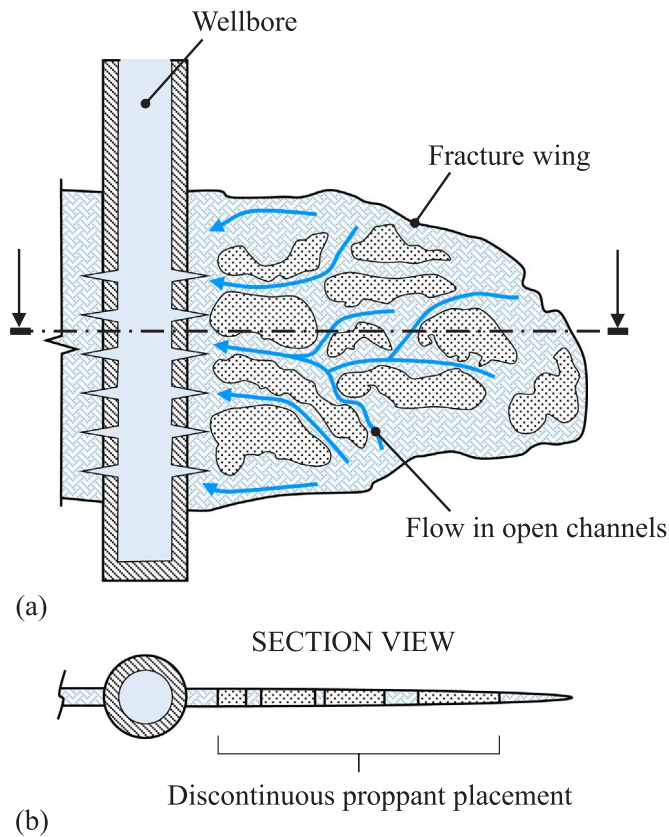


Fig. 1. (a) Schematic diagram (not-to-scale) of a partially filled fracture created using the channel fracturing technique, (b) The section view shows the initial (undeformed) fracture opening during the proppant injection stage.

single horizontal wellbore.¹⁵

The ‘channel fracturing’ technique involves the injection of proppant-laden fluid into the fracture in short pulses that are alternated with pulses of proppant-free fluid.^{16,17} Fibers or agglomerating gels are added throughout the operation to mitigate the dispersion of the proppant-laden pulses as they travel through surface equipment, along the wellbore and within the fracture.^{8,11} The relative duration of the proppant-laden pulses during the injection stage governs the volume fraction of the proppant-free channel network and the spacing between the adjacent proppant columns.

It is expected that an increment in the proppant column spacing or channel volume fraction would be beneficial up to a certain point, since

it would result in a greater increase in the overall fracture conductivity. However, this trend cannot be sustained indefinitely and too large of a column spacing would result in excessive deformation of the channels, and an overall decrease in the fracture conductivity. Hence, there must exist an optimal volume fraction of the channel network, i.e. an optimal spacing between the proppant columns, for which the overall fracture conductivity gain is maximised.

The objective of the present article is to demonstrate the existence of an optimal value of the proppant column spacing (or volume fraction), and to provide numerical results which demonstrate the potential benefits and limitations of this technique under typical field conditions. Although studies with a similar motivation have recently appeared in the literature,^{18–20} the novelty of the present study lies in its refined modelling approach and the insight provided by its numerical results. In the next section, the formulation of the problem is presented along with the modelling assumptions. In Section 3, the details of the solution procedure are presented. The dependence of the fracture residual opening and conductivity on the mechanical properties of the rock and proppant, magnitude of compressive stress, and the spacing between proppant columns is described through a set of parametric studies in Section 4.

2. Problem formulation

Consider the problem of a hydraulic fracture created in a homogeneous, elastic and isotropic rock layer and filled partially with proppant particles. As illustrated in Fig. 1a, the geometry of a hydraulic fracture is planar and the distribution of proppant in the fracture is irregular. Determining the planar distribution of proppant in the fracture in terms of the proppant injection schedule or perforation spacing at the wellbore is beyond the scope of the present work. Instead, the main interest is to investigate the dependence of the fracture residual opening and fluid conductivity on the size of the proppant columns and gaps between them. For simplicity, the arrangement of the proppant columns in the fracture is considered to be regular and a 2D equivalent of the actual 3D problem geometry is considered.

In this simplified problem, shown in Fig. 2a, the rock layer extends along the x - y plane and the fracture is aligned with the x -axis. The proppant columns are considered to be equal in width, $2b$, and the spacing between adjacent columns, $2a > 2b$ is uniform along the length of the fracture, $2L$. Since the fracture length is significantly greater than all other characteristic dimension of the problem, i.e. $L \gg a, b, \delta_0$, the problem geometry can be idealised as periodic, with unit cell shown in Fig. 2b. The column width to spacing ratio, a/b in the simplified problem (Fig. 2b) corresponds to the volume fraction of proppant-filled regions in the actual fracture geometry (Fig. 1a).

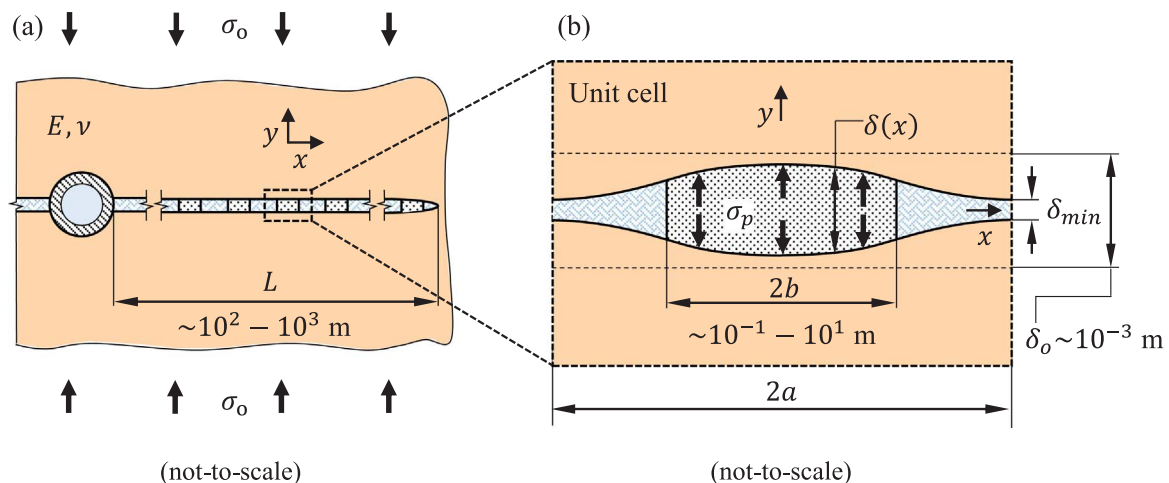


Fig. 2. (a) 2D model of a hydraulic fracture supported by equispaced proppant columns, and (b) detailed view of the unit cell of the periodic fracture geometry.

The lateral in-situ stress, σ_o acts normal to the fracture length and is opposed by the normal stress $\sigma_p(x)$ generated by the proppant columns. The residual opening of the partially-filled fracture, $\delta(x)$ is smaller than its initial opening δ_o , during the fluid injection stage due to the compressibility of the proppant pack. The loss of fracture opening is considered to be due to the consolidation of the proppant pack and the elastic deformation of the rock. Loss of fracture opening due to the embedment of proppant grains into the rock is neglected. Later in the paper, a method for estimating the effective conductivity of the planar fracture geometry (Fig. 1a) from the residual opening profile of the unit cell will also be presented.

2.1. Mechanical response of the proppant columns

A proppant column can be treated as an assembly of particles held together by the cohesive, capillary and frictional forces. The stability of the column depends upon a number of parameters, including the particle size and shape distribution, the opening of the fracture, the magnitude of the confining lateral stress, and the fluid drag force acting on the column walls during the production stage.^{21,22} High speed flow in the open channels surrounding the proppant columns tend to reduce their stability.²¹ In order to counteract this effect, additives or coatings are utilised during the implementation of the channel fracturing technique. Examples of additives include chopped fibers^{23,24} and thermo-plastic strips²⁵ and examples of coatings are surface modification agents²⁶ and curable resins.²⁷ In this study, it is assumed that the proppant columns resist erosion during the production stage.

The compressive loading on the proppant columns leads to the reduction of the column height accompanied by lateral expansion along the column width. The lateral expansion of the column has the effect of reducing the gap between the proppant columns and redistributing the stresses within the proppant column. However, the limited experimental results available in the literature¹⁷ suggest that the lateral expansion of the column approaches a steady value and the lateral strain decreases monotonically with increasing column width (see Fig. 3). This implies that the lateral expansion of proppant columns is non-uniform, occurring mostly near the perimeter of the column while the interior remains laterally constrained.

By extrapolating the available experimental results it can be argued that the lateral strain would be negligible at field-scale, where columns can be several meters wide. For example, at a confining stress of 20.7 MPa and column width of 50 cm (smallest value considered in our numerical study) the lateral strain as extrapolated from Fig. 3 would be ~ 2%, which corresponds to an increase in column width by ~ 1 cm. In this instance, the effect of the lateral expansion cannot be ignored if the gap between the columns, $2(a - b)$ is also of the order of few centimetres. However, for simplicity of the problem formulation, the lateral

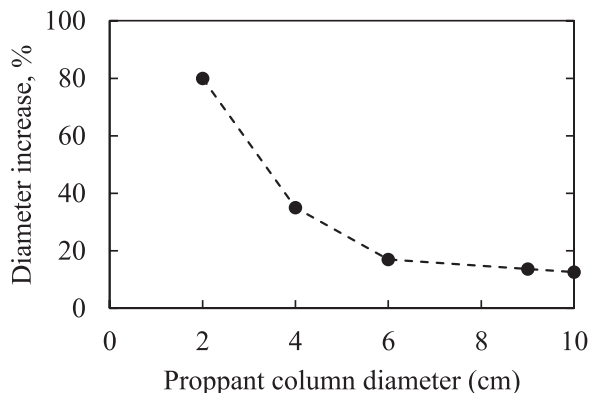


Fig. 3. Laboratory measurements for the lateral expansion of proppant columns under a compressive stress of 20.7 MPa.¹⁷ The fiber-laden proppant columns were fabricated from 20/40 mesh size ceramic proppant.

expansion of the column is ignored, the consequence of which is yet to be investigated.

Since the stiffness and strength of individual particles is quite high, the uniaxial deformation or consolidation of the proppant columns is largely achieved through particle rearrangement into a tighter packing. Particle rearrangement into a more compact configuration results from particle slip and rotation as well as through particle damage.²⁸ The particle damage mechanisms include the abrasion or grinding of particle surface asperities, breaking or crushing of particle surface protrusions and sharp corners and edges, and fracture, splitting or shattering of particles.^{28–31} The degree of particle damage together with inter-particle slip and rotation determine the mechanical response of a particular proppant pack.²⁸

Several consolidation models have been proposed in the literature to describe the mechanical response of granular assemblies over a wide range of applied stresses.³² Although these models take into account the physical mechanisms for consolidation, their accuracy increases only at the expense of an increasing number of unknown material parameters. Therefore, the present study adopts a simple empirical model for uniaxial proppant consolidation which is calibrated by experimental results for uniaxial compression of proppant columns. The compressive stress in the proppant column, σ_p is related to the proppant settlement ratio, λ according to the following power-law relationship:

$$\sigma_p = \sigma_{p0} \alpha \left(\frac{\lambda}{1-\lambda} \right)^\beta, \tag{1}$$

where α and β are the dimensionless fitting parameters. The settlement ratio, λ is defined as the ratio between the change in the height of the proppant column and the original height, i.e.

$$\lambda = (\delta_o - \delta) / \delta_o, \tag{2}$$

where δ_o is the initial height of the unloaded proppant column and δ is the height of the column at some compressive stress, σ_p . The value of λ lies in the interval (0, 1) and Eq. (1) correctly predicts that $\sigma_p = 0$ at $\lambda = 0$ and $\sigma_p \rightarrow \infty$ as $\lambda \rightarrow 1$. Note that the constant σ_{p0} is solely introduced to ensure that Eq. (1) is dimensionally correct. It has the same units as the experimentally measured stress, σ_p and has a numerical value of unity. For example, if the stress σ_p is measured in MPa, the value of $\sigma_{p0} = 1$ MPa.

Experimental results obtained by d'Huteau et al.¹⁷ are used to calibrate the model (Fig. 4) and to obtain the values of the fitting parameters. In these tests, the initial height of the proppant columns, δ_o was 6 mm and the proppant columns were placed in a hydraulic press equipped with sensors for monitoring the load and the distance between the press rams. Compressive stresses of up to 228 MPa were applied and the experimental results in the range of 0–50 MPa have been used to fit the empirical model. The calibrated empirical model is used to describe the compressive behaviour of the proppant pack in the next section.

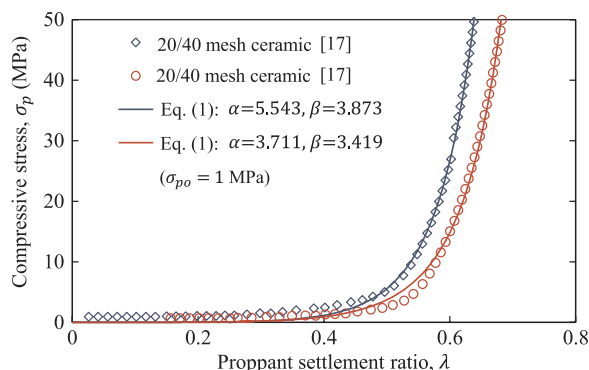


Fig. 4. Experimentally observed relationship between the compressive stress and the proppant column settlement. The solid lines represent the best fit obtained using Eq. (1).

It should be highlighted that the obtained values of the fitting parameters can vary greatly with the choice of the proppant, presence or absence of additives (resin coatings, fibers), degree of fluid saturation of the proppant columns, and the type of applied loading (uniaxial vs triaxial). Hence, for the practical application of the approach developed in this paper, the fitting constants must be re-determined for the selected proppant and experiments conditions must be selected to closely resemble the anticipated in-situ conditions.

2.2. Governing equations for the residual opening of the fracture

The distributed dislocation technique (DDT), which is based on the pioneering works of Bilby, Cottrell and Swinden,³³ and Bilby and Eshelby³⁴ is used to formulate the crack problem. In this technique, the displacement discontinuity, i.e. the relative opening or slip between the crack faces, is modelled by a continuous distribution of ‘strain nuclei’ or point sources of strain. The basic strategy is to then distribute these strain nuclei in a manner such that the traction boundary conditions along the crack faces are satisfied. The stress field induced by a single strain nucleus satisfies the equilibrium, constitutive and compatibility equations of the theory of classical linear elasticity and serves as the fundamental solution or Green’s function for obtaining the stress field induced by the continuous distribution of strain nuclei.

In the case of plane (two-dimensional) elasticity problems, the appropriate strain nucleus is the familiar edge dislocation, and although it has precisely the same characteristics as the edge dislocation arising as a lattice defect in crystalline solids, the quantity is used here for generating a controlled state of stress in the elastic medium and the presence of any lattice defects is not implied. Prior to developing the governing equations for the elasticity problem, we briefly review the fundamental solution for the stress field arising due to a single edge dislocation in an infinite body. A dislocation located $x = 0, y = 0$ with Burger’s vector $\mathbf{b} = 0\mathbf{i} + b_y\mathbf{j}$ produces a displacement jump

$$v(x, y = 0^+) - v(x, y = 0^-) = b_y H(-x), \tag{3}$$

where $v(x, y)$ is the y -component of the displacement field. The displacement jump is equivalent to making a cut along $x < 0, y = 0$, pulling the material apart and inserting a strip of material of thickness, b_y , before re-joining. The stress field arising from the displacement jump (3) is known to be³⁵

$$\tilde{\sigma}_{xx}(x, y) = \frac{\bar{E}}{4\pi} b_y \frac{x}{r^4} (x^2 - y^2), \tag{4}$$

$$\tilde{\sigma}_{yy}(x, y) = \frac{\bar{E}}{4\pi} b_y \frac{x}{r^4} (x^2 + 3y^2), \tag{5}$$

$$\tilde{\sigma}_{xy}(x, y) = \frac{\bar{E}}{4\pi} b_y \frac{y}{r^4} (x^2 - y^2), \tag{6}$$

where $r^2 = x^2 + y^2$ and \bar{E} is the generalised Young’s modulus, defined as $\bar{E} = E$ under plane stress conditions or $\bar{E} = E/(1-\nu^2)$ under plane strain conditions.

Now consider a continuous distribution of dislocations along $-\infty < x < \infty, y = 0$, such that the strength of an infinitesimal dislocation lying between $x = \xi$ and $x = \xi + d\xi$ is $db_y = B_y d\xi$. The stress field induced by the continuous distribution of dislocations is obtained by integrating the fundamental solution for a single dislocation, as follows

$$\tilde{\sigma}_{xx}(x, y) = \frac{\bar{E}}{4\pi} \int_{-\infty}^{\infty} B_y(\xi) \frac{(x-\xi)((x-\xi)^2 - y^2)}{((x-\xi)^2 + y^2)^2} d\xi, \tag{7}$$

$$\tilde{\sigma}_{yy}(x, y) = \frac{\bar{E}}{4\pi} \int_{-\infty}^{\infty} B_y(\xi) \frac{(x-\xi)((x-\xi)^2 + 3y^2)}{((x-\xi)^2 + y^2)^2} d\xi, \tag{8}$$

$$\tilde{\sigma}_{xy}(x, y) = \frac{\bar{E}}{4\pi} \int_{-\infty}^{\infty} B_y(\xi) \frac{y((x-\xi)^2 - y^2)}{((x-\xi)^2 + y^2)^2} d\xi. \tag{9}$$

The functional form of the dislocation density function, $B_y(\xi)$, is determined based on physical considerations relevant to the problem at hand. For the unit cell of the problem geometry, shown in Fig. 2, the symmetry of the problem geometry about the x -axis implies that:

$$\sigma_{xy}(x, y) = 0, \quad y = 0, \tag{10}$$

and the periodicity of the problem requires that

$$\sigma_{xy}(x, y) = 0, \quad x = 0, \tag{11a}$$

$$\sigma_{xy}(x, y) = 0, \quad x = \pm a. \tag{11b}$$

Since no external shear stresses act on the unit cell, it is the shear stress induced by the distributed dislocations, $\tilde{\sigma}_{xy}(x, y)$, that must satisfy these boundary conditions. The traction boundary condition along the crack faces can be stated as

$$\sigma_{yy}(x, y) = \begin{cases} \sigma_p(x), & |x| < b \\ 0, & b < |x| < a \end{cases}, \quad y = 0, \tag{12}$$

where $\sigma_p(x)$ is the continuous normal traction applied to crack surface by the proppant pack. The lateral in-situ stress acting normal to the crack can be expressed as

$$\sigma_{yy}(x, y) = -\sigma_0, \quad \sqrt{x^2 + y^2} \rightarrow \infty. \tag{13}$$

In Eqs. (12) and (13), the normal stresses are considered to be positive under tension.

To deduce the correct functional form of the dislocation density, first consider the shear stress induced by the distributed dislocations along the line $x = 0$, which can be obtained from Eq. (9) as

$$\tilde{\sigma}_{xy}(0, y) = \frac{\bar{E}}{4\pi} y \int_{-\infty}^{\infty} B_y(\xi) \frac{(\xi^2 - y^2)}{(\xi^2 + y^2)^2} d\xi. \tag{14}$$

The symmetry condition (11a), i.e. $\tilde{\sigma}_{xy}(0, y) = 0$ can only be satisfied by Eq. (14) if the dislocation density is an odd function of ξ i.e. $B_y(-\xi) = -B(\xi)$. Additionally, since the dislocation density must vary continuously as it changes sign from positive to negative, it must be equal to zero at $\xi = 0$. A similar argument can be made regarding the symmetry condition (11b). The shear stresses along $x = \pm a$ are given by

$$\tilde{\sigma}_{xy}(\pm a, y) = \frac{\bar{E}}{4\pi} y \int_{-\infty}^{\infty} B_y(\xi) \frac{((a \mp \xi)^2 - y^2)}{((a \mp \xi)^2 + y^2)^2} d\xi. \tag{15}$$

The requirement $\tilde{\sigma}_{xy}(\pm a, y) = 0$ can be satisfied by Eq. (15) only if the dislocation density is odd about $x = \pm a$. Keeping in mind the periodic nature of the problem, this condition can be satisfied by setting the dislocation density function to be equal to zero at $x = \pm a$ and requiring it to be periodic, such that $b_y(x + 2an) = b_y(x)$, $n = 0, \pm 1, \pm 2, \dots$. It can also be checked that the symmetry condition (10) is satisfied by Eq. (9) for all $B_y(\xi)$.

We now proceed to the application of DDT to obtaining the governing integral equation for the dislocation density function. It follows from the superposition principle that the stress state in the cracked body can be written as a summation of the stress state in the body in the absence of the crack and the stress state induced by the separation of the crack faces, i.e. the continuous distribution of dislocations.³⁶ For example, the normal stress in the y -direction can be written as

$$\begin{aligned} \sigma_{yy}(x, y) &= -\sigma_0 + \tilde{\sigma}_{yy}(x, y) \\ &= -\sigma_0 + \frac{\bar{E}}{4\pi} \int_{-\infty}^{\infty} B_y(\xi) \frac{(x-\xi)((x-\xi)^2 + 3y^2)}{((x-\xi)^2 + y^2)^2} d\xi, \end{aligned} \tag{16}$$

The stress field induced by the distributed dislocations vanishes as $\sqrt{x^2 + y^2} \rightarrow \infty$, hence the expression for σ_{yy} obtained above satisfies the boundary condition (13). The normal traction along $y = 0$ can be obtained from Eq. (16) as

$$\sigma_{yy}(x, y) = -\sigma_0 + \frac{E}{4\pi} \int_{-\infty}^{\infty} \frac{B_y(\xi)}{x-\xi} d\xi, \tag{17}$$

Exploiting the periodic nature of the dislocation density function, above expression can be reduced, after some algebraic manipulations, to the following

$$\sigma_{yy}(x, y) = -\sigma_0 + \frac{E}{4\pi} \int_{-a}^a B_y(\xi) \left[\frac{1}{x-\xi} + \sum_{n=1}^{\infty} \frac{2(x-\xi)}{(x-\xi)^2 - 4a^2n^2} \right] d\xi, \quad |x| < a \tag{18}$$

Utilising the symmetry of the dislocation density function about $x = 0$, Eq. (18) can be further reduced to

$$\sigma_{yy}(x, 0) = -\sigma_0 + \frac{E}{4\pi} \int_{-a}^a B_y(\xi) \left[\frac{2\xi}{x^2-\xi^2} + K(x, \xi) \right] d\xi, \quad 0 < |x| < a, \tag{19}$$

where the kernel $K(x, \xi)$ is given by

$$K(x, \xi) = \sum_{n=1}^{\infty} \frac{4\xi(x^2 - \xi^2 + 4a^2n^2)}{\{(x - \xi)^2 - 4a^2n^2\}\{(x + \xi)^2 - 4a^2n^2\}}. \tag{20}$$

In order to satisfy the traction boundary condition (12), it is required that

$$-\sigma_0 + \frac{E}{4\pi} \int_{-a}^a B_y(\xi) \left[\frac{2\xi}{x^2-\xi^2} + K(x, \xi) \right] d\xi = \begin{cases} \sigma_p(x), & |x| < b, \\ 0, & b < |x| < a, \end{cases} \tag{21}$$

or

$$\frac{E}{4\pi} \int_{-a}^a B_y(\xi) \left[\frac{2\xi}{x^2-\xi^2} + K(x, \xi) \right] d\xi = \sigma_0 - \sigma_p(x)H(b - |x|), \quad 0 < x < a, \tag{22}$$

where $H()$ is the Heaviside step function. Eq. (22) is the governing singular integral equation for the unknown dislocation density function, $B_y(\xi)$.

There is obviously a close relationship between the dislocation density and the relative separation between the crack faces at any point, $\delta(x) = v(x, y = 0^+) - v(x, y = 0^-)$. To establish this relationship, we note that $\delta(x = a) = \delta_{min}$, Fig. 2b, and that the insertion of dislocations along $x < a$ increases the crack opening,³⁷ so that

$$\delta(x) = \delta_{min} + \int_x^a B_y(\xi) d\xi, \quad B_y(\xi) = \frac{d\delta(\xi)}{d\xi}, \quad 0 < x < a. \tag{23}$$

The reaction stress due to the proppant column, $\sigma_p(x)$ can be related to the crack opening $\delta(x)$ by substituting Eq. (2) into the empirical relationship, (1), i.e.

$$\sigma_p(x) = \sigma_{p0} \alpha \left(\frac{\delta_0}{\delta(x)} - 1 \right)^\beta. \tag{24}$$

This dependence of the proppant reaction stress on the crack opening and consequently, on the dislocation density, renders the singular integral Eq. (22) non-linear. Equations of this form arises in the formulation of a range of other crack problems which involve a continuous distribution of tractions on the crack faces. Some examples include fatigue cracks in aircraft panels repaired by composite patches³⁸ and matrix cracks in fiber-reinforced composites.³⁹ Analytical solution to such singular integral equations is not possible and the numerical solution procedure for this class of integral equations, and Eq. (22) in particular, is presented next.

3. Solution procedure

The first step of the solution procedure is normalising the interval in Eqs. (22)–(23) from $[0, a]$ to $[-1, 1]$. The substitution $x = (a/2)(t + 1)$ and $\xi = (a/2)(s + 1)$ yields the normalised form for the integral equation as follows:

$$\begin{aligned} \frac{1}{\pi} \int_{-1}^1 B_y(s) \left[\frac{(s+1)}{2(t-s)(t+s+2)} + K'(t, s) \right] ds \dots \\ = \frac{\sigma_0}{E} - \frac{\sigma_p(t)}{E} H\left(\frac{2b}{a} - t - 1\right), \quad -1 < t < 1. \end{aligned} \tag{25}$$

where the regular part of the kernel,

$$K'(t, s) = \sum_{n=1}^{\infty} \frac{(s+1)((t-s)(t+s+2)+16n^2)}{\{(t-s)^2-16n^2\}\{(t+s+2)^2-16n^2\}},$$

and the proppant reaction stress

$$\sigma_p(t) = \sigma_{p0} \alpha \left(\frac{\delta_0}{\delta(t)} - 1 \right)^\beta.$$

The crack opening displacement $\delta(t)$ over the normalised interval can be obtained from Eq. (23) as follows:

$$\delta(t) = \delta_{min} + \frac{a}{2} \int_{-1}^1 B_y(s) ds, \quad -1 < t < 1. \tag{26}$$

The dislocation density function, $B_y(s)$, is then represented as the product of an unknown regular function, $\phi(s)$, and a fundamental function, $\omega(s)$, which takes into account the asymptotic behaviour of the solution for dislocation density at $s = \pm 1$.⁴⁰ As discussed previously, the symmetry of the present problem requires that the dislocation density be equal to zero at $\xi = 0$, a i.e. $B_y(s) = 0$ at $s = \pm 1$. The appropriate form for the fundamental function, $\omega(s)$ which satisfies this requirement is $\omega(s) = \sqrt{(1-s^2)}$.^{36,40} For the chosen fundamental function, the Gauss-Chebyshev quadrature is used to reduce the singular integral Eq. (25) to the following system of algebraic equations

$$\begin{aligned} \frac{1}{N+1} \sum_{i=1}^N (1-s_i^2) \left[\frac{(s_i+1)}{2(t_k-s_i)(t_k+s_i+2)} + K'(t_k, s_i) \right] \phi(s_i) \dots \\ + \frac{\sigma_p(t_k)}{E} H\left(\frac{2b}{a} - t_k - 1\right) - \frac{\sigma_0}{E} = 0, \quad k = 1, 2, \dots, N+1. \end{aligned} \tag{27}$$

where

$$K'(t_k, s_i) = \sum_{n=1}^{\infty} \frac{(s_i+1)((t_k-s_i)(t_k+s_i+2)+16n^2)}{\{(t_k-s_i)^2-16n^2\}\{(t_k+s_i+2)^2-16n^2\}},$$

$$\sigma_p(t_k) = \sigma_{p0} \alpha \left(\frac{\delta_0}{\delta(t_k)} - 1 \right)^\beta,$$

and

$$\delta(t_k) = \delta_{min} + \frac{\pi a}{2(N+1)} \sum_{i=1}^{k-1} (1-s_i^2) \phi(s_i). \tag{28}$$

The set of N discrete integration points are given by³⁶

$$s_i = \cos\left(\pi \frac{i}{N+1}\right), \quad i = 1, \dots, N, \tag{29}$$

and the N collocation points are given by³⁶

$$t_k = \cos\left(\pi \frac{2k-1}{2(N+1)}\right), \quad k = 1, \dots, N+1. \tag{30}$$

The system of Eq. (27) is non-linear and requires iterative solution.^{39,41} Let the array $\{\phi\} = \{\phi_1, \phi_2, \dots, \phi_N\}^T = \{\phi(s_1), \phi(s_2), \dots, \phi(s_N)\}^T$ contain the unknown values of the function $\phi(s)$ at the N integration points along the crack. Also, let the array $\{F\} = [F_1(\phi), F_2(\phi), \dots, F_{N+1}(\phi)]$ represent the left hand side of (27) evaluated at $\{\phi\}$. Then the value of $\{\phi\}$ which satisfies the system of equations, $\{F\} = 0$, within some allowed tolerance or error, is the solution or root to the system of Eq. (27). The iterative solution procedure requires an initial guess for the solution, $\{\phi\}_0$ as well as the Jacobian matrix, which contains all first-order partial derivatives of the vector-valued function $\{F\}$. For the present problem, the elements of the Jacobian matrix $[J]$ can be obtained as:

$$J_{k,i} = \frac{\partial F_k}{\partial \phi_i} = \frac{(1-s_i^2)}{N+1} \left[\frac{(s_i+1)}{2(t_k-s_i)(t_k+s_i+2)} + K'(t_k, s_i) \right] \dots - \frac{\sigma_p(t_k)}{E} H\left(\frac{2b}{a} - t_k - 1\right) \frac{\delta_0 \beta}{\delta(t_k)[\delta_0 - \delta(t_k)]} \frac{\pi a}{2(N+1)} (1-s_i^2) H(k-i-1). \tag{31}$$

The initial guess solution is chosen to be $\{\phi\}_0 = \{\phi_1, \phi_2, \dots, \phi_N\}_0^T = \epsilon\{1, 1, \dots, 1\}^T$, where $\epsilon \rightarrow 0$. This guess solution corresponds to zero dislocation density along the crack i.e. a constant initial crack opening. The parameter ϵ is kept infinitesimally small but non-zero to avoid the elements of the Jacobian matrix from becoming singular. The least-square solution to the overdetermined system of equations is obtained using the MATLAB nonlinear solver ‘fsolve’ which utilises the trust-region reflective algorithm.

In order to obtain a solution to the system of Eq. (27), it is first required to guess the value of the integration constant, δ_{min} , which corresponds to the residual opening at $x = \pm a$. This is because the system of governing equations is written in terms of the dislocation density, i.e. the derivative of the residual opening, rather than directly in terms of the residual opening. The system of Eq. (27) is solvable, provided that the selected value of the unknown constant δ_{min} in Eq. (28), lies between 0 and δ_{1D} , where $\delta_{min} = 0$ corresponds to the contact between the fracture faces at $x = \pm a$, and $\delta_{min} = \delta_{1D}$ corresponds to the case when the entire unit cell is filled with proppant. In the latter case, the proppant column is subjected to uniaxial strain and the constant residual opening of the unit cell can be obtained by substituting $\sigma_p = \sigma_0$ into Eq. (1) as follows:

$$\delta_{1D} = \delta_0 \left[1 + \left(\frac{\sigma_0}{\sigma_{po}\alpha} \right)^{\frac{1}{\beta}} \right]^{-1}. \tag{32}$$

The correct value of δ_{min} lies between these two limits and is selected by trial-and-error, such that the obtained solution satisfies the condition for stress equilibrium in the y-direction:

$$\frac{1}{2} \int_{-1}^{+1} \sigma_p(t) dt - \sigma_0 = 0. \tag{33}$$

The integral in Eq. (33) can be evaluated using the trapezoidal rule from the solution for σ_p obtained at the $N + 1$ collocation points.

At any given proppant column width, $2b$, the value of δ_{min} decreases from δ_{1D} to 0 as the value of column spacing, $2a$ increases from $2b$ to some critical value, $2a^*$. If the column spacing is increased beyond this critical value, the crack faces would come in contact over $a^* \leq |x| \leq a$. The presence of the contact region does not significantly alter the solution procedure due to the symmetry of the problem. When $a > a^*$, the residual opening over $|x| < a^*$ can be obtained by taking $a = a^*$ in the solution procedure and the residual opening over the contact region $a^* \leq |x| \leq a$ would be equal to zero. However, this case corresponds to partially-closed channels and hence is of little practical interest.

4. Numerical results

In this section, the effects of partial filling of the fracture are examined through a series of numerical calculations. The governing parameters of the developed theoretical model are: the column spacing, $2a$ and width, $2b$, initial opening of the fracture, δ_0 , the magnitude of the lateral in-situ stress, σ_0 , Young’s modulus of the rock, E and the mechanical properties of the proppant pack, σ_{po} , α , and β . The numerical values of δ_0 , E , σ_{po} , α , and β are kept fixed throughout the calculations. Keeping the column width $2b$ and lateral stress σ_0 fixed, the value of the column spacing $2a$ is varied to alter the volume fraction of proppant in the fracture and the residual opening and fracture transmissivity are calculated at each increment of column spacing. This analysis is conducted for a combination of three different values of the column aspect ratio $2b/\delta_0$ and two values of the lateral stress, σ_0 . The values of the governing parameters selected for the numerical calculations are representative of typical field values and are summarised in Table 1.

Table 1
Selected numerical values of governing parameters.

Parameter	Value
δ_0	5 mm
$2b$	0.5, 2.5, 5.0
σ_0	10, 50 MPa
E	10 GPa
σ_{po}	1 MPa (Fig. 4)
α	5.543 (Fig. 4)
β	3.873 (Fig. 4)

4.1. Residual opening profile of the unit-cell

The conductivity of a fracture is strongly dependent on its opening,^{42,43} hence we begin by examining the influence of the governing parameters on the residual opening profile of the partially-filled fracture, $\delta(x)$. The numerical results for the residual opening are presented in Figs. 5 and 6 for lateral in-situ stresses, $\sigma_0 = 10$ and 50 MPa, respectively. At each value of stress, three values of the column width, $2b = 0.5, 2.5$ and 5 m are considered and plots are presented for each combination of σ_0 and $2b$. In each plot, the proppant column width, $2b$ is kept fixed and the value of the column spacing, $2a$ is increased until $\delta_{min} = \delta(x = a)$ becomes close to zero. Increasing the column spacing in the 2D model corresponds to decreasing the proppant volume fraction in the actual fracture geometry (Fig. 1).

Plots (a), (c) and (e) of both figures show the variation of the residual opening over interval $0 < x < a$ i.e. along one half of the unit cell. Due to symmetry of the problem geometry about $x = 0$, the residual opening along the other half of the unit cell is simply $\delta(-x) = \delta(x)$. The residual opening along the length of the fracture is periodic such that $\delta(x + 2an) = \delta(x)$, where $n = 0, \pm 1, \pm 2, \dots$. The residual opening at key locations, $x = b$ and $x = a$, is presented separately in plots (b), (d) and (f), as a function of the gap between adjacent proppant columns, $2(a - b)$. The average residual opening over $0 < x < b$, denoted by δ_1 , and over $b < x < a$, denoted by δ_2 , are also displayed on these plots. The parameters δ_1 and δ_2 correspond to the average proppant column height and the average channel opening, respectively.

The average column height, δ_1 was found to decrease only slightly with increasing gap between the proppant columns and this effect was most pronounced for $b = 50$ cm. The average channel opening, δ_2 decreased more rapidly with increase in the gap between columns. However, the dependence of the average channel opening on the width of the columns was less prominent. Comparing plots (b), (d) and (f), we find that the maximum permissible gap between the column, corresponding to $a = a^*$, increased by roughly 30% at $\sigma_0 = 10$ MPa and roughly 5% at $\sigma_0 = 50$ MPa, as the column width increased ten-fold from 50 cm to 5 m. This weak dependence is observed because the selected values of column width, $2b$ were much greater than the initial column height, δ_0 . A similar dependence was observed in previous studies dealing with the residual opening due to a single rigid inclusion.^{44,45}

The dependence of the cross-section area of the open channels on the gap between proppant columns is shown in Fig. 7. The channel cross-section area, A_c initially increases and reaches a maximum value before decreasing as the gap between the columns, $2(a - b)$, increases. The decrease in the cross-section area is due to the rapid decrease in average channel opening as the column spacing approaches its critical value $2a^*$. It should be noted that the column spacing $2a$ at which the cross-section area is maximised is not the optimal spacing. The optimal spacing is determined in the next section based on the calculations of the average fracture conductivity. As in the case of the channel residual opening before, the cross-sectional area of the channels depends weakly on the column width, provided that $2b \gg \delta_0$. The dependence of the channel cross-section area on the lateral stress is more pronounced.

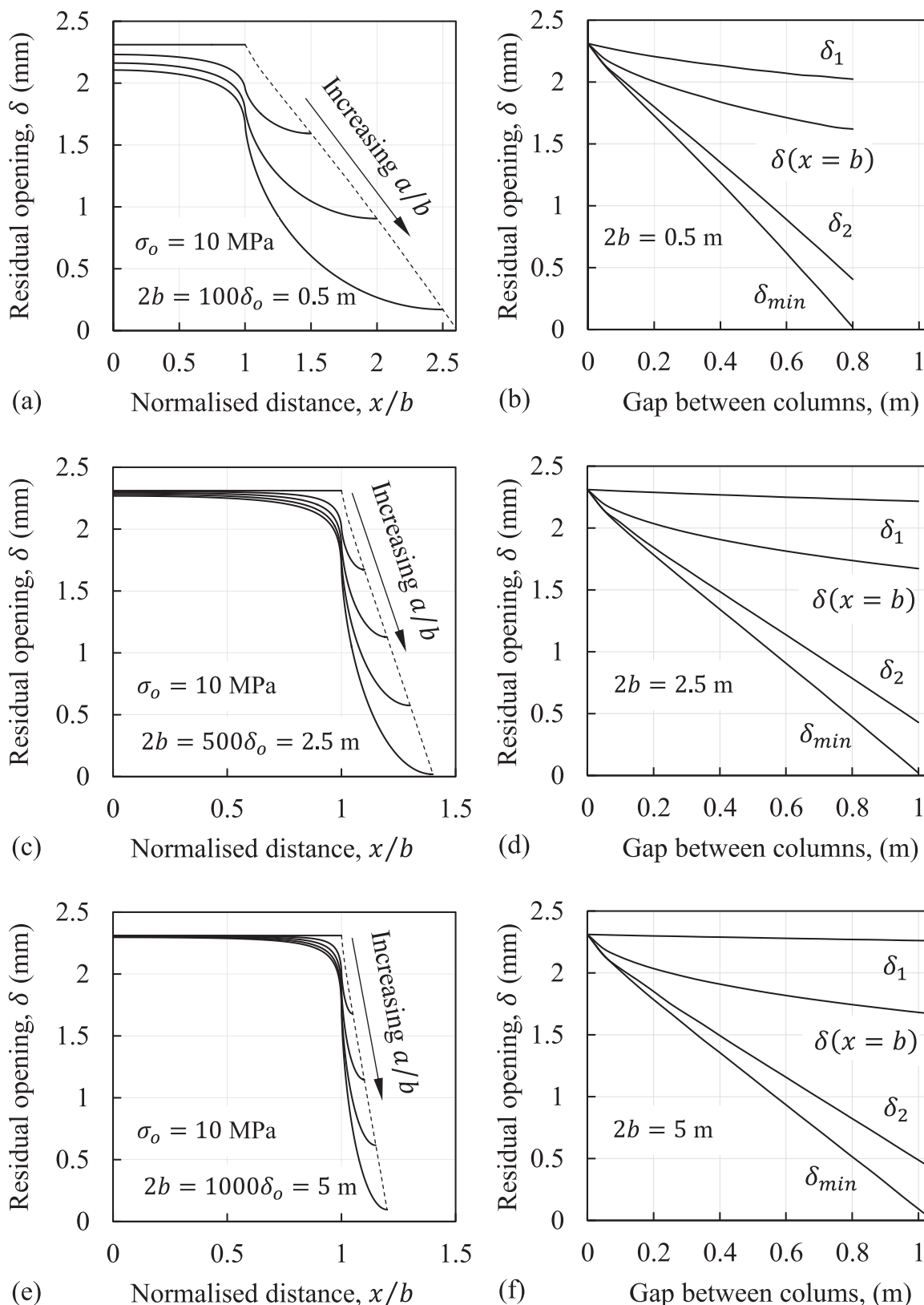


Fig. 5. Effect of the width of proppant columns and the gaps between them on the residual opening profile at a lateral in-situ stress of 10 MPa.

Increasing σ_o from 10 MPa to 50 MPa leads to an order of magnitude decrease in the channel cross-section area and roughly a five-fold decrease in the maximum permissible gap between columns.

4.2. Average conductivity of the fracture

Three key features of the fluid-flow in partially-filled fractures are: (1) the fluid flows through a two-phase medium, comprising of porous proppant columns alternating with open channels, (2) the fracture

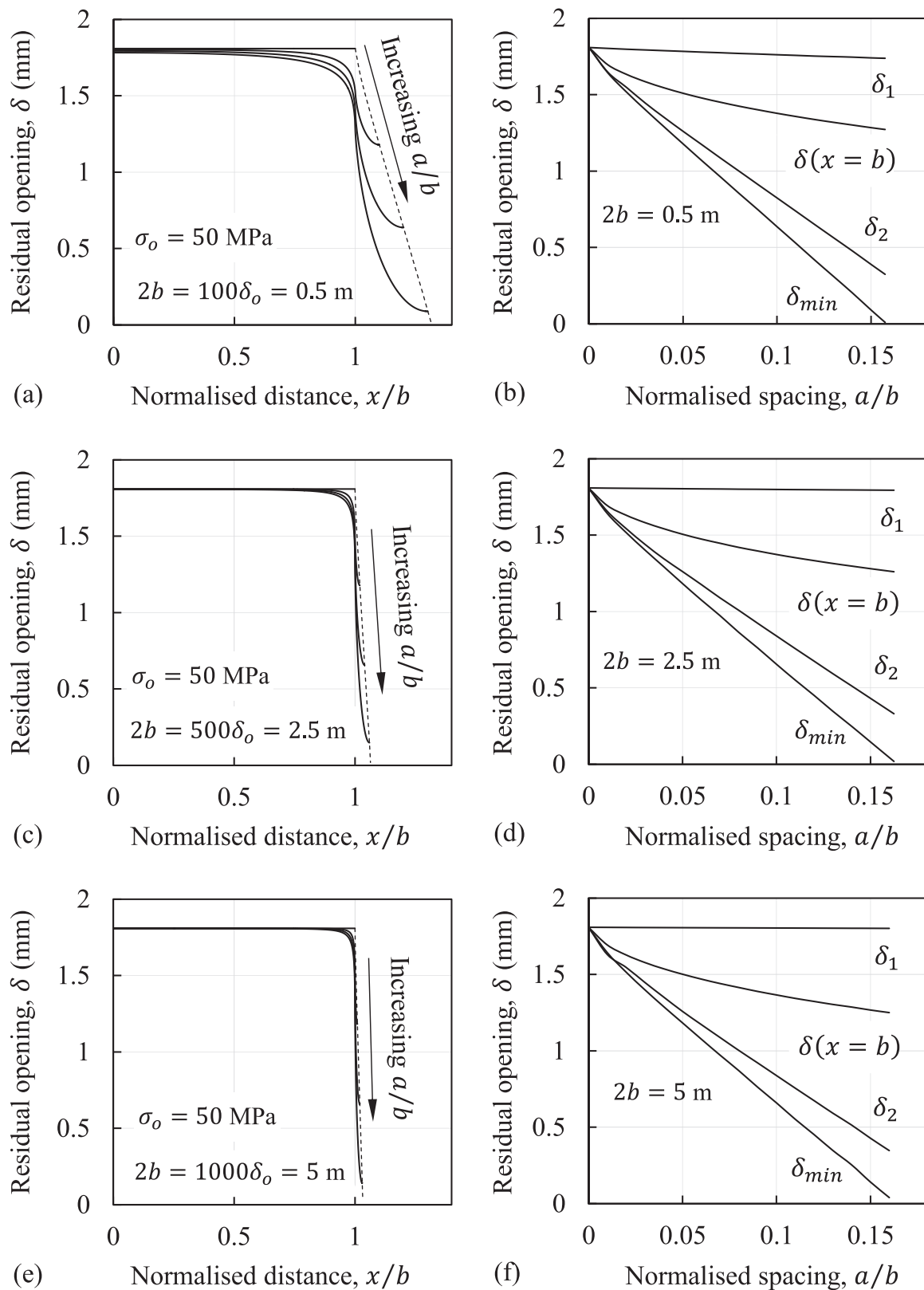


Fig. 6. Effect of the width of proppant columns and the gaps between them on the residual opening profile at a lateral in-situ stress of 50 MPa.

aperture varies along the fracture length, and (2) the local streamlines are not aligned with the global pressure gradient (see Fig. 1). The governing Navier-Stokes equations are not amenable to solution by means of analytical techniques for the problem under consideration; however, they can be simplified greatly if certain kinematic and

geometric conditions are satisfied. Provided that the viscous forces dominate the inertial forces and the fracture aperture does not vary abruptly,⁴⁶ which is generally the case for rock fractures, the flow in the open channels can be described by the Reynolds lubrication equation and the flow in the proppant columns can be described by Darcy's

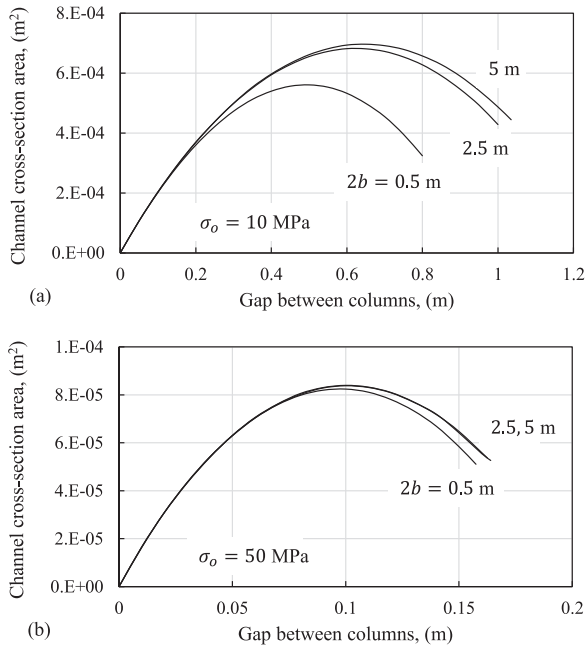


Fig. 7. Effect of the width of proppant columns and the gaps between them on the cross-section area of the open channels.

law.⁴⁶ The coupling of these equations and their upscaling from the fine scale (unit-cell) to the coarse scale (fracture) is still a challenging task, requiring the aid of numerical techniques such as the finite element method.¹⁸

Instead we provide an estimate for the effective fracture conductivity which lies between upper and lower bounds obtained in accordance with variational principles as follows^{47,48}

$$\langle 1/k \rangle^{-1} < k_{eff} < \langle k \rangle. \tag{34}$$

For a heterogeneous conductive medium, the lower bound, $\langle 1/k \rangle^{-1}$ corresponds to the situation in which all the conductive elements are arranged in series, whereas the upper bound, $\langle k \rangle$ corresponds to a parallel arrangement of the individual elements.⁴⁷ For the problem geometry shown in Fig. 2, these extreme cases correspond to one-dimensional fluid flow along the x -direction (along the fracture length) or z -direction (into the page), respectively.

In our problem, it is expected that at some points along the fracture,

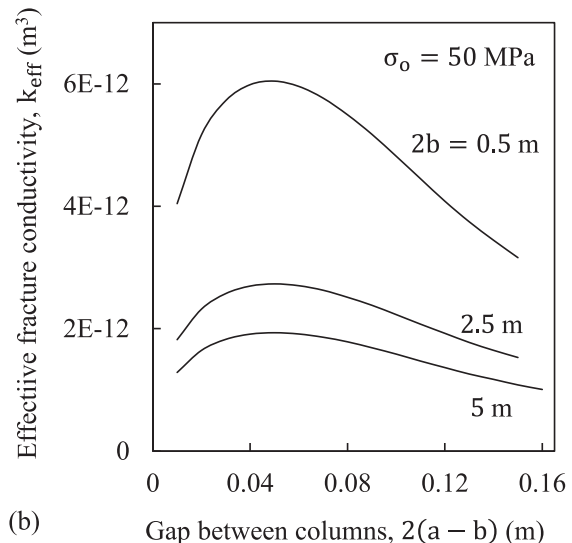
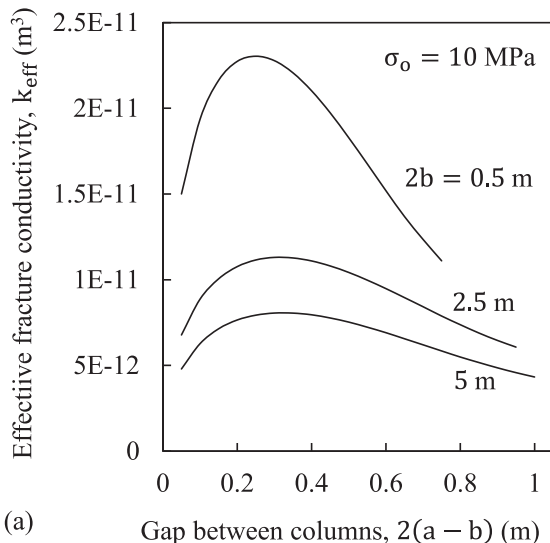


Fig. 8. Effect of the width of proppant columns and the gaps between them on the effective fracture conductivity.

the fluid will flow along the x -direction, whereas at other points, it will flow along the z -direction. As a result, the assumption of series (or parallel) arrangement of conductive elements would underestimate (or overestimate) the actual effective conductivity.⁴⁷ Hence, we estimate the effective conductivity of the fracture as the geometric mean of the upper and lower bounds, i.e.

$$k_{eff} = \sqrt{\langle 1/k \rangle^{-1} \langle k \rangle} \tag{35}$$

The above expression was obtained by Zimmerman et al.⁴⁷ who also showed that Eq. (35) provides similar estimates for the effective fracture conductivity as the geometric mean of the narrower Hashin-Shtrikman bounds.

The local conductivity at a point along the unit cell, k is defined in accordance with the Darcy and ‘cubic’ laws as follows⁴²

$$k(x) = \begin{cases} K_p \delta(x), & |x| < b, \\ \delta(x)^3, & b < |x| < a, \end{cases} \tag{36}$$

where K_p is the proppant column permeability and $\delta(x)$ is the residual opening profile of the fracture. The column permeability is considered to be constant along $|x| < b$ and its dependence on the compressive stress acting on the proppant column is neglected. This assumption does not introduce any significant error in the analysis since the permeability of typical proppant columns ($\sim 10^{-10} \text{ m}^2$) is already several order of magnitudes lower than the effective permeability of open channels, $\delta^2/12$ ($\sim 10^{-7} \text{ m}^2$ for $\delta = 1 \text{ mm}$).

Substituting Eq. (36) into (34) yields the lower (series) and upper (parallel) bounds for the fracture conductivity as follows:

$$\langle 1/k \rangle^{-1} = a \left(\int_0^b \frac{dx}{K_p \delta(x)} + \int_b^a \frac{dx}{\delta^3(x)} \right)^{-1}, \quad \langle k \rangle = \frac{1}{a} \left(\int_0^b K_p \delta(x) dx + \int_b^a \delta^3(x) dx \right). \tag{37}$$

The estimate for the effective fracture conductivity is obtained using (35) as

$$k_{eff} = \left[\left(\int_0^b K_p \delta(x) dx + \int_b^a \delta^3(x) dx \right) \left(\int_0^b \frac{dx}{K_p \delta(x)} + \int_b^a \frac{dx}{\delta^3(x)} \right) \right]^{\frac{1}{2}} \tag{38}$$

Results for k_{eff} vs. the gap between columns are presented in Fig. 8 for $K_p = 10^{-10} \text{ m}^2$. For this selected value of proppant column permeability, the maximum conductivity of a fully-filled fracture with an

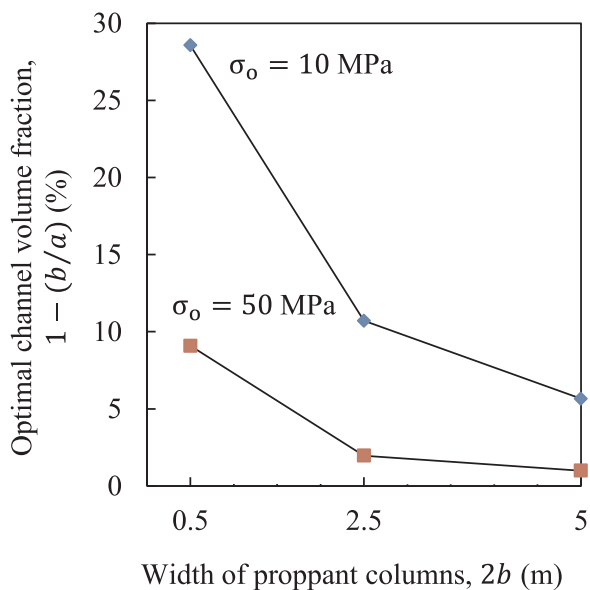


Fig. 9. Optimal values of the channel volume fraction under typical field conditions.

initial crack opening, $\delta_0 = 5$ mm is $K_p \delta_0 = 5 \times 10^{-13} \text{ m}^3$. In Fig. 8, the effective fracture conductivity of the partially-filled fractures was found to always exceed this value in the presence of open channels. At any given column spacing and stress, the effective fracture conductivity increased with decreasing column width, $2b$. Hence, it is desirable to minimise the column width, i.e. the relative time duration of the proppant-laded pulses, during the implementation of the channel-fracturing technique.

An optimal gap between the proppant columns is identified, for which the effective fracture conductivity is maximised. This optimal gap was found to depend weakly on the column width ($2b \gg \delta_0$), and significantly on the lateral in-situ stress. At $\sigma_0 = 10$ MPa, the optimal gap, $2(a - b)$ was roughly 0.3 m, which corresponds to $a/b = 1.5, 1.12$ and 1.06 at $2b = 0.5, 2.5$ and 5 m, respectively. At $\sigma_0 = 50$ MPa, this

optimal gap reduced to approximately 0.05 m, which corresponds to $a/b = 1.1, 1.02$ and 1.01 at $2b = 0.5, 2.5$ and 5 m, respectively. It becomes apparent that the columns need to be placed quite close to one another, especially at high levels of lateral in-situ stress. Fig. 9 shows the optimal volume fraction of the open channels (i.e. the amount of proppant saved) for the considered values of in-situ stress and column width.

An important governing parameter not considered so far in the parametric study is the Young's modulus of the rock, E . All previous calculations were performed for $E = 10$ GPa, which is a typical value for many oil/gas bearing rocks. Also, only two values of in-situ stress (10 MPa and 50 MPa) were considered. In Fig. 10, some main results are presented for Young's moduli of up to 50 GPa as well as for intermediate values of in-situ stress. In these calculations, the proppant column width $2b$ is taken as 1 m. From Fig. 10a it becomes apparent that optimal implementation of the channel fracturing technique, i.e. discontinuous proppant placement, may result in one to two orders of magnitude increase in the fracture fluid conductivity under a wide range of in-situ conditions. Fig. 10b shows that the reduction in proppant use arising from the optimal application of the channel fracturing technique can vary significantly, from a mere 5% ($\sigma_0 = 50$ MPa, $E = 10$ GPa) up to 50% ($\sigma_0 = 10$ MPa, $E = 50$ GPa).

It is important to reiterate that all of the above results have been obtained for specific values of the fitting parameters α and β (Fig. 4) and the effects of proppant embedment in the rock and lateral expansion of the proppant columns have been ignored. Hence, these results pertain to a specific type of proppant and serve as an 'upper limit' for the maximum achievable increase in fracture conductivity and reduction in proppant use by the discontinuous proppant placement.

4.3. Compressive stress induced in the proppant column

Aside from the fracture conductivity, another important consideration when selecting the proppant column spacing is the compressive stress induced in the proppant column. As the gap between the columns increases, the compressive stress acting on the columns increases, especially near the column edges. The additional compressive stresses may lead to localised effects, such as the embedment of proppant

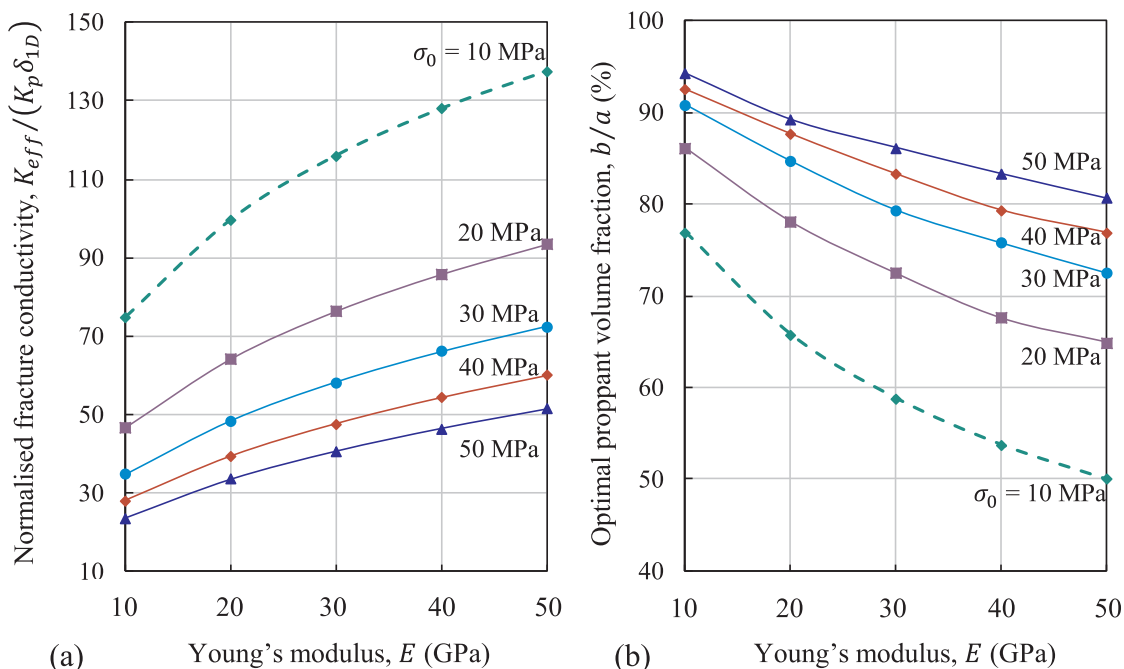


Fig. 10. (a) the dependence of maximum effective conductivity on Young's modulus and in-situ stress. The case of $K_{eff}/(K_p \delta_{1D}) = 1$ corresponds to fully-propped fracture; (b) the dependence of optimal proppant volume fraction on Young's modulus and in-situ stress. The case of $b/a^* = 100\%$ corresponds to fully-propped fracture.

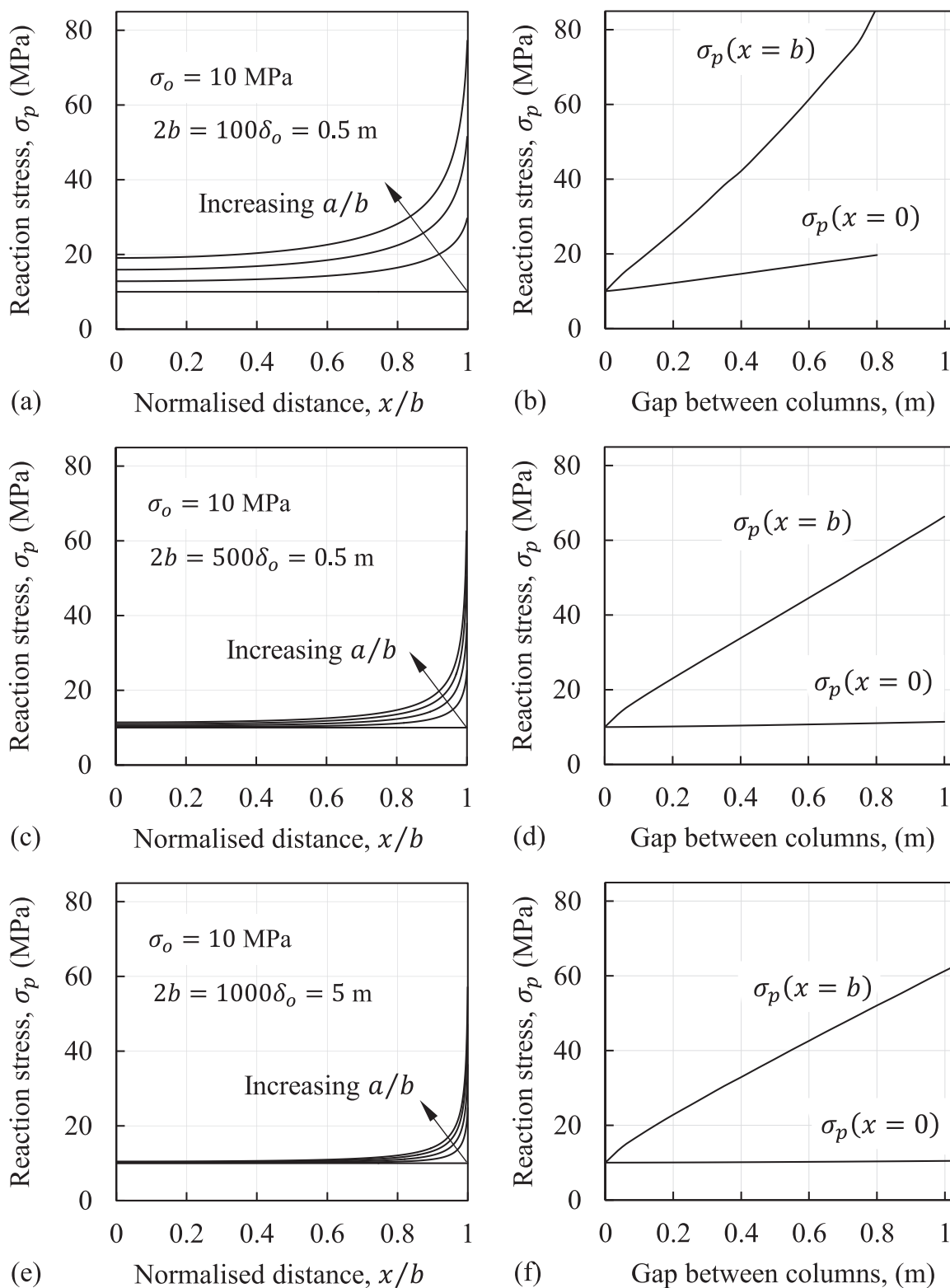


Fig. 11. Effect of the width of proppant columns and the gaps between them on the proppant reaction stress at a lateral in-situ stress of 10 MPa.

particles in the rock, or more severe effects, such as the collapse of the columns. We do not try to incorporate these effects into our model, but simply provide numerical results for the stress distribution in the proppant columns.

The compressive stress induced in the proppant column, $\sigma_p(x)$ is related to the residual opening $\delta(x)$ along the column width $|x| < b$ according to Eq. (24). The variation of $\sigma_p(x)$ along the normalised column

width, x/b , is shown in Figs. 11 and 12. For a fully filled fracture, i.e. $a = b$, the reaction stress in the proppant pack is equal to the lateral in-situ stress σ_o and remains constant along the length of the fracture. As the gap between the columns, $2(a - b)$ increases, the reaction stress σ_p increases non-uniformly along the width of the column. The greatest increase occurs at the edges of the column, $|x| = b$ and the smallest increase occurs at the center of the column, i.e. $x = 0$. The distribution

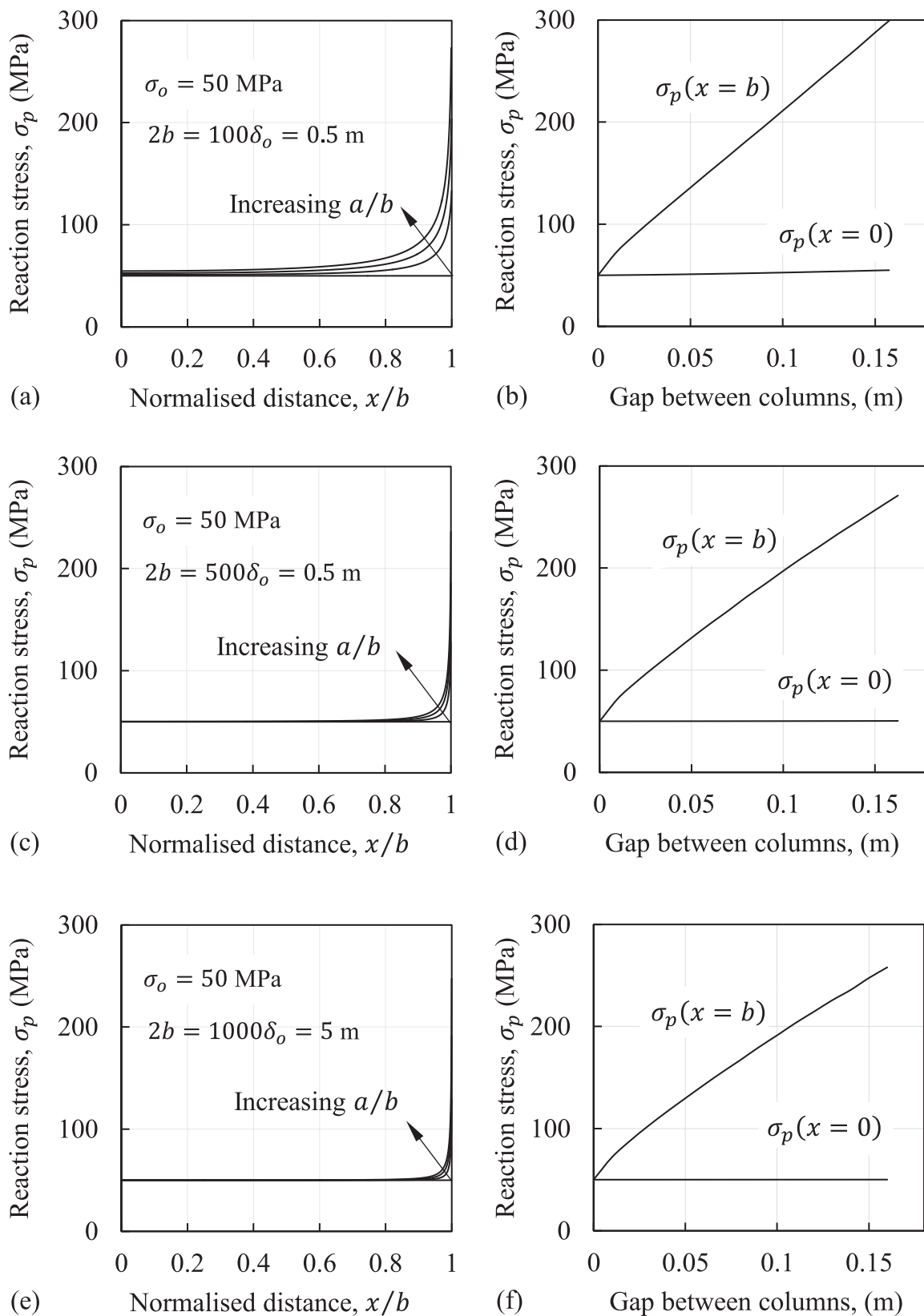


Fig. 12. Effect of the width of proppant columns and the gaps between them on the proppant reaction stress at a lateral in-situ stress of 50 MPa.

of the reaction stress is such that the average value $\sigma_{p,avg} = \sigma_o a/b$, i.e. the equilibrium condition (33) is satisfied.

The numerical values for the maximum compressive stress in the proppant pack at the optimal column spacing are provided in Table 2

The maximum stress in the proppant pack is found to be roughly 2.5 times greater than lateral in-situ stress based on the present calculations. Hence, localised effects, such as proppant crushing or embedment, would be more prominent near the column edges.

Table 2

Ratio of the maximum to average compressive stress in the proppant pack at the critical column spacing $2a^*$.

$2b$ (m)	$\sigma_0 = 10$ MPa			$\sigma_0 = 50$ MPa		
	$2(a_{opt}-b)$ (m)	a_{opt}/b	$\sigma_p(x=b)$ (MPa)	$2(a_{opt}-b)$ (m)	a_{opt}/b	$\sigma_p(x=b)$ (MPa)
0.5	0.25	1.40	25.88	0.05	1.10	135.8
2.5	0.3	1.12	28.46	0.05	1.02	131.6
5.0	0.3	1.06	27.93	0.05	1.01	129.7

5. Conclusion

A simplified theoretical model was developed to obtain optimal estimates for the residual opening and effective conductivity of partially-filled fractures created using the channel fracturing technique. The key strength of the model lies in the use of an experimentally calibrated ‘traction law’ to accurately capture the compressive behaviour of fiber-laden proppant columns, in contrast with previous studies, which assume the column to be linearly elastic and hence over-estimate the residual opening of the fractures.^{18–20} The resulting non-linear problem is formulated using DDT, and an efficient numerical solution procedure is developed to solve the governing equations. A method for estimating the effective conductivity of the 3D fracture geometry from the residual opening profile of the 2D unit cell is also presented.

Detailed numerical results are presented for the fracture residual opening, effective fracture conductivity and reaction stress in the proppant column. The obtained results are for one particular type of proppant (fiber-laden 20/40 mesh ceramic) and are based on several simplifying assumptions. Effects of proppant embedment and lateral expansion of proppant columns can be incorporated to further improve the developed approach. The main significance of the present results lies in the qualitative trends which may guide engineers in the optimal implementation of the channel fracturing technique. It is recommended to minimise the column width, i.e. the relative duration of the proppant-laden pulse during the injection stage of the fracturing treatment. It is also recommended to account for high compressive stresses near the column edges during the design stage of the fracturing treatment. The developed approach can be readily extended towards the analysis of hydraulic fractures in multilayered reservoirs.⁴⁹

References

- Valko P, Economides MJ. *Hydraulic fracture mechanics*. Chichester: Wiley; 1995.
- Barree RD, Cox SA, Barree VL, Conway MW. Realistic assessment of proppant pack conductivity for material selection. *SPE*. 2003;84306<http://dx.doi.org/10.2118/84306-MS>.
- Weaver JD, van Batenburg DW, Parker MA, Nguyen PD. Sustaining conductivity. *SPE*. 2006;98236<http://dx.doi.org/10.2118/98236-MS>.
- Wen Q, Zhang S, Wang L, Liu Y, Li X. The effect of proppant embedment upon the long-term conductivity of fractures. *J Pet Sci Eng*. 2007;55:221–227. <http://dx.doi.org/10.1016/j.petrol.2006.08.010>.
- Reinicke A, Rybacki E, Stanchits S, Huenges E, Dresen G. Hydraulic fracturing stimulation techniques and formation damage mechanisms—Implications from laboratory testing of tight sandstone-proppant systems. *Chem Erde*. 2010;70:107–117. <http://dx.doi.org/10.1016/j.chemer.2010.05.016>.
- Liang F, Sayed M, Al-Muntasheri GA, Chang FF, Li L. A comprehensive review on proppant technologies. *Petroleum*. 2016;2:26–39. <http://dx.doi.org/10.1016/j.petim.2015.11.001>.
- Tinsley JM, Williams Jr JR. A new method for providing increased fracture conductivity and improving stimulation results. *J Pet Technol*. 1975;27:1319–1325. <http://dx.doi.org/10.2118/4676-PA>.
- Inyang UA, Nguyen PD, Cortez J. Development and field applications of highly conductive proppant-free channel fracturing method. *SPE*. 2014;168996<http://dx.doi.org/10.2118/168996-MS>.
- Barasia A, Pankaj P. Tail-in proppant and its importance in channel fracturing technique. *SPE*. 2014;169227<http://dx.doi.org/10.2118/169227-MS>.
- Malhotra S, Lehman ER, Sharma MM. Proppant placement using alternate-slug fracturing. *SPE J*. 2014;19:974–985. <http://dx.doi.org/10.2118/163851-PA>.
- Medvedev A, Yudina K, Panga MK, Kraemer CC, Pena A. On the mechanisms of channel fracturing. *SPE*. 2013;163836<http://dx.doi.org/10.2118/163836-MS>.

- Khanna A, Keshavarz A, Mobbs K, Davis M, Bedrikovetsky P. Stimulation of the natural fracture system by graded proppant injection. *J Pet Sci Eng*. 2013;111:71–77. <http://dx.doi.org/10.1016/j.petrol.2013.07.004>.
- Khanna A, Kotousov A, Sobey J, Weller P. Conductivity of narrow fractures filled with a proppant monolayer. *J Pet Sci Eng*. 2013;100:9–13. <http://dx.doi.org/10.1016/j.petrol.2012.11.016>.
- Bedrikovetsky PG, Keshavarz A, Khanna A, McKenzie KM, Kotousov A. Stimulation of natural cleats for gas production from coal beds by graded proppant injection. *SPE*. 2012;158761<http://dx.doi.org/10.2118/158761-MS>.
- Khanna A, Kotousov A. Controlling the height of multiple hydraulic fractures in layered media. *SPE J*. 2016;21:256–263. <http://dx.doi.org/10.2118/176017-PA>.
- Gillard M, Medvedev O, Pena A, Medvedev A, Penacorada F, d'Huteau E. A new approach to generating fracture conductivity. *SPE*. 2010;135034<http://dx.doi.org/10.2118/135034-MS>.
- d'Huteau E, Gillard M, Miller M, et al. Open-channel fracturing - a fast track to production. *Oilfield Rev*. 2011;23:4–17 [Retrieved from:]. https://www.slb.com/resources/publications/industry_articles/oilfield_review/2011/or2011_chaut01_open.aspx.
- Yan X, Huang Z, Yao J, Song W, Li Y, Gong L. Theoretical analysis of fracture conductivity created by the channel fracturing technique. *J Nat Gas Sci Eng*. 2016;31:320–330. <http://dx.doi.org/10.1016/j.jngse.2016.03.038>.
- Hou T, Zhang S, Yu B, Lv X, Zhang J, Han J, Li D. Theoretical Analysis and Experimental Research of Channel Fracturing in Unconventional Reservoir. *SPE-180105-MS*, 2016. <http://dx.doi.org/10.2118/180105-MS>.
- Hou B, Zheng X, Chen M, Ye Z, Chen D. Parameter simulation and optimization in channel fracturing. *J Nat Gas Sci Eng*. 2016;35(A):122–130. <http://dx.doi.org/10.1016/j.jngse.2016.08.046>.
- Milton-Taylor D, Stephenson C, Asgian MI. Factors affecting the stability of proppant in propped fractures: results of a laboratory study. *SPE*. 1992;24821<http://dx.doi.org/10.2118/24821-MS>.
- Asgian MI, Cundall PA, Brady BH. Mechanical stability of propped hydraulic fractures: a numerical study. *J Pet Tech*. 1995;47:203–208. <http://dx.doi.org/10.2118/28510-PA>.
- Romero J, Feraud JP. Stability of proppant pack reinforced with fiber for proppant flowback control. *SPE*. 1996;31093<http://dx.doi.org/10.2118/31093-MS>.
- Burukhin AA, Kalinin S, Abott J, et al. Novel interconnected bonded structure enhances proppant flowback control. *SPE*. 2012;151861<http://dx.doi.org/10.2118/151861-MS>.
- Nguyen PD, Weaver JD, Parker MA, King DG. Thermoplastic film prevents proppant flowback. *Oil Gas J*. 1996;94:60–62.
- Weaver J, Baker J, Woolverton S, Parker M. Application of surface-modification agent in wells with high flow rates. *SPE*. 1999;53923<http://dx.doi.org/10.2118/53923-MS>.
- Sinclair AR, Graham JW, Sinclair CP. Improved well stimulation with resin-coated Proppants. *SPE*. 1993;11579<http://dx.doi.org/10.2118/11579-MS>.
- Mesri G, Vardhanabhuti B. Compression of granular materials. *Can Geotech J*. 2009;46:369–392. <http://dx.doi.org/10.1139/T08-123>.
- Roberts JE, de Souza JM. The compressibility of sands. *Proc Am Soc Test Mater*. 1958;58:1269–1272.
- Hardin BO. Crushing of soil particles. *J Geotech Geoenviron Eng*. 1985;10:1177–1192. [http://dx.doi.org/10.1061/\(ASCE\)0733-9410\(1985\)111:10\(1177\)](http://dx.doi.org/10.1061/(ASCE)0733-9410(1985)111:10(1177)).
- Coop MR. The mechanics of uncemented carbonate sands. *Geotechnique*. 1990;40:607–626. <http://dx.doi.org/10.1680/geot.1990.40.4.607>.
- Pestana JM, Whittle AJ. Compression model for cohesionless soils. *Geotechnique*. 1995;45:611–631. <http://dx.doi.org/10.1680/geot.1995.45.4.611>.
- Bilby BA, Cottrell AH, Swinden KH. The spread of plastic yield from a notch. *Proc R Soc Lond Ser A*. 1963;272:304–314. <http://dx.doi.org/10.1098/rspa.1963.0055>.
- Bilby B, Eshelby J. Dislocations and the theory of fracture. In: Liebowitz H, ed. *Fracture: An Advanced Treatise*. 1. New York: Academic Press; 1968:99–182.
- Hirth JP, Lothe J. *Theory of dislocations*. New York: McGraw-Hill; 1968.
- Hills DA, Kelly PA, Dai DN, Korsunsky AM. *Solution of crack problems: the distributed dislocation technique*. Dordrecht: Kluwer Academic Publishers; 1996.
- Kotousov A, Bortolan Neto L, Khanna A. On a rigid inclusion pressed between two elastic half spaces. *Mech Mater*. 2014;68:38–44. <http://dx.doi.org/10.1016/j.mechmat.2013.08.004>.
- Cox BN, Rose LRF. A self-consistent approximation for crack bridging by elastic/perfectly plastic ligaments. *Mech Mater*. 1996;22:249–263. [http://dx.doi.org/10.1016/0167-6636\(95\)00025-9](http://dx.doi.org/10.1016/0167-6636(95)00025-9).
- Khanna A, Kotousov A. Stress analysis of a crack in a fiber-reinforced layered composite. *Compos Struct*. 2014;118:139–148. <http://dx.doi.org/10.1016/j.compstruct.2014.07.024>.
- Erdogan F, Gupta GD, Cook TS, Sih GC, ed. *Leyden: Noordhoff International*; 1973:368–425. Numerical solution of singular integral equations, in *Mechanics of Fracture*; 1.
- Bortolan Neto L, Khanna A, Kotousov A. Conductivity and performance of hydraulic fractures partially filled with compressible proppant packs. *Int J Rock Mech Min Sci*. 2015;74:1–9. <http://dx.doi.org/10.1016/j.ijrmm.2014.11.005>.
- Witherspoon PA, Wang JSY, Iwai K, Gale JE. Validity of cubic law for fluid flow in a deformable rock fracture. *Water Resour Res*. 1980;16:1016–1024. <http://dx.doi.org/10.1029/WR016i006p01016>.
- Zimmerman RW, Yeo IW. Fluid flow in rock fractures: from the navier-stokes equations to the cubic law. *Dyn Fluids Fract Rock*. 2000:213–224. <http://dx.doi.org/10.1029/GM122>.
- Selvadurai APS. A unilateral contact problem for a rigid disc inclusion embedded between two dissimilar elastic half-spaces. *Q J Mech Appl Math*. 1994;47:493–510. <http://dx.doi.org/10.1093/qjmam/47.3.493>.

45. Khanna A, Bortolan Neto L, Kotousov A. Effect of residual opening on the inflow performance of a hydraulic fracture. *Int J Eng Sci.* 2014;74:80–90. <http://dx.doi.org/10.1016/j.ijengsci.2013.08.012>.
46. Zimmerman RW, Bodvarsson GS. Hydraulic conductivity of rock fractures. *Transp Porous Media.* 1996;23:1–30. <http://dx.doi.org/10.1007/BF00145263>.
47. Zimmerman RW, Kumar S, Bodvarsson GS. Lubrication theory analysis of the permeability of rough-walled fractures. *Int J Rock Mech Min Sci Geomech Abstr.* 1991;28:325–331. [http://dx.doi.org/10.1016/0148-9062\(91\)90597-F](http://dx.doi.org/10.1016/0148-9062(91)90597-F).
48. Zimmerman RW, Bodvarsson GS. Effective transmissivity of two-dimensional fracture networks. *Int J Rock Mech Min Sci Geomech Abstr.* 1996;33:433–438. [http://dx.doi.org/10.1016/0148-9062\(95\)00067-4](http://dx.doi.org/10.1016/0148-9062(95)00067-4).
49. Khanna A, Kotousov A. The stress field due to an interfacial edge dislocation in a multi-layered medium. *Int J Solids Struct.* 2015;72:1–10. <http://dx.doi.org/10.1016/j.ijsolstr.2015.06.030>.

Chapter 5

Optimisation of proppant use in the application
of the channel fracturing technique

ISBN 978-1-925627-02-2

Optimisation of proppant use in the application of the channel fracturing technique

Hao Luong¹

¹ School of Mechanical Engineering, The University of Adelaide
SA 5005, Australia

E-mail: hao.luong@adelaide.edu.au

Abstract: *The channel fracturing technique is a recent development in the area of hydraulic fracturing which allows for discontinuous proppant placement within the fracture. The discontinuous placement results in a network of interconnected open channels within the fracture, which can significantly enhance the efficacy of fluid conductivity in the fracture. The purpose of this article is to investigate the optimal usage of the proppant in order to maximise the efficacy of the fracture conductivity. To this end, the study utilises a mathematical model to describe the effects of the mechanical properties of the rock and the proppant assembly, the magnitude of the compressive in-situ stresses and the arrangement of the proppant columns in the partially-filled fracture, upon its residual opening and effective conductivity. Mechanisms including the elastic deformation of the rock, the non-linear consolidation of the proppant assembly and the indentation of the fracture rock by proppant particles are considered. The numerical results provide estimates for the increase in fracture conductivity and decrease in proppant use under realistic conditions. In particular, attention is focused on rocks with high Young's modulus and hardness, which are ideal candidates for the channel fracturing technique.*

Keywords: *Channel fracturing, fracture opening, optimal proppant usage, proppant deformation, proppant arrangement, fracture conductivity.*

1. INTRODUCTION

Proppant packs play the dual role of providing mechanical support and a pathway for fluid flow within a fracture. [1] However, several damage mechanisms lead to the plugging of the pore space of the proppant pack, and impair the permeability of the proppant-pack in practice. [2] Attempts to counteract these damage mechanisms and improve the proppant pack permeability generally increase the cost of the fracturing treatment. An alternative and cost-effective solution is to decouple the load bearing task of the proppant pack from that of providing a fluid pathway. Such a decoupling is achieved by discontinuous proppant placement within the fracture, with the intent of creating a stable network of open channels within the hydraulic fracture. [3-6] Discontinuous proppant placement may also result in cost savings, especially in the case of large fracturing jobs requiring several hundred tons of proppant to be placed within the fracture.

Non-uniform proppant placement is achieved by injecting proppant-laden fluids into the fracture in short pulses that are alternated with pulses of proppant-free fluid. [7,8] Fibers or agglomerating gels are added throughout the operation to mitigate the dispersion of the proppant-laden pulses as they travel through the surface equipment, along the wellbore and within the fracture. [9,10] Although the idea of discontinuous proppant placement was proposed in the early days of hydraulic fracturing, [3] the technique has only recently been adopted in practice. Current research efforts in the area are mainly directed towards the development of technologies and engineering practices necessary for the field application of this technique. [11] Limited attention has been paid to the mathematical modelling of the conductivity enhancing mechanisms in the channel fracturing technique. [12-15]

The aim of the present article is to investigate the influences of mechanical properties of rock layer and proppant assembly, compressive in-situ stress, and proppant placement on the residual opening and effective conductivity of the fracture. From the results, an optimal proppant usage to maximise the effective conductivity is identified.

2. PROBLEM FORMULATION

The problem of a hydraulic fracture created in a homogeneous, elastic, and isotropic rock is considered. For simplicity, the problem geometry is idealised as two dimensional and the proppant placement within the fracture is presumed to be uniform (Fig. 1). The in-situ stress σ_0 normal to the fracture length is balanced by normal stress $\sigma_p(x)$ generated from the proppant columns. Since the length of the fracture, $2L$, is significantly greater than column width, $2b$, and the column spacing, $2a$, the problem geometry can be considered to be periodic, and the representative unit cell is shown in Fig. 1b. Due to the compressibility of the proppant, the residual opening of the fracture, $\delta(x)$, is smaller than the initial crack opening, δ_0 , during fluid injection. The reduction of the crack opening due to embedment is neglected.

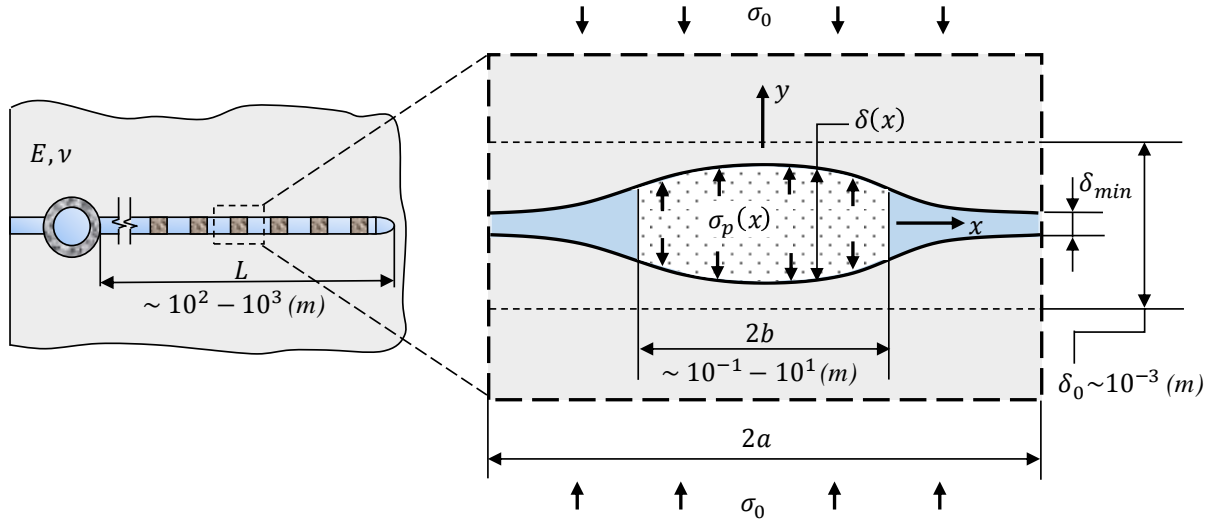


Figure 1 - (a) 2D fracture geometry with discontinuous proppant placement; (b) unit-cell showing the residual opening of the partially-filled fracture.

The deformation or consolidation of proppant columns is considered to be uniaxial. The stiffness and strength of proppant particles is quite high, therefore the consolidation of the proppant columns is largely achieved through particle rearrangement. The mechanical response of the proppant pack is described by an empirical model, whereby the compressive stress generated by the proppant columns, σ_p , is related to the column height, δ , through the following power-law relationship, [16]

$$\sigma_p = \sigma_{p0} \alpha \left(\frac{\lambda}{1 - \lambda} \right)^\beta, \quad (1)$$

where σ_{p0} is the multiplicative constant with the units of stress, α and β are the fitting parameters, and λ is the settlement ratio.

$$\lambda = \frac{(\delta_0 - \delta)}{\delta_0}, \quad (2)$$

where δ_0 is the initial height of the proppant column at unloaded conditions, and δ is the proppant column height at the compressive stress σ_p . The value of λ lies in the interval $[0, 1)$.

3. MATHEMATICAL MODEL

3.1. Residual opening profile

The crack problem shown in Fig. 1b can be formulated in the framework of the distributed dislocation technique, and the crack opening can be represented by a continuous distribution of edge

dislocations. The stress field induced by a single edge dislocation in an infinite body serves as the Green's function for obtaining the stress field induced by the continuous edge dislocations and it only remains to distribute the dislocations in a manner that the traction boundary conditions along the crack line and at infinity are satisfied. After some standard algebraic manipulations, the governing integral equation for the dislocation density can be obtained as [16,17]:

$$\frac{\bar{E}}{4\pi} \int_0^a B_y(\xi) \left[\frac{2\xi}{x^2 - \xi^2} + K(x, \xi) \right] d\xi = \sigma_0 - \sigma_p(x)H(b - |x|), \quad 0 < x < a, \quad (3)$$

where $H(\cdot)$ is the Heaviside step function, \bar{E} is the generalised plane strain (stress) Young's modulus, and the kernel $K(x, \xi)$ is given as

$$K(x, \xi) = \sum_{n=1}^{\infty} \frac{4\xi(x^2 - \xi^2 + 4a^2n^2)}{\{(x - \xi)^2 - 4a^2n^2\}\{(x + \xi)^2 - 4a^2n^2\}}. \quad (4)$$

The relationship between dislocation density, $B_y(\xi)$, and crack opening at any point, $\delta(x)$, is given according to [18,19]

$$\delta(x) = \delta_{\min} + \int_x^a B_y(\xi) d\xi, \quad B_y(\xi) = \frac{d\delta(\xi)}{d\xi}, \quad 0 < x < a. \quad (5)$$

By substituting (2) into (1), the dependence of proppant reaction stress on crack opening can be obtained as

$$\sigma_p(x) = \sigma_{p0} \alpha \left(\frac{\delta_0}{\delta(x)} - 1 \right)^\beta \quad (6)$$

The solution to the governing integral equation (3) yields the unknown dislocation density function, and the residual opening profile and proppant reaction stress can then be determined from Eqs. (5) and (6), respectively. The Gauss-Chebyshev quadrature technique is used to discretise the integral Eq. (3) into a system of non-linear algebraic equations, and the resulting equations are solved using the Newton-Raphson method. Details of the numerical solution procedure are provided elsewhere. [20,21]

3.2. Effective fracture conductivity

The effective conductivity of the partially-filled fracture can be estimated to lie between the lower and upper bounds based on variational principles [22,23]:

$$\left[\frac{1}{k} \right] < k_{\text{eff}} < [k]. \quad (7)$$

With reference to Fig. 1, the lower bound $[1/k]$ corresponds to one-dimensional flow along the x -direction (along the fracture length), and the upper bound, $[k]$ corresponds to one-dimensional flow in the z -direction (into the page). In other words, the lower bound corresponds to the case when the conductive elements (open channels and proppant columns) are arranged in series, and the upper bound corresponds to the conductive elements arranged in parallel. The effective fracture conductivity is expected to lie between these two bounds and was estimated as the geometric mean of the lower and the upper bounds, [22,23] i.e.

$$k_{\text{eff}} = \sqrt{\left[\frac{1}{k} \right] [k]}. \quad (8)$$

The local conductivity of a point along the fracture depends on its position within the fracture. The flow in the open channels can be described by the Reynolds lubrication equation and the flow in the proppant columns can be described by Darcy's law. [24] Hence,

$$k(x) = \begin{cases} K_p \delta(x), & 0 < |x| < b \\ \delta(x)^3, & b < |x| < a \end{cases} \quad (9)$$

where K_p is permeability of the proppant column and $\delta(x)$ is residual opening profile of the fracture.

4. RESULTS AND DISCUSSION

The influence of proppant column spacing, Young's modulus of rock mass, and in-situ stress on residual opening profile and conductivity of the partially-filled fracture are investigated via numerical calculations. The governed parameters for the calculation are selected and presented in Table 1. Throughout the calculation, $b, \delta_0, \alpha, \beta,$ and σ_{p0} are kept fixed while proppant column space is incremented until the minimum channel opening approaches zero. For each column space increment, the residual opening profile and the conductivity are calculated. The calculations are performed for the combination of five values of Young's modulus with five values of lateral in-situ stress.

Table 1: Selected values of governing parameters for the numerical calculations

Parameter	Value	Unit
Proppant column width, $2b$	1	m
Initial fracture opening, δ_0	5	mm
In-situ lateral (closure) stress, σ_0	10, 20, 30, 40, 50	MPa
Generalised Young's modulus, E	10, 20, 30, 40, 50	GPa
Fitting parameters for the proppant consolidation model		
σ_p	1	MPa
α, β	5.543, 3.873	—

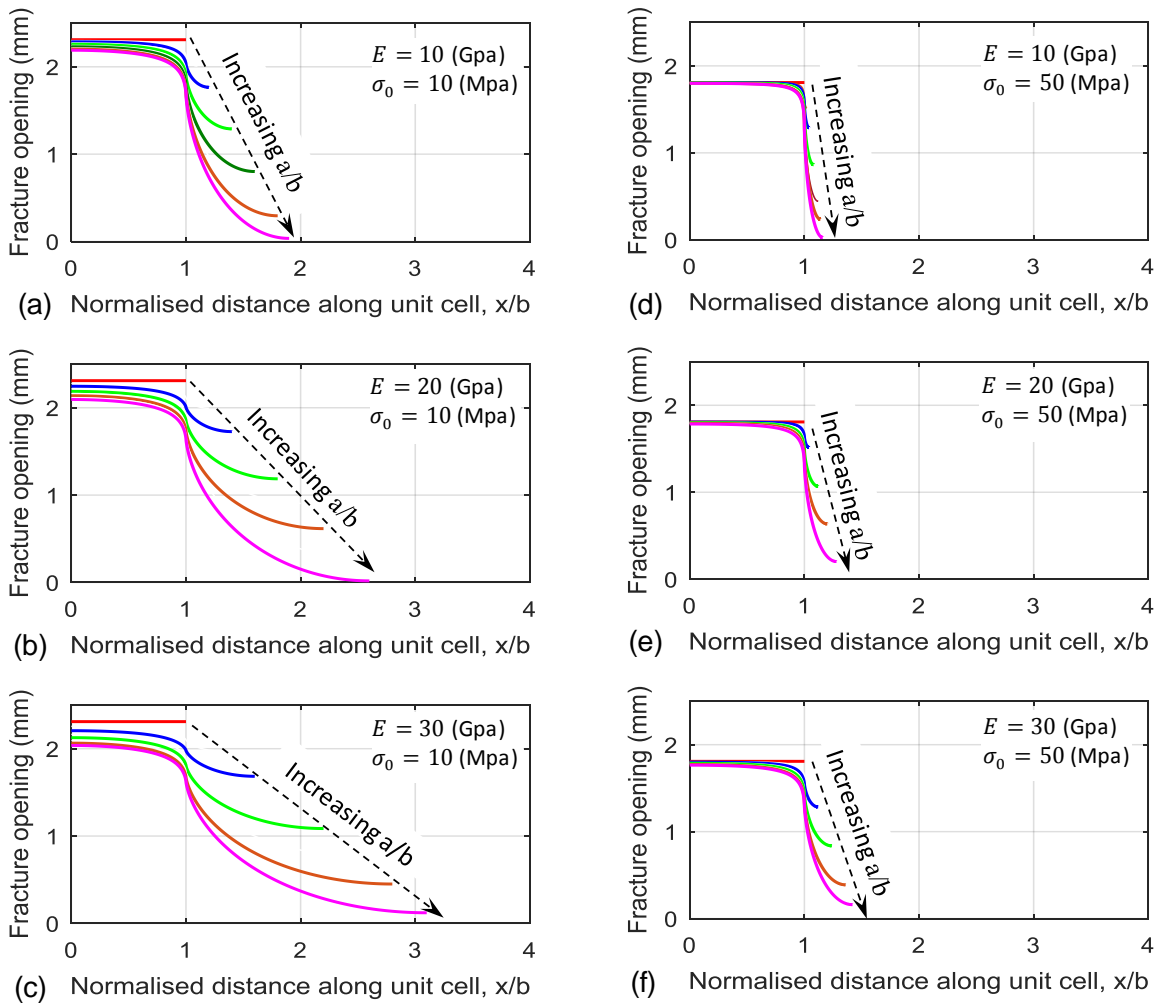


Figure 2 – The variation of residual opening of the unit cell with increase in column spacing. Plots (a)-(c) correspond to an in-situ stress of 10 MPa and plots (d)-(f) correspond to a stress of 50 MPa.

The dependence of residual opening profile on the Young's modulus of the rock mass and compressive in-situ stress is shown in Fig. 2. The residual opening of a unit cell is investigated by

gradually increasing proppant column space from fully-filled fracture, $a = b$, until the minimum residual opening of the fracture reaches close to zero at $x = a$. Under the fixed in-situ stress, it is observed that a higher value of Young's modulus results in a larger residual opening as well as a larger maximum permissible column spacing. Also, at a high level of stress, $\sigma_0 = 50 \text{ MPa}$, the rock mass and proppant column suffer an extensive deformation which leads to a significant decrease in both the residual opening and the maximum column space in comparison to those at a low stress, $\sigma_0 = 10 \text{ MPa}$.

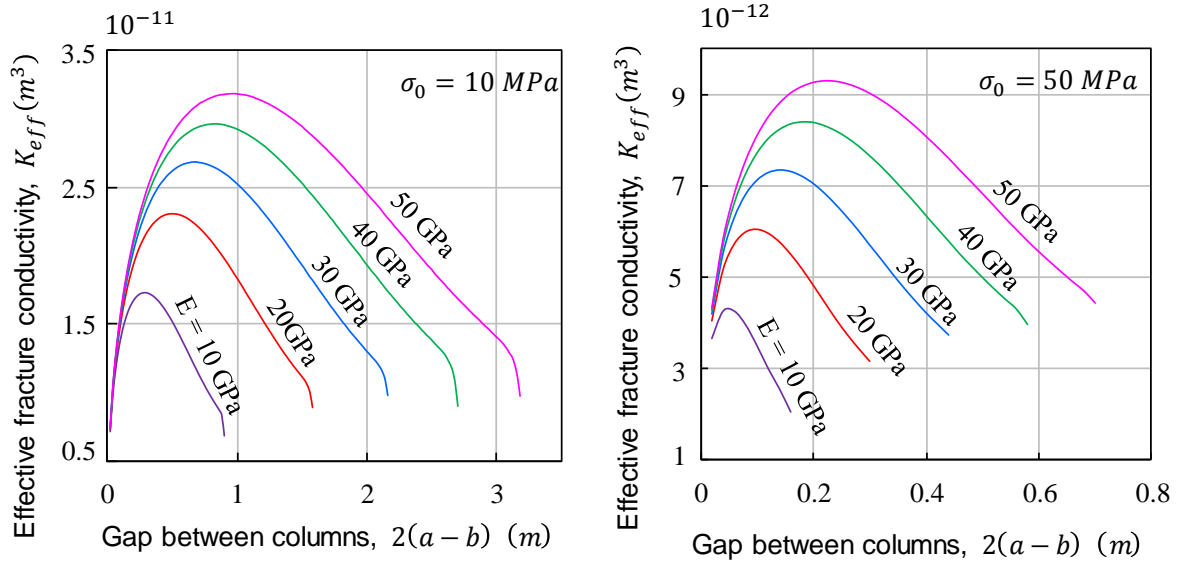


Figure 3 – The variation of effective fracture conductivity with the increasing gap between columns.

The dependence of effective conductivity on the strength of the rock mass and compressive in-situ stress is presented in Fig. 3. With the selected proppant permeability $K_p = 10^{-12} \text{ (m}^2\text{)}$, the calculated conductivity in fully-filled fracture, $K_p \delta_0 = 5 \times 10^{-13} \text{ (m}^3\text{)}$, is always lower than that that of a partially-filled fracture. At any column spacing and compressive stress, the effective conductivity increases with the increase of Young's modulus. The reverse effect is observed in the case of increase in the in-situ stress. An increase of stress from $\sigma_0 = 10 \text{ MPa}$ to 50 MPa , results in a roughly three times decrease in the effective fracture conductivity. Most notably, the optimal gap or spacing between columns is strongly affected by the magnitude of the in-situ stress.

The maximum effective conductivity in partially-filled fracture containing open-channels greatly exceeds the conductivity in fully-filled fracture, and the comparison between these two cases is presented in Fig. 4a. At a low level of stress $\sigma_0 = 10 \text{ MPa}$, the ratio between the maximum effective conductivity in partially-filled fracture and full-filled fracture $K_{\text{eff-max}} / (K_p \delta_0)$ increases from 74.8 to 138 with the increase of E from 10 GPa to 50 GPa . This ratio is lower at a higher in-situ stress. At a high level of stress, $\sigma_0 = 50 \text{ MPa}$, the ratio lies in a range from 23.5 to 51.4 according to increasing $E = 10 \text{ GPa}$ to 50 GPa .

At each set of Young's modulus and lateral in-situ stress, an optimal column spacing $2a^*$, which maximises the effective conductivity, can be defined. The ratio b/a^* , which can be understood as the optimal proppant volume fraction, strongly depends on both the Young's modulus and the in-situ stress, as shown in Fig. 4b. At stress $\sigma_0 = 10 \text{ MPa}$, the optimal proppant volume fraction decreases from 76.92% to 50% when Young's modulus increases from $E = 10 \text{ GPa}$ to 50 GPa . At stress $\sigma_0 = 50 \text{ MPa}$, the effective conductivity is maximised when the optimal proppant volume fraction is 94.3% and 80.6% at $E = 10 \text{ GPa}$ and 50 GPa , respectively. This suggests that significant reduction in proppant usage can be achieved, even at high stress levels, for rocks with high Young's modulus. The savings in proppant use in the case of rocks with low Young's modulus are only significant under low-stress conditions.

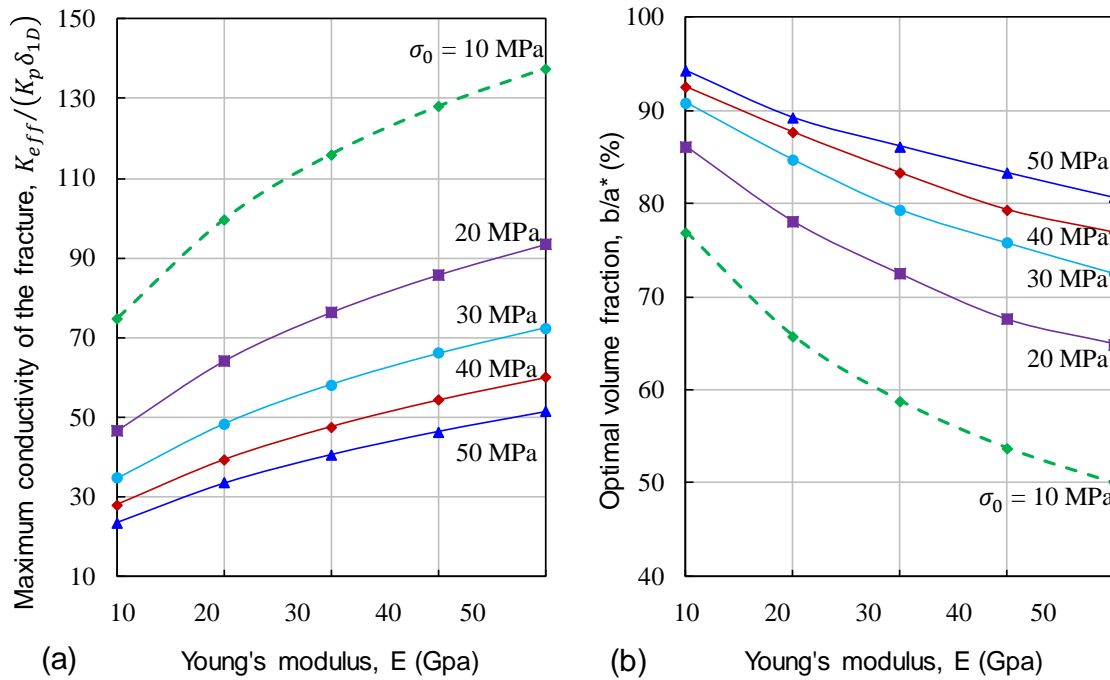


Figure 4 - (a) the dependence of maximum effective conductivity on Young's modulus and in-situ stress. The case of $K_{eff}/(K_p \delta_{1D}) = 1$ corresponds to fully-propped fracture; (b) the dependence of optimal proppant volume fraction on Young's modulus and in-situ stress. The case of $b/a^* = 100\%$ corresponds to fully-propped fracture.

5. CONCLUSION

A mathematical model is proposed to evaluate the residual opening and effective conductivity of partially-filled fractures, with applications to the optimisation of the channel fracturing technique. In the research, proppant consolidation is considered to be non-linear which more accurately describes the response of the proppant columns under compression. Attention is focussed on hard rock formations, in which proppant embedment is negligible. It is demonstrated that the fracture conductivity can be increased by several fold through the optimal application of the channel fracturing technique. It is also shown that rock with high Young's modulus and hardness are ideal for the application of the channel fracturing technique. A further extension of the above analysis could be towards the examination of residual opening of fractures created in layered reservoirs, using the method presented in [25-27].

6. ACKNOWLEDGEMENTS

The research is completed under the guidance of A/Prof Andrei Kotousov and Dr Aditya Khanna.

7. REFERENCES

1. Valko P, Economides MJ. Hydraulic fracture mechanics. Chichester: Wiley, 1995.
2. Liang F, Sayed M, Al-Muntasheri GA, Chang FF, Li, L. A comprehensive review on proppant technologies. Petroleum 2016;2(1):26-39.

3. Tinsley JM, Williams Jr. JR. A new method for providing increased fracture conductivity and improving stimulation results. *J. Pet. Technol.* 1975;27(11):1319-1325. SPE-4676-PA.
4. Bedrikovetsky PG, Keshavarz A, Khanna A, McKenzie KM, Kotousov A. Stimulation of natural cleats for gas production from coal beds by graded proppant injection. Presented at the SPE Asia Pacific Oil and Gas Conference and Exhibition, Perth, Australia, 22-24 October 2012. SPE-158761-MS.
5. Khanna A, Keshavarz A, Mobbs K, Davis M, Bedrikoversky P. Stimulation of the natural fracture system by graded proppant injection. *J. Pet. Sci. Eng.* 2013;111:71-77.
6. Khanna A, Kotousov A, Sobey J, Weller P. Conductivity of narrow fractures filled with a proppant monolayer. *J. Pet. Sci. Eng.* 2012;100:9-13.
7. Gillard, M., Medvedev, O., Pena, A., Medvedev, A., Penacorada, F. and d'Huteau, E. A New Approach to Generating Fracture Conductivity. Presented at the SPE Annual Technical Conference and Exhibition, Florence, Italy, 19-22 September. SPE-135034-MS.
8. Inyang UA, Nguyen PD, Cortez J. 2014. Development and Field Applications of Highly Conductive Proppant-free Channel Fracturing Method. Presented at the SPE Unconventional Resources Conference, The Woodlands, Texas 1-3 April 2010. SPE-168996-MS.
9. d'Huteau E, Gillard M, Miller M, Pena A, Johnson J, Turner M, Medvedev O, Rhein T, Willberg D. 2011. Open-channel Fracturing - A Fast Track to Production. *Oilfield Rev.* 2010: 23:4-17. [cited 2017 Jul 4]. Available from:
https://www.slb.com/~media/Files/resources/oilfield_review/ors11/aut11/01_open_channel.pdf
10. Medvedev A, Yudina K, Panga MK, Kraemer CC, Pena A. On the Mechanisms of Channel Fracturing. Presented at the SPE Hydraulic Fracturing Technology Conference, The Woodlands, Texas, 4-6 February 2013. SPE-163836-MS.
11. Malhotra S, Lehman ER, Sharma MM. Proppant Placement Using Alternate-Slug Fracturing. *SPE J.* 2014;19(5): 974-985. SPE-163851-PA.
12. Hou B, Zheng X, Chen M, Ye Z, Chen D. Parameter simulation and optimization in channel fracturing. *J. Nat. Gas Sci. Eng.* 2016;35(A):122-130.
13. Morris JP, Chugunov N, Meouchy G. Understanding heterogeneously propped hydraulic fractures through combined fluid mechanics, geomechanics, and statistical analysis. Presented at the 48th US Rock Mechanics / Geomechanics Symposium, Minneapolis, Minnesota, 1-4 June 2014. ARMA 14-7408.
14. Yan X, Huang Z, Yao J, Song W, Li Y and Gong L. Theoretical analysis of fracture conductivity created by the channel fracturing technique. *J. Nat. Gas Sci. Eng.* 2016;31:320-330.
15. Zheng X, Chen M, Hou B, Ye Z, Wang W, Yin C and Chen X. Effect of proppant distribution pattern on fracture conductivity and permeability in channel fracturing. *J. Pet. Sci. Eng.* 2017;149:98-106.
16. Khanna A, Luong H, Kotousov A, Nguyen GD, Rose F. Residual opening of hydraulic fractures created using the channel fracturing technique. *Int. J. Rock Mech. Mining Sci.* 2017; Under review. [Submitted on 08 Feb 2017].
17. Khanna A, Kotousov A, Luong H. On the application of the channel-fracturing technique to soft rock formations. *SPE J.* 2017; Under review. [Submitted on 20 May 2017].
18. Khanna A, Bortolan Neto L, Kotousov A. Effect of residual opening on the inflow performance of a hydraulic fracture. *Int. J. Eng. Sci.* 2014;74:80-90.

19. Kotousov A, Bortolan Neto L, Khanna A. On a rigid inclusion pressed between two elastic half spaces. *Mech. Mater.* 2014;68:38-44.
20. Bortolan Neto L, Khanna A, Kotousov A. Conductivity and performance of hydraulic fractures partially filled with compressible proppant packs. *Int. J. Rock Mech. Mining Sci.* 74;1-9.
21. Khanna A, Kotousov A. 2014. Stress analysis of a crack in a fiber-reinforced layered composite. *Compos. Struct.* 2015;118:139-148.
22. Zimmerman RW, Bodvarsson GS. Hydraulic Conductivity of Rock Fractures. *Transp. Porous Media.* 1996;23:1-30.
23. Zimmerman RW, Kumar S, Bodvarsson GS. Lubrication theory analysis of the permeability of rough-walled fractures. *Int. J. Rock Mech. Min. Sci. & Geomech. Abstr.* 1991;28:325-331.
24. Zimmerman RW, Yeo IW. Fluid Flow in Rock Fractures: From the Navier-Stokes Equations to the Cubic Law. In B. Faybishenko, P.A. Witherspoon, S.M. Benson , editors, *Dynamics of fluids in fractured rock*. Washington, DC: American Geophysical Union; 2000. p. 213-224.
25. Khanna A, Kotousov A. Controlling the Height of Multiple Hydraulic Fractures in Layered Media. *SPE J.* 2016;21(1):256:253.
26. Khanna A, Kotousov A. The stress field due to an interfacial edge dislocation in a multi-layered medium. *Int. J. Solids Struct.* 2015;72:1-10.
27. Khanna A. Stress analysis of a crack near an elastic layer [online]. In: 8th Australasian Congress on Applied Mechanics: ACAM 8. Barton, ACT: Engineers Australia, 2014: 103-111. [cited 04 Jul 17]. Available from:
<<http://search.informit.com.au/documentSummary;dn=193768398529753;res=IELENG>>

Chapter 6

On the application of the channel-fracturing
technique to soft rock formations

Statement of Authorship

Title of Paper	On the application of the channel-fracturing technique to soft rock formations
Publication Status	<input type="checkbox"/> Published <input type="checkbox"/> Accepted for Publication <input checked="" type="checkbox"/> Submitted for Publication <input type="checkbox"/> Unpublished and Unsubmitted work written in manuscript style
Publication Details	Society of Petroleum Engineers Journals (SPE Journals)

Principal Author

Name of Principal Author	Aditya Khanna		
Contribution to the Paper	Supervised the development of the theoretical models, wrote manuscript and acted as corresponding author.		
Overall percentage (%)	50		
Signature	Date	10/07/2018	

Co-Author Contributions

By signing the Statement of Authorship, each author certifies that:

- i. the candidate's stated contribution to the publication is accurate (as detailed above);
- ii. permission is granted for the candidate to include the publication in the thesis; and
- iii. the sum of all co-author contributions is equal to 100% less the candidate's stated contribution.

Name of Co-Author (Candidate)	Andrei Kotousov		
Contribution to the Paper	Supervised development of work, helped in data interpretation and manuscript evaluation.		
Overall percentage (%)	30		
Signature	Date	10/07/2018	

Name of Co-Author	Hao Thanh Luong		
Contribution to the Paper	Developed the models and performed analyses		
Overall percentage (%)	20		
Certification:	This paper reports on original research I conducted during the period of my Higher Degree by Research candidature and is not subject to any obligations or contractual agreements with a third party that would constrain its inclusion in this thesis. I am the 3 rd author of this paper		
Signature	Date	10/07/2018	

On the Application of the Channel-Fracturing Technique to Soft Rock Formations

Aditya Khanna, Andrei Kotousov, and Hao Thanh Luong, University of Adelaide

Summary

The application of the channel-fracturing technique can result in a significant increase in the conductivity of hydraulic fractures and reduced proppant usage. In soft rock formations, the conductivity of the partially propped fractures would depend not only on the volume fraction of the open channels, but also on the elastic deformation of open channels and fracture closure resulting from proppant consolidation and embedment. In this study, an analytical approach is developed for identifying the optimal proppant column spacing that maximizes the effective conductivity. The latter parameter can guide the design of the proppant-injection schedule and well-perforation scheme. To demonstrate the approach, we conduct a parametric study under realistic field conditions and identify the folds of increase in fracture conductivity and reduction in proppant use resulting from the optimized application of the channel-fracturing technique. The outcomes of the parametric study could be particularly useful in the application of the developed approach to soft rock formations.

Introduction

During the hydraulic stimulation of low-permeability rocks, a pressurized suspension of proppant particles is generally injected into the natural or manmade fractures to fill the fracture volume with proppant particles. The deposited particles are expected to prevent the complete closure of the fracture once the injection-fluid pressure is relieved. The assemblies of these granular particles also provide a highly conductive pathway for fluid flow (Valko and Economides 1995). Several past studies have demonstrated that the porosity and permeability of proppant packs degrade with time under the in-situ conditions due to a number of damage mechanisms (Barree et al. 2003; Weaver et al. 2006; Wen et al. 2007; Reinicke et al. 2010; Liang et al. 2016). The diminished permeability of the pack limits the fluid conductivity of the fracture and can undermine the overall effectiveness of the hydraulic stimulation.

The long-term decline of proppant pack conductivity was apparent to the early pioneers in hydraulic fracturing, who proposed several concepts for decoupling the load-bearing task of the proppant pack from that of providing a fluid-transport pathway. Most notably, Darin and Huitt (1959) proposed the partial-monolayer concept and Tinsley and Williams (1975) suggested that a staggered arrangement of proppant multilayers be used. Both concepts envisaged the development of a network of proppant-free channels within the fracture, which could generate an alternative fluid-transport pathway and an increase in the effective conductivity of the fracture (Bedrikovetsky et al. 2012; Khanna et al. 2013). Discontinuous or partial filling of the fracture with proppant multilayers instead of a single monolayer offered the additional benefit of a larger fracture opening in soft rock formations prone to embedment. The latter concept is often referred to as the channel-fracturing technique, and recent technological advancements have made it possible to achieve such a discontinuous placement of proppants in the fracture (Gillard et al. 2010; Inyang et al. 2014; Malhotra et al. 2014). Field studies have demonstrated that partially filled fractures generally have comparable or higher fluid conductivities than continuously filled fractures (d'Huteau et al. 2011; Medvedev et al. 2013).

Motivated by the successful field trials, several modeling studies on the optimization of the channel-fracturing technique have appeared in recent literature (Hou et al. 2016a, b; Morris et al. 2014; Yan et al. 2016; Zhang and Hou 2016; Zheng et al. 2017). Although these modeling studies provide many useful practical recommendations, the choice of the fracture-deformation models used in these studies is not entirely justified in the context of channel fracturing. For example, Hou et al. (2016a) and Zheng et al. (2017) modeled the proppant columns as rigid cylindrical indenters and used the Hertz contact theory to determine the fracture opening. This approach is more suitable for determining the opening of fractures supported by a monolayer of proppant particles (Khanna et al. 2012), and greatly overestimates the fracture residual opening in the case of proppant multilayers (Khanna et al. 2014; Bortolan Neto et al. 2015).

Morris et al. (2014) and Yan et al. (2016) modeled the proppant columns as linear elastic cylinders with constant stiffness in an attempt to incorporate the effect of proppant-pack deformation on the residual opening of the fracture. However, experimental observations suggest that the consolidation response of granular assemblies, such as proppant packs, is nonlinear, because the settlement or consolidation is largely achieved through particle rearrangement into a tighter packing rather than the elastic deformation of individual particles (Mesri and Vardhanabhuti 2009). The particle rearrangement into a more compact configuration is caused by several mechanisms, including particle slip and rotation and particle damage. The degree of particle damage and interparticle slip and rotation determine the unique and nonlinear mechanical response of any specific granular assembly (Roberts and de Souza 1958; Hardin 1985; Coop 1990; Mesri and Vardhanabhuti 2009). In fact, several consolidation models exist in the literature to describe the mechanical response of various granular assemblies over a wide range of applied stresses (Pestana and Whittle 1995).

A micromechanical approach for calculating the deformation of partially filled fractures was developed by Hou et al. (2016b) and Zhang and Hou (2016). Their approach uses the elementary solution for two elastic spheres squeezed by a pair of normal point forces to evaluate the deformation of the proppant pack as well as the embedment of the proppant particles into the rock (Gao et al. 2013; Li et al. 2015). Although this approach is more general than linear spring models, it cannot adequately capture the deformation of a multi-layered proppant pack because the system of forces acting on individual particles in a multilayer (Reinicke 2011) is more complex than that assumed by the authors. It is believed that an experimentally calibrated consolidation model would be more appropriate for describing the deformation of proppant columns compared with micromechanical approaches using elementary solutions. The present article aims to address the above-mentioned shortcomings in previous modeling studies and presents a general framework for determining the

residual opening and effective conductivity of partially filled fractures. Like its predecessors, the developed framework is also dependent on a set of simplifying assumptions regarding the fracture geometry, proppant distribution, and mechanical response of the rock and proppant pack. These assumptions are discussed in more detail in the next section.

Problem Formulation and Modeling Assumptions

We consider a planar hydraulic fracture emanating from a vertical wellbore and partially filled with proppant particles. The fracture geometry is described by the Kristianovich-Geertsma-de Klerk (KGD) model; the plane-strain assumption is used, and variations in fracture opening, fracture-fluid pressure, and confining stress are neglected in the vertical direction. The proppant distribution within the fracture is idealized by a regular arrangement of identical proppant columns of width $2b$, evenly spaced by distance $2s$ between adjacent columns. The fracture geometry under consideration has three characteristic dimensions: the half-length of the fracture L , the half-width of the proppant column b , and the initial opening or aperture of the fracture, δ_o , such that $L \gg b \gg \delta_o$ (Fig. 1). The initial opening of the fracture δ_o , the fluid pressure within the fracture p_f , and the remote in-situ stress normal to the fracture plane σ_o^∞ vary spatially along the fracture length. However, the variations of these quantities are expected to be negligible at small distances compared with the width of the proppant column [i.e., $x \approx O(b \ll L)$], except close to the wellbore ($X = 0$) or the fracture tips ($|X| = \pm L$). Hence, the problem geometry is periodic at the length scale of the proppant columns (see Fig. 1).

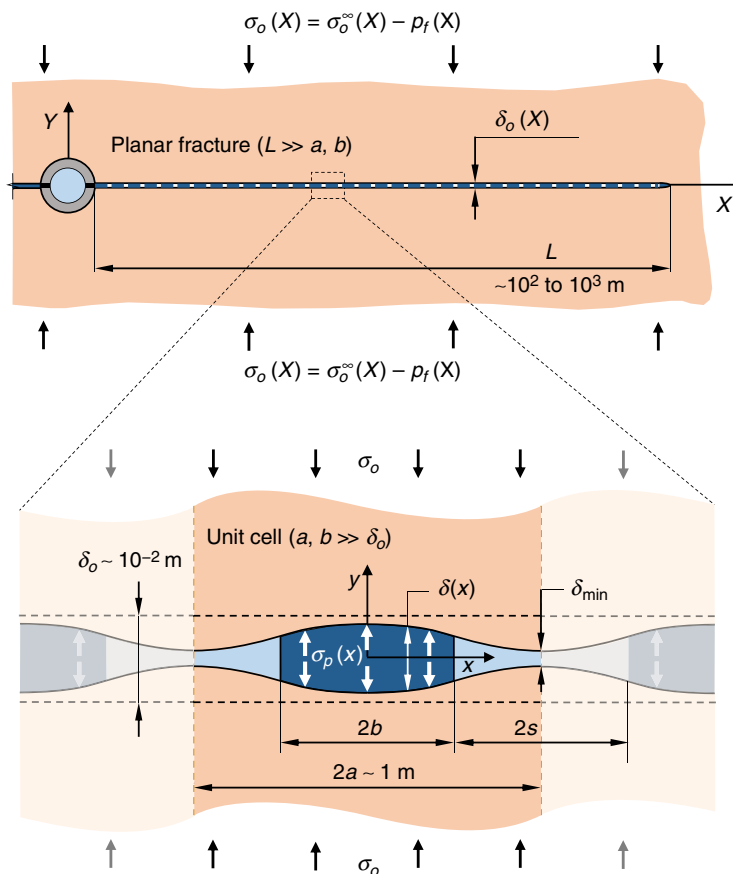


Fig. 1—Schematic of the 2D problem geometry showing two characteristic length scales, $X \approx O(L)$ and $x \approx O(a)$. The effective confining stress σ_o and initial fracture opening δ_o can be treated as constants over the width of the unit cell but vary along the length of the fracture.

Laboratory-scale experiments indicate that pulsed proppant injection produces an irregular distribution of proppant within a planar fracture, as opposed to the periodic arrangement assumed in the present work (Malhotra et al. 2014). The irregular distribution of proppant in the fracture is controlled by numerous factors, including the proppant-injection schedule, arrangement of the perforations along the wellbore, geometry of the fracture, size distribution of proppant particles, settlement of proppant in the fracture, and the rheological properties of the fracturing fluid. Modeling of proppant transport and placement in a fracture is beyond the scope of the present work. The effects of proppant flowback during fluid production are also ignored in the present work. Additives or coatings are generally used during the implementation of the channel-fracturing technique to improve the stability of the proppant columns and minimize proppant flowback. Examples of additives include chopped fibers (Romero and Feraud 1996; Burukhin et al. 2012) and thermoplastic strips (Nguyen et al. 1996), and examples of coatings are surface-modification agents (Weaver et al. 1999) and curable resins (Sinclair et al. 1993).

Poroelasticity effects are also disregarded in the present work for simplicity reasons (i.e., the effects of fluid-pressure diffusion are neglected). Nonetheless, it is vital to discuss the influence of this simplifying assumption on the modeling outcomes. There are two distinct poroelastic effects in fluid-saturated porous media: the dilation/contraction of the porous matrix caused by a change in pore pressure, and the perturbation of the pore pressure induced by changes in the mean stress under undrained conditions (Detournay and Cheng 1991). The volumetric strain associated with the first poroelastic effect is proportional to the Biot coefficient α , and the pore-pressure change associated with the second poroelastic effect is proportional to the difference between the undrained and drained Poisson's ratios $(\nu_u - \nu)$ (Rice and Cleary 1976). The second poroelastic effect can be ignored for compressible fluids ($\nu_u \approx \nu$) or large times,

$\tau \gg \ell^2/c$, where ℓ is the characteristic length and c is the coefficient of diffusivity of the porous medium (Rice and Cleary 1976). Hence, only the first poroelastic effect is of significance in the present context. It is well-known that long-term fluid production from reservoirs causes a decline in the reservoir pore pressure and tends to induce contraction in a reservoir. Hydraulic-fracturing field measurements show that σ_h , the minimum horizontal stress normal to the fracture plane, decreases (become more tensile) with decreasing reservoir pore pressure p_o with the ratio $\Delta\sigma_h/\Delta p_o$ of approximately 0.5 to 0.8 (Segall and Fitzgerald 1998). Because the change in confining stress is smaller than the change in pore pressure, the effective stress normal to the fracture increases with reservoir depletion. The increase in effective stress normal to the fracture would result in a decrease in the residual opening with reservoir depletion (Segall and Fitzgerald 1998). The model to be presented in the following sections can be used for the determination of the long-term residual opening of the unit cell by selecting a suitable value of the net confining stress, which implicitly incorporates this poroelastic effect.

It is important to note that although the mathematical model is developed for periodic-problem geometry, it can be extended toward the analysis of the more realistic situation where the initial fracture opening δ_o , fracture-fluid pressure p_f , and the remote in-situ normal stress σ_o^∞ vary along the fracture length. Provided that these parameters vary gradually along the fracture length, a homogenization procedure can be developed to solve the nonperiodic problem in a computationally efficient manner. The purpose of the homogenization or averaging procedure is to replace the numerous discrete proppant columns by an effective medium, which fills the entire fracture. The “traction law” or stress-displacement relationship for the effective medium can be obtained from the unit-cell solution using the energy-conservation principle (Rose 1987). Once the traction law for the effective medium is derived, it only remains to solve the problem of the hydraulic fracture uniformly filled with the effective medium subjected to the appropriate stress and displacement boundary conditions (Rose 1987). The method of solution of the latter boundary-value problem was presented by Bortolan Neto et al. (2015). A similar approach is used in the analysis of other multiscale problems of mechanics, such as when modeling crack propagation in fiber-reinforced composites (Budiansky et al. 1986).

The numerous assumptions introduced into the current approach and discussed previously are common and unavoidable for analytical, semianalytical, and numerical modeling of hydraulic simulations. Indeed, in the current work some of the simplifications are relaxed compared with previous studies because of the application of a more advanced computational technique and mechanical-behavior model, which will be discussed next.

Mechanical Behavior of Rock and Proppant Columns

The change in opening of hydraulic fractures during the fluid-production stage can be attributed to the deformation of the rock, embedment of proppant particles into the fracture faces, and consolidation of the proppant pack into a more compact arrangement. The latter two mechanisms are illustrated in Fig. 2. In the present study, the rock is modeled as a linearly elastic, isotropic, and homogeneous medium with Young’s modulus E and Poisson’s ratio ν . This assumption is justified because the inelastic deformation of the rock arising from proppant embedment is localized to a small depth approximately $O(\delta_o \ll b, a)$ from the fracture surface, and does not significantly affect the elastic response of the bulk of the rock. The same assumption is used in the modeling of crack problems in ductile materials under small-scale yielding conditions (Codrington and Kotousov 2009) and in the modeling of rock joints (Le et al. 2017).

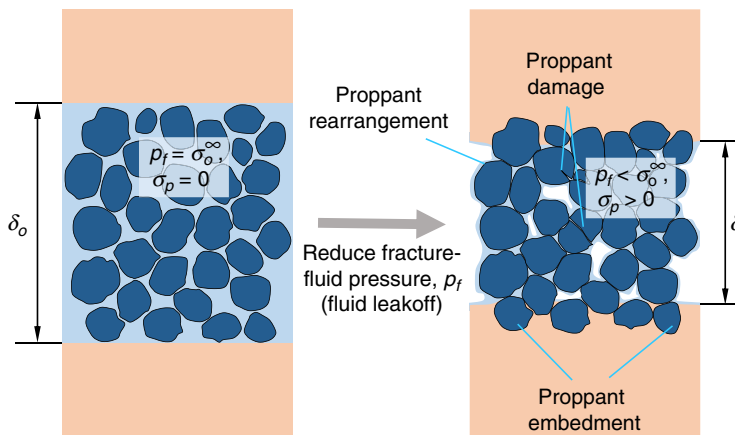


Fig. 2—Schematic showing two mechanisms leading to fracture closure: proppant consolidation (rearrangement and damage) and proppant embedment.

In hard rocks, experiments conducted under typical reservoir conditions indicate that the embedment depth is generally approximately one-half of the proppant-grain diameter (Much and Penny 1987). On the other hand, embedment depths of up to three grain diameters have been reported in soft rocks, such as weakly consolidated sandstones (Lacy et al. 1998; Zhang et al. 2015). It is therefore essential to consider the effects of proppant embedment during the application of the channel-fracturing technique to soft formations. However, the theoretical modeling of proppant embedment is a very challenging task because of the nonlinear response of rocks to indentation (Momber 2004), the dependence of a rock’s mechanical properties on the degree of water saturation (Lacy et al. 1998), and the mutual contact and interaction between indenting proppant particles (Reinicke 2011; Deng et al. 2014). Consequently, empirical approaches have been adopted to calculate the embedment depths of proppant monolayers (Huitt and McGlothlin 1958; Volk et al. 1981) and multilayers (Guo et al. 2008; Palisch et al. 2010). The present study, similar to past empirical approaches, adopts a linear relationship between the stress in the proppant pack σ_p and the loss of fracture opening caused by proppant embedment, $(\delta_o - \delta)$,

$$\sigma_p = \gamma(\delta_o - \delta), \dots \dots \dots (1)$$

where the parameter γ is referred to as the “embedment stiffness.” The larger the embedment stiffness, the smaller the loss of fracture opening at a given closure-stress level. Fig. 3a, in particular, shows that the adopted empirical model allows a satisfactory correlation with experimental tendencies (Lacy et al. 1998). However, more-complex embedment models can be used within the developed framework without any restrictions, but at the expense of additional fitting parameters.

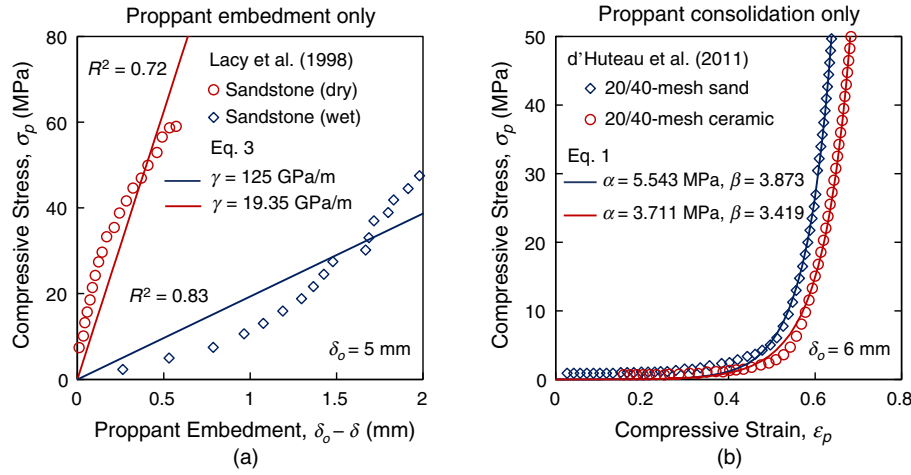


Fig. 3—Obtaining the fitting parameters of the empirical models for (a) proppant-column consolidation and (b) proppant embedment.

The deformation of proppant columns under compressive loading is nonlinear because it largely occurs as a result of inelastic processes of proppant rearrangement and damage, as discussed in the Introduction. Although numerous consolidation models have been proposed in the literature (Pestana and Whittle 1995), their accuracy increases only at the expense of an increasing number of fitting parameters, which in turn need more-extensive experimental data. Such data are often unavailable or very limited. Therefore, the present study adopts a simple empirical model for proppant consolidation, which is calibrated using available experimental data. The consolidation model is 1D (i.e., the lateral expansion of the proppant columns is ignored). In the case of sufficiently wide columns ($b \gg \delta_o$), it is expected that the lateral expansion of the columns would occur mostly near the perimeter of the column while the interior remains laterally constrained [i.e., the average lateral strain ($\Delta b/b$) caused by axial loading would be negligible]. Laboratory tests conducted by d’Huteau et al. (2011) are in a general agreement with this hypothesis and also indicate that the average lateral strain in axially loaded proppant columns decreases rapidly with an increase in proppant-column diameter.

The compressive stress in the proppant column σ_p is related to the uniaxial compressive strain ϵ_p using the power-law relationship,

$$\sigma_p = \alpha \left(\frac{\epsilon_p}{1 - \epsilon_p} \right)^\beta, \dots \dots \dots (2)$$

where α and β are fitting parameters and

$$\epsilon_p = (\delta_o - \delta) / \delta_o = \Delta / \delta_o, \dots \dots \dots (3)$$

where δ_o and δ are the initial and final heights of the proppant column and Δ is the fracture closure at some compressive stress σ_p . The value of ϵ_p lies in the interval $[0, 1]$, and Eq. 2 implies that $\sigma_p = 0$ at $\epsilon_p = 0$ and $\sigma_p \rightarrow \infty$ as $\epsilon_p \rightarrow 1$. Experimental results obtained by d’Huteau et al. (2011) are used to calibrate the model and to obtain representative values of the fitting parameters (Fig. 3b). The experimental results show that certain proppant columns can undergo finite deformation (i.e., the compressive strain ϵ_p is not infinitesimal). This does not adversely affect the formulation of the present problem because the governing equations derived in the next section describe the stress and displacement field in the linearly elastic rock, not in the proppant columns. The proppant columns serve only as a means for generating displacement-dependent normal tractions in the current mathematical model.

In the present work, δ_o is used interchangeably for the initial opening of the unit cell and the initial height of the proppant column. Hence, the initial condition corresponds to the instant when the proppant particles cannot freely mobilize within the fracture and the proppant slurry conforms into a pack. The critical porosity of the proppant slurry at this instant is closely connected to the size distribution and packing arrangement of the proppant grains, and is in general determined from geometric considerations (Bortolan Neto et al. 2011). It is understood that the opening of a hydraulic fracture during the proppant-injection stage must be larger than the desired height of the proppant columns, to prevent proppant bridging.

The effects of proppant embedment and consolidation can be combined by considering the embedment stiffness γ and the instantaneous proppant-column stiffness $K_{n,p}$ to act in series. The latter can be obtained by differentiating Eq. 2 as

$$K_{n,p} = \frac{\partial \sigma_p}{\partial \Delta} = - \frac{\partial \sigma_p}{\partial \delta} = \frac{\alpha \beta \delta_o}{\delta^2} \left(\frac{\delta_o}{\delta} - 1 \right)^{\beta-1} \dots \dots \dots (4)$$

Hence, the effective stiffness of the proppant-filled regions of the fracture becomes

$$K_{n,eff} = \left(\frac{1}{\gamma} + \frac{1}{K_{n,p}} \right)^{-1} = \frac{\alpha \beta \gamma \delta_o (\delta_o - \delta)^{\beta-1}}{\gamma \delta^{\beta+1} + 2 \alpha \beta \delta_o (\delta_o - \delta)^{\beta-1}}, \dots \dots \dots (5)$$

and the compressive stress in the proppant pack at any given fracture opening, $\delta \leq \delta_o$, can be determined as

$$\sigma_p(\delta) = \int_{\delta}^{\delta_o} K_{n,eff}(\rho) d\rho, \quad 0 \leq \delta \leq \delta_o \dots \dots \dots (6)$$

The interplay between proppant-pack consolidation and proppant embedment and the resulting variation of the effective fracture stiffness is demonstrated in Fig. 4. During the initial stages of fracture closure ($\Delta \rightarrow 0$), the proppant column stiffness $K_{n,p}$ is negligible and hence the initial loss of fracture opening is caused by the consolidation of the proppant pack. Physically, this corresponds to the

rearrangement of the proppant grains into a more compact configuration and the expulsion of the fracturing fluid from the pore space of the proppant column. With further fracture closure, the stiffness of the proppant column increases rapidly, becoming comparable with and eventually exceeding the rock's embedment stiffness. In the final stages of fracture closure, ($\Delta \rightarrow \delta_o$), the loss of fracture opening is largely caused by the embedment of proppant grains in the rock.

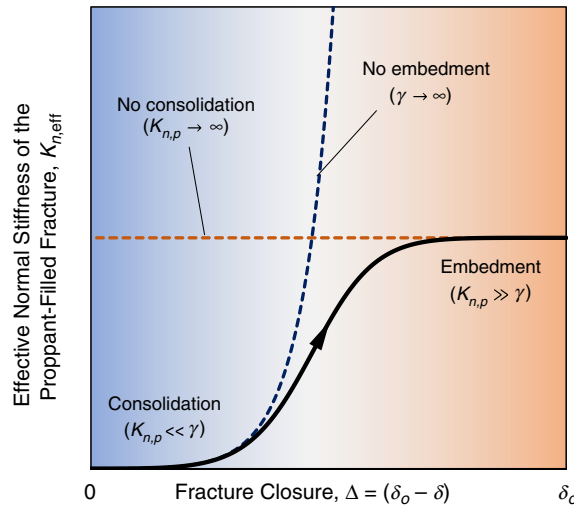


Fig. 4—Schematic showing the variation in the effective normal stiffness of the propped fracture with the degree of fracture closure. The limiting cases of no proppant consolidation and no embedment are also shown.

It must be noted that Fig. 4 is only a schematic and the choice of values for the model variables α , β , and γ will determine which of the two mechanisms dominates during the application of the confining pressure at the production stage. The two limiting cases of no consolidation and no embedment are also shown in Fig. 4. The developed empirical model for the mechanical response of the proppant pack is used in the next section to determine the residual opening of partially filled fractures.

Governing Equations for the Residual Opening of the Unit Cell

For the unit cell of the problem geometry, shown in Fig. 1, the periodicity of the problem requires that

$$u_x(x = \pm a, y) = 0, \quad \sigma_{xy}(x = \pm a, y) = 0. \quad \dots \dots \dots (7)$$

The traction boundary condition along the crack faces can be stated as

$$\sigma_{yy}(x, y = 0_{\pm}) = \begin{cases} \sigma_p(x) + p_f, & |x| < b \\ p_f, & b < |x| < a, \end{cases} \quad \dots \dots \dots (8)$$

$$\sigma_{xy}(x, y = 0_{\pm}) = 0, \quad \dots \dots \dots (9)$$

where p_f is the fracture-fluid pressure and $\sigma_p(x)$ is the continuous normal traction applied to the crack surface by the proppant pack. The latter can be defined in terms of the crack-opening displacement, $\delta(x) = u_y(x, y = 0^+) - u_y(x, y = 0^-)$, using Eq. 6. The remote boundary condition can be expressed as

$$\sigma_{yy}(x, y \rightarrow \infty) = -\sigma_o^{\infty}, \quad \sigma_{xy}(x, y \rightarrow \infty) = 0. \quad \dots \dots \dots (10)$$

In Eqs. 8 and 10, the normal stresses are positive under tension. Finally, the equilibrium equation for the forces in the y-direction can be stated as

$$\int_{-b}^b \sigma_p(x) dx - 2a(\sigma_o^{\infty} - p_f) = 0. \quad \dots \dots \dots (11)$$

For a given column width $2b$ and initial height δ_o , the solution to the problem formulated by Eqs. 7 through 11 comprises the residual opening profile $\delta(x)$ and the proppant-reaction stress $\sigma_p(x)$. To ensure that the unsupported fracture faces do not come into contact, the gap between the adjacent columns, $2s = 2(a - b)$, must be selected such that $\delta_{\min} = \delta(x = a)$ remains greater than zero (see Fig. 1).

The distributed-dislocation technique (DDT), which is based on the pioneering work of Bilby et al. (1963) and Bilby and Eshelby (1968), is used to obtain the solution to the formulated crack problem. The relative opening between the crack faces, $\delta(x)$, is modeled by a continuous distribution of “edge dislocations.” The edge dislocation is used here as a “strain nucleus” (i.e., a means for generating a controlled state of stress in the elastic medium), and the presence of any lattice defects is not implied. Because the stress field induced by a single edge dislocation satisfies the equilibrium, constitutive, and compatibility equations of the theory of classical linear elasticity, these equations are also satisfied by a continuous distribution of dislocations. What remains is to distribute these dislocations in a manner such that the boundary conditions, Eqs. 7 through 10, are satisfied. The singular integral equation that governs the distribution of the dislocations is derived in Appendix A and can be written as

$$\frac{\bar{E}}{4\pi} \int_0^a B_y(\xi) \left[\frac{2\xi}{x^2 - \xi^2} + K(x, \xi) \right] d\xi = \sigma_o^{\infty} - p_f - \sigma_p(x) H(b - |x|), \quad 0 < x < a, \quad \dots \dots \dots (12)$$

where $B_y(\xi)$ is the unknown dislocation-density function that represents the continuous distribution of dislocations, $H(\cdot)$ is the Heaviside step function, and the kernel $K(x, \xi)$ given by Eq. A-17 incorporates the effect of periodicity of the problem geometry. The singular integral equation, Eq. 12, can be generalized to consider layered reservoirs or multiple hydraulic fractures using an approach developed previously (Khanna and Kotousov 2015, 2016). By defining the net confining stress as $\sigma_o = \sigma_o^\infty - p_f$, the governing equation (Eq. 12) can be rewritten as

$$\frac{\bar{E}}{4\pi} \int_0^a B_y(\xi) \left[\frac{2\xi}{x^2 - \xi^2} + K(x, \xi) \right] d\xi = \sigma_o - \sigma_p(x)H(b - |x|), \quad 0 < x < a. \quad (13)$$

There is a close relationship between the dislocation density and the relative separation between the crack faces at any point, $\delta(x) = u_y(x, y = 0^+) - u_y(x, y = 0^-)$. To establish this relationship, we note that $\delta(x = a) = \delta_{\min}$ (Fig. 1), and that the insertion of dislocations along $x < a$ increases the crack opening (Kotousov et al. 2014) so that

$$\delta(x) = \delta_{\min} + \int_x^a B_y(\xi) d\xi, \quad B_y(\xi) = \frac{d\delta(\xi)}{d\xi}, \quad 0 < x < a. \quad (14)$$

The reaction stress caused by the proppant column $\sigma_p(x)$ can be related to the crack opening $\delta(x)$ by substituting Eq. 5 into Eq. 6,

$$\sigma_p(x) = \int_{\delta(x)}^{\delta_o} \frac{\alpha\beta\gamma\delta_o(\delta_o - \rho)^{\beta-1}}{\gamma\rho^{\beta+1} + 2\alpha\beta\delta_o(\delta_o - \rho)^{\beta-1}} d\rho. \quad (15)$$

In the present work, we model the proppant column as a bundle of “springs,” which deform independently of each other, similar to previous analytical studies (Bortolan Neto et al. 2015). This is because the proppant column is a cohesionless granular medium rather than an elastic medium. Hence, Eq. 6, which represents the averaged response of a proppant column subject to uniaxial strain, also represents the stress-displacement relationship for the individual “springs” in the column (i.e., Eq. 15). This approach is widely used in civil-engineering calculations to describe the interaction between elastic bodies and cohesionless soils, such as in the well-known Winkler model. We simply extend this well-established approach to a similar problem of the interaction between the elastic rock and cohesionless proppant pack. The fitting parameters in Eq. 15 can be obtained experimentally, with the restriction that the test specimen must undergo uniaxial strain, which is uniform across the specimen width. The experimental data used in the present work were obtained from tests that meet this requirement.

This dependence of the proppant-reaction stress on the crack opening and consequently on the dislocation density renders the singular integral equation, Eq. 13, nonlinear. Equations of this form arise in the formulation of a range of other crack problems that involve a continuous distribution of tractions on the crack faces. Some examples include fatigue cracks in aircraft panels repaired by composite patches (Cox and Rose 1996), and matrix cracks in fiber-reinforced composites (Khanna and Kotousov 2014). An analytical solution to such singular-integral equations is not possible, and the numerical-solution procedure for this class of integral equations, and Eq. 13, is presented in Appendix B. Once the solution for the dislocation density $B_y(x)$ is determined, the solution for the residual opening profile $\delta(x)$ and the compressive stress distribution in the proppant columns $\sigma_p(x)$ can be obtained using Eqs. 14 and 15, respectively. The numerical-solution procedure is illustrated by means of a flow chart in Fig. 5.

Effective Conductivity of the Unit Cell

The problem of fluid flow in a partially propped fracture is complex because the fluid flow occurs in a heterogeneous medium comprising irregularly shaped porous proppant columns and a network of open channels. In addition, the fracture opening varies with position along the fracture. Consequently, the exact solution to the Navier-Stokes equations, which govern the motion of Newtonian fluids, cannot be obtained for the problem under consideration. However, these equations can be simplified greatly if certain kinematic and geometric conditions are satisfied. Provided that the viscous forces dominate the inertial forces and the fracture aperture does not vary abruptly, which is generally the case for rock fractures, the flow in the open channels can be described by the Reynolds lubrication equation and the flow in the proppant columns can be described by Darcy’s law (Witherspoon et al. 1980; Zimmerman and Yeo 2000). The coupling of these equations and their upscaling from the fine scale (unit cell) to the coarse scale (fracture) are still challenging tasks, requiring the aid of numerical techniques (Khanna et al. 2012; Yan et al. 2016).

In the present work, a more straightforward approach is adopted to obtain a closed-form expression for the effective conductivity of the unit cell. We provide an estimate for the effective unit-cell conductivity that lies between upper and lower bounds obtained in accordance with variational principles (Zimmerman et al. 1991; Zimmerman and Bodvarsson 1996),

$$\langle 1/k \rangle < k_{\text{eff}} < \langle k \rangle. \quad (16)$$

For a heterogeneous conductive medium, the lower bound $\langle 1/k \rangle$ corresponds to the situation in which all the conductive elements are arranged in series, whereas the upper bound $\langle k \rangle$ corresponds to a parallel arrangement of the individual elements (Zimmerman and Bodvarsson 1996). For the problem geometry shown in Fig. 1, these extreme cases correspond to 1D fluid flow along the x -direction (along the fracture length) or z -direction (into the page), respectively.

However, in the real-fracture geometry, it is expected that the fluid will flow mainly along the x -direction at some points, whereas at other points, it will flow mainly along the z -direction. As a result, the assumption of a series (or parallel) arrangement of conductive elements would underestimate (or overestimate) the actual effective conductivity (Zimmerman et al. 1991). An estimate for the effective conductivity of the unit cell can be obtained as the geometric mean of the upper and lower bounds,

$$k_{\text{eff}} = \sqrt{\langle 1/k \rangle^{-1} \langle k \rangle}. \quad (17)$$

Eq. 17 was obtained by Zimmerman et al. (1991), who also showed that it provides similar estimates for the effective fracture conductivity as the geometric mean of the narrower Hashin-Shtrikman bounds (Hashin and Shtrikman 1962).

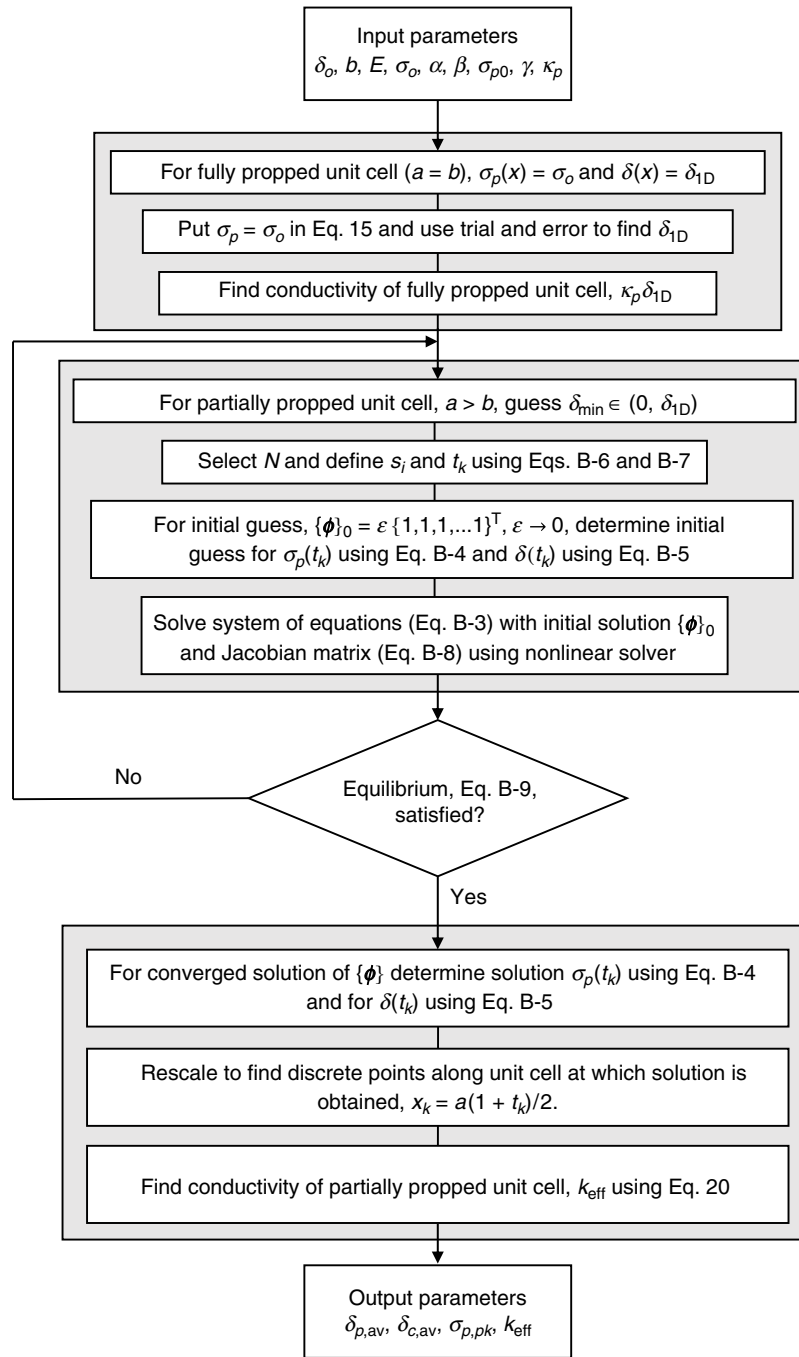


Fig. 5—Flow chart of numerical-solution procedure.

The local conductivity at a point along the unit cell k is defined in accordance with the Darcy and cubic laws,

$$k(x) = \begin{cases} \kappa_p \delta(x), & |x| < b, \\ \frac{\delta(x)^3}{12}, & b < |x| < a, \end{cases} \dots \dots \dots (18)$$

where κ_p is the proppant-column permeability and $\delta(x)$ is the residual opening profile of the unit cell. The column permeability κ_p is considered to be constant, and its reduction with proppant consolidation and embedment is neglected. This assumption does not introduce any significant error in the analysis because the permeability of typical proppant columns (approximately 10^{-10} m² or 100 darcies) is already several orders of magnitude lower than the effective permeability of open channels, $\delta^2/12$ (approximately 10^{-7} m² or 100,000 darcies for $\delta = 1$ mm).

Substituting Eq. 18 into Eq. 16 yields the lower (series) and upper (parallel) bounds for the unit-cell conductivity as (Khanna et al. 2017)

$$\langle 1/k \rangle = a \left[\int_0^b \frac{dx}{\kappa_p \delta(x)} + 12 \int_b^a \frac{dx}{\delta^3(x)} \right], \quad \langle k \rangle = \frac{1}{a} \left[\int_0^b \kappa_p \delta(x) dx + \frac{1}{12} \int_b^a \delta^3(x) dx \right]. \dots \dots \dots (19)$$

The estimate for the effective unit-cell conductivity is finally obtained using Eq. 18,

$$k_{\text{eff}} = \left\{ \left[\int_0^b K_p \delta(x) dx + \frac{1}{12} \int_b^a \delta^3(x) dx \right] / \left[\int_0^b \frac{dx}{K_p \delta(x)} + 12 \int_b^a \frac{dx}{\delta^3(x)} \right] \right\}^{\frac{1}{2}} \dots \dots \dots (20)$$

Parametric Study

Using the theoretical models and the numerical procedures developed in the preceding sections, an extensive parametric study is conducted to investigate the effects of the proppant-column spacing, magnitude of the net confining stress, and rock-embedment stiffness on the residual opening and effective conductivity of the unit cell. The selected values of the governing parameters are representative of typical field situations and are summarized in **Table 1**. The values of the rock Young’s modulus and Poisson’s ratio as well as the fitting parameters for the proppant-consolidation model are kept fixed in the calculations. However, numerous values of the rock-embedment stiffness are considered to investigate the influence of proppant embedment on the effectiveness of the channel-fracturing technique. A wide range of values for the fracture-closure stress or the net confining stress is also considered because the closure stress varies greatly from reservoir to reservoir. Finally, two values of the initial fracture opening are considered. For 20/40-mesh-size proppant used frequently in hydraulic-fracturing treatments, the selected values for the initial fracture opening (5 and 10 mm) roughly correspond to a proppant-pack density or concentration of 2 and 4 lbm/ft² (Lacy et al. 1998).

Parameter	Value	Units
Initial fracture opening, δ_o	5, 10	mm
Proppant-column width, $2b$	1	m
In-situ lateral (closure) stress, σ_o	10, 20, 30, 40, 50	MPa
Generalized Young’s modulus, \bar{E}	10	GPa
Fitting parameter for the proppant-consolidation model, α	5.543	MPa
Fitting parameter for the proppant-consolidation model, β	3.873	MPa
Rock-embedment stiffness, γ	20, 40, 60, 80, 100	GPa/m

Table 1—Numerical values of the governing parameters.

Typical results for the residual opening profile $\delta(x)$ and the compressive stress in the proppant pack $\sigma_p(x)$ are shown in **Fig. 6**. The compressive stress in the proppant columns $\sigma_p(x)$ is distributed in a manner such that the net opening force exerted by the proppant column on the fracture faces is balanced by the closing force exerted by the net confining stress σ_o (i.e., the average stress in the proppant column, $\sigma_{p,av}$, is $\sigma_o a/b$). The actual stress distribution is nonuniform across the column width. The stress rises sharply near the edge of the column, $x = b$, and its peak value is denoted as $\sigma_{p,pk}$. The sharp rise in the proppant-pack compressive stress can be explained in terms of the well-known principle of stress concentration in linear elasticity, which states that any abrupt changes in geometry, material properties, or loading conditions cause a localized increase in stresses in the vicinity of the abrupt change (Peterson 1953). In the present problem, there is a sudden change in the normal stiffness of the fracture at the edges of the proppant column. The point $|x| \rightarrow b_-$ is supported by the proppant column, whereas the point $|x| \rightarrow b_+$ is unsupported. Therefore, the stress field varies rapidly near the edge of the column. The observed stress distribution is similar to the solution for contact stress in the related problem of an elastic half-space indented by a rigid flat punch (Barber 2010). The residual opening of the unit cell also decreases sharply around the edge of the proppant column (i.e., $|x| = b$). Because of the lack of support from the proppant column, the residual opening of the channel ($b \leq |x| \leq a$) decreases monotonically until reaching a minimum value δ_{min} at $x = a$. The average channel opening can be obtained as $\delta_{c,av} = 1/(a - b) \int_b^a \delta(x) dx$.

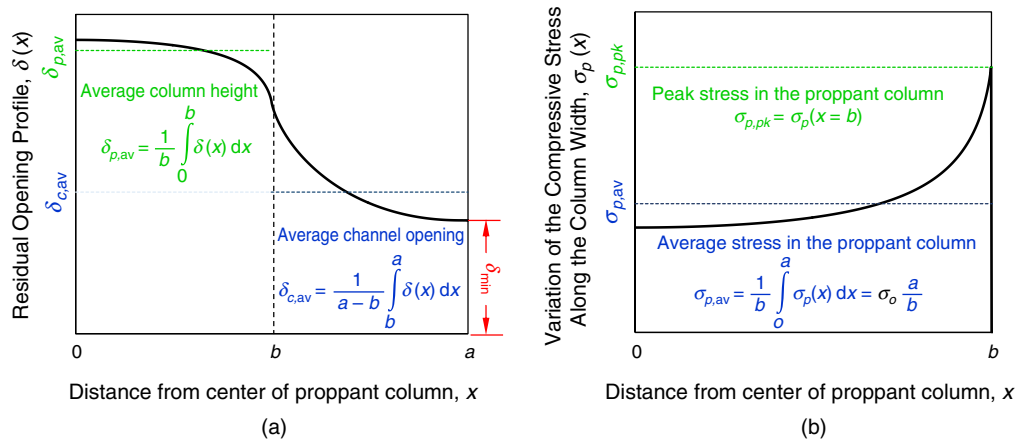


Fig. 6—Representative results for (a) the residual opening profile of the unit cell and (b) the compressive stress in the proppant column. The proppant column lies along $|x| < b$, and the open channel lies along $b \leq |x| \leq a$.

Poroelastic effects associated with the consolidation of the proppant columns are ignored in the present work, as discussed in the Introduction. However, it is of interest to mention the well-known Mandel-Cryer effect in poroelasticity, which predicts that the sudden compaction of a fluid-saturated porous column between two rigid plates produces a nonuniform distribution of the axial stress across the column width. The resulting poroelastic stress distribution is opposite to that in Fig. 6; i.e., the maximum poroelastic stress occurs at the center of the column and the minimum occurs at the edges (Abousleiman et al. 1996; Liu et al. 2018). This poroelastic effect is transient, and at sufficiently large times, the axial-stress distribution in the column becomes uniform (Abousleiman et al. 1996). This is in agreement with the present model, which predicts uniformly distributed stress in the column [i.e., $\sigma_p(x) = \sigma_o$] for the trivial case of a fully propped fracture (i.e., $a = b$).

When performing the numerical calculations, we begin with the case of a fully propped fracture (i.e., and the gap between the proppant columns is $2s = 0$). For this trivial case, there is no need to solve the singular-integral equation for the dislocation density, and the constant residual opening of the unit cell can be directly obtained from Eqs. 5 and 6. This value of residual opening is denoted by δ_{ID} . The effective unit-cell conductivity is simply $\kappa_p \delta_{ID}$, where κ_p is the permeability of the proppant pack. If the proppant-column width $2b$ is kept fixed and the gap between the columns $2s$ is increased, the value of δ_{min} decreases from δ_{ID} to 0 as the gap between the columns $2s$ increases from 0 to some critical value, $2s_{cr}$. At this critical gap between columns, the channel walls come into contact at $x = a$. If it is required to calculate the residual opening beyond this critical column gap, the problem formulation presented in the preceding section needs to be generalized to account for the possibility of contact between the crack faces. However, this was not deemed necessary because the latter case corresponds to partially closed channels and is of little practical interest. The dependence of the critical gap on the embedment stiffness, closure stress, and the initial fracture opening is shown in Fig. 7. It should also be noted that for certain combinations of embedment stiffness and closure stress, this critical gap is zero (i.e., complete fracture closure occurs even when the fracture is fully propped, which corresponds to the situation of very high closure stress or very low embedment stiffness). For other combinations of the governing-parameter values, critical gap size is comparable with or greater than the column width, $2b = 1$ m.

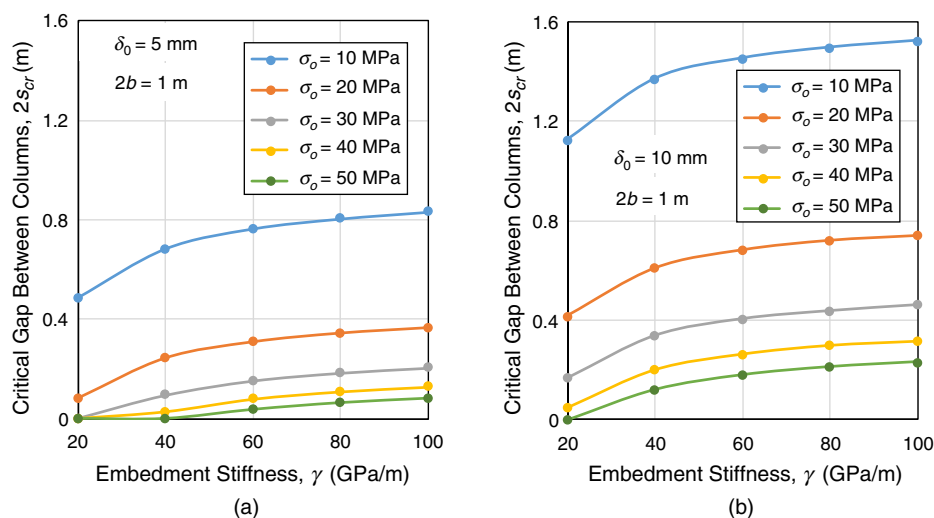


Fig. 7—The dependence of the critical gap between columns on the embedment stiffness, net confining stress, and initial fracture opening. The critical gap corresponds to $\delta_{min} = 0$ (i.e., when the channel walls come into contact).

The dependence of the average channel opening on the governing parameters is shown in Fig. 8. It is observed, as expected, that the average channel opening decreases with an increase in the gap between columns $2s$, a decrease in the embedment stiffness γ , and an increase in the net confining stress σ_o . By comparing Figs. 8a through 8d with 8e through 8h, it can be deduced that the effects of proppant embedment and high confining stress can be compensated to some extent by increasing the initial fracture opening (i.e., the proppant-pack density or concentration). The dependence of the peak stress in the column on the governing parameters is shown in Fig. 9. At some combinations of values of the governing parameters, the peak compressive stress in the proppant columns was up to four times greater than the net confining stress for the case of partially propped fractures. However, the peak stress in the proppant pack approached the net confining stress with a decreasing gap between the columns. The peak stress in the proppant pack was found to be lower for small values of the embedment stiffness.

The effective conductivity of partially propped fractures is found to always exceed the conductivity of the fully filled fracture, as shown in Fig. 10. However, an optimal column spacing exists that maximizes the conductivity of the unit cell. This optimal spacing between columns, $2a^*$, is smaller than the maximum permissible spacing between columns, $2a_{cr}$. The optimal spacing is found to weakly depend on the embedment stiffness and strongly depend on the net confining stress and initial fracture opening. The ratio of the column width $2b$ and the optimal column spacing $2a^*$ provides a measure for the optimal volume fraction of proppant in the partially filled unit cell.

Fig. 11 shows the dependence of the optimal proppant-volume fraction on the net confining stress and rock-embedment stiffness. For example, if the optimal proppant-volume fraction is 80%, according to Fig. 10, that means that the fracture conductivity will be maximized if the width of the proppant columns $2b$ is 80% of the width of the unit cell $2a$ (see Fig. 1). Because the proppant arrangement in the fracture is assumed to be periodic, the proppant-volume fraction also represents the percentage fraction of the fracture volume that must be filled with proppant. According to this interpretation, the proppant-volume fraction is an indicator of the ratio of proppant used in discontinuous (channel fracturing) vs. continuous (traditional) proppant placement. From this point of view, Fig. 11 suggests that if it is decided to implement an optimal channel-fracturing treatment, one can expect to save roughly 5 to 15% in proppant use under typical field conditions.

The strong dependence of the optimal column spacing on the initial fracture opening and net confining stress suggests that regular column spacing throughout the fracture length might not be the optimal solution. This is because the initial fracture opening and net confining stress vary gradually, but significantly, from the wellbore toward the fracture tip. Instead, a quasiregular column spacing might be selected in such a manner that the spacing at any given distance from the wellbore is the optimal value for the initial fracture opening and net confining stress at that location. Further investigations are required to identify the optimal quasiregular proppant-column spacing along the fracture length.

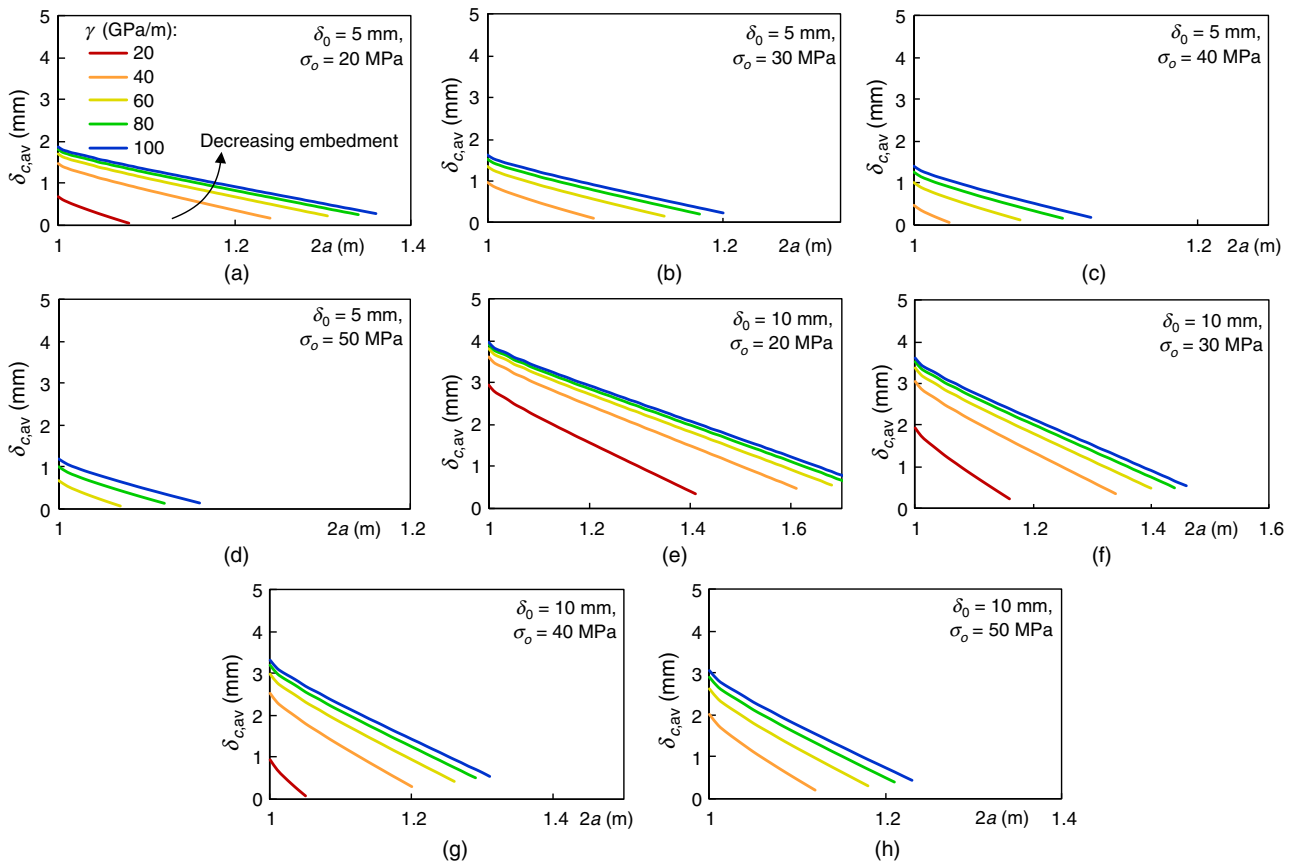


Fig. 8—The dependence of the average channel opening on the unit-cell width, embedment stiffness, net confining stress, and proppant concentration. The case of $2a = 1$ m corresponds to a fully propped fracture.

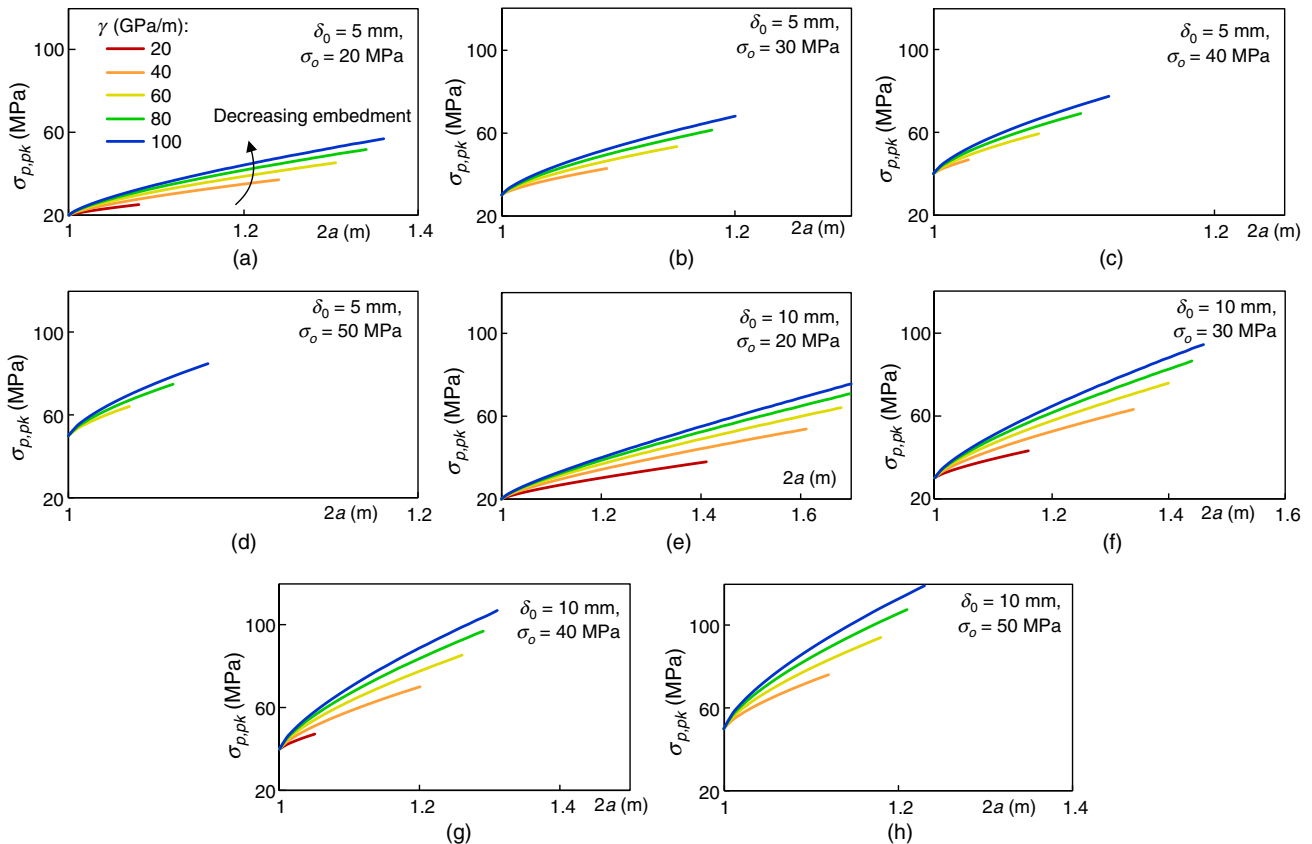


Fig. 9—The dependence of the peak stress in the proppant pack on the unit-cell width, embedment stiffness, net confining stress, and proppant concentration. The case of $2a = 1$ m corresponds to a fully propped fracture.

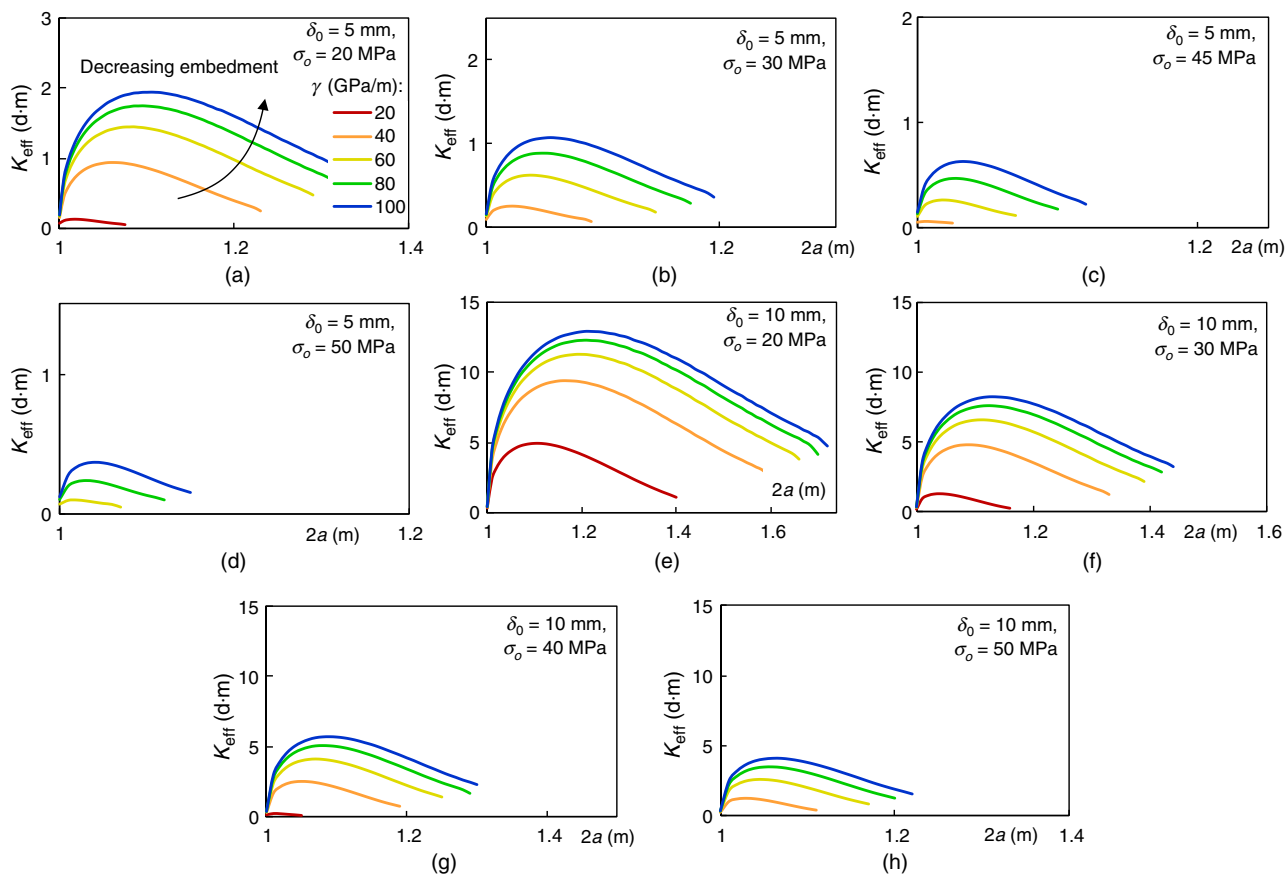


Fig. 10—The dependence of the effective fracture conductivity on the unit-cell width, embedment stiffness, net confining stress, and proppant concentration. The case of $2a = 1$ m corresponds to a fully propped fracture.

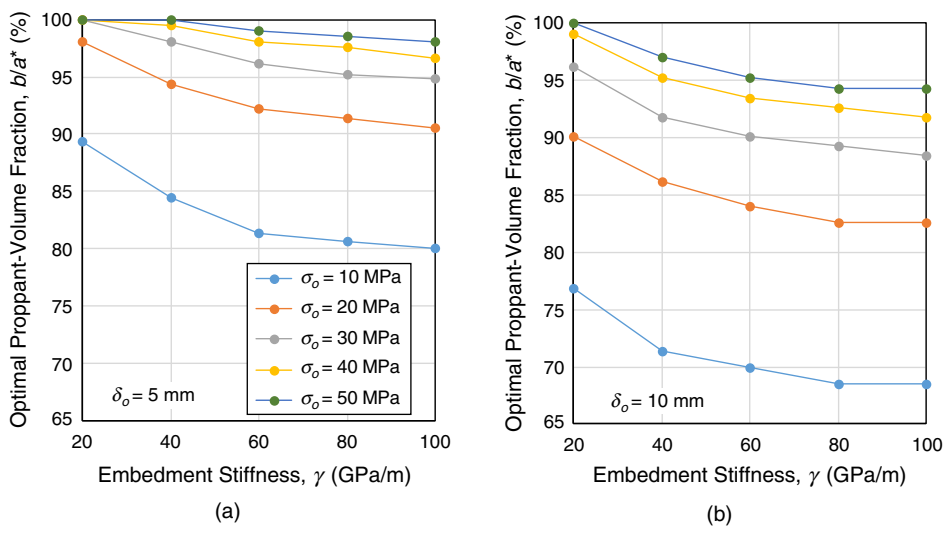


Fig. 11—The dependence of the optimal proppant-volume fraction on the embedment stiffness, net confining stress, and proppant concentration. The case of $b/a^* = 100\%$ corresponds to a fully propped fracture.

Finally, we provide some estimates for the folds of the possible increase in the effective conductivity resulting from the optimized application of the channel-fracturing technique. **Fig. 12** shows that the unit-cell conductivity can be increased by one to two orders of magnitude under a wide range of net confining stresses. These results also indicate that the channel-fracturing technique can be beneficial even in the case of soft rock formations, exhibiting significant proppant embedment, provided that the initial fracture opening is sufficiently large. It is also believed that the adopted simplifications, which are required for this kind of modeling approach, cannot alone explain the large increase in the effective conductivity at optimized conditions. Therefore, one would expect significant benefits from the optimization of channel-fracturing stimulations, which can be dependent on modeling, expert advice, or trial-and-error approaches.

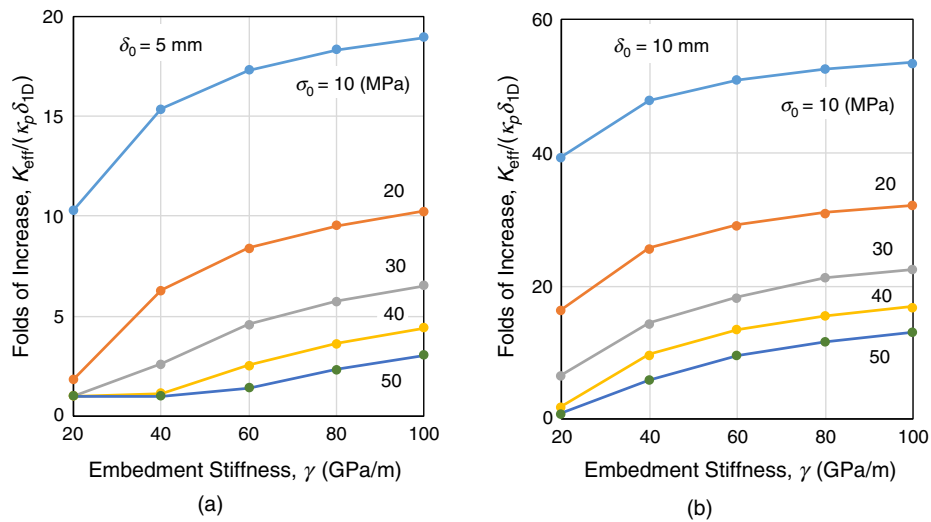


Fig. 12—The dependence of the folds of increase in the fracture conductivity on the embedment stiffness, net confining stress, and proppant concentration. The case of $K_{\text{eff}}/(\kappa_p \delta_{1D}) = 1$ corresponds to a fully propped fracture.

Conclusions

In this paper, we developed an analytical approach for the evaluation of the optimal parameters of the channel-fracturing technique. The approach relies on a rigorous mathematical formulation using the DDT and considers the dominant mechanisms of the proppant-pack response to the applied loading: compaction and embedment. The latter was not adequately represented in the current literature existing on this topic. New empirical models for proppant consolidation and embedment were proposed to adequately describe experimental tendencies while keeping the number of fitting parameters at a minimum. However, the analytical approach using the DDT can be readily adapted to incorporate more-sophisticated models describing the consolidation and embedment of proppant. In any case, the fitting parameters of the empirical models are not unique and need to be determined experimentally for a given rock/proppant combination.

With the developed approach, a suitable proppant-injection schedule can be identified so the full closure of the fracture and sharp decay in the conductivity of fractures can be avoided. The analytical approach also allows the evaluation of optimal spacing between proppant columns of the channel-fracturing stimulation by conducting a multiparametric study, which is often impossible for numerical-based approaches. In the considered characteristic example, it was demonstrated that despite the proppant-volume reduction in the case of channel fracturing being marginal (approximately 10%), the increase in the conductivity is significantly greater compared with continuous proppant placement. The calculations suggest a high sensitivity of the outcomes of the stimulation to the selected values of the net confining stresses, initial opening, and fitting parameters of the proppant-response model. For the practical application of the developed approach, the uncertainty of the input data and the possible error associated with the modeling assumptions must be considered.

Nomenclature

- $1/k$ = lower bound for the conductivity of the unit cell, assuming a series arrangement of conductive elements, L^3, m^3
- $2a$ = width of a unit cell of the periodic-problem geometry, L, m
- $2b$ = width of the proppant columns or pillars, L, m
- $2s$ = gap between adjacent proppant columns, L, m
- b_x, b_y = Cartesian components of the Burger's vector of an edge dislocation, L, m
- $B_y(x)$ = dislocation-density function, dimensionless
- E = Young's modulus of the rock formation, $ML^{-1}T^{-2}$, Pa
- \bar{E} = generalized Young's modulus, $\bar{E} = E$ for plane stress and $\bar{E} = E/(1 - \nu^2)$ for plane strain
- k = upper bound for the conductivity of the unit cell, assuming a parallel arrangement of conductive elements, L^3, m^3
- k_{eff} = effective fluid conductivity of the unit cell and the fracture, L^3, m^3
- $k(x)$ = local fluid conductivity at a point in the unit cell, L^3, m^3
- $K_{n,\text{eff}}$ = effective normal stiffness of the proppant-filled regions of the fracture, $ML^{-2}T^{-2}$, Pa/m
- $K_{n,p}$ = instantaneous normal stiffness of proppant column, $ML^{-2}T^{-2}$, Pa/m
- $K(x, \xi)$ = regular kernel in the governing integral equation, describing the influence of the periodic-problem geometry, L^{-1}, m^{-1}
- L = fracture half-length, L, m
- N = number of integration and collocation points in the numerical solution of the governing integral equation for dislocation density, dimensionless
- $p_f(X)$ = fluid pressure within the fracture, $ML^{-1}T^{-2}$, Pa
- s = normalized integration variable, dimensionless
- s_i, t_k = integration and collocation points for the Gauss-Chebyshev quadrature, dimensionless
- t = normalized coordinate along the crack length, dimensionless
- u_x, u_y = displacement components in the rock, L, m
- x, y = local coordinate axes at the scale of the unit cell
- X, Y = global coordinate axes at the scale of the fracture
- α = fitting parameter to describe the consolidation response of the proppant pack, $ML^{-1}T^{-2}$, Pa
- β = fitting parameter to describe the consolidation response of the proppant pack, dimensionless

- γ = rock-embedment stiffness, $\text{ML}^{-2}\text{T}^{-2}$, Pa/m
- δ_{av} = average residual opening over $0 < |x| < a$, or the average opening of unit cell, L, m
- $\delta_{c,\text{av}}$ = average residual opening over $b < |x| < a$, or the average channel opening, L, m
- δ_{min} = minimum residual opening of a partially filled unit cell, $\delta(x)$ at $x = a$, L, m
- δ_o = initial opening (width) of the unit cell, L, m
- $\delta_{p,\text{av}}$ = average residual opening over $|x| < b$, or the average proppant-column height, L, m
- $\delta(x)$ = residual opening (width) distribution along the unit cell, L, m
- $\Delta(x)$ = fracture closure, $\delta_o - \delta(x)$, L, m
- κ_p = permeability of the proppant pack, L^2 , m^2
- ν = Poisson's ratio of the rock formation, dimensionless
- ξ, ρ = dummy integration variables, L, m
- σ_o = net confining stress acting on the unit cell, $\sigma_o = \sigma_o^\infty - p_f$, $\text{ML}^{-1}\text{T}^{-2}$, Pa
- $\sigma_p(x)$ = compressive stress acting on the proppant columns, $\text{ML}^{-1}\text{T}^{-2}$, Pa
- $\sigma_{p,\text{pk}}$ = peak value of the compressive stress on the proppant columns, $\sigma_p(x = b)$, $\text{ML}^{-1}\text{T}^{-2}$, Pa
- σ_{xx}, σ_{yy} = normal-stress components in the rock, $\text{ML}^{-1}\text{T}^{-2}$, Pa
- σ_{xy} = shear stress in the rock, $\text{ML}^{-1}\text{T}^{-2}$, Pa
- $\sigma_o^\infty(X)$ = remote in-situ stress acting normal to the fracture plane, $\text{ML}^{-1}\text{T}^{-2}$, Pa
- $\hat{\sigma}_{xx}, \hat{\sigma}_{yy}, \hat{\sigma}_{xy}$ = stresses in an infinite elastic medium generated because of an edge dislocation at the origin of the Cartesian coordinate system, $\text{ML}^{-1}\text{T}^{-2}$, Pa
- $\phi(s)$ = unknown regular function, such that $B_y(s) = \omega(s)\phi(s)$, dimensionless
- $\omega(s)$ = fundamental function describing the asymptotic behavior of the dislocation-density function at the endpoints, $s = \pm 1$, dimensionless

References

Abousleiman, Y., Cheng, A. H. D., Cui, L. et al. 1996. Mandel's Problem Revisited. *Géotechnique* **46** (2): 187–195. <https://doi.org/10.1680/geot.1996.46.2.187>.

Barber, J. R. 2010. *Elasticity*, third revised edition. Dordrecht, The Netherlands: Springer.

Barree, R. D., Cox, S. A., Barree, V. L. et al. 2003. Realistic Assessment of Proppant Pack Conductivity for Material Selection. Presented at the SPE Annual Technical Conference and Exhibition, Denver, 5–8 October. SPE-84306-MS. <https://doi.org/10.2118/84306-MS>.

Bedrikovetsky, P. G., Keshavarz, A., Khanna, A. et al. 2012. Stimulation of Natural Cleats for Gas Production From Coal Beds by Graded Proppant Injection. Presented at the SPE Asia Pacific Oil and Gas Conference and Exhibition, Perth, Australia, 22–24 October. SPE-158761-MS. <https://doi.org/10.2118/158761-MS>.

Bilby, B. and Eshelby, J. 1968. Dislocations and The Theory of Fracture. In *Fracture: An Advanced Treatise*, Vol. 1, ed. H. Liebowitz, 99–182. New York City: Academic Press.

Bilby, B. A., Cottrell, A. H., and Swinden, K. H. 1963. The Spread of Plastic Yield From a Notch. *Proc. Roy. Soc. London A* **272** (1350): 304–314. <https://doi.org/10.1098/rspa.1963.0055>.

Bortolan Neto, L., Kotousov, A., and Bedrikovetsky, P. 2011. Elastic Properties of Porous Media in the Vicinity of the Percolation Limit. *J. Pet. Sci. Eng.* **78** (2): 328–333. <https://doi.org/10.1016/j.petrol.2011.06.026>.

Bortolan Neto, L., Khanna, A., and Kotousov, A. 2015. Conductivity and Performance of Hydraulic Fractures Partially Filled With Compressible Proppant Packs. *Int. J. Rock Mech. Min.* **74** (February): 1–9. <https://doi.org/10.1016/j.ijrmms.2014.11.005>.

Budiansky, B., Hutchinson, J. W., and Evans, A. G. 1986. Matrix Fracture in Fiber-Reinforced Ceramics. *J. Mech. Phys. Solids* **34** (2): 167–189. [https://doi.org/10.1016/0022-5096\(86\)90035-9](https://doi.org/10.1016/0022-5096(86)90035-9).

Burukhin, A. A., Kalinin, S., Abott, J. et al. 2012. Novel Interconnected Bonded Structure Enhances Proppant Flowback Control. Presented at the SPE International Symposium and Exhibition on Formation Damage Control, Lafayette, Louisiana, 15–17 February. SPE-151861-MS. <https://doi.org/10.2118/151861-MS>.

Codrington, J. and Kotousov, A. 2009. A Crack Closure Model of Fatigue Crack Growth in Plates of Finite Thickness Under Small-Scale Yielding Conditions. *Mech. Mater.* **41** (2): 165–173. <https://doi.org/10.1016/j.mechmat.2008.10.002>.

Coop, M. R. 1990. The Mechanics of Uncemented Carbonate Sands. *Géotechnique* **40** (4): 607–626. <https://doi.org/10.1680/geot.1990.40.4.607>.

Cox, B. N. and Rose, L. R. F. 1996. A Self-Consistent Approximation for Crack Bridging by Elastic/Perfectly Plastic Ligaments. *Mech. Mater.* **22** (4): 249–263. [https://doi.org/10.1016/0167-6636\(95\)00025-9](https://doi.org/10.1016/0167-6636(95)00025-9).

d'Huteau, E., Gillard, M., Miller, M. et al. 2011. Open-Channel Fracturing—A Fast Track to Production. *Oilfield Rev.* **23** (3): 4–17, https://www.slb.com/~media/Files/resources/oilfield_review/ors11/aut11/01_open_channel.pdf (accessed 12 May 2017).

Darin, S. R. and Huit, J. L. 1959. Effect of a Partial Monolayer of Propping Agent on Fracture Flow Capacity. SPE-1291-G.

Deng, S., Haibo, L., Guowei, M. et al. 2014. Simulation of Shale-Proppant Interaction in Hydraulic Fracturing by the Discrete Element Method. *Int. J. Rock Mech. Min.* **70** (September): 219–228. <https://doi.org/10.1016/j.ijrmms.2014.04.011>.

Detournay, E. and Cheng, A. H.-D. 1991. Plane Strain Analysis of a Stationary Hydraulic Fracture in a Poroelastic Medium. *Int. J. Solids Struct.* **27** (13): 1645–1662. [https://doi.org/10.1016/0020-7683\(91\)90067-P](https://doi.org/10.1016/0020-7683(91)90067-P).

Erdogan, F., Gupta, G. D., and Cook, T. S. 1973. Numerical Solution of Singular Integral Equations. In *Mechanics of Fracture*, Vol. 1, ed. G. C. Sih, 368–425. Leyden, The Netherlands: Noordhoff International.

Gao, Y., Lv, Y., Wang, M. et al. 2013. New Mathematical Models for Calculating the Proppant Embedment and Conductivity. Oral presentation given at IPTC 2013: International Petroleum Technology Conference, Beijing, 26–28 March.

Gillard, M. R., Medvedev, O. O., Hosein, P. R. et al. 2010. A New Approach to Generating Fracture Conductivity. Presented at the SPE Annual Technical Conference and Exhibition, Florence, Italy, 19–22 September. SPE-135034-MS. <https://doi.org/10.2118/135034-MS>.

Guo, J.-C., Lu, C., Zhao, J.-Z. et al. 2008. Experimental Research on Proppant Embedment. *J. China Coal Soc.* **33** (6): 661–664.

Hardin, B. O. 1985. Crushing of Soil Particles. *J. Geotech. Eng.* **111** (10): 1177–1192. [https://doi.org/10.1061/\(ASCE\)0733-9410\(1985\)111:10\(1177\)](https://doi.org/10.1061/(ASCE)0733-9410(1985)111:10(1177)).

Hashin, Z. and Shtrikman, S. 1962. A Variational Approach to the Theory of the Effective Magnetic Permeability of Multiphase Materials. *J. Appl. Phys.* **33**: 3125–3131. <https://doi.org/10.1063/1.1728579>.

Hills, D. A., Kelly, P. A., Dai, D. N. et al. 1996. *Solution of Crack Problems: The Distributed Dislocation Technique*. Dordrecht, The Netherlands: Kluwer Academic Publishers.

Hirth, J. P. and Lothe, J. 1968. *Theory of Dislocations*. New York City: McGraw-Hill.

- Hou, B., Zheng, X., Chen, M. et al. 2016a. Parameter Simulation and Optimization in Channel Fracturing. *J. Nat. Gas Sci. Eng.* **35A** (September): 122–130. <https://doi.org/10.1016/j.jngse.2016.08.046>.
- Hou, T., Zhang, S., Yu, B. et al. 2016b. Theoretical Analysis and Experimental Research of Channel Fracturing in Unconventional Reservoir. Presented at SPE Europec featured at the 78th EAGE Conference and Exhibition, Vienna, Austria, 30 May–2 June. SPE-180105-MS. <https://doi.org/10.2118/180105-MS>.
- Huitt, J. L. and McGlothlin, B. B. Jr. 1958. The Propping of Fractures in Formations Susceptible to Propping-Sand Embedment. API-58-115.
- Inyang, U. A., Nguyen, P. D., and Cortez, J. 2014. Development and Field Applications of Highly Conductive Proppant-Free Channel Fracturing Method. Presented at the SPE Unconventional Resources Conference, The Woodlands, Texas, 1–3 April. SPE-168996-MS. <https://doi.org/10.2118/168996-MS>.
- Khanna, A. and Kotousov, A. 2014. Stress Analysis of a Crack in a Fiber-Reinforced Layered Composite. *Compos. Struct.* **118** (December): 139–148. <https://doi.org/10.1016/j.compstruct.2014.07.024>.
- Khanna, A. and Kotousov, A. 2015. Controlling the Height of Multiple Hydraulic Fractures in Layered Media. *SPE J.* **21** (1): 256–263. SPE-176017-PA. <https://doi.org/10.2118/176017-PA>.
- Khanna, A. and Kotousov, A. 2016. The Stress Field Due to an Interfacial Edge Dislocation in a Multi-Layered Medium. *Int. J. Solids Struct.* **72** (15 October): 1–10. <https://doi.org/10.1016/j.ijsolstr.2015.06.030>.
- Khanna, A., Bortolan Neto, L., and Kotousov, A. 2014. Effect of Residual Opening on the Inflow Performance of a Hydraulic Fracture. *Int. J. Eng. Sci.* **74** (January): 80–90. <https://doi.org/10.1016/j.ijengsci.2013.08.012>.
- Khanna, A., Keshavarz, A., Mobbs, K. et al. 2013. Stimulation of the Natural Fracture System by Graded Proppant Injection. *J. Pet. Sci. Eng.* **111** (November): 71–77. <https://doi.org/10.1016/j.petrol.2013.07.004>.
- Khanna, A., Kotousov, A., Sobey, J. et al. 2012. Conductivity of Narrow Fractures Filled With a Proppant Monolayer. *J. Pet. Sci. Eng.* **100** (December): 9–13. <https://doi.org/10.1016/j.petrol.2012.11.016>.
- Khanna, A., Luong, H., Kotousov, A. et al. 2017. Residual Opening of Hydraulic Fractures Created Using the Channel-Fracturing Technique. *Int. J. Rock Mech. Min.* **100** (December): 124–137. <https://doi.org/10.1016/j.ijrmms.2017.10.023>.
- Kotousov, A., Bortolan Neto, L., and Khanna, A. 2014. On a Rigid Inclusion Pressed Between Two Elastic Half Spaces. *Mech. Mater.* **68** (January): 38–44. <https://doi.org/10.1016/j.mechmat.2013.08.004>.
- Lacy, L. L., Rickards, A. R., and Bilden, D. M. 1998. Fracture Width and Embedment Testing in Soft Reservoir Sandstone. *SPE Drill & Compl* **13** (1): 25–29. SPE-36421-PA. <https://doi.org/10.2118/36421-PA>.
- Le, L. A., Nguyen, G. D., Bui, H. H. et al. 2017. Modelling Jointed Rock Mass as a Continuum With an Embedded Cohesive-Frictional Model. *Eng. Geol.* **228** (13 October): 107–120. <https://doi.org/10.1016/j.enggeo.2017.07.011>.
- Li, K., Gao, Y., Lyu, Y. et al. 2015. New Mathematical Models for Calculating Proppant Embedment and Fracture Conductivity. *SPE J.* **20** (3): 496–507. SPE-155954-PA. <https://doi.org/10.2118/155954-PA>.
- Liang, F., Sayed, M., Al-Muntasheri, G. A. et al. 2016. A Comprehensive Review on Proppant Technologies. *Petroleum* **2** (1): 26–39. <https://doi.org/10.1016/j.petlm.2015.11.001>.
- Liu, C., Hoang, S. K., and Abousleiman, Y. N. 2018. Responses of Chemically Active and Naturally Fractured Shale Under Time-Dependent Mechanical Loading and Ionic Solution Exposure. *Int. J. Numer. Anal. Met.* **42** (1): 34–69. <https://doi.org/10.1002/nag.2713>.
- Malhotra, S., Lehman, E. R., and Sharma, M. M. 2014. Proppant Placement Using Alternate-Slug Fracturing. *SPE J.* **19** (5): 974–985. SPE-163851-PA. <https://doi.org/10.2118/163851-PA>.
- Medvedev, A. V., Kraemer, C. C., Pena, A. A. et al. 2013. On the Mechanisms of Channel Fracturing. Presented at the SPE Hydraulic Fracturing Technology Conference, The Woodlands, Texas, 4–6 February. SPE-163836-MS. <https://doi.org/10.2118/163836-MS>.
- Mesri, G. and Vardhanabhati, B. 2009. Compression of Granular Materials. *Can. Geotech. J.* **46** (4): 369–392. <https://doi.org/10.1139/T08-123>.
- Momber, A. W. 2004. Deformation and Fracture of Rocks Loaded With Spherical Indenters. *Int. J. Fract.* **125** (3–4): 263–279. <https://doi.org/10.1023/B:FRAC.0000022240.64448.2f>.
- Morris, J. P., Chugunov, N., and Meouchy, G. 2014. Understanding Heterogeneously Propped Hydraulic Fractures Through Combined Fluid Mechanics, Geomechanics, and Statistical Analysis. Presented at the 48th US Rock Mechanics/Geomechanics Symposium, Minneapolis, Minnesota, 1–4 June. ARMA-2014-7408.
- Much, M. G. and Penny, G. S. 1987. Long-Term Performance of Proppants Under Simulated Reservoir Conditions. Presented at the Low Permeability Reservoirs Symposium, Denver, 18–19 May. SPE-16415-MS. <https://doi.org/10.2118/16415-MS>.
- Nguyen, P. D., Weaver, J. D., Parker, M. A. et al. 1996. Thermoplastic Film Prevents Proppant Flowback. *Oil Gas J.* **94**: 60–62.
- Palisch, T. T., Vincent, M., and Handren, P. J. 2010. Slickwater Fracturing: Food for Thought. *SPE Prod & Oper* **25** (3): 327–344. SPE-115766-PA. <https://doi.org/10.2118/115766-PA>.
- Pestana, J. M. and Whittle, A. J. 1995. Compression Model for Cohesionless Soils. *Géotechnique* **45** (4): 611–631. <https://doi.org/10.1680/geot.1995.45.4.611>.
- Peterson, R. E. 1953. *Stress Concentration Design Factors*. New York City: Wiley.
- Reinicke, A. 2011. *Mechanical and Hydraulic Aspects of Rock-Proppant Systems: Laboratory Experiments and Modelling Approaches*. PhD dissertation, GFZ German Research Centre for Geosciences, Potsdam, Germany.
- Reinicke, A., Rybacki, E., Stanchits, S. et al. 2010. Hydraulic Fracturing Stimulation Techniques and Formation Damage Mechanisms—Implications From Laboratory Testing of Tight Sandstone–Proppant Systems. *Chem. Erde Geochem.* **70** (August): 107–117. <https://doi.org/10.1016/j.chemer.2010.05.016>.
- Rice, J. R. and Cleary, M. P. 1976. Some Basic Stress Diffusion Solutions for Fluid-Saturated Elastic Porous Media With Compressible Constituents. *Rev. Geophys.* **14** (2): 227–241. <https://doi.org/10.1029/RG014i002p00227>.
- Roberts, J. E. and de Souza, J. M. 1958. The Compressibility of Sands. *Proc. Am. Soc. Test. Mater.* **58**: 1269–1272.
- Romero, J. and Feraud, J. P. 1996. Stability of Proppant Pack Reinforced With Fiber for Proppant Flowback Control. Presented at the SPE Formation Damage Control Symposium, Lafayette, Louisiana, 14–15 February. SPE-31093-MS. <https://doi.org/10.2118/31093-MS>.
- Rose, L. R. F. 1987. Effective Spring Constant for Unbroken Ligaments Between Crack Faces. *Int. J. Fract.* **33** (2): 145–152. <https://doi.org/10.1007/BF00033746>.
- Segall, P. and Fitzgerald, S. D. 1998. A Note on Induced Stress Changes in Hydrocarbon and Geothermal Reservoirs. *Tectonophysics* **289** (1–3): 117–128. [https://doi.org/10.1016/S0040-1951\(97\)00311-9](https://doi.org/10.1016/S0040-1951(97)00311-9).
- Sinclair, A. R., Graham, J. W., and Sinclair, C. P. 1993. Improved Well Stimulation With Resincoated Proppants. Presented at the SPE Production Operations Symposium, Oklahoma City, Oklahoma, 27 February–1 March. SPE-11579-MS. <https://doi.org/10.2118/11579-MS>.
- Tinsley, J. M. and Williams, J. R. Jr. 1975. A New Method for Providing Increased Fracture Conductivity and Improving Stimulation Results. *J. Pet Technol* **27** (11): 1319–1325. SPE-4676-PA. <https://doi.org/10.2118/4676-PA>.
- Valko, P. and Economides, M. J. 1995. *Hydraulic Fracture Mechanics*. Chichester, UK: Wiley.

Volk, L. J., Raible, C. J., Carroll, H. B. et al. 1981. Embedment of High Strength Proppant Into Low-Permeability Reservoir Rock. Presented at the SPE/DOE Low Permeability Gas Reservoirs Symposium, Denver, 27–29 May. SPE-9867-MS. <https://doi.org/10.2118/9867-MS>.

Weaver, J. D., Baker, J. D., Woolverton, S. et al. 1999. Application of Surface-Modification Agent in Wells With High Flow Rates. Presented at the Latin American and Caribbean Petroleum Engineering Conference, Caracas, 21–23 April. SPE-53923-MS. <https://doi.org/10.2118/53923-MS>.

Weaver, J. D., van Batenburg, D. W., Parker, M. A. et al. 2006. Sustaining Conductivity. Presented at the SPE International Symposium and Exhibition on Formation Damage Control, Lafayette, Louisiana, 15–17 February. SPE-98236-MS. <https://doi.org/10.2118/98236-MS>.

Wen, Q., Zhang, S., Wang, L. et al. 2007. The Effect of Proppant Embedment Upon the Long-Term Conductivity of Fractures. *J. Pet. Sci. Eng.* **55** (3–4): 221–227. <https://doi.org/10.1016/j.petrol.2006.08.010>.

Witherspoon, P. A., Wang, J. S. Y., Iwai, K. et al. 1980. Validity of Cubic Law for Fluid Flow in a Deformable Rock Fracture. *Water Resour. Res.* **16** (6): 1016–2024. <https://doi.org/10.1029/WR016i006p01016>.

Yan, X., Huang, Z., Yao, J. et al. 2016. Theoretical Analysis of Fracture Conductivity Created by the Channel-Fracturing Technique. *J. Nat. Gas Sci. Eng.* **31** (April): 320–330. <https://doi.org/10.1016/j.jngse.2016.03.038>.

Zhang, J. and Hou, J. 2016. Theoretical Conductivity Analysis of Surface Modification Agent Treated Proppant II—Channel Fracturing Application. *Fuel* **165** (1 February): 28–32. <https://doi.org/10.1016/j.fuel.2015.10.026>.

Zhang, J., Ouyang, L., Zhu, D. et al. 2015. Experimental and Numerical Studies of Reduced Fracture Conductivity Due to Proppant Embedment in the Shale Reservoir. *J. Pet. Sci. Eng.* **130** (June): 37–45. <https://doi.org/10.1016/j.petrol.2015.04.004>.

Zheng, X., Chen, M., Hou, B. et al. 2017. Effect of Proppant Distribution Pattern on Fracture Conductivity and Permeability in Channel Fracturing. *J. Pet. Sci. Eng.* **149** (20 January): 98–106. <https://doi.org/10.1016/j.petrol.2016.10.023>.

Zimmerman, R. W. and Bodvarsson, G. S. 1996. Hydraulic Conductivity of Rock Fractures. *Transport Porous Med.* **23** (1): 1–30. <https://doi.org/10.1007/BF00145263>.

Zimmerman, R. W. and Yeo, I. W. 2000. Fluid Flow in Rock Fractures: From the Navier-Stokes Equations to the Cubic Law. In *Dynamics of Fluids in Fractured Rock*, Vol. 122, eds. B. Faybishenko, P. A. Witherspoon, S. M. Benson, 213–224, Washington, DC: American Geophysical Union.

Zimmerman, R. W., Kumar, S., and Bodvarsson, G. S. 1991. Lubrication Theory Analysis of the Permeability of Rough-Walled Fractures. *Int. J. Rock Mech. Min.* **28** (4): 325–331. [https://doi.org/10.1016/0148-9062\(91\)90597-F](https://doi.org/10.1016/0148-9062(91)90597-F).

Appendix A—Singular-Integral Equation for Dislocation Density

Before developing the governing equations for the elasticity problem, we briefly review the fundamental solution for the stress field arising from a single edge dislocation in an infinite body. Consider the 2D problem of an edge dislocation with Burger’s vector $\mathbf{b} = 0\mathbf{i} + b_y\mathbf{j}$, located at the origin $x = 0, y = 0$ of an infinite elastic medium. The dislocation produces a displacement jump,

$$u_y(x, y = 0^+) - u_y(x, y = 0^-) = b_y H(-x), \dots \dots \dots \text{(A-1)}$$

in the elastic medium, where $u_y(x, y)$ is the y -component of the displacement field. The displacement jump is equivalent to making a cut along $x < 0, y = 0$, pulling the material apart and inserting a strip of material of thickness b_y before rejoining. The stress field arising from the displacement jump (Eq. A-1) is known to be (Hirth and Lothe 1968)

$$\hat{\sigma}_{xx}(x, y) = \frac{\bar{E}}{4\pi} b_y \frac{x}{r^4} (x^2 - y^2), \dots \dots \dots \text{(A-2)}$$

$$\hat{\sigma}_{yy}(x, y) = \frac{\bar{E}}{4\pi} b_y \frac{x}{r^4} (x^2 + 3y^2), \dots \dots \dots \text{(A-3)}$$

$$\hat{\sigma}_{xy}(x, y) = \frac{\bar{E}}{4\pi} b_y \frac{y}{r^4} (x^2 - y^2), \dots \dots \dots \text{(A-4)}$$

where $r^2 = x^2 + y^2$ and \bar{E} is the generalized Young’s modulus, defined as $\bar{E} = E$ under plane-stress conditions or $\bar{E} = E/(1 - \nu^2)$ under plane-strain conditions.

Now consider a continuous distribution of dislocations along $-\infty < x < \infty, y = 0$, such that the strength of an infinitesimal dislocation lying between $x = \xi$ and $x = \xi + d\xi$ is $db_y = B_y d\xi$. The stress field induced by the continuous distribution of dislocations is obtained by integrating the fundamental solution for a single dislocation (i.e., Eqs. A-2 through A-4). It follows from the superposition principle that the stress state in the cracked body can be then be written as a summation of the stress state in the body in the absence of the crack and the stress state induced by the separation of the crack faces (i.e., the continuous distribution of dislocations),

$$\sigma_{xx}(x, y) = \frac{\bar{E}}{4\pi} \int_{-\infty}^{\infty} B_y(\xi) \frac{(x - \xi)[(x - \xi)^2 - y^2]}{[(x - \xi)^2 + y^2]^2} d\xi, \dots \dots \dots \text{(A-5)}$$

$$\sigma_{yy}(x, y) = -\sigma_o + p_f + \frac{\bar{E}}{4\pi} \int_{-\infty}^{\infty} B_y(\xi) \frac{(x - \xi)[(x - \xi)^2 + 3y^2]}{[(x - \xi)^2 + y^2]^2} d\xi, \dots \dots \dots \text{(A-6)}$$

$$\sigma_{xy}(x, y) = \frac{\bar{E}}{4\pi} \int_{-\infty}^{\infty} B_y(\xi) \frac{y[(x - \xi)^2 - y^2]}{[(x - \xi)^2 + y^2]^2} d\xi. \dots \dots \dots \text{(A-7)}$$

The functional form of the dislocation-density function, $B_y(\xi)$, is determined using the physical considerations relevant to the problem at hand.

It can be observed that the symmetry condition, Eq. 9 [i.e., $\sigma_{xy}(x, y = 0_{\pm}) = 0$], is automatically satisfied by Eq. A-7. It is also noted that the integral in Eq. A-6 vanishes as $y \rightarrow \infty$; hence, the boundary condition at infinity, Eq. 10, is also satisfied. Next, consider the shear stresses along $x = \pm a$, which are given by

$$\sigma_{xy}(x = \pm a, y) = \frac{\bar{E}}{4\pi} y \int_{-\infty}^{\infty} B_y(\xi) \frac{[(a \mp \xi)^2 - y^2]}{[(a \mp \xi)^2 + y^2]^2} d\xi. \dots \dots \dots \text{(A-8)}$$

Because of the periodicity of the unit-cell geometry, the residual opening of the fracture, $\delta(x)$, must be even about $x = \pm a$, i.e., the dislocation-density function, $B_y(\xi) = d\delta(\xi)/d\xi$ must be an odd function about $\xi = \pm a$, i.e., of the form $B_y(\xi + 2an) = B_y(\xi)$, $n = 0, \pm 1, \pm 2, \dots$. The periodicity boundary condition, Eq. 7, i.e., $\sigma_{xy}(x = \pm a, y) = 0$, can be satisfied by Eq. A-8 only if the dislocation density is equal to zero at $\xi = 2an$.

A similar argument can be made regarding the shear stress induced by the distributed dislocations along the line $x = 0$, which can also be obtained from Eq. A-7 as

$$\sigma_{xy}(0, y) = \frac{\bar{E}}{4\pi} y \int_{-\infty}^{\infty} B_y(\xi) \frac{(\xi^2 - y^2)}{(\xi^2 + y^2)^2} d\xi \dots \dots \dots (A-9)$$

The residual opening of the unit cell must be symmetric at approximately $x = 0$; i.e., the dislocation density must be an odd function at approximately $\xi = 0$, or $B_y(-\xi) = -B_y(\xi)$. In addition, because the dislocation density must vary continuously as it changes sign from positive to negative, it must be equal to zero at $\xi = 0$.

We now proceed to the application of the DDT to obtaining the governing integral equation for the dislocation-density function. The normal traction along $y = 0$ can be obtained from Eq. A-6 as

$$\sigma_{yy}(x, 0) = -\sigma_o^\infty + p_f + \frac{\bar{E}}{4\pi} \int_{-\infty}^{\infty} \frac{B_y(\xi)}{x - \xi} d\xi \dots \dots \dots (A-10)$$

The indefinite integral in Eq. A-10 can be subdivided into smaller intervals, such that

$$\sigma_{yy}(x, 0) = -\sigma_o^\infty + p_f + \frac{\bar{E}}{4\pi} \sum_{-\infty}^{\infty} \int_{(2n-1)a}^{(2n+1)a} \frac{B_y(\xi_n)}{x - \xi_n} d\xi_n, \quad \xi_n = \bar{\xi} + 2an, \quad -a < \bar{\xi} < a \dots \dots \dots (A-11)$$

Noting that $d\xi_n = d\bar{\xi}$ and $B_y(\xi_n) = B_y(\bar{\xi} + 2an) = B_y(\bar{\xi})$, the integrals within the summation can be rewritten as

$$\sigma_{yy}(x, 0) = -\sigma_o^\infty + p_f + \frac{\bar{E}}{4\pi} \sum_{-\infty}^{\infty} \int_a^a \frac{B_y(\bar{\xi})}{x - \bar{\xi} - 2an} d\bar{\xi} \dots \dots \dots (A-12)$$

Further, the summation operator can be moved inside the integral to yield

$$\sigma_{yy}(x, 0) = -\sigma_o^\infty + p_f + \frac{\bar{E}}{4\pi} \int_a^a B_y(\bar{\xi}) \sum_{-\infty}^{\infty} \frac{1}{x - \bar{\xi} - 2an} d\bar{\xi} \dots \dots \dots (A-13)$$

The summation in Eq. A-13 can be rewritten by isolating the term corresponding to $n = 0$ and combining the $+n$ and $-n$ terms,

$$\begin{aligned} \sigma_{yy}(x, 0) &= -\sigma_o^\infty + p_f + \frac{\bar{E}}{4\pi} \int_a^a B_y(\bar{\xi}) \left[\frac{1}{x - \bar{\xi}} + \sum_{n=1}^{\infty} \left(\frac{1}{x - \bar{\xi} - 2an} + \frac{1}{x - \bar{\xi} + 2an} \right) \right] d\bar{\xi} \\ &= -\sigma_o^\infty + p_f + \frac{\bar{E}}{4\pi} \int_a^a B_y(\bar{\xi}) \left\{ \frac{1}{x - \bar{\xi}} + \sum_{n=1}^{\infty} \left[\frac{2(x - \bar{\xi})}{(x - \bar{\xi})^2 - 4a^2n^2} \right] \right\} d\bar{\xi} \dots \dots \dots (A-14) \end{aligned}$$

Dropping the overbar from $\bar{\xi}$, the governing equation for the dislocation density over the unit cell $|x| < a$ can be written as

$$\sigma_{yy}(x, 0) = -\sigma_o^\infty + p_f + \frac{\bar{E}}{4\pi} \int_a^a B_y(\xi) \left\{ \frac{1}{x - \xi} + \sum_{n=1}^{\infty} \left[\frac{2(x - \xi)}{(x - \xi)^2 - 4a^2n^2} \right] \right\} d\xi, \quad |x| < a \dots \dots \dots (A-15)$$

Using the symmetry of the dislocation-density function at approximately $x = 0$, Eq. A-15 can be further reduced to

$$\sigma_{yy}(x, 0) = -\sigma_o^\infty + p_f + \frac{\bar{E}}{4\pi} \int_0^a B_y(\xi) \left[\frac{2\xi}{x^2 - \xi^2} + K(x, \xi) \right] d\xi, \quad 0 < x < a, \dots \dots \dots (A-16)$$

where the kernel $K(x, \xi)$ is given by

$$K(x, \xi) = \sum_{n=1}^{\infty} \frac{4\xi(x^2 - \xi^2 + 4a^2n^2)}{[(x - \xi)^2 - 4a^2n^2][(x + \xi)^2 - 4a^2n^2]} \dots \dots \dots (A-17)$$

To satisfy the traction boundary condition, Eq. 8, it is required that

$$-\sigma_o^\infty + p_f + \frac{\bar{E}}{4\pi} \int_0^a B_y(\xi) \left[\frac{2\xi}{x^2 - \xi^2} + K(x, \xi) \right] d\xi = \begin{cases} \sigma_p(x), & |x| < b, \\ 0, & b < |x| < a \end{cases} \dots \dots \dots (A-18)$$

or

$$\frac{\bar{E}}{4\pi} \int_0^a B_y(\xi) \left[\frac{2\xi}{x^2 - \xi^2} + K(x, \xi) \right] d\xi = -\sigma_o^\infty + p_f - \sigma_p(x)H(b - |x|), \quad 0 < x < a, \quad \dots \quad (\text{A-19})$$

where $H(\cdot)$ is the Heaviside step function.

Appendix B—Numerical-Solution Procedure of the Singular-Integral Equation

The first step of the numerical-solution procedure is to normalize the interval in Eqs. 13 and 14 from $[0, a]$ to $[-1, 1]$. The substitution $x = (a/2)(t + 1)$ and $\xi = (a/2)(s + 1)$ yields the normalized form for the integral equation,

$$\frac{1}{\pi} \int_{-1}^1 B_y(s) \left[\frac{(s + 1)}{2(t - s)(t + s + 2)} + K'(t, s) \right] ds = \frac{\sigma_o}{E} - \frac{\sigma_p(t)}{E} H\left(\frac{2b}{a} - t - 1\right), \quad -1 < t < 1, \quad \dots \quad (\text{B-1})$$

where the regular part of the kernel becomes

$$K'(t, s) = \sum_{n=1}^\infty \frac{(s + 1)[(t - s)(t + s + 2) + 16n^2]}{[(t - s)^2 - 16n^2][(t + s + 2)^2 - 16n^2]}.$$

The crack-opening displacement $\delta(t)$ over the normalized interval can be normalized in a similar manner to yield

$$\delta(t) = \delta_{\min} + \frac{a}{2} \int_t^1 B_y(s) ds, \quad -1 < t < 1. \quad \dots \quad (\text{B-2})$$

The dislocation-density function, $B_y(s)$, is then represented as the product of an unknown regular function $\phi(s)$ and a fundamental function $\omega(s)$ that takes into account the asymptotic behavior of the solution for dislocation density at $s = \pm 1$ (Erdogan et al. 1973). As discussed previously, the symmetry of the present problem requires that the dislocation density be equal to zero at $\xi = 0, a$ [i.e., $B_y(s) = 0$ at $s = \pm 1$]. The appropriate form for the fundamental function $\omega(s)$ that satisfies this requirement is $\omega(s) = \sqrt{(1 - s^2)}$ (Erdogan et al. 1973; Hills et al. 1996). For the chosen fundamental function, the Gauss-Chebyshev quadrature is used to reduce the singular integral, Eq. 25, to the following system of algebraic equations:

$$\frac{1}{N + 1} \sum_{i=1}^N (1 - s_i^2) \left[\frac{(s_i + 1)}{2(t_k - s_i)(t_k + s_i + 2)} + K'(t_k, s_i) \right] \phi(s_i) + \frac{\sigma_p(t_k)}{E} H\left(\frac{2b}{a} - t_k - 1\right) - \frac{\sigma_o}{E} = 0, \quad k = 1, 2, \dots, N + 1, \quad \dots \quad (\text{B-3})$$

where

$$K'(t_k, s_i) = \sum_{n=1}^\infty \frac{(s_i + 1)[(t_k - s_i)(t_k + s_i + 2) + 16n^2]}{[(t_k - s_i)^2 - 16n^2][(t_k + s_i + 2)^2 - 16n^2]}.$$

The proppant-reaction stress and residual opening at discrete points t_k are

$$\sigma_p(t_k) = \int_{\delta(t_k)}^{\delta_o} \frac{\sigma_{po} \alpha \beta \gamma \delta_o (\delta_o - \rho)^{\beta-1}}{\gamma \rho^{\beta+1} + 2\sigma_{po} \alpha \beta \delta_o (\delta_o - \rho)^{\beta-1}} d\rho \quad \dots \quad (\text{B-4})$$

and

$$\delta(t_k) = \delta_{\min} + \frac{\pi a}{2(N + 1)} \sum_{i=1}^{k-1} (1 - s_i^2) \phi(s_i). \quad \dots \quad (\text{B-5})$$

The expression for $\sigma_p(t_k)$ is obtained by numerical integration. The integration and collocation points are roots of Chebyshev polynomials (Erdogan et al. 1973),

$$U_N(s_i) = 0, \quad s_i = \cos\left(\pi \frac{i}{N + 1}\right), \quad i = 1, \dots, N, \quad \dots \quad (\text{B-6})$$

$$T_{N+1}(t_k) = 0, \quad t_k = \cos\left(\frac{\pi 2k - 1}{2N + 1}\right), \quad k = 1, \dots, N + 1, \quad \dots \quad (\text{B-7})$$

where $U_N(s)$ is a Chebyshev polynomial of second order N and $T_{N+1}(t)$ is a Chebyshev polynomial of first order $N + 1$. The system of equations in Eq. B-3 is nonlinear and requires an iterative solution (Khanna and Kotousov 2014; Bortolan Neto et al. 2015). Let the array $\{\phi\} = \{\phi_1, \phi_2, \dots, \phi_N\}^T = \{\phi(s_1), \phi(s_2), \dots, \phi(s_N)\}^T$ contain the unknown values of the function $\phi(s)$ at the N integration points along the crack. Also, let the array $\{F\} = [F_1(\phi), F_2(\phi), \dots, F_{N+1}(\phi)]$ represent the left-hand side of Eq. B-3 evaluated at $\{\phi\}$. Then, the value of $\{\phi\}$ that satisfies the system of equations, $\{F\} = 0$, within some allowed tolerance or error, is the solution or root to the system of equations in Eq. B-3. The iterative solution procedure requires an initial guess for the solution, $\{\phi\}_0$, as well as the Jacobian matrix, which contains all first-order partial derivatives of the vector-valued function $\{F\}$. For the present problem, the elements of the Jacobian matrix $[J]$ can be obtained as

$$J_{k,i} = \frac{\partial F_k}{\partial \phi_i} = \frac{(1 - s_i^2)}{N + 1} \left[\frac{(s_i + 1)}{2(t_k - s_i)(t_k + s_i + 2)} + K'(t_k, s_i) \right] - \frac{1}{E} H \left(\frac{2b}{a} - t_k - 1 \right) \frac{\sigma_{po} \alpha \beta \gamma \delta_o (\delta_o - \delta)^{\beta-1}}{\gamma \delta^{\beta+1} + 2 \sigma_{po} \alpha \beta \delta_o (\delta_o - \delta)^{\beta-1}} \frac{\pi a}{2(N + 1)} \times (1 - s_i^2) H(k - i - 1). \dots \dots \dots (B-8)$$

The initial-guess solution is chosen to be $\{\phi\}_0 = \{\phi_1, \phi_2, \dots, \phi_N\}_0^T = \varepsilon \{1, 1, \dots, 1\}^T$, where $\varepsilon \rightarrow 0$. This guess solution corresponds to zero dislocation density along the crack (i.e., a constant initial crack opening). The parameter ε is kept infinitesimally small but nonzero to avoid the elements of the Jacobian matrix from becoming singular. The least-squares solution to the overdetermined system of equations is obtained using the MATLAB nonlinear solver `fsolve` that uses the trust-region reflective algorithm.

To obtain a unique solution to the system of Eq. B-3, the value of δ_{min} in Eq. B-5 must be specified. The upper limit for δ_{min} corresponds to the case when the entire unit cell is filled with proppant (i.e., $a = b$). In this case, the proppant column is then subjected to uniaxial strain and the constant residual opening of the unit cell δ_{1D} can be obtained by substituting $\sigma_p = \sigma_o$ into Eq. 6 and then solving the resulting equation by trial and error. The lower limit for δ_{min} is zero, which corresponds to the contact between the fracture faces at $x = \pm a$. The correct value of δ_{min} lies between these two limits and is selected by trial and error, such that the obtained solution satisfies the condition for stress equilibrium in the y -direction (Eq. 11). The latter can be written in normalized form as

$$\frac{1}{2} \int_{-1}^{+1} \sigma_p(t) dt - \sigma_o = 0. \dots \dots \dots (B-9)$$

The integral in Eq. B-9 can be evaluated using the trapezoidal rule from the solution for σ_p obtained at the $N + 1$ collocation points.

Aditya Khanna is a post-doctoral-degree research associate at the University of Adelaide. Khanna holds a PhD degree in mechanical engineering from the University of Adelaide.

Andrei Kotousov is a professor in the School of Mechanical Engineering at the University of Adelaide. He has broad experience in theoretical and experimental fracture mechanics, biomechanics, structural health monitoring, and composite materials. Kotousov has contributed to more than 150 peer-reviewed publications in these areas. He holds a PhD degree from the Russian Academy of Sciences.

Hao Thanh Luong is a master's-degree student at the School of Mechanical Engineering at the University of Adelaide. He holds a bachelor's degree from Hanoi University of Science and Technology, Vietnam.

Chapter 7

On the coarse-scale residual opening of
hydraulic fractures created using
the channel fracturing technique

Statement of Authorship

Title of Paper	On the coarse-scale residual opening of hydraulic fractures created using the Channel Fracturing technique
Publication Status	<input type="checkbox"/> Published <input type="checkbox"/> Accepted for Publication <input checked="" type="checkbox"/> Submitted for Publication <input type="checkbox"/> Unpublished and Unsubmitted work written in manuscript style
Publication Details	11th International Conference on Structural Integrity and Failure (SIF-2018), 3 - 6 December 2018, Perth, Australia

Principal Author

Name of Principal Author	Hao Luong		
Contribution to the Paper	Developed the method, performed all numerical calculations, prepared manuscript and figures.		
Overall percentage (%)	50		
Certification:	This paper reports on original research I conducted during the period of my Higher Degree by Research candidature and is not subject to any obligations or contractual agreements with a third party that would constrain its inclusion in this thesis. I am the 1 st author of this paper		
Signature		Date	10/07/2018

Co-Author Contributions

By signing the Statement of Authorship, each author certifies that:

- i. the candidate's stated contribution to the publication is accurate (as detailed above);
- ii. permission is granted for the candidate to include the publication in the thesis; and
- iii. the sum of all co-author contributions is equal to 100% less the candidate's stated contribution.

Name of Co-Author (Candidate)	Aditya Khanna		
Contribution to the Paper	Assisted with the formulation of the homogenisation procedure		
Overall percentage (%)	20		
Signature		Date	10/07/2018

Name of Co-Author	Andrei Kotousov		
Contribution to the Paper	Assisted with the conceptual framework of the paper		
Overall percentage (%)	10		
Signature		Date	10/07/2018

Name of Co-Author	Francis Rose		
Contribution to the Paper	Assisted with the formulation of the homogenisation procedure		
Overall percentage (%)	20		
Signature		Date	10/07/2018

1 **On the coarse-scale residual opening of hydraulic fractures**
2 **created using the Channel Fracturing technique**

3 Hao Luong^{1*}, Aditya Khanna¹, Andrei Kotousov¹ and L.R. Francis Rose²

4 ¹School of Mechanical Engineering, The University of Adelaide, Adelaide, SA
5 5005, Australia

6 ²Aerospace Division, DST Group, Melbourne, VIC 3207, Australia

7 *Authors' email – hao.luong@adelaide.edu.au

8 **Abstract**

9 Hydraulic fracturing is a well-stimulation technology used in the oil and gas
10 industry for enhancing hydrocarbon recovery from low permeability reservoirs.
11 Under reservoir conditions when the fluid conductivity of the fracture limits
12 the recovery rate, it is desirable to enhance the fracture conductivity by
13 discontinuous proppant placement. Channel fracturing is one of the techniques
14 utilised to achieve discontinuous proppant placement, i.e. a network of open
15 channels or voids between the proppant-filled regions (proppant columns).

16 The problem of deformation and fluid flow in a partially-filled fracture
17 involves two length scales: a large scale comparable to the length of the
18 fracture $\sim O(10^2)$ m and a fine scale comparable to the length of the proppant
19 filled regions or ‘columns’ $\sim O(1)$ m. It is understood that the effective stress
20 normal to the fracture plane, the initial fracture aperture as well as the spacing
21 between the proppant columns can vary with position along the fracture. In this
22 paper, a homogenisation procedure is developed to obtain the residual opening
23 profile and effective fracture conductivity at the large scale from the solution
24 of a ‘unit-cell’ problem at the fine scale. The application of the model in a
25 practical scenario is demonstrated by performing a mock numerical simulation.

26

27 Introduction

28 The Channel Fracturing Technique is the novel fracturing technique
29 successfully developed in recent years. The idea of the technique is creating
30 discontinuous proppant placement within the hydraulic fracture to obtain open
31 channels between the proppant columns (Gillard et al. 2010; Inyang et al.
32 2014). The open channels are very conductive pathways for fluid flow from
33 oil/gas reservoir to the wellbore, so the effective fracture conductivity can be
34 increased up to several folds higher than that using the conventional hydraulic
35 fracturing techniques (Khanna et al. 2017).

36 The effective fracture conductivity can be maximised by selecting the optimal
37 width of the open channels, i.e. the optimal spacing between the proppant-
38 filled regions or ‘columns’. The optimisation requires solution to the problem
39 of rock deformation and fluid flow in a partially-filled fracture at two length-
40 scales: a coarse length-scale, \hat{X} comparable to the half-length of the fracture,
41 $L \sim O(10^2)$ m, and a fine length-scale, \hat{x} comparable to the half-length of the
42 proppant-filled regions or ‘columns’, $b \sim O(1)$ m. The initial opening of the
43 fracture, δ_o , the fluid pressure within the fracture, p_f , as well as the
44 compressive overburden stress normal to the fracture plane, σ_{yy}^∞ , vary at the
45 coarse scale. However, these variations are expected to be negligible at the fine
46 scale, except close to the wellbore ($X = 0$) or the fracture tips ($|X| = \pm L$).
47 Hence, the problem geometry can be treated as periodic at the length-scale of
48 the proppant columns (see Fig. 1) (Khanna et al. 2017).

49 Based on the assumption of periodicity, a ‘unit-cell’ problem can be
50 formulated at the fine scale. Upon the application of the compressive stress of
51 magnitude $\sigma_0 = \sigma_{yy}^\infty - p_f$, the proppant column and elastic rock undergo
52 deformation in such a manner that the residual opening of the unit-cell, $\delta(x)$,
53 $|x| \leq a$, is less than the constant initial opening δ_o (Fig. 1). In the proppant-
54 filled region of the unit-cell, i.e. $|x| \leq b$, δ_o and $\delta(x)$ also represent the initial
55 and final height of the proppant column. The fluid conductivity of the
56 proppant-filled regions and open channels in the deformed configuration can

57 be determined from the solution of the residual opening profile using the
 58 Darcy's law and Poiseuille law, respectively (Witherspoon et al. 1980;
 59 Zimmerman & Yeo 2000). The effective conductivity of the unit-cell can be
 60 estimated from the conductivity of the two media using a suitable averaging
 61 procedure (Khanna et al. 2017). It is then straightforward to determine the
 62 optimal spacing between the proppant-filled regions, $2a$, which maximises the
 63 effective conductivity of the unit-cell for given values of the parameters $2b$, δ_o ,
 64 and σ_o .

65 From a practical viewpoint, it is of
 66 greater interest to consider the effective
 67 conductivity of the entire fracture, rather
 68 than a unit-cell. The solution at the
 69 coarse scale can be obtained in a
 70 computationally efficient manner by
 71 adopting a homogenisation procedure.
 72 The homogenisation or averaging
 73 procedure replaces the numerous
 74 discrete proppant columns along the
 75 fracture length by a continuously-
 76 distributed 'fictitious' porous medium.
 77 The purpose of this paper is to develop

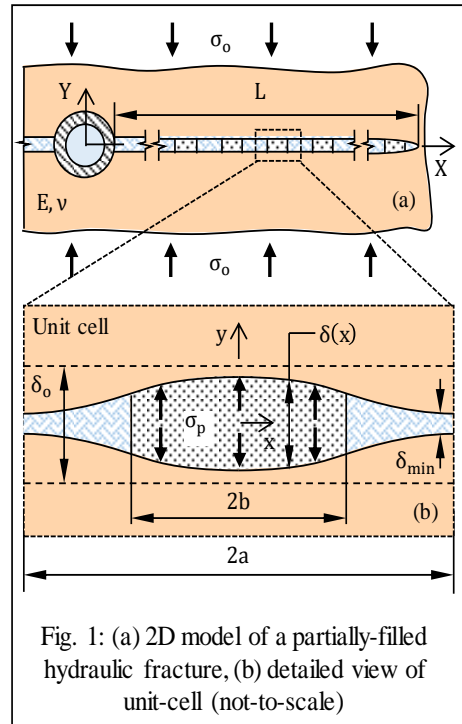


Fig. 1: (a) 2D model of a partially-filled hydraulic fracture, (b) detailed view of unit-cell (not-to-scale)

78 the displacement-dependent traction and conductivity relationships for the
 79 fictitious medium, which is a necessary first step towards the solution of
 80 homogenised problem. The formulation of the unit-cell problem and the
 81 method of solution are briefly discussed first.

82 Formulation of the unit-cell problem

83 For the unit cell of the problem geometry, shown in Fig. 1b, the periodicity of
 84 the problem requires that:

$$u_x(x = \pm a, y) = 0, \quad \sigma_{xy}(x = \pm a, y) = 0, \quad (1)$$

85 The traction boundary conditions along the crack faces can be stated as

$$\sigma_{yy}(x, y = 0_{\pm}) = \begin{cases} -\sigma_p(x), & |x| < b \\ 0, & b < |x| < a' \end{cases} \quad (2a)$$

$$\sigma_{xy}(x, y = 0_{\pm}) = 0. \quad (2b)$$

86 where $\sigma_p(x)$ is the continuous normal traction applied to crack surface by the
 87 proppant pack. The latter can be defined in terms of the crack opening
 88 displacement, $\delta(x) = u_y(x, y = 0_+) - u_y(x, y = 0_-)$, using the traction law
 89 adopted for describing the uniaxial consolidation of the proppant pack. The
 90 remote boundary condition for the stress acting normal to the crack can be
 91 expressed as

$$\sigma_{yy}(x, y \rightarrow \infty) = -\sigma_o, \quad (3a)$$

$$\sigma_{xy}(x, y \rightarrow \infty) = 0. \quad (3b)$$

92 In Eqs. (2a)-(3a), the normal stresses are positive under tension. Finally, the
 93 equilibrium equation for the forces in the y-direction can be stated as

$$\int_{-b}^b \sigma_p(x) dx - 2a\sigma_o = 0. \quad (4)$$

94 The present study adopts a simple one-dimensional model for proppant
 95 consolidation, i.e. the lateral expansion of the proppant columns is ignored.
 96 The compressive stress at a given location in the proppant column, $\sigma_p(x)$ is
 97 related to the change in height of the proppant column, $\delta_o - \delta(x)$ using the
 98 following power-law relationship (Khanna et al. 2017):

$$\sigma_p(x) = \alpha \left(\frac{\delta_o - \delta(x)}{\delta(x)} \right)^{\beta}. \quad (5)$$

99 In the above equation, the constants α and β are the fitting parameters
 100 determined from experimental data. The height of the proppant column $\delta(x)$
 101 lies in the interval $(0, \delta_o]$ and Eq. (5) implies that $\sigma_p = 0$ at $\delta(x) = \delta_o$ and
 102 $\sigma_p \rightarrow \infty$ as $\delta(x) \rightarrow 0$.

103 For a unit-cell completely filled with proppant, i.e. $a = b$ (see Fig. 1), the rock
 104 undergoes uniaxial deformation, i.e. the residual opening of the unit-cell is

105 constant. The latter can be obtained by substituting $\sigma_p = \sigma_o$ into Eq. (5) as
 106 follows

$$\delta(x) = \delta_{1D} = \delta_o \left(1 + \left(\frac{\sigma_o}{\alpha} \right)^{\frac{1}{\beta}} \right)^{-1}, \quad |x| \leq a. \quad (6)$$

107 For the more general case of a partially filled unit-cell, the residual opening
 108 varies as a function of the position x and the resulting stress and displacement
 109 field in the elastic rock must satisfy the boundary conditions given by Eqs. (1)-
 110 (4). To ensure that the unsupported fracture faces do not come in contact, the
 111 spacing between the columns must be selected such that $\delta_{\min} = \delta(x = a)$
 112 remains greater than zero (see Fig. 1).

113 **Method of solution: Distributed Dislocation Technique**

114 The relative opening between the crack faces, $\delta(x)$, is modelled by a
 115 continuous distribution of ‘edge dislocations’. The singular integral equation
 116 which governs the distribution of the dislocations is derived in Khanna et al.
 117 (2017) and can be written as

$$\frac{\bar{E}}{4\pi} \int_0^a B_y(\xi) \left[\frac{2\xi}{x^2 - \xi^2} + K(x, \xi) \right] d\xi = \sigma_o - \sigma_p(x)H(b - |x|), \quad 0 < x < a, \quad (7)$$

118 where $B_y(\xi)$ is the unknown dislocation density function which represents the
 119 continuous distribution of dislocations, $H(\)$ is the Heaviside step function
 120 and the kernel $K(x, \xi)$ is given by

$$K(x, \xi) = \sum_{n=1}^{\infty} \frac{4\xi(x^2 - \xi^2 + 4a^2n^2)}{\{(x - \xi)^2 - 4a^2n^2\}\{(x + \xi)^2 - 4a^2n^2\}}. \quad (8)$$

121 The dislocation density is related to the residual opening profile according to

$$\delta(x) = \delta_{\min} + \int_x^a B_y(\xi) d\xi, \quad B_y(\xi) = \frac{d\delta(\xi)}{d\xi}, \quad 0 < x < a. \quad (9)$$

122 The method of solution of the governing Eq. (7) is described in Khanna et al.
 123 (2017) and will not be discussed here. The elastic stress field in the rock in the

124 interval $x \in [0, a]$, $y \in [0, \infty)$ can be obtained from the superposition of the
 125 stress field in the absence of the fracture and the stress field induced by the
 126 dislocation density, $B_y(\xi)$, i.e.

$$\sigma_{xx}(x, y) = \frac{\bar{E}}{4\pi} \int_0^a B_y(\xi) [f_{xx}(x - \xi, y) - f_{xx}(x + \xi, y)] d\xi, \quad (10)$$

$$\sigma_{yy}(x, y) = -\sigma_o + \frac{\bar{E}}{4\pi} \int_0^a B_y(\xi) [f_{yy}(x - \xi, y) - f_{yy}(x + \xi, y)] d\xi, \quad (11)$$

$$\sigma_{xy}(x, y) = \frac{\bar{E}}{4\pi} \int_0^a B_y(\xi) [f_{xy}(x - \xi, y) - f_{xy}(x + \xi, y)] d\xi. \quad (12)$$

127 where the kernels f_{ij} , which account for the periodic boundary condition can be
 128 obtained using the method described in Khanna et al. (2017) as

$$f_{xx}(x, y) = \sum_{n=-\infty}^{\infty} \frac{(x - 2an)((x - 2an)^2 - y^2)}{((x - 2an)^2 + y^2)^2}, \quad (13)$$

$$f_{yy}(x, y) = \sum_{n=-\infty}^{\infty} \frac{(x - 2an)((x - 2an)^2 + 3y^2)}{((x - 2an)^2 + y^2)^2}, \quad (14)$$

$$f_{xy}(x, y) = \sum_{n=-\infty}^{\infty} \frac{y((x - 2an)^2 - y^2)}{((x - 2an)^2 + y^2)^2}. \quad (15)$$

129 Similarly, the displacement field in the rock in the interval $x \in [0, a]$, $y \in$
 130 $[0, \infty)$ can be obtained from the superposition of displacements in the absence
 131 of the fracture, the displacements induced by the dislocation density, and the
 132 rigid body motion at $y = 0$ due to the closure of the fracture under the remote
 133 compressive loading. Of particular interest is the y -component of the
 134 displacement, which can be written as

$$\begin{aligned}
u_y(x, y \geq 0) = & -\frac{\sigma_o}{E} y \\
& + \frac{1}{8\pi(1-\nu)} \int_0^a B_y(\xi) [g_y(x-\xi, y) - g_y(x+\xi, y)] d\xi \\
& - \frac{(\delta_o - \delta_{\min})}{2},
\end{aligned} \tag{16}$$

135 where

$$g_y(x, y) = \sum_{n=-\infty}^{\infty} \left[4(1-\nu) \tan^{-1} \frac{y}{(x-2an)} - \frac{2(x-2an)y}{(x-2an)^2 + y^2} \right], \tag{17}$$

136 The integrals in Eqs. (10)-(12) and (16) can be evaluated using the Gauss-
137 Chebyshev quadrature method or numerically (Erdogan et al. 1973). The
138 infinite summations in Eqs. (13)-(15) and (17) can be truncated at a suitably
139 large value of n.

140 **Homogenisation procedure**

141 The aim of the homogenisation procedure is to replace the proppant column,
142 which partially occupies the unit-cell, by an effective medium which fills the
143 entire unit-cell. The nonlinear response of the effective medium is also
144 described by Eq. (5), except for a multiplicative constant C, which varies with
145 the geometrical parameters a, b and δ_o and the remote stress, σ_o . The constant
146 C must be found in such a manner than the potential energy of the unit-cell,
147 defined below, remains conserved.

$$\Pi = U_1 + U_2 + W. \tag{18}$$

148 In Eq. (18), U_1 is the strain energy of the rock in the deformed configuration
149 over the region $x \in [-a, a]$, $y \in (-\infty, \infty)$ and can be written as:

$$U_1 = 4 \int_0^{\infty} \int_0^{+a} \left(\frac{\sigma_{xx}^2 + \sigma_{yy}^2 - 2\nu\sigma_{xx}\sigma_{yy}}{2\bar{E}} + \frac{\sigma_{xy}^2}{2G} \right) dx dy, \tag{19}$$

150 where the stress components can be obtained from Eqs. (10)-(12). The above
 151 integral does not converge since the stress component $\sigma_{yy}(x, y \rightarrow \infty) = -\sigma_o$.
 152 However, it can be evaluated by truncating the outer integral at a sufficiently
 153 large value of y at which the kernels given by Eqs. (13)-(15) tend to zero. From
 154 a numerical convergence study, $y = (2b) \times 10^6$ was found to be a sufficiently
 155 remote boundary at which the stress field corresponded to Eq. (4).

156 The term U_2 in Eq. (18) corresponds to the strain energy stored in the deformed
 157 proppant column and can be obtained as:

$$U_2 = 2 \int_0^{+b} \int_0^{\delta_o - \delta(x)} \alpha \left(\frac{u}{\delta_o - u} \right)^\beta du dx, \quad (20)$$

158 where $u = \delta_o - \delta$ denotes the change in height of the proppant column.

159 Finally, the term W in Eq. (18) represent the work done due to the
 160 displacement of the remote boundary upon which the compressive traction
 161 $\sigma_{yy}(x, y \rightarrow \pm\infty) = -\sigma_o$ is applied. It can be written as

$$W = -4 \int_0^{+a} u_y(x, y \rightarrow \infty) \sigma_{yy}(x, y \rightarrow \infty) dx. \quad (21)$$

162 Since the displacement field due to the dislocation density, i.e. the kernel
 163 $g_y(x, y)$ in Eq. (16) tends to zero at the remote boundary $y \rightarrow \infty$, the work done
 164 can be written as

$$W = \lim_{y \rightarrow \infty} \left(-4a \frac{\sigma_o^2}{E} y \right) - 2a(\delta_o - \delta_{\min})\sigma_o. \quad (22)$$

165 A unit-cell filled entirely with the effective medium undergoes uniaxial
 166 compression and the strain energy stored in the rock over the region $x \in$
 167 $[-a, a]$, $y \in (-\infty, \infty)$ is simply given by

$$U_1^* = 4 \int_0^\infty \int_0^{+a} \left(\frac{\sigma_o^2}{2E} \right) dx dy. \quad (23)$$

168 The strain energy stored in the effective medium can be written as

$$U_2^* = 2 \int_0^{+a} \int_0^{\delta_0 - \delta^*} C \alpha \left(\frac{u}{\delta_0 - u} \right)^\beta du dx, \quad (24)$$

169 where δ^* is the constant opening of the fracture filled with the effective
170 medium, and can be obtained similar to Eq. (6) as:

$$\delta^* = \delta_0 \left(1 + \left(\frac{\sigma_0}{C\alpha} \right)^{\frac{1}{\beta}} \right)^{-1}. \quad (25)$$

171 Analogous to (22), the work done at the remote boundary is

$$W^* = \lim_{y \rightarrow \infty} \left(-4a \frac{\sigma_0^2}{E} y \right) - 2a(\delta_0 - \delta^*)\sigma_0. \quad (26)$$

172 The equivalence of potential energy requires that $\Pi = \Pi^*$, i.e. $U_1 + U_2 + W =$
173 $U_1^* + U_2^* + W^*$. Utilising Eqs. (19)-(26), the potential energy equivalence
174 requirement can be stated as

$$\begin{aligned} & 4 \int_0^\infty \int_0^{+a} \left(\frac{\sigma_{xx}^2 + \sigma_{yy}^2 - 2\nu\sigma_{xx}\sigma_{yy}}{2\bar{E}} + \frac{\sigma_{xy}^2}{2G} - \frac{\sigma_0^2}{2\bar{E}} \right) dx dy \\ & + 2 \int_0^{+b} \int_0^{\delta_0 - \delta(x)} \alpha \left(\frac{u}{\delta_0 - u} \right)^\beta du dx \\ & - 2 \int_0^{+a} \int_0^{\delta_0 - \delta^*} C \alpha \left(\frac{u}{\delta_0 - u} \right)^\beta du dx - 2a(\delta^* - \delta_{\min})\sigma_0 \\ & = 0. \end{aligned} \quad (27)$$

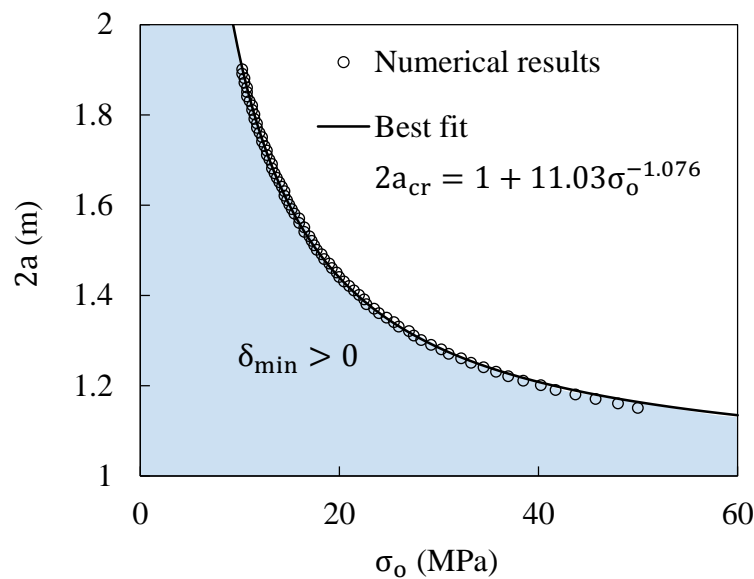
175 Eq. (27) is satisfied by a unique value of the constant C which can be obtained
176 using a suitable root finding algorithm.

177 **Numerical results**

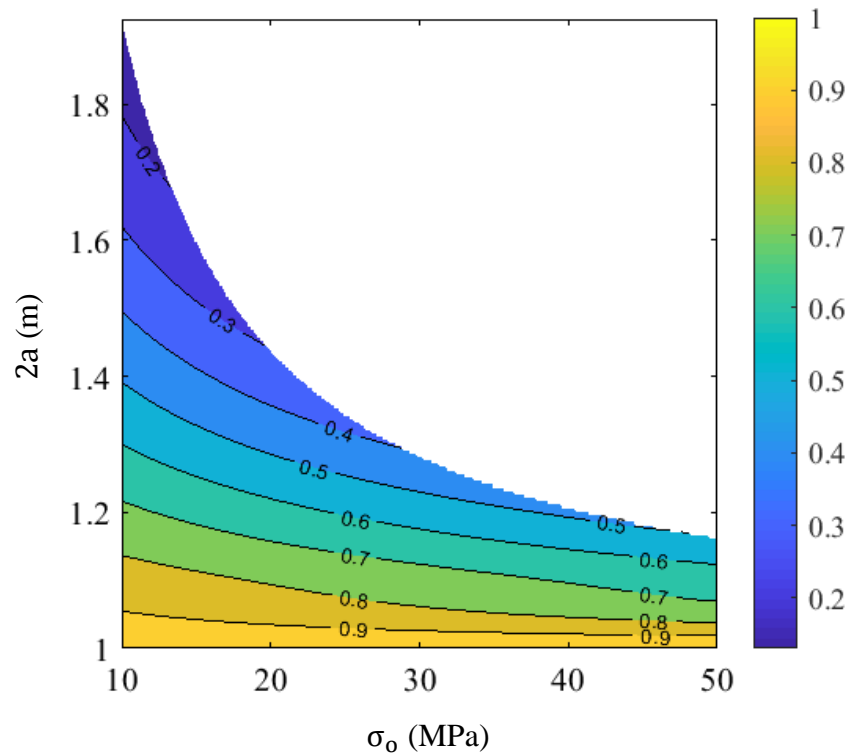
178 In this section, some numerical results are presented for the effective properties
179 of the homogenised medium. In these numerical calculations, the initial
180 opening δ_0 is fixed at 5 mm and the width of the proppant filled region, $2b$ is

181 fixed at 1 m. The Young's modulus and Poisson's ratio of the rock are selected
 182 to be $E = 10$ GPa and $\nu = 0.3$, which are typical values for oil/gas bearing
 183 rocks. The fitting parameters in Eq. (5) are selected to be $\alpha = 5.543$ MPa and
 184 $\beta = 3.873$.

185 The first step of the analysis is to determine the critical spacing between the
 186 proppant columns, $2a$, at which the minimum residual opening of the unit-cell,
 187 $\delta_{\min} = \delta(|x| = a)$ equals to zero, i.e. the fracture walls come in contact (see
 188 Fig. 1b). This critical value of proppant column spacing, $2a_{\text{cr}}$, corresponds to a
 189 drastic reduction in the fluid conductivity of the open channels. The selection
 190 of proppant column spacing greater than this critical value will result in sub-
 191 optimal increase in the effective fracture conductivity, hence represents a case
 192 of little practical interest. The dependence of a_{cr} on the remotely applied
 193 compressive stress σ_o was obtained through an extensive parametric study and
 194 the results are presented in Fig. 2. The best fit equation recovers the limiting
 195 cases, i.e. $2a_{\text{cr}} \rightarrow \infty$ as $\sigma_o \rightarrow 0$ and $2a_{\text{cr}} \rightarrow 2b = 1$ m as $\sigma_o \rightarrow \infty$.



196
 197 Fig. 2: Envelope showing combinations of proppant column spacing, $2a$ and remotely
 198 applied compressive stress, σ_o which ensure that the fracture faces do not come in
 199 contact.
 200



201

202 Fig. 3: Contour plot showing the variation of the effective medium stiffness constant C
 203 upon proppant column spacing and remotely applied stress..

204 Numerical results for the constant C are obtained for the remotely applied
 205 stress in the range $10 < \sigma_0 < 50$ MPa with increments of 1 MPa and the
 206 proppant column spacing in the range $1.0 < 2a < 2.0$ m, with increments of
 207 0.05 m. A spline function was fitted through the discrete data points to obtain
 208 the interpolated value of the constant C for any combination of parameters $2a$
 209 and σ_0 which yield $\delta_{\min} > 0$ as shown in Fig. 3.

210 Conclusion

211 In this paper, the periodic system of proppant columns within a hydraulic
 212 fracture is replaced by a continuous distribution of springs along the fracture
 213 length using a homogeneous procedure. The energy conservation principle and
 214 the solution for “unit-cell” developed in Khanna et al (2017) are utilised to
 215 define the traction-law for the nonlinear springs. The numerical results present
 216 the effective medium stiffness constant C according to any combination of

217 proppant column spacing and the confining stress. The application of the
218 effective medium stiffness concept allows a significant reduction of the
219 complexity of the problem and an application of well-developed methods of
220 Fracture Mechanics to evaluate the residual opening of a periodically
221 supported fracture. The outcomes of this work provide the first necessary step
222 to analyse the hydraulic channel fracturing technique, which is of great interest
223 for gas and oil industries.

224 **References**

225 Erdogan, F., Gupta, G.D. & Cook, T.S. 1973, 'Numerical solution of singular integral
226 equations', In: Sih G.C. (eds) *Methods of analysis and solutions of crack problems.*
227 *Mechanics of fracture*, vol. 1.

228 Gillard, M.R., Medvedev, O.O., Hosein, P.R., Medvedev, A., Peñacorada, F., apos &
229 Huteau, E. 2010, 'A new approach to generating fracture conductivity', paper
230 presented at SPE Annual Technical Conference and Exhibition, Florence, Italy.

231 Inyang, U.A., Nguyen, P.D. & Cortez, J. 2014, 'Development and field applications of
232 highly conductive proppant-free channel fracturing method', paper presented at SPE
233 Unconventional Resources Conference, The Woodlands, Texas, USA.

234 Khanna, A., Luong, H., Kotousov, A., Nguyen, G.D. & Rose, L.R.F. 2017, 'Residual
235 opening of hydraulic fractures created using the channel fracturing technique',
236 *International Journal of Rock Mechanics and Mining Sciences*, vol. 100, pp. 124-137,
237 DOI <https://doi.org/10.1016/j.ijrmms.2017.10.023>.

238 Witherspoon, P.A., Wang, J.S.Y., Iwai, K. & GaleJ, E. 1980, 'Validity of cubic law for
239 fluid flow in a deformable rock fracture', *Water Resources Research*, vol. 16, no. 6,
240 pp. 1016-1024, DOI doi:10.1029/WR016i006p01016.

241 Zimmerman, R.W. & Yeo, I. 2000, 'Fluid flow in rock fractures: From the navier -
242 stokes equations to the cubic law', in *Dynamics of fluids in fractured rock*, pp. 213-
243 224.

244

Chapter 8

Summary and recommendations

Chapter 8

Summary and recommendations

8.1. Summary of the outcomes

In this thesis, a number of advanced analytical models were developed, which are capable to incorporate the several important governing mechanisms and effects associated with deformation and discontinuous placement of proppant, initial hydraulic fracture opening and fluid flow in narrow channels. By using an analytical framework, a number of multi-parametric studies were conducted to evaluate the optimal normalised spacing between proppant columns that maximises the overall fluid conductivity of channel fractures as a function of different stress conditions, mechanical properties of the proppant and rock formation. The developed solutions also capture the size effect of the proppant columns, which is impossible to investigate in-situ or experimentally due to the relatively small size of laboratory samples in comparison with the actual hydraulic fracture dimensions. The evaluation and validation of the developed models in this thesis was accomplished via the sensitivity studies and by comparing the theoretical predictions with available field observations. It is also recognised that more work is needed to find the fitting constants in the proposed empirical equations describing the properties and interaction of rock and proppant as well as to validate the developed mathematical models, theoretical solutions and general conclusions. Further, the main outcomes of the present thesis will be described chapter by chapter excluding the first three introductory chapters, which were included into the thesis to provide the cohesiveness and completeness of the thesis.

Chapter 4: Residual opening of hydraulic fractures created using the channel fracturing technique

In this Chapter, a general solution was developed to analyse a partially-filled fracture created by the channel fracturing technique. For simplicity, the

actual 3D problem was simplified and the problem geometry was reduced to 2D shape. The proppant packs (columns) were assumed to be regularly distributed along the fracture length. So, the problem was analysed using one representative unit cell instead of considering the whole of fracture length. The mechanical response of the proppant columns under compression was simulated based on an empirical equation accounting for the proppant consolidation phenomenon. The equation was calibrated using available experimental results. A numerical procedure was developed based on Newton Raphson iterative scheme to allow for a parametric study in order to identify the optimal conditions, which maximise the fluid conductivity.

Chapter 5: Optimisation of proppant use in the application of the channel fracturing technique

This Chapter largely extends the theoretical framework presented in the previous Chapter. An advanced mathematical model was proposed to incorporate the effects of the mechanical properties of the rock formation and proppant packs, the magnitude of the compressive in-situ stresses, as well as the different proppant placement patterns on the residual opening profiles and effective fluid conductivity. Various important deformation mechanisms including the linear elastic deformation of the rock, the non-linear consolidation of the proppant packs and the indentation of proppant particles into the rock formation were incorporated into this advanced model. In particular, it was demonstrated that the channel fracturing technique is much more efficient for hard rock rather than for soft rock formations.

Chapter 6: On the application of the channel-fracturing technique to soft rock formations

This Chapter is specifically focused on the application of the channel fracturing technique for soft rock formations, in which the influence of the proppant embedment on the fracture conductivity can be quite significant, so it needs to be properly incorporated into the modelling. The soft rock formation

was modelled as previously: as a linearly elastic, isotropic, and homogeneous medium. The proppant response was represented as a synthesis of the nonlinear response of the proppant to the consolidation and the linear response to the embedment. The empirical models for the proppant consolidation and proppant embedment were proposed based on the previously published experimental results, which are quite limited. An analytical approach, as elsewhere in this thesis, was based on the Distributed Dislocation Technique, which was adopted for particular problems, e.g. in this Chapter to evaluate the optimal parameters of the channel fracturing technique. A parametric study under typical field conditions was conducted to identify the optimal parameters leading to the maximum fluid conductivity enhancement.

Chapter 7: On the coarse-scale residual opening of hydraulic fractures created using the Channel Fracturing technique

In this Chapter, the discontinuous placement of proppant within a fracture was considered taking into account the variation of the confining stress and the opening along the fracture length. The discrete proppant columns were replaced by a continuous distribution of nonlinear springs along the fracture length, and the effective mechanical response of these springs on a large scale was selected to be equivalent to the discrete columns. The traction-law for these springs was developed using the energy conservations along with the solution for the “unit-cell” proposed in the previous chapters. The results were presented in terms of the effective medium stiffness constant for various combinations of the normalised proppant column spacing.

8.2. Recommendations for future work

It is well known that analytical models normally offer a high degree of the transparency, repeatability, reproducibility and computational efficiency. However, this type of models suffers from unavoidable simplifications and reliance on a number of rather radical assumptions. It is clear that this reliance can affect the accuracy and adequacy of the theoretical results. Despite that a

number of modelling assumptions have been utilised in many similar analytical studies in the past, some of them still need to be validated and further assessed. It seems, there is a common agreement that the main value of analytical models is in their ability to predict the tendencies rather than particular values of a complex process, such as the hydraulic stimulation. Another advantage of analytical models and analytical approaches is their suitability for the optimisation purposes, here they can compete with more sophisticated numerical methods. These two aspects of analytical models are the main drivers behind the current project, and, as expected, for the future studies.

As mentioned above, the validation of the adopted proppant consolidation and embedment models are vital for the accurate predictions of the well efficiency. Therefore, the future work should strongly focus on the experimental validation of the adopted empirical models. However, it is expected that there will be no significant impact on the developed modelling approach if more appropriate empirical equations describing the proppant consolidation and embedment or fluid flow or proppant placement models to be used in the future. Thus, the theoretical developments described in this thesis can be easily adopted, adjusted and modified in accordance with the future finding, if necessary.

From practical point of view, the outcomes of this thesis can be used as a guidance in the improvement and optimisation of the channel fracturing technique in order to maximise production rates as well as to decrease proppant use by controlling the relative duration of the proppant-laden pulses during the injection state. However, the application of these theoretical models needs a strong support from the industry and quite significant financial commitments. As mentioned before in the Introduction, the increased competitiveness of the current resources and commodities marked could encourage the industry to search for more efficient ways to recover the energy resources and, eventually, adopt some of the modelling approaches to direct and guide the further developments and technologies.